Glacier mass balance and runoff in the tropical Cordillera Blanca, Perú.

DISSERTATION

zur Erlangung des akademischen Grades eines
Doktors der Naturwissenschaften
an der Leopold-Franzens-Universität Innsbruck.

Eingereicht von: Mag. rer. nat. Irmgard Juen
Betreut von: A. Univ. Prof. Dr. Georg Kaser

Innsbruck, September 2006

Institute of Geography

Tropical
Glaciology Group
University of Innsbruck

vorgeschlagene Begutachter:
Dir. de Recherche Dr. Bernard Pouyaud (IRD, Montpellier);
A. Uni. Prof. Dr. Fritz Schöberl (Geographie, Univ. Innsbruck);
Univ. Prof. Dr. Pierre Ribstein (Univ. Jussieu, Paris)

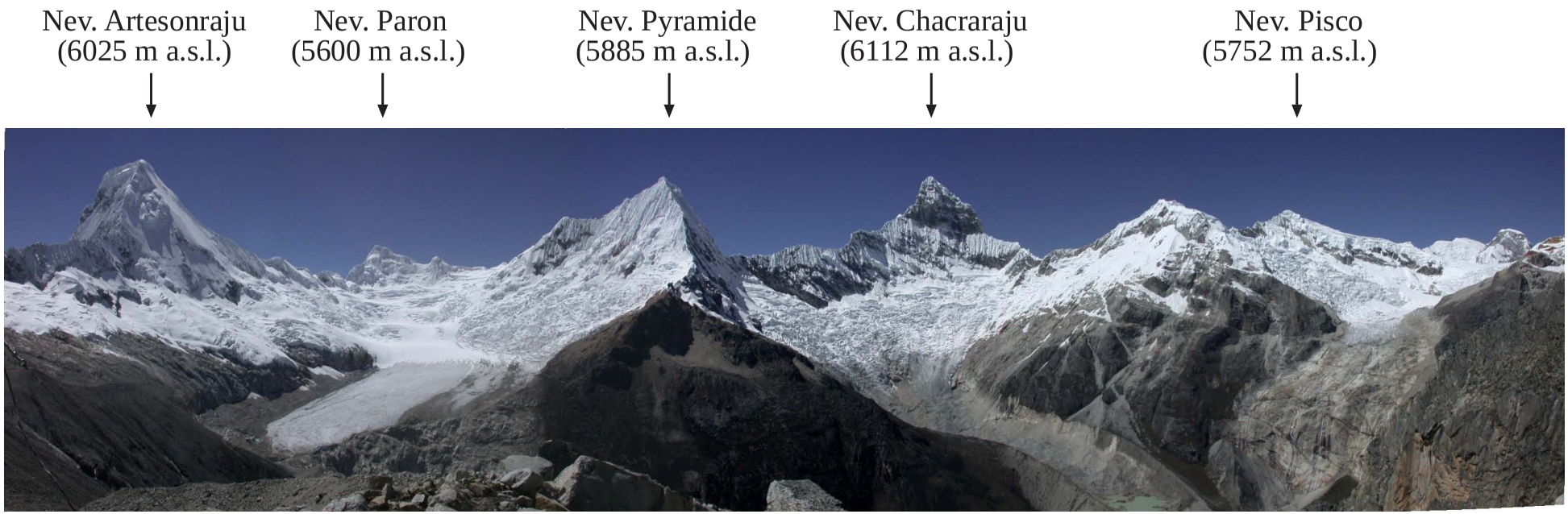

Panorama of Glacier Artesonraju and Chacraraju in the Parón valley. Photo taken by Irmgard Juen in May 2005.

Table of content

TABLE OF CONTENT ..... *I*

LIST OF FIGURES ..... *IV*

LIST OF TABLES ..... *XII*

PREFACE ..... *XV*

ABSTRACT *1*

1. INTRODUCTION *3*

1.1 Investigation area *3*

1.2 Objectives *7*

1.3 Structure of the Thesis *9*

2. STUDY SITES AND AVAILABLE DATA *11*

2.1 Digital elevation model and glacier extent mappings *11*

2.2 Long term records *17*

2.2.1 Precipitation and runoff records *17*

2.2.2 Air temperature records *21*

2.3 Glaciological records *22*

2.4 Data from automatic stations *24*

3. CLIMATE AND GLACIERS IN THE CORDILLERA BLANCA 27

3.1 Long term climate conditions 27

3.2 Glacier fluctuations 32

4. APPLIED METHODS 35

4.1 Mass balance reconstructions from hydrological balance (MBH) ... 35

4.1.1 Determination of runoff characteristics 35

4.1.2 The calculation of mass balance 39

4.2 Mass balance reconstruction from a vertical mass balance profile model (ITGG-2.0) 41

4.3 Runoff modelling (ITGG-2.0-R) 48

4.4 Energy balance calculation 52

5. RESULTS AND DISCUSSION 56

5.1 Mass balance reconstructions 1953 – 1994 56

5.2 Runoff reconstruction for a highly glacierised catchment 61

5.2.1 Calibration period 1965 − 74 and validation period 1975 − 84 62

5.2.2 Runoff simulation for the period 1953 − 1997 65

5.3 Runoff predictions under changing climate conditions 68

5.3.1 Runoff predictions for climate change scenarios 69

5.3.2 Runoff predictions for IPCC climate change scenarios 72

5.4 Energy balance investigations on a tropical glacier tongue 81

5.4.1 Climate conditions at the glacier surface 81

5.4.2 The energy balance at the glacier surface 88

5.4.3 Glacier mass balance, glacier melt and runoff 97

6. SUMMARY AND CONCLUSIONS 104

BIBLIOGRAPHY ***109***

PUBLICATIONS ***119***

APPENDIXES ***123***

A. Generating a digital elevation model (DEM) *123*

B. Watershed deviation from DEM *127*

1. Berechnung der hydrologischen Einzugsgebiete vom GeländEModell cblat (Lattice) *127*

2. Berechnung der hydrologischen Einzugsgebiete vom GeländEModell cbsurfer *130*

3. Expostions- und Neigungsanalysen der beiden DEM *130*

C. Field work report *133*

Glacier Chinchey *135*

Glacier Vallunaraju *138*

Glacier Shallap *140*

Glacier Artesonraju *144*

Data from automatic stations *146*

Hydrological data *154*

D. Data gaps at the energy balance station *157*

E. Additional Figures to chapter 5.3 ..... *159*

F. Additional Figures to chapter 5.4 ..... *162*

List of Figures

Top of Nevado Vallunaraju (5686 m a.s.l.) before (left) and after (right) the demolition on November 18th 2001. Photos are taken by Georg Kaser and Nelson Santillan in 2000 and 2001, respectively..... XVIII

Figure 1.1: Location of the Cordillera Blanca, Perú. 4

Figure 1.2: Annual variation of air temperature ΔT_a (°C) as calculated from the monthly means depending on geographical latitude (φ). Data are from high elevation stations in South America, Africa and Irian Jaya (after Kaser and Osmaston, 2002). The station Querococha in the Cordillera Blanca is marked with a circle..... 5

Figure 2.1: Shaded DEM of the Cordillera Blanca, Perú including catchment borders for hydrological investigations, glacier sites referred to in the text and the glacier extent in 1990. 12

Figure 2.2: Area altitude distribution (50 m altitude steps) of the different catchments including their glacier areas. 15

Figure 2.3: Area altitude distribution (50 m altitude steps) of the glacier areas in the different catchments. 16

Figure 2.4: Mean seasonal variations of precipitation in the Cordillera Blanca depicted from January to December (after Niedertscheider, 1990). 19

Figure 2.5: Mean seasonal variations of runoff in the Cordillera Blanca depicted from January to December (after Niedertscheider, 1990). 20

Figure 2.6: EBS on the tongue of Glacier Artesonraju (4850 m a.s.l.). The station in the background is the RBS. Photo taken by Irmgard Juen in July 2004..... 25

Figure 2.7: Runoff gauge at the outlet of Lake Artesococha (4200 m a.s.l.). Photo taken by Bernard Pouyaud. 25

Figure 3.1: Mean seasonal cycle in precipitation and air temperature from 1949 – 2004. Precipitation is measured at station Parón (4200 m a.s.l.); air temperature is from NCEP-NCAR Reanalysis (500 hPa level). The graph shows the arithmetic mean (cross), limits of the lower and upper quartile (orange box, 25 and 75 %), 90 % quantile (vertical bar), and maximum and minimum values. 28

Figure 3.2: Deviation of annual precipitation sums (delta P) and mean air temperature (delta Ta) from the long term mean climate conditions 1949 – 2004. Precipitation is measured at station Parón (4200 m a.s.l.), air temperature is the NCEP-NCAR Reanalysis data set from the 500 hPa level..... 29

Figure 3.3: Change in the glacier terminus positions of three glaciers in the Cordillera Blanca from 1948 – 1994. 33

Figure 4.1: Mean monthly variation of runoff and precipitation coefficients from 1953 – 1994 (hydrological year from October to September) for six differently glacierised catchments. 36

Figure 4.2: Seasonal storage coefficient S of six differently glacierised catchments against the percentage of glaciation. Que: Quererococha, Pac: Pachacoto, Ch: Chancos, Qui: Quillcay, Ll: Llanganuco, Par: Parón..... 38

Figure 4.3: The modelling of the mass balance variation with altitude under A) dry and B) wet conditions. Calculations start with the determination of accumulation c and ablation a at z_r. From there, the mass balance varies with altitude depending on the vertical variation of accumulation c(z), albedo $\alpha(z)$, and air Temperature $T_a(z)$. Above the ELA and the 0°C level the contribution of $\alpha(z)$ and of $T_a(z)$ cease respectively. More details are given in the text (figure by Georg Kaser). 43

Figure 4.4: Vertical mass balance profiles calculated wit the ITGG-2.0 model with input variables from Table 4.1 for very dry and very wet conditions. 46

Figure 4.5: Schematic structure of the ITGG-2.0-R model. T_a is air temperature, P precipitation, A_G glacier area, A_N glacier-free area, q_G glacier melt, $m|_{zref}$ melt at reference level, VBP vertical balance profile, P_A precipitation volume, $\partial P/\partial z$ vertical gradient of P, and q_T total runoff depth. 49

Figure 4.6: Daily mean measured and modelled surface temperature. The correlation coefficient is $r^2=0.76$, n=404. 55

Figure 5.1: Annual specific mass balance for five catchments in the Cordillera Blanca for the hydrological years 1953/1954 – 1993/1994 modelled from the hydrological balance (MBH) and with the ITGG-2.0 mass balance model (ITGG). The MBH is scaled by 54 %. The catchments are sorted from low to high percentage of glacierisation and from North to South. 57

Figure 5.2: A) Mean cumulative annual specific mass balance for five catchments for the hydrological years 1953/1954 – 1993/1994 modelled from the hydrological balance (MBH) and with the ITGG-2.0 mass balance model (ITGG). The MBH is scaled by 54 %. B) Change in glacier terminus position of three glaciers in the Cordillera Blanca from 1948 – 1994. 59

Figure 5.3: Modelled (qmod) and measured (qmeas) monthly mean runoff depths for the calibration period 1965 to 1975 with a) measured air temperature at Querococha station and b) air temperature from NCEP-NCAR Reanalysis. 63

Figure 5.4: Modelled (qmod) and measured (qmeas) monthly mean runoff depths for the validation period 1975 to 1985 with a) measured air temperature at Querococha station and b) air temperature from NCEP-NCAR Reanalysis. Additionally, runoff is modelled with a reduced sublimation/melt ratio f during the dry period 1983 (dashed line, see text for further explanation)..... 64

Figure 5.5: Results for the 44 years time series from 1953 to 1997 with air temperature input from NCEP-NCAR Reanalysis: a) modelled (qmod) and measured (qmeas) monthly mean runoff depth, b) difference between modelled and measured runoff with the standard deviation of measured runoff in dashed lines), and c) cumulative monthly difference. 66

Figure 5.6: Long-term mean seasonal variation of modelled (qmod) and measured (qmeas) runoff for the hydrological year (October – September). Vertical and horizontal bars depict the standard deviation of measured and modelled runoff, respectively..... 67

Figure 5.7: Modelled influence of a climate change on the amount of glacier melt for a) a change in air temperature of +/− 0.2−2 °C and b) a change in precipitation by +/− 2−20 %. Lines with circles indicate the immediate change in the amount of glacier melt and filled triangles the change after the glacier has reached steady-

state conditions with the respective new climate. Blue represents a decrease, orange an increase of the respective climate variable..... 70

Figure 5.8: Relative change in glacier area (delta AG 1990) to reach steady-state glacier extent for mean climate conditions from 1961−1990 dependent on A) the arithmetic mean and median altitude of the glaciers in the individual catchments and B) on the percentage of glacier area above mean ELA (5100 m a.s.l.). The abbreviations for the single catchments are: par=Parón, lla=Llanganuco, cha=Chancos, qui=Quillcay, pac=Pachacoto, quer=Querococha. 75

Figure 5.9: Predicted monthly relative change in total runoff (delta Q) for the two IPCC climate chance scenarios in 2050 and 2080 in the different catchments..... 78

Figure 5.10: The daily cycle in measured air temperature, wind speed, and vapour pressure at the surface of Glacier Artesonraju (4850 m a.s.l.). The graph shows the arithmetic mean (cross), limits of the lower and upper quartile (orange box, 25 and 75 %), 90 % quantile (vertical bar), and maximum and minimum values..... 83

Figure 5.11: Daily mean wind speed, air temperature, and vapour pressure measured at the surface of Glacier Artesonraju (4850 m a.s.l.) from 1.4. 2004 – 31.03. 2005 (black lines). The blue, orange, and thick black lines are 7 day running means of the daily maximum, minimum, and mean values, respectively. Horizontal lines represent the 0 °C air temperature and the vapour pressure of a saturated glacier surface at melting point (6.1 hPa), respectively. 85

Figure 5.12: Frequency of wind directions (45 ° bins) measured at Glacier Artesonraju (4850 m a.s.l.) for each month from April 2004 – March 2005. 86

Figure 5.13: The daily cycle in measured SW_{in}, SW_{out}, and albedo at the surface of Glacier Artesonraju (4850 m a.s.l.). The graph shows the arithmetic mean (cross), limits of the lower and upper quartile (orange box, 25 and 75 %), 90 % quantile (vertical bar), and maximum and minimum values..... 89

Figure 5.14: The daily cycle in measured LW_{in}, LW_{out}, and the calculated sensible (H) and latent (LE) turbulent fluxes at the surface of Glacier Artesonraju (4850 m a.s.l.). The graph shows the arithmetic mean (cross), limits of the lower and upper quartile (orange box, 25 and 75 %), 90 % quantile (vertical bar), and maximum and minimum values. For legend see Figure 5.13. 90

Figure 5.15: Statistics of daily means of the SW radiation terms and albedo measured at the EBS at the surface of Glacier Artesonraju (4850 m a.s.l.) for each month. The graph shows the arithmetic mean (cross), limits of the lower and upper quartile (orange box, 25 and 75 %), 90 % quantile (vertical bars), and maximum and minimum daily values. For legend see Figure 5.13. 92

Figure 5.16: EBS on Glacier Artesonraju (4850 m a.s.l.) at 11:30 a.m. The left photo is taken by Irmgard Juen during a dry period in August 2005. The right Photo is taken by Robert Galliere after a snowfall event during the night in March 2004. . 93

Figure 5.17: Statistics of daily means of the LW radiation terms measured at the EBS at the surface of Glacier Artesonraju (4850 m a.s.l.) and calculated turbulent fluxes (H and LE) for each month. The graph shows the arithmetic mean (cross), limits of the lower and upper quartile (orange box, 25 and 75 %), 90 % quantile (vertical bars), and maximum and minimum daily mean values. For legend see Figure 5.13. 94

Figure 5.18: Measured (RBS, ultrasonic height sensor) and calculated cumulative net mass balance (EBS, melt + sublimation – accumulation) from 2. – 18. April 2005 at the tongue of Glacier Artesonraju (4750 and 4850 m a.s.l., respectively). Accumulation is obtained from precipitation measurements at the AWS outside the glacier (4850 m a.s.l.). 98

Figure 5.19: Net mass balance rates as measured at four ablation stakes close to the EBS (striped bars with error bars of the standard deviation) and net ablation rates calculated from the EB (sublimation + melt; empty bars). The black bars are net ablation rates from sublimation. Albedo is averaged over the respective time period (right hand axis). 99

Figure 5.20: Mean daily cycle in glacier melt calculated from the EB at the tongue of Glacier Artesonraju (4850 m a.s.l.) and runoff measured at the outlet of Lake Artesoncocha (4200 m a.s.l.). The dashed line is calculated glacier melt applying a linear reservoir equation with a storage parameter ks=7. 100

Figure 5.21: Comparison of runoff (blue) measured at the outlet of Lake Artesoncocha (4200 m a.s.l.) and calculated glacier melt (black) from Glacier Artesonraju for period P1 (Day 73 – 120, 2004). Glacier melt is calculated from the EB at 4850 m a.s.l. applying a linear reservoir equation with A) ks=7 and B) ks=55. 101

Figure 5.22: Daily mean runoff as measured at the outlet of Lake Artesoncocha (4200 m a.s.l.) and delayed glacier melt calculated from the energy balance at Glacier Artesonraju at 4850 m a.s.l. from day 73, 2004 to 58, 2005. 102

Figure 6.1: Mean monthly energy fluxes from SW_{net} (SW) and LW_{net} (LW) radiation, and the turbulent fluxes (H, LE) on the surface of Glacier Artesonraju (4850 m a.s.l.) from April 2004 to March 2005. 107

Figure C.1: Map of Glacier Chinchey its station equipment, stake and terminus position (measured with DGPS)..... 136

Figure C.2: Map of Glacier Vallunaraju its station equipment, stake and terminus position (measured with DGPS)..... 139

Figure C.3: Map of Glacier Shallap its station equipment and stake position. 141

Figure C.4: Seasonal stake ablation at Glacier Shallap between 4785 to 4940 m a.s.l. from April 2002 to March 2004. The dry season is defined from April to September, the wet season from October to March. The lines indicate the regression between the stakes (dashed line is 2003/2004). 142

Figure C.5: Mean net mass balance derived from ablation stake measurements at Glacier Shallap averaged over three months..... 143

Figure C.6: Map of Glacier Artesonraju its station equipment and stake position. AWS = automatic weather station; RBS = radiation balance station (moved to lower side on 17th of November 2004); EBS = energy balance station. 144

Figure C.7: Daily means (9-day running mean) of solar incoming radiation (SWin), ventilated air temperature (calculated for 5000 m a.s.l.), relative humidity and vapour pressure (e) humidity, and wind speed as measured at the AWS at Chinchey-low and –high, Vallunaraju, Shallap, Artesonraju-north and -south, and EBS Artesonraju..... 147

Figure C.8: Mean annual and seasonal daily cycle of solar incoming radiation (Swin), air temperature, specific humidity, and wind speed as recorded at AWS Chinchey-low (red) and –high (blue), Vallunaraju (green), Shallap (black) and the EBS Artesonraju (orange)..... 149

Figure C.9: AWS-south at Glacier Artesonraju (4850 m a.s.l.) with a precipitation gauge. Photo taken by Irmgard Juen in July 2004. 150

Figure C.10: AWS-north (Artesonraju) at 5100 m a.s.l. with two digital cameras. Photo taken by Georg Kaser in July 2004. The cameras take a picture of Glacier Artesonraju and Chacraraju at 10 and 15 l. t. each day. 150

Figure C.11: Connection of the instruments to a Campbell Datalogger CR10X at station AWS-north including pressure sensor (Setra) and storage module. Photo taken by Irmgard Juen in November 2005. 151

Figure C.12: Photo of Glacier Artesonraju from the digital camera 1 at AWS-north. 152

Figure C.13: Photo of Glacier Chacraraju from the digital camera 2 at AWS-north. 152

Figure C.14: RBS at Glacier Artesonraju (4850 m a.s.l.). Photo taken by Irmgard Juen in July 2004. 153

Figure C.15: Campbell Datalogger CR23X installed at the RBS on Glacier Artesonraju. Photo taken by Irmgard Juen in March 2004. 153

Figure C.16: Daily mean runoff recorded at station Chinchey (first graph) and Artesoncocha (38 % and 75 % glacierised, respectively) and daily sums of precipitation measured at lake Parón (4200 m a.s.l.). The dry season is defined from May to September, the humid season from October to April. 154

Figure C.17: Weekly precipitation sums at Llupa, 3600 m a.s.l. 155

Figure C.18: EPROM Datalogger installed at Lake Artesoncocha (4200 m a.s.l.) where runoff is recorded. Photo taken by Bernard Pouyaud. 156

Figure C.19: Calibration measurement at the runoff station at Glacier Chinchey (4200 m a.s.l.). Photo taken by Georg Kaser in November 2001..... 156

Figure D.1: Mean daily cycle in air temperature from 27.3. – 5.4. 2004 measured at the EBS and at the RBS, and from 12.2. – 21.2. measured at the EBS and AWS. The lower graphs show the mean difference in the daily cycle between EBS and RBS and EBS and AWS, respectively. 158

Figure E.1: Predicted change in direct runoff from precipitation (delta Qn) for five differently glacierised catchments in the Cordillera Blanca in 2050 and 2080. For detailed information see chapter 5.3. 159

Figure E.2: predicted change in the amount of glacier melt (delta Qg) for five differently glacierised catchments in the Cordillera Blanca in 2050 and 2080. For detailed information see chapter 5.3. 160

Figure E.3: Predicted change in total runoff (delta QT) for five differently glacierised catchments in the Cordillera Blanca in 2050 and 2080. For detailed information see chapter 5.3. 160
Figure F.1: Monthly daily cycle of wind speed. 162
Figure F.2: Monthly daily cycle of air temperature. 163
Figure F.3: Monthly daily cycle of air humidity. 163
Figure F.4: Monthly daily cycle of vapour pressure (e). 164
Figure F.5: Monthly daily cycle of albedo. 164
Figure F.6: Monthly daily cycle of SW_{in}. 165
Figure F.7: Monthly daily cycle of SW_{out}. 165
Figure F.8: Monthly daily cycle of LW_{in}. 166
Figure F.9: Monthly daily cycle of LW_{out}. 166
Figure F.10: Monthly daily cycle of sensible heat flux (H). 167
Figure F.11: Monthly daily cycle of latent heat flux (LE). 167
Figure F.12: Monthly daily cycle of SW_{net}. 168
Figure F.13: Monthly daily cycle of LW_{net}. 168
Figure F.14: Daily mean values of wind speed, air temperature and vapour pressure each month. 169
Figure F.15: Daily mean values of SW_{net}, LW_{net} and total net radiation each month. 169
Figure F.16: Runoff and delayed glacier melt with ks=7 and ks=55 (P2: day 158 – 209). 172
Figure F.17: Runoff and delayed glacier melt with ks=7 and ks=55 (P3: day 245 – 311). 173
Figure F.18: Runoff and delayed glacier melt with ks=7 and ks=103 (P4: day 346 – 58). 173

List of Tables

Table 2.1: Runoff stations in the Cordillera Blanca and some key values for the catchments. The glacier extent is taken from surveys in 1990. ..... *14*

Table 2.2: Glaciological observations in the Cordillera Blanca, Perú. The altitude range refers to the lowest and highest point of mass balance measurements, respectively. *22*

Table 2.3: Equipment of the individual automatic stations that collect data in the Cordillera Blanca. SWin, SWout, LWin, and LWout are the shortwave and longwave radiation fluxes, respectively. Air temperature and relative air humidity sensors at the AWS were replaced in July 2004 (second line).The accuracy is given according to manufacturers. *26*

Table 3.1: Frequency of months with different precipitation amounts and air temperature means at the 500 hPa level 1949 – 2004 and for the periods before and after 1977. ..... *30*

Table 3.2: Long term (1949 – 2004) mean annual precipitation sums (P) and air temperature (T_a) and their deviation for the period before and after 1977 and for each decade separately. Precipitation is measured at station Parón (4200 m a.s.l.), air temperature is the NCEP-NCAR Reanalysis data set from the 500 hPa level. . *31*

Table 3.3: Glacier extents in the Cordillera Blanca during the 20th century (glacier area from Georges (2004, 2005)). The reduction in glacier area (ΔA_G) is calculated with respect to the 1990 glacier extent (100 %). *32*

Table 4.1: Value ranges as measured for different variables and model input for monthly application as rounded from the measured ranges. *45*

Table 5.1: Input variables and model parameters for the ITGG-2.0-R model to obtain best fit between measured and modelled runoff. *61*

Table 5.2: Monthly and seasonal coefficients of determination between modelled and measured runoff. 66

Table 5.3: The immediate and long term change in mean annual glacier melt (q_G) for a change in air temperature (T_a) and precipitation (P). ΔA_G is the change in the glacier area for a new steady-state glacier extent. 71

Table 5.4: Predicted mean annual change in air temperature Δ Ta and precipitation Δ P (sea level) for two IPCC climate change scenarios (b1-low, a2-high) with respect to the mean conditions from 1961−1990 (IPCC, 2001; Hulme and Sheard, 1999). Values are taken as a mean from the four GCM grid points surrounding the Cordillera Blanca..... 73

Table 5.5: Modeled mean specific mass balance for the mean climate conditions from 1961 – 1990 ($\overline{B}$ 1961 – 1990) and the required change in air temperature (ΔT_a) or precipitation (Δ P) to reach steady-state glacier extents with the 1990 glacier area extent in the individual catchments..... 74

Table 5.6: Change in annual total runoff q_T, glacier melt q_G, and direct runoff q_N for a new steady-state glacier extent for two IPCC climate change scenarios for the individual catchments as predicted for the years 2050 and 2080. A_G is the change in the glacier area relative to the steady-state glacier extent for mean climate conditions from 1961 – 1990. The catchments are listed from a high to low ratio of glacier area/total catchment. 77

Table 5.7: Statistical mean, median (50%), standard deviation (σ), minimum and maximum, and lower and upper quartile (25 and 75 %, respectively) of measured wind speed, air temperature, and vapour pressure at the tongue of Glacier Artesonraju (4850 m a.s.l.) from April 1st 2004 to March 31st 2005. First line: hourly measurements; second line: daily means..... 82

Table 5.8: Statistical mean, median (50%), standard deviation (σ), lower and upper quartile (25 and 75 %, respectively), and minimum and maximum of the energy fluxes at the tongue of Glacier Artesonraju (4850 m a.s.l.) from April 1st 2004 to March 31st 2005. First line: hourly values; second line: daily means..... 88

Table 5.9: Mean monthly, seasonal and annual energy fluxes by shortwave and longwave net radiation (SW_{net}, LW_{net}) and the turbulent fluxes (H and LE). Albedo

is derived from the ratio of SW_{in} and SW_{out}. The amount of melt (m) and sublimation (s) is calculated from the EB from station Artesonraju (4850 m a.s.l.) and calculated as monthly and annual sums, and seasonal mean monthly sum, respectively. The core dry and wet seasons are defined from June to August and from January to March, respectively. 95

Table C.1: Field visits in the Cordillera Blanca during the two FWF projects P13567-GEO and P13116-N06 134

Table C.2: Automatic stations in the Cordillera Blanca during the two FWF projects P13567-GEO and P13116-N06 134

Table C.3: Seasonal and annual stake movements obtained from DGPS measurements on Glacier Chinchey from October 1999 to November 2001. 137

Table C.4: Seasonal net mass balance on Glacier Chinchey from October 1999 to November 2000. 138

Table C.5: Seasonal and annual stake movements obtained from GPS measurements and stake ablation on Glacier Vallunaraju from May 2000 to May 2001..... 140

Table C.6: Seasonal stake ablation measured at Glacier Shallap at 4800, 4850 and 4900 m a.s.l. 142

Table C.7: Daily sublimation as measured during field trips in July and November 2004 and in August 2005. Measurements were made at 10 a.m. each day. 145

Table E.1: Predicted seasonal change in total runoff (q_T), direct runoff (q_N), and runoff from glacier melt (q_G) for the core wet and the core dry season in 2050 and 2080. The catchments are listed with decreasing percentage of glacier area from top to bottom. For more detail see chapter 5.3. The core wet season is from January to March, the dry season from June to August..... 161

Table F.1: Mean monthly (April 2004 to March 2005) and seasonal climate variables measured at the EBS on Glacier Artesonraju (4850 m a.s.l.). The dry season is defined from June to August, the wet season from January to March. 170

Table F.2: Mean monthly (April 2004 to March 2005) and seasonal radiation fluxes measured at the EBS on Glacier Artesonraju (4850 m a.s.l.). Resulting energy available for melt Q_M is derived from the energy balance calculation (see chapter 4.4). The dry season is defined from June to August, the wet season from January to March. 171

Preface

A research nightmare…

The time in which scientists risked their life in order to obtain scientific data and increase humanity's knowledge about nature and its laws may long be over. Yet, nature's unpredictability presents a constant threat to scientists and more than one of them has endangered his or her life in course of his work. Fortunately, one is usually unaware of the possible dangers and can easily ignore any threats nature might present to the innocent scientist. A life-endangering and almost fatal incident in course of my first expedition to Peru in 2001 made me change my notions about the inherent dangers of my work.

From the very beginning on the Cordillera Blanca glacier mass balance project had been under an unlucky star. Two sites had been chosen for glacier mass balance and climate studies: Glacier Rajupaquinan on the west side and Glacier Chinchey on the east, more humid side. On each site an automatic weather station (*AWS*), several rain gauges and ablation stakes were installed in 1999. The following rains, however, did not provide enough precipitation. Hence, the local people near Glacier Rajupaquinan superstitiously blamed our instruments for the lack of rain and removed them to stow it away in prison where they probably still are. Fortunately, they did not know the exact position of our *AWS* and therefore it was safe. As a consequence, the expedition leader Georg Kaser decided to give up the site and recoved the *AWS* at the dead of night. A new site had to be found in order to continue collecting data on the west side of the Cordillera Blanca. This new site was Glacier Vallunaraju, which would become the place of disastrous events two years later.

Bad weather conditions did not improve over the following two years. Despite their best efforts, Georg Kaser and his team were unable to gather full mass balance measurements. Heavy snowfall and the dreaded crevasses even prevented the team from getting to the accumulation area. Once again a new site had to be found in order to continue observations. This was the state of affairs when I joined the Cordillera Blanca glacier mass balance project in autumn 2001.

My first trip to Peru was scheduled for October 16th , 2001. Bad luck persisted. My plane from Innsbruck to Lima had to return to the airport soon after takeoff due to technical problems. My flight was cancelled and I had to make arrangements to get to Peru via Amsterdam one day later. After a week of preparation in Huaraz we successfully built a runoff gauge below Glacier Chinchey, which should provide the basis for my thesis. Additional preparatory work on Glacier Shallap convinced us that we had finally discovered the right place to do our long-due mass balance measurements. We planed to return to Shallap after our field trip to Vallunaraju.

The field trip to Vallunaraju started on November 15th, 2001. Our team consisted of my supervisor, Georg Kaser, a glaciologist from the local institution of INRENA, Jesus Gomez, a cook, Uldarico Oropezo, a porter, Hector Oropezo and me. Like so many times before tents were put up on the dam of Lake Mullaca at an altitude of 4600 m a.s.l. Since the surrounding terrain was very rough, rocky and prone to falling rocks we considered the even concrete dam a perfectly safe place. The unforeseen incident took place in the night of November 17th.

The night was exceptionally clear and chilly with a beautiful, starlit sky. An almost full moon provided some pale light. I tend to sleep quite well even at high altitudes, which I usually consider quite an advantage. But this night this advantage almost proved disastrous. A low, rumbling noise woke me up. I heard my colleagues shout my name. Without wasting any time to unzip my sleeping bag I opened my tent. The sight that met my eyes was incredibly shocking: a wave of about one to two meters height was towering above the edge of the dam and was approaching quickly.

Despite the desperate efforts of my colleagues I did not manage to get out of the tent to safety in time. The wave hit me like a solid object and took me with it. I was swept along in the tidal wave, felling utterly helpless and being unable to control my movements in the torrent. Every now and then I caught sight of the lights of the settlements down in the valley and I was tormented by the thought that the tidal wave would hit the settlements without warning. I was still being hurled around in the waters and had great difficulty breathing. After what seemed like an eternity I had no longer the perception of movement, although my breathing was still laboured.

The dining tent that had been swept along with the tidal wave was hanging on a rock and I was caught in the ropes of the tent. I managed to climb up the rock to find myself surrounded by the torrent. For a long time I was fully occupied with trying to calm down my breathing, unable to do anything else. The water level had not fallen significantly and was still irregular and I was afraid of being hit by another tidal wave. Since I was sure my team colleagues were either seriously injured or even dead I tried to get away from the rock on my own. Just when I had given up all hope and was overcome with fear I saw tiny dots of light coming down the hill and heard my

colleagues shouting my name. With numb fingers I tried to switch on the lamp that miraculously was still on my head. I did not succeed but still they became aware of my presence. It took some time to find a way to cross the torrent and rescue me from the rock. Finally, Hector managed to cross the torrent by risking his own life.

Our camp had totally vanished except my tent. Georg had salvaged an air mattress and the badly damaged tent, which was everything we had to bring us through the night. After a while Hector went down to the valley to get help. The rest of us spent a terrible night in the open air with only little to protect us from the cold and dull the pain we were in. I was terribly afraid of frostbite since I had trouble with my blood circulation. In the first daylight Uldarico thoroughly searched of the river and was able to recover our medical supplies. At about 9 a.m. we began our descent to the valley, I being carried in turns by Uldarico and Jesus. Georg had lost his shoes and hat to walk on bare feet. The path had been washed away which made the decent a most dangerous and horrifying experience. Twice we had to cross the river whose water levels were still exceptionally high. Halfway down we met the search team led by Hector that had set out to rescue us. More than 18 hours after the tidal wave had washed away our camp we reached the hospital in Huaraz where we received medical treatment. I had suffered a cut on my right knee, my left upper arm had almost been pierced by a tent pole and I had contusions all over my body. A day later the doctors discovered that I had a fracture at my eighth vertebra. Although I could have been injured far worse, it took me about two months to recover.

From a personal point of view such a near-death experience of course had the deepest impact imaginable. But from a scientific point of view the facts about the tidal wave are most impressive, too. At bout 1:30 a.m. on November 18th, a part of Vallunaraju's mountain top broke off, resulting in a gigantic rock- and ice-slide. Scientists form INREANA estimated the amount of rock and ice at 25 000 m³. The material hit the glacier, leading to an enormous avalanche of ice. Over a length of I km and to a breadth of 200 to 400 m the glacier was eroded to its bed by the sheer force of the impact. Taken all in all about 10 million m³ of rock, ice and snow moved downhill with an incredible average speed of 60 m/s. The material completely filled up a lake at the base of the glacier, edging out the water and sending the water and the remaining material down to the two larger lakes. 70 % of the material landed in the southern Lake Mullaca where our camp was located. The first wave made the lake slop over; the second one flooded the dam. Fortunately, the dam had been build with special safety constructions in 1953, in course of which its waterline was lowered by four meters. Otherwise the moraine dam probably would not have been able to resist the enormous water masses and would have broken. As a result, a huge area would have been flooded, the tidal wave killing dozens of people.

In July 2002, I returned to Huaraz. Our team had already decided to abandon mass balance measurements at Glacier Vallunaraju in favour of Shallap. However, our *AWS* was still on the ridge of Vallunaraju at an altitude of 5000 m a.s.l. Imagine our surprise when – after a four-hour ascent – none of our instruments were to be found. Luckily an old man whom we met on the way down was able to give us crucial information about the thief and his address. After long dreadful hours at the police office in Huaraz we got our equipment back, but data of almost a year were irretrievably lost. In July 2003, we had to abandon our plans to erect a runoff station at the outlet of Lake Shallap because of the construction of a hydroelectric power plant at the lake. The runoff station at Chinchey, whose data was intended as the basis for my thesis, was stolen in March 2004.

After all this bad luck and futile efforts we decided to join our efforts with the French scientists of IRD and concentrate most of our field work on Glacier Artesonraju where they already run a runoff station at Lake Artesoncocha since April 2000. Fortunately, Dr. Bernard Pouyaud consent to share his data with our team. This, after all, provided enough data to allow me to continue the research for my PHD.

English text by Iris Schmied

Top of Nevado Vallunaraju (5686 m a.s.l.) before (left) and after (right) the demolition on November 18th 2001. Photos are taken by Georg Kaser and Nelson Santillan in 2000 and 2001, respectively.

Many thanks to all the people that supported my work either in the field or with helpful discussions and ideas...

Thanks especially to

Alcides Ames and family

Bernd Öggl

Bernard Pouyaud

Christian Georges

Georg Kaser

Gernot Groder

Hector Oropeza

Jesus Gomez

Lisette Klok

Marco Zapato

Martin Hölzli

Michael Winkler

Nicolas Cullen

Norbert Span

Patrick Wagnon

Thomas Mölg

And also to many others like the Peruvian Glaciologists, Porters, Drivers, Cook, the Technicians from the Meteorological Institute of Innsbruck, my friends and my family …

The financial background for my work was guaranteed within the frame of two scientific projects (P136567-GEO and P16113-N06) supported by the Austrian Science foundation FWF.

Abstract

The Cordillera Blanca, Perú, is the most intensively glacierised tropical high mountain range with a glacier area of 618 km² in 1990. Its regional climate shows only minor variability in air temperature but high differences in moisture content of the atmosphere during the year, with a core wet (January – March) and dry season (June – August). In the dry season, runoff in the intensively populated Rio Santa valley mainly originates from water due to glacier melt. To model runoff, it is thus necessary to study and understand the processes that drive glacier mass balance in this tropical climate setting.

To model the glacier mass balance of five catchments in the Cordillera Blanca over 1953 – 1994, two models are applied: one based on the hydrological balance, and a vertical mass balance profile model (ITGG-2.0). A comparison of simulated mass balance fluctuations with measurements of terminus positions in the Cordillera Blanca shows good agreement. The general trend of retreat is interrupted by a series of positive mass balances in 1970 – 1975 and in the 1980s. Associated advances of the glacier terminus occur with a time delay of 3 – 5 years.

To model total runoff in the catchments, runoff from glacier melt is obtained from the ITGG-2.0 model and added to direct runoff from precipitation. The reconstruction of monthly mean runoff 1953 – 1997 in a highly glacierised catchment agrees well with measured total runoff. To predict the change in total runoff in 2050 and 2080 from climate change scenarios, it is assumed that the glaciers' extents will be in balance with the respective climate. The change in the seasonal cycle of total runoff is highest in catchments with high portion of glacier area and decreases with the percentage of glacierisation. In 2080 it has to be expected that total runoff in the catchment of Parón (highest glacierisation: 41 %) increases by 18 – 42 % in the core wet season and decrease by 20 – 28 % in the core dry season. Such a situation in the dry season indicates a sharp contrast between the steadily increasing water demand, and actual water availability.

The energy and mass fluxes at the glacier-atmosphere interface provide the key to the physical processes that determine mass balance. Thus they are studied in detail in the finalizing part of this thesis, to detect potential future improvements for

parameterisations in the current ITGG-2.0 model. Data are obtained from an energy balance (*EB*) station (March 2004 to April 2005) installed in the ablation are of Glacier Artesonraju (4850 m a.s.l.). During the dry season the amount of energy that is available for melting is significantly reduced compared to the wet season. This is due to reduced energy from several components of the *EB*: (i) high albedo which decreases net shortwave radiation, (ii) reduced incoming longwave radiation due to low atmospheric moisture content that decreases atmospheric emissivity, and (iii) enhanced latent heat loss due to high gradients in vapour pressure between the atmosphere and the glacier surface and high wind speeds that force the turbulent exchange. The hourly variability of total runoff measured at the outlet of Lake Artesoncocha (4200 m a.s.l.) could best be simulated by applying a linear reservoir model with a storage parameter of 55 hours in the wet season and 103 hours in the dry and intermediate season. With this approach, 73 % of the daily variability in total runoff can be explained by runoff variability from glacier melt. The amount of glacier melt in the altitude band of the station (4825 – 4875 m a.s.l.; 5 % of total glacier area) accounts for 13.2 % of total runoff during the wet, and for 21.5 % of total runoff during the dry season.

For upcoming versions of the ITGG-2.0 model, it is proposed to consider that

- albedo increases under very dry conditions;
- the surface temperature is frequently below zero in the dry season and thus melting is reduced; and
- sublimation in the dry season is lower than expected.

For runoff modelling it is also suggested to change the delay in runoff from melt water in the firn area which is higher during the dry than during the wet season.

1. Introduction

1.1 Investigation area

The investigation area for this thesis is the tropical Cordillera Blanca in Perú (8°30'−10°10'S). This high alpine mountain ridge stretches 180 km from NNW to SSE as part of the South American Andes. The longitudinal extent of the mountain is only 30 km (77°8'−78° W). 27 peaks reach elevations above 6000 m a.s.l., the top of Nevado Huascáran Sur (6.768 m a.s.l.) is the highest peak in Perú (Figure 1.1). The highly glacierised mountain range harbours 25 % of all tropical glaciers with respect to surface area (Kaser and Osmaston, 2002). The Cordillera Blanca is part of the continental water divide and drains on its eastern side into the Rio Marañon to the Atlantic and at the western side into the Rio Santa to the Pacific. The population in the Callejon the Huaylas (valley of Rio Santa) but also in the coastal region has markedly increased during the last decades. E. g., the population of the respective political district of Ancash has increased from 726 215 in 1972 to 1,067 282 in 2000, the city of Huaraz has grown from 85 063 to 144 894 inhabitants during the same time period (Instituto Nacional de Estadistica e Informatica, Perú). In addition, human activities and lifestyle have changed dramatically towards an increasing consumption of energy and fresh water. Intensified and modernised agriculture, the recently intensified mining activities, and the "westernizing" of their live style not only consume a high amount of water but also pollute it. The problem is, as a matter of course, particularly obvious during the dry season and the still ongoing change of society from a traditional subsistence structure to a profit orientated and consuming one will aggravate the already arising conflicts. Yet, only very little work has been dedicated so far to the hydrology of glaciated tropical catchment areas (Fliri, 1968; Ribstein et al., 1995; Tamayo, 1996; Schuler, 1997; Wagnon et al., 1999b; Kaser and Osmaston, 2002; Sicart, 2002; Kaser et al., 2003; Juen et al., 2006).

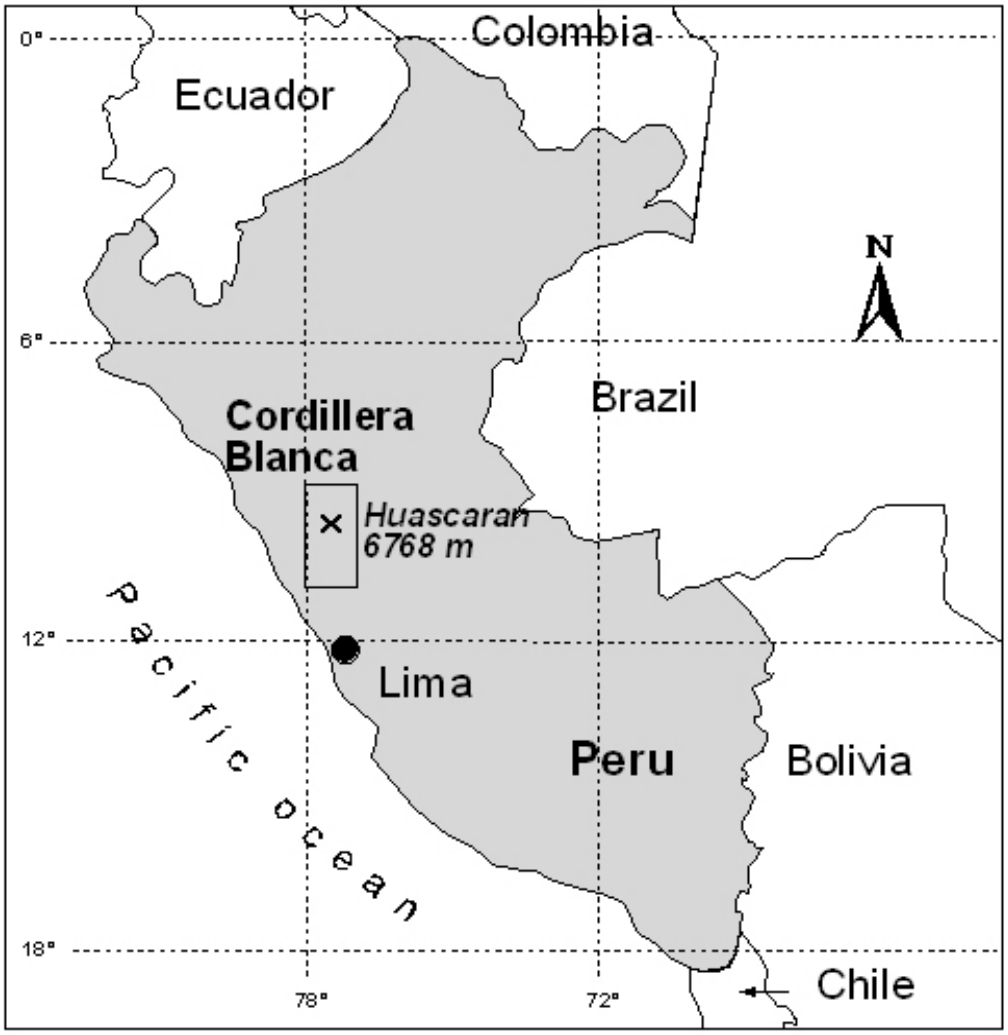

Figure 1.1: Location of the Cordillera Blanca, Perú.

The tropical atmosphere, in general, is characterised by homogeneous thermal conditions with very small annual variations in air temperature. Figure 1.2 shows these variations at low latitude and high elevation stations in South America, Africa, and Irian Jaya. A high altitude station in the Cordillera Blanca at 3980 m a.s.l. (indicated with a circle in Figure 1.2) shows a particularly small annual variation of only 0.8°C. In contrast, the seasonal variations of all humidity related variables such as cloudiness and precipitation is high. They are governed by the oscillation of the Inter Tropical Convergence Zone (ITCZ) which approaches the Cordillera Blanca from East between October and April (Kaser et al., 1990) when about 70 to 80% of the annual precipitation fall. From May to September, in turn, the ITCZ is far north and a trade wind system causes dry conditions. Thus, this *outer tropical climate regime* switches between a tropical and a subtropical one. The shape and setting make the Cordillera Blanca a pronounced barrier to the easterly dominated

atmospheric currents and separate the dry Pacific side from the humid Amazon side. Marked windward and lee-side effects are the result (Kinzl, 1942; Fliri, 1968). Thus, pronounced seasonal changes and spatial gradients have to be expected in air humidity and all related variables.

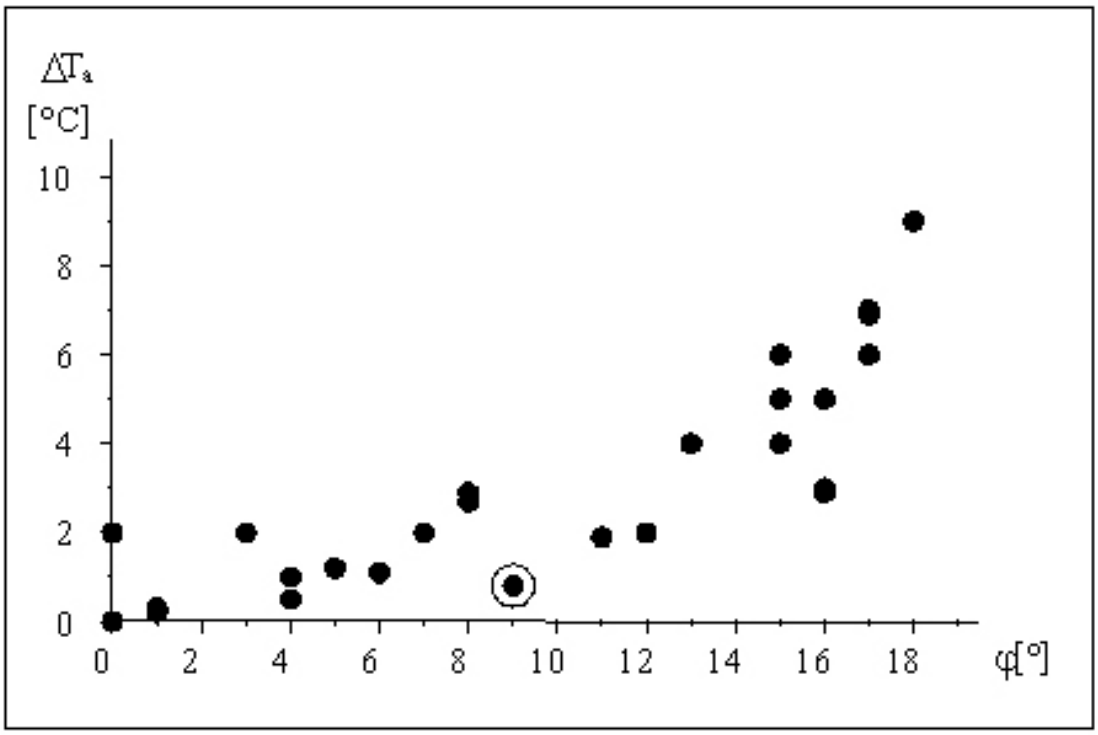

Figure 1.2: Annual variation of air temperature ΔT_a (°C) as calculated from the monthly means depending on geographical latitude (φ). Data are from high elevation stations in South America, Africa and Irian Jaya (after Kaser and Osmaston, 2002). The station Quererococha in the Cordillera Blanca is marked with a circle.

The glacier regimes under tropical conditions have been discussed intensively by Lliboutry et al. (1977), Ageta and Higuchi (1984), Hastenrath (1984), Francou et al. (1995), Kaser (1995), Kaser et al. (1996b), Kaser and Georges (1999), Wagnon et al. (1999a), Kaser (2001), Kaser and Osmaston (2002), Wagnon et al. (2001). The dominant effect on glaciers is the missing thermal seasonality. Accordingly, ablation occurs all year round although sublimation reduces the rates during dry seasons to some extent. Accumulation, in turn, occurs basically on the higher portions of the glaciers and mainly during the wet season. These conditions lead to a very particular distribution of mass balance with altitude (Kaser, 2001), but also causes problems in measuring the glacier mass balance which is the crucial term for understanding the glacier climate interaction (Kaser and Georges, 1999; Kaser and Osmaston, 2002). The difficulties are due to the isothermal structure of the snow cover which, in addition to daily melting on the surface up to high elevations, prevents from any

layering. Consequently, impermeable ice layers, dust layers, and density changes in the snow pack are usually missing. Because of geological and tectonic circumstances, glaciers in the Cordillera Blanca are very steep and, consequently, rather shallow and crevassed which increases the difficulties of in situ measurements. Thus, mass balance studies on tropical glaciers are rare and only one long term series has been maintained on Lewis Glacier, Mt. Kenya (Hastenrath, 1984, 1991). Short period field studies have been performed on glaciers of the Ruwenzori massif (Bergstrøm, 1955; Whittow et al., 1963), Kilimanjaro (Mölg and Hardy, 2004), and Irian Jaya (Hope et al., 1976). On Glacier Zongo and Glacier Chacaltaya in the Cordillera Real (Bolivia), mass balance programs have been maintained since 1991 (Francou et al., 1995, Pouyaud et al. 1995; Ramirez et al. 2001, Wagnon et al. 2001). In the Cordillera Blanca the mass balance was measured in the ablation zone of two glaciers since the 1970s until the mid 1990s (Ames 1985, Kaser et al., 1990).

1.2 Objectives

During the last decades glaciers all over the world have retreated (e.g. Hastenrath and Kruss, 1992; Peterson and Peterson, 1997; Kaser, 1999; Oerlemans, 2000; Oerlemans, 2001; Ramírez et al., 2001; Reynolds and Young, 1997). The reduction in volume and glacier area changes both the intensity of runoff seasons and the inter-annual variation (e.g. Braun et al., 2000; Jansson et al., 2003). Thus, the knowledge about the influence of a changing climate on glacier runoff is of great importance for regional water supplies all over the world, as widely discussed for alpine regions (e.g. Collins, 1987; Collins, 1989; Chen and Ohmura, 1990; Braun et al., 2000), as well as on a global scale (e.g. Gleick, 1987; McMahon et al., 1987; Arnell, 1996). In order to understand, analyse and predict glacier runoff, a variety of models has been developed for catchments in the mid and high latitudes (as e.g. summarised in Hock, 1998 and 2003). Sophisticated energy balance models (e.g. Arnold et al., 1996; Sicart, 2002) need a considerable amount of measured data with high temporal resolution (e.g. hours), which are usually only available for short experimental periods. Thus, statistical temperature-index-models, with air temperature as only input, are widely used. The high correlation between the sum of positive degree days and melt rates (e.g. Hock, 1998; Hock, 1999; Braithwaite and Zhang, 2000; Oerlemans and Reichert, 2000) makes these models very successful for the mid and high latitudes (Ohmura, 2001), where temperature governs seasonality.

Contrary to the mid- and high-latitudes, low-latitude climate is characterised by a pronounced variation in atmospheric moisture content and related variables, whereas the thermal variation is minor (Hastenrath, 1991; Kaser, 2001; Kaser and Osmaston, 2002). Especially for the tropical South American Andes, where runoff during the dry season (May – September) can originate up to100 % from glacier melt (Mark and Seltzer, 2003), the retreat of glaciers can lead to a considerable seasonal water shortage. Nevertheless, knowledge on runoff from glacierised catchments in the tropical Andes is still limited (Fliri, 1968; Francou et al., 1995; Ribstein et al., 1995; Tamayo, 1996; Schuler, 1997; Wagnon et al., 1999b; Sicart, 2002; Kaser et al., 2003). Ribstein et al. (1995) found a rather good correlation between runoff from Glacier Zongo (16°S, Bolivia) and the duration of air temperature above 3 °C combined with incident solar radiation, both recorded at a nearby station. Still, energy balance investigations at the same site demonstrate the high importance of sublimation (Wagnon et al., 1999a), net longwave radiation, and albedo (Francou et

al., 2003) for ablation. They are all directly related to air humidity and atmospheric moisture content. In the tropical Cordillera Blanca (app. 8 – 10 °S), the correlation between monthly mean air temperature and runoff is very poor (r^2=< 0.2) and, thus, temperature-index models are not expected to reproduce the seasonality of runoff.

Therefore, suitable mass balance models have to be found for the particular tropical climate conditions in order to model glacier mass balance and glacier melt for runoff simulations. Detailed studies on the energy balance on the glacier surface provide more profound knowledge about the relation of melt water production and climate change.

The objectives of this thesis are

- to develop and apply models that are able to represent the glacier mass balance under tropical climate conditions,
- to reconstruct and predict glacier melt and total runoff for different catchments in the Cordillera Blanca, and
- to improve the knowledge about the influence of climate conditions on the amount of glacier melt by studying the energy balance on a tropical glacier surface.

The specific working steps are as follows:

Glacier mass balance is

i) reconstructed from the hydrological balance (chapter 4.1, 5.1), and
ii) with an extended vertical balance profile model (ITGG-2.0) that was developed especially for tropical climate conditions (chapter 4.2, 5.1);

Runoff is

i) simulated with the ITGG-2.0 model with an additional module to derive direct runoff (chapter 4.3, 5.2),
ii) predicted for different IPCC climate change scenarios in 2050 and 2080 (chapter 5.3), and
iii) compared with glacier melt calculated from the energy balance on a tropical glacier tongue (chapter 4.4, 5.4).

1.3 Structure of the Thesis

The development and application of mass balance reconstructions from the hydrological balance is published in the Journal of Hydrology (Kaser et al., 2003). A paper where runoff simulation and prediction with the ITGG-2.0-R model is performed for a 31 % glacierised catchment is in accepted for Global and Planetary Change and already in press (Juen et al., 2006). All other parts are not published yet but have been presented at international scientific conferences (see Publications). Results from the analyses of the energy balance on the surface of Glacier Artesonraju are in preparation for publication.

Chapter 2 gives an overview of the study sites and available data. The data used for this thesis, i.e. a digital elevation model and the 1990 glacier extent (chapter 2.1), long-term climate records (chapter 2.2), glaciological records (chapter 2.3), as well as high resolution data from automatic stations in the Cordillera Blanca (chapter 2.4) are presented in this chapter.

In chapter 3 the climate conditions in the Cordillera Blanca during the 2nd half of the 20th century are reviewed. After a description of the long term trends in precipitation and air temperature (chapter 3.1) glacier extents and terminus changes are discussed (chapter 3.2).

The methods that are used for this thesis are object of chapter 4. To derive the mass balance from the hydrological balance (4.1) the runoff characteristic in the Cordillera Blanca is analysed for differently glacierised catchments first (chapter 4.1.1). The calculation of mass balance from the hydrological balance (MBH) is then described in chapter 4.1.2. Next, an extended vertical mass balance profile model (ITGG-2.0, chapter 4.2) is introduced. To simulate runoff for glacierised catchments a feature to derive direct runoff was added to the ITGG-2.0 model which is described in chapter 4.3. The methods of calculating the energy balance on the glacier surface and its validation are thoroughly described in this chapter 4.4.

The results of all investigations made for this thesis are presented and discussed in chapter 5. First, the two reconstructed glacier mass balances from the hydrological balance (MBH) and the glacier mass balance model ITGG-2.0 are compared to each other. Additionally, reconstructed mean cumulative mass balances for the two

different model runs are compared to available measurements of the terminus position of three glaciers in the Cordillera Blanca (chapter 5.1). The simulation of runoff from 1953 − 1997 for a highly glacierised catchment is performed in chapter 5.2, which is the base for the following runoff predictions for changing climate conditions (chapter 5.3). With data from an energy balance station installed on a tropical glacier tongue in the Cordillera Blanca the climate conditions of the glacier surface over one year are discussed in detail in chapter 5.4.1. Detailed studies on the energy balance of the glacier surface are discussed in chapter 5.4.2. Finally, resulting runoff from glacier melt is compared to measured total runoff (chapter 5.4.3).

Chapter 6 gives a summary and conclusion of the findings in this thesis.

2. Study sites and available data

2.1 Digital elevation model and glacier extent mappings

For hydrological and glaciological investigations, a digital elevation model (*DEM*) may provide important information for, e.g., dividing watersheds (Appendix B) or projecting satellite images. A *DEM* for the whole Cordillera Blanca (Figure 2.1) was produced using contour lines from the Carta Nacional del Perú from 1987, scale 1:100 000. Equidistance of the contour lines is 50 m, in some small parts it is reduced to 25 m. To cover the whole mountain range the contour lines of five sheets (18 – 20 h; 19 – 20 i) were digitised. Two differently processed *DEM*s were created with 20 m grid resolution using ARC/INFO software, version 7.1. (Georges, 2005) and SURFER, version 6. (Appendix A). For hydrological analyses the *DEM* generated with SURFER was used, the catchments were defined by watershed analyses (Appendix B).

Evaluations on the extent of the glacier area in the Cordillera Blanca exist for 1970, 1990, 1997 and for the southern part also for the year 2002. A rough estimate of the glacier extent for the 1930s (indicated as 1935 glacier extent) is given on the maps Cordillera Blanca (Borchers, 1935a) and Cordillera Blanca – Südteil (Deutscher Alpenverein, 1945). The aerial extent was derived using terrestrial photogrammetry techniques. The northern part dates from 1932 (Borcher, 1935b), the southern part was surveyed in 1939 (Kinzl, 1942; Kinzl, 1949). The 1970 glacier extent was derived from aerial photographs taken in 1970 (Ames et al., 1989) with the objective to establish a first glacier inventory for the whole of Perú. A second inventory was evaluated from satellite images from 1997 (Morales Arnao, 2000). For the 1990 glacier extent two SPOT XS satellite scenes from 1991 (northern part) and 1987 were used (Georges, 2004). The glaciation of the southern part of the Cordillera Blanca in 2002 was mapped from optical satellite data LANDSAT 7 (Georges, 2005).

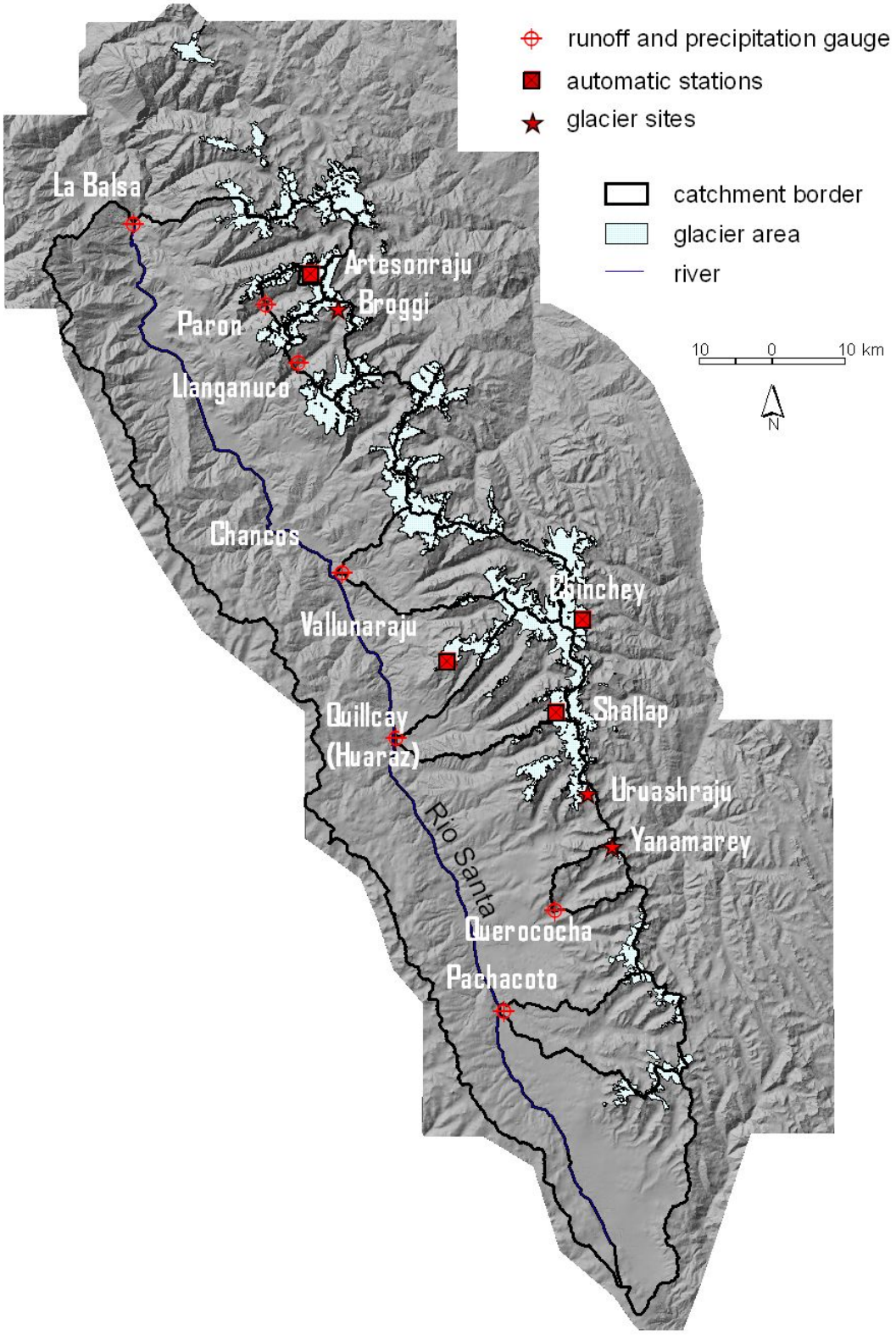

Figure 2.1: Shaded DEM of the Cordillera Blanca, Perú including catchment borders for hydrological investigations, glacier sites referred to in the text and the glacier extent in 1990.

Due to the differences in the data base and aim of the respective evaluation of glacier extents the quality of the mapping is not homogenous. E.g. the accuracy of the large scale evaluation of the glacier extents in 1970 and 1997 is not very high. This has been demonstrated for the Huascarán − Chopicalqui massif in the Cordillera Blanca where glaciation was reanalysed in a very detailed way on the basis of the same air photographs as used for the 1970 glacier inventory (Kaser et al., 1996a). A re-evaluation for several mountain groups in the Cordillera Blanca (Georges, 2004) came to a glacier area that is 6 – 9 % smaller than the inventory values. According to point checks (Georges, 2005), the 1997 analysis (Morales Arnao, 2000) is even more vague and the results are highly questionable. The most reliable and accurate evaluation of the glacier extent in the Cordillera Blanca is the 1990 glacier extent which is the base for all investigations in this thesis. A thorough evaluation of the glacier extents during the 20th century is performed by Georges (2004). Additionally, the maximum glacier extent has been approximated from the 1920 moraines (Georges, 2004) which are similar to the Little Ice Age (LIA) moraines in the Cordillera Blanca around 1860 (Kinzl, 1949; Kaser and Osmaston, 2002). The glacier extent in 2002 was evaluated for three mountain groups in the southern part which cover 1/3 of the whole glaciers in the Cordillera Blanca (Georges, 2005).

Catchment areas and their glacierisation

Out of the 10 catchments in the Cordillera Blanca with available runoff data (chapter 2.2.1) the six catchments of Parón, Llanganuco, Chancos, Quillcay, Pachacoto and Querococha (Figure 2.1) are selected for glaciological and hydrological studies. The catchments Recreta, Quitaracsa, Colcas and Los Cedros seem not to be suitable for the studies carried out in this thesis. They are characterised by extended swamps, intense artificial irrigation, or Lake regulation which strongly influences the seasonal pattern in runoff (Kaser et al., 2003). Thus, these catchments are not considered here. The watersheds were defined from the *DEM* (Appendix A and B).

The six selected catchments are very different in sise and altitude range (Figure 2.2, Table 2.1). The catchment of Chancos is the largest (271 km²), reaches down to the lowest point of 2840 m a.s.l. and has the highest range in altitude (3434 m). The highest station is Parón at 4185 m a.s.l., the catchment is the smallest with only 47 km², and glacierisation is highest with 41 %. The catchment with the lowest portion of glacier area is Querococha (66 km², 3.2 %), it only range 1227 m in altitude and ends at 5207 m a.s.l.. The highest point of all catchments is in the area of Llanganuco which contains the second highest peak of the Cordillera Blanca (Huascaran-Norte 6664 m a.s.l.).

Table 2.1: Runoff stations in the Cordillera Blanca and some key values for the catchments. The glacier extent is taken from surveys in 1990.

Station name	Total area [km²]	Altitude from – to [m a.s.l.]	Altitude range [m]	Glacier area [km²]	Glacier terminus [m]	Glacier altitude range [m]	Ratio of glaciation [%]
Parón	47	4185−6112	1927	19,2	4650	1450	40,9
Llanganuco	86	3850−6664	2914	26,8	4550	2100	31
Chancos	271	2840−6274	3434	65,3	4400	1850	24,1
Quillcay	250	3063−6309	3246	43,4	4400	1900	17,4
Pachacoto	210	3760−5688	1928	20,3	4700	950	9,7
Querococha	66	3980−5207	1227	2,1	4650	550	3,2

The glacier extent in Table 2.1 represents the 1990 glacier area as obtained from satellite images around 1990 (Georges, 2004). The glacier terminus in the different catchments reaches down to 4400 – 4700 m a.s.l., the altitude range of the glaciers is 550 – 2100 m (Figure 2.3, Table 2.1). In the catchment of Llanganuco the glaciers reach to the highest point of all catchments (6664 m a.s.l.) and range over 2100 m. The lowest upper limit for the glaciers is in the area of Querococha at 5207 m a.s.l.. The glaciers in the catchment of Pachacoto are spread over an altitude range of 950 m and end at 5688 m a.s.l. The other catchments reach to altitudes above 6100 m a.s.l. and range over 1450 – 1900 m in altitude. The area altitude distribution shows that the main glacier area is found between 4900 and 5300 m a.s.l. (Figure 2.3), which is also the altitude range in which mean *ELA* and mean 0°C−level mainly oscillate. Thus, changes in both the *ELA* and/or the mean 0°C−level always affects huge parts of the glacier area and thus can easily switch positive to negative mass balances and vice versa.

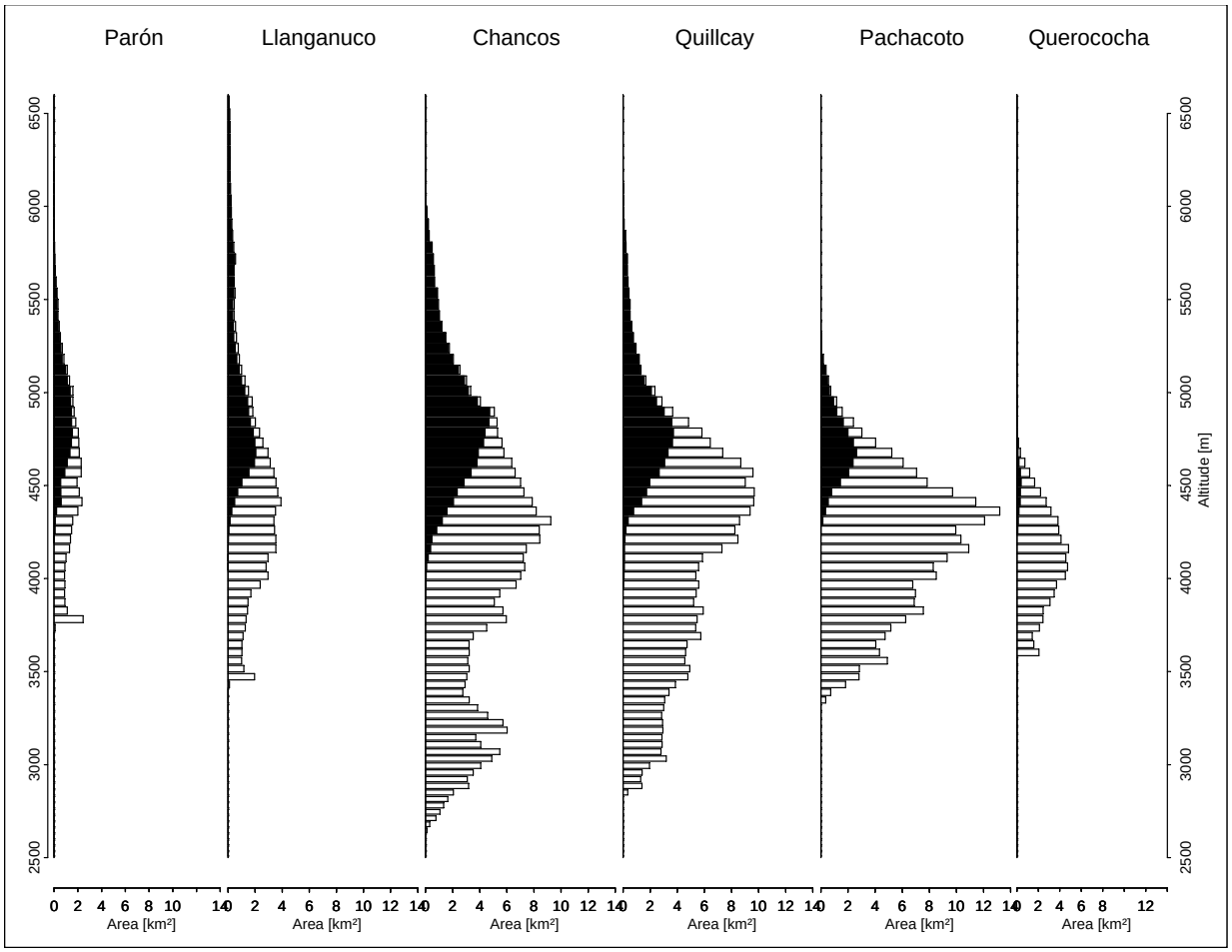

Figure 2.2: Area altitude distribution (50 m altitude steps) of the different catchments including their glacier areas.

Beside the six catchments discussed above predictions of runoff from glacier melt were also made for the whole Rio Santa valley. The hydroelectric power station of La Balsa (Figure 2.1) at the entry to the Canon del Pato collects the water from the whole Callejon de Huaylas. The main river named Rio Santa origins in the Lake Goñococha at 4220 m a.s.l. in the South of the Cordillera Blanca and drains into the Pacific at Chimbote in the North. The Rio Santa catchment reaches from the highest point of the Cordillera Blanca the Nevado Huascarán Sur with 6768 m a.s.l. to the station of La Balsa in the Canon del Pato at 1861 m a.s.l. On the west side of the river the water comes from the glacier free and dry Cordillera Negra. This area makes around one third of the whole catchment of 4870 km². The glaciers are all situated in the west ridge of the Cordillera Blanca and reach from the top of Nevado Huascarán Sur down to almost 4350 m a.s.l. They cover an area of 410 km² which is 8.4 % of the catchment area.

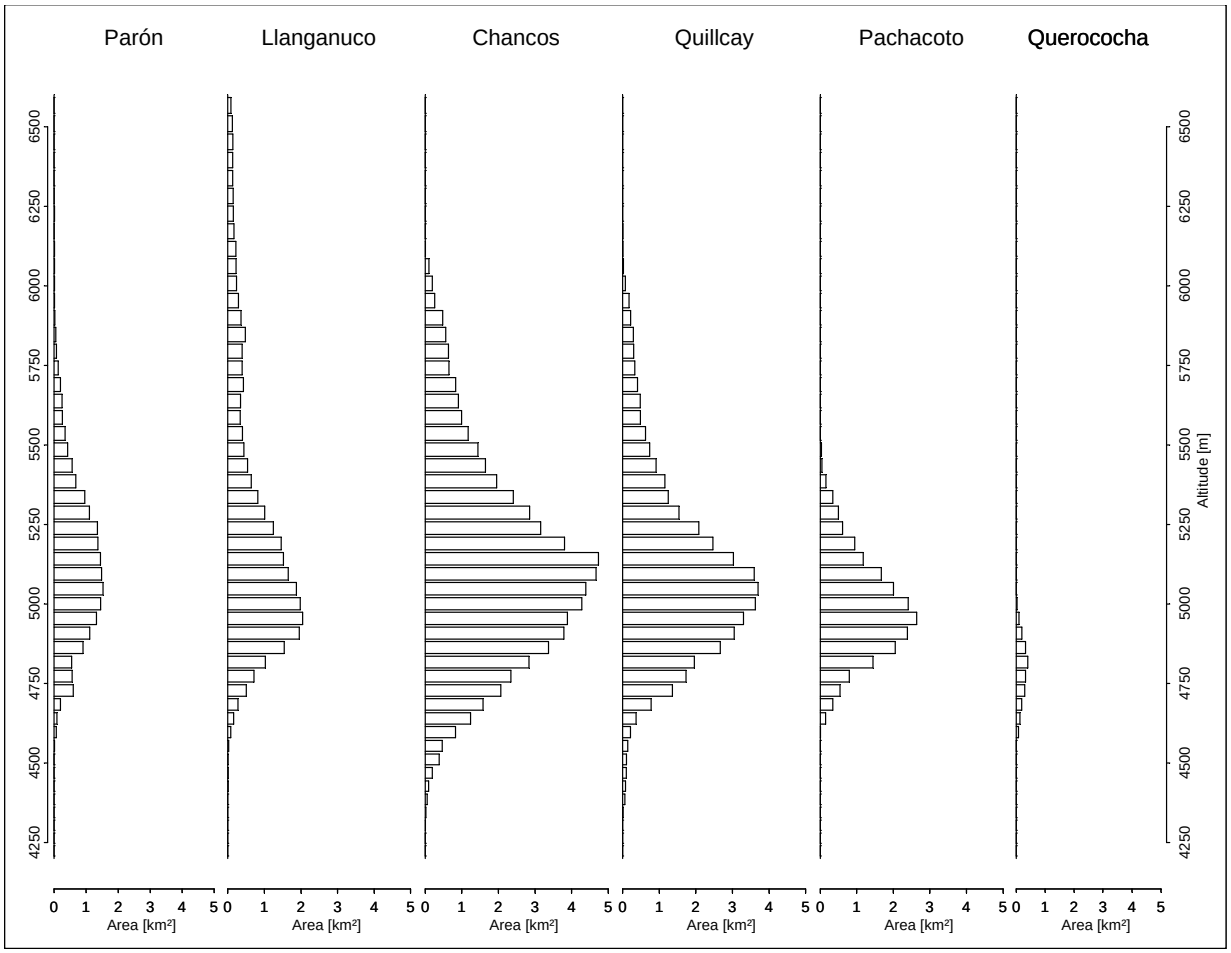

Figure 2.3: Area altitude distribution (50 m altitude steps) of the glacier areas in the different catchments.

Detailed studies on runoff from glacier melt at Glacier Artesonraju and runoff are performed for a sub catchment in the Parón region (Figure 2.1). There, a runoff gauge at Lake Artesoncocha (4200 m a.s.l.) operates since 2000 and measures runoff from the Glacier Artesonraju (see also chapter 2.4). The catchment area is 7.7 km², the glaciers cover an area of 5.7 km² which is 74 % of the total area. The highest point in the catchment is Nevado Artesonraju with 6025 m a.s.l., the glacier reaches down to app. 4750 m a.s.l.. For a detailed map of the catchment see Appendix C, Figure C.6.

2.2 Long term records

2.2.1 Precipitation and runoff records

In the Callejon de Huaylas several series of monthly sums of precipitation and monthly means of runoff are available since 1953, precipitation measurements at the Station of Parón (Figure 2.1) already started in 1949. The data have been collected and have generously been made available by Electroperú S. A. Unfortunately, measurements have been interrupted in 1994 with the privatisation of the respective institutions and most of the stations were abandoned. Runoff records after that are only available for the catchment of Llanganuco (Figure 2.1) until 1997. Some precipitation records could recently be extended until 2000, the station Parón is still operating.

In some cases, the quality of the available data is limited. This is particularly true for the precipitation records and for data after 1994. Although Niedertscheider (1990) has made a basic control, correction, and completion until 1986 and the same has been done for the rest of the data, a thorough proof of some uncertainties cannot be provided since the original sources are not accessible anymore. Still, if the data are used as averages over time and/or space, whenever this is possible, the problem is widely diminished.

Figure 2.4 shows the mean annual cycle of precipitation for all stations available in the Cordillera Blanca. The spatial variety in the total amount of precipitation is rather complex due to orographic effects (Niedertscheider, 1990). Mean annual precipitation amounts vary from exceptional 1520 mm at Safuna (4275 m a.s.l.) to 165 mm at Hidroelectra (1386 m a.s.l., Table 2.2). They are obviously highest along the glacier covered Cordillera Blanca chain whereas the valley floor of the Callejon de Huaylas shows low precipitation amounts particularly in the northern and lower part. This, in turn, is the most extensively used part for agriculture but cannot be cultivated without additional water supply. On the other hand, the pronounced seasonality which is related to the oscillation of the ITCZ is highly uniform over the entire area, which justifies using mean precipitation from several station as representative value for the individual regions.

Table 2.2: All gauging stations in the Cordillera Blanca and the mean of the available precipitation and runoff records from 1953 – 1994, listed from north to south.

Station name	Elevation [m a.s.l.]	Precipitation [mm/a]	Runoff [m³/s]
Huillca	3995	841*	
Hidroelectra	1386	165*	
Quitaracsa	1480		10,9
Los Cedros	1990		3,5
La Balsa	2050		83,6*
Colcas	1880		5,7
Safuna	4275	1520*	
Parón	4185	787	1,9
Caraz	2286	180*	
Llanganuco	3850	629	3,0
Yungay	2535	312*	
Chancos	2840	548	8,2
Huaraz/Quillcay	3063	665	7,3
Cahuish	4550	985	
Querococha	3980	967	1,7
Ticapampa	3480	730*	
Shacaypampa	3600	630*	
Huancapeti	4420	430*	
Pachacoto	3760	581	4,3
Collota	3800	485*	
Recreta	3990	440	2,8
Yanacocha	4460	868*	
Punta Mojon	4390	675*	
Lampes Alto	4030	722	

* one or more years missing.

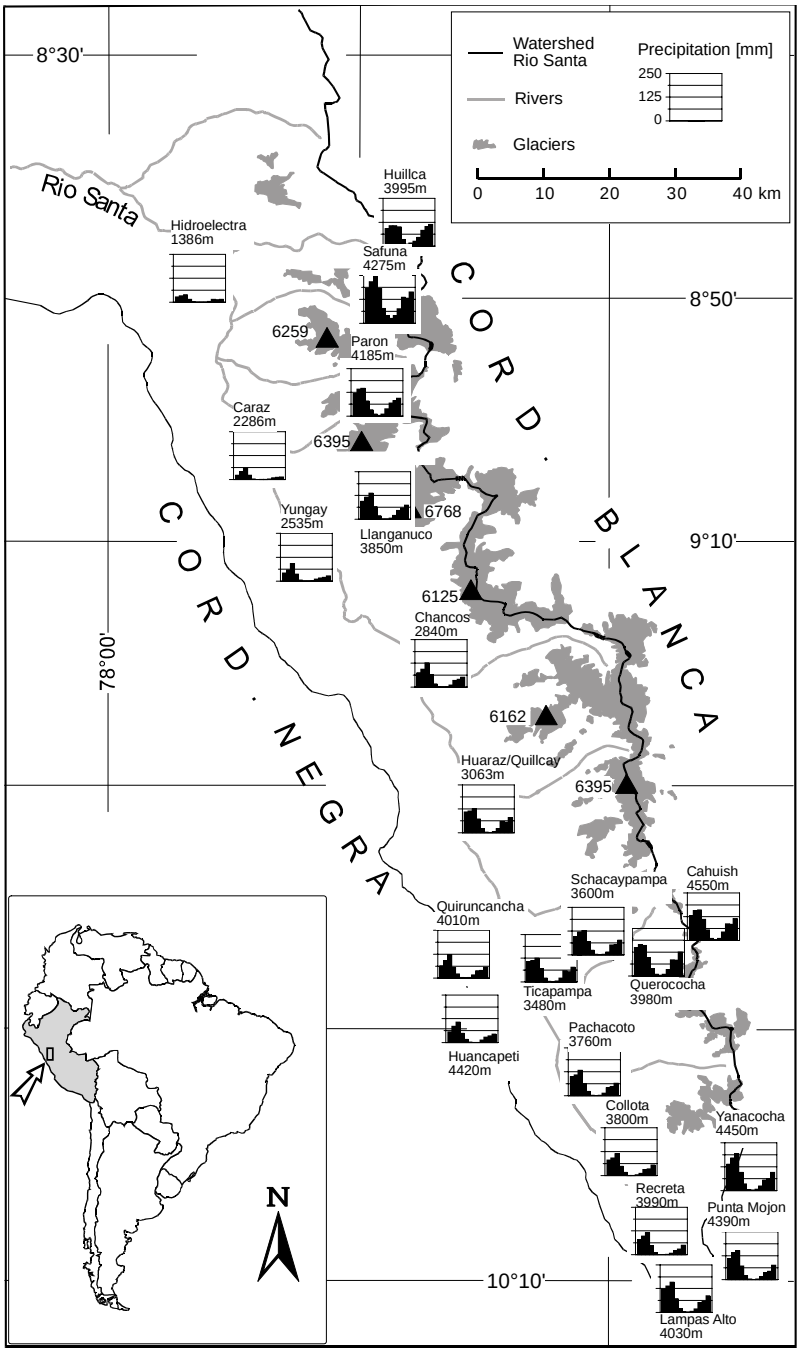

Figure 2.4: Mean seasonal variations of precipitation in the Cordillera Blanca depicted from January to December (after Niedertscheider, 1990).

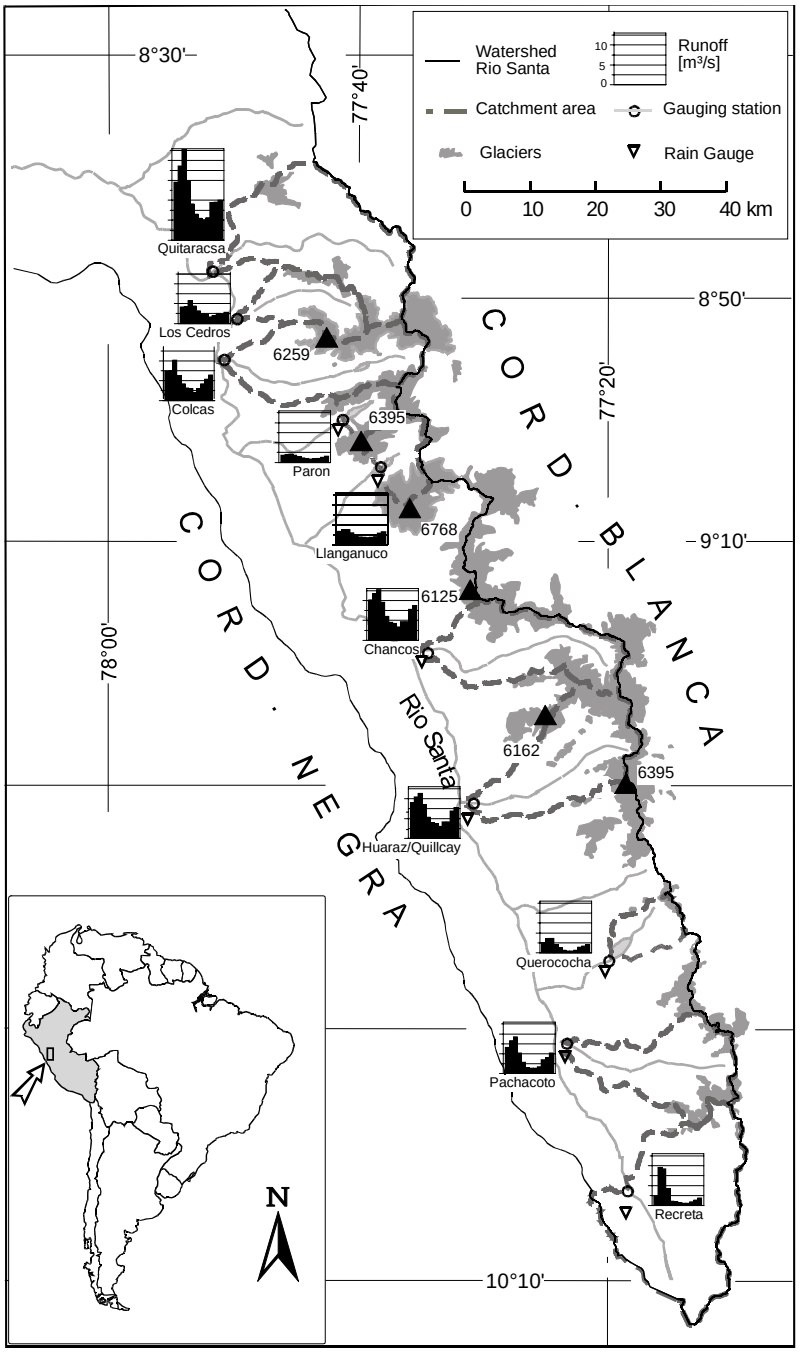

Figure 2.5: Mean seasonal variations of runoff in the Cordillera Blanca depicted from January to December (after Niedertscheider, 1990).

The seasonal variation of the runoff (Figure 2.5) is strongly correlated with the cycle of precipitation with low values during the dry season on a first view. Clear exceptions, however, show the graphs of the catchment areas of Llanganuco and Parón where runoff is rather balanced throughout the year indicating the marked impact of the respective extended glacierisation (see also chapter 4.1.1). The mean annual runoff (Table 2.2) depends on the glacier extent of the respective catchment area, as a matter of course.

2.2.2 Air temperature records

In the Cordillera Blanca only one time series of monthly mean, maximum and minimum air temperature measured at station Querococha at 3980 m a.s.l. exists 1965 – 1994. However, the data of this station are very doubtful and do not cover the whole time period of interest. A continuous record of air temperature from 1949 to 2004 can only be derived from the NCEP-NCAR Reanalysis data set (Kistler et al., 2001). The pronounced spatial thermal homogeneity in the tropics justifies the use of large scaled data to obtain general patterns in air temperature variability. Whenever NCAP−NCAR Reanalysis air temperature is used in this paper it is calculated as a mean over the four surrounding grid points of the Cordillera Blanca (75 and 77.5° W; 7.5 and 10° S). Monthly mean air temperature at 4000 m a.s.l. varies between 6 to 9.5 °C and 5.6 to 9 °C at station Querococha and at the 500 hPa level (calculated with a vertical gradient of air temperature $dT/dz=0.0065$ °C m^{-1} for the period 1965 – 1994), respectively.

2.3 Glaciological records

Since the early 1970s, ablation measurements have been carried out on the Yanamarey and the Uruashraju Glaciers (Figure 2.1, Table 2.2) in the Perúvian Cordillera Blanca (Ames, 1985; Kaser et al., 1990) but repeated attempts to measure the accumulation failed because of the lack of impermeable layers from the previous season. Soot marks set at the end of the previous dry season had disappeared due to continuously percolating melt water (Ames, personal communication). This corresponds with the theoretical framework (Kaser and Osmaston, 2002). The difficulties are due to the isothermal structure of the snow cover which prevents any layering. Consequently, impermeable ice layers, dust layers, and density changes in the snow pack are usually missing. Mass balance measurements during field works from 1999 to 2004 (Appendix C) also failed to obtain data from the accumulation area (Table 2.2). Thus, no full measured mass balance record is available for the Cordillera Blanca so far, only point information from the ablation areas could be obtained (Table 2.2). Still, net balance of glacier Yanamarey could be estimated from volume changes (Hastenrath and Ames, 1995b) for several dates from 1939 – 1988.

Table 2.2: Glaciological observations in the Cordillera Blanca, Perú. The altitude range refers to the lowest and highest point of mass balance measurements, respectively.

Glacier	**Mass balance**	**Altitude range [m]**	**Surface velocity**	**Terminus position**
Yanamarey	1977 – 1988	4600 – 4960	1977 – 1988	1968 – 1994
Uruashraju	1977 – 1987	4610 – 4900	1979 – 1987	1968 – 1994
Broggi				1968 – 1994
Chinchey	1999 – 2000	4780 – 5070	1999 – 2001	2000
Vallunaraju	2000 – 2001	4850 – 5110	2000 – 2001	2000 – 2001
Shallap	2002 – 2004	4780 – 4940		
Artesonraju	2000 − 2004	4750 – 5000		

The change of the terminus position from three small glaciers in the Cordillera Blanca (Table 2.2) was measured every year from the 1960s until 1994 (Ames and Francou, 1995; Ames et al., 1989). From 1999 to 2001 the terminus position of Glacier Vallunaraju and Chinchey (Appendix C) was measured using differential GPS (global position system). Information about former glacier terminus variations was either obtained from map extents or from moraine position.

Detailed studies on the ice flow dynamic have been carried out on glacier Yanamarey (Hastenrath and Ames, 1995a; 1995b) and on glacier Uruashraju (Ames and Hastenrath, 1996) during the 1980s. The surface velocity was obtained from repeated survey of the stake positions. Using the same method, ice velocity in the ablation areas of Glacier Vallunaraju and Chinchey was surveyed during the field works from 1999 to 2002 (Appendix C). A series of daily pictures taken from the ablation area of Glacier Chinchey gave additional information about the flow velocity.

2.4 Data from automatic stations

Since 1999 several climatological and hydrological stations were installed by the Tropical Glaciology Group (ITGG, Austria) and by the Institut de Recherche pour le Développement (IRD, France) at different sites (Figure 2.1, Appendix C). To obtain the climate conditions close to the equilibrium line of the glacier (app. 5000 m a.s.l.) three automatic weather stations (*AWS*) were installed at different sites at the moraine or rocks close to the glacier at altitudes between 4600 – 5100 m a.s.l.. The *AWS* are equipped with instruments to measure wind speed and direction, air temperature and relative humidity, and incoming shortwave radiation (Table 2.3) at a height of 2 m above the surface. In 2004 two stations were extended with a precipitation balance. Not a single station could be run over the whole time period at the same site due to differing troubles (Appendix C). Still, combining the data from all different sites a continuous time series from 2000 – 2005 can be derived (Appendix C). For energy balance studies an energy balance station (*EBS*) and a radiation balance station (*RBS*) were installed on the surface of Glacier Artesonraju at 4850 and 4750 m a.s.l., respectively. They both measure the four components of the radiation balance (shortwave and longwave incoming and outgoing radiation) since March 2004. The *RBS* additionally measures the ablation with an ultrasonic height sensor, the *EBS* is also equipped with wind speed and direction, and air temperature and relative humidity instruments (Table 2.3).

Just below Glacier Artesonraju runoff is measured at the outlet of Lake Artesoncocha (4200 m a.s.l., Figure 2.7, see also chapter 2.2) since 2000. The pressure sensor used (Chloe-Elsyde) for measuring runoff only writes when a change in the pressure exceeds a certain trashhold. This corresponds to a change in the water level of 1 cm which is thus the lowest accuracy that can be obtained. The digital memorial used is from EPROM (Figure F..

For this thesis primarily data from the *EBS* at Glacier Artesonraju (Figure 2.6) and the runoff measured at Artesoncocha from March 2004 to April 2005 are used. In some cases, data gaps from the *EBS* were filled using the data from the *RBS* and the nearby *AWS* outside the glacier (Appendix D). For the year of interest precipitation measurements at Lake Parón were of bad quality and failed for two months since 2004 (June and November). The precipitation gauge installed at the *AWS* close to the glacier operates since end of November 2004. Thus, no continuous record of precipitation amounts during the entire period of interest could be obtained.

Figure 2.6: EBS on the tongue of Glacier Artesonraju (4850 m a.s.l.). The station in the background is the RBS. Photo taken by Irmgard Juen in July 2004.

Figure 2.7: Runoff gauge at the outlet of Lake Artesococha (4200 m a.s.l.). Photo taken by Bernard Pouyaud.

Table 2.3: Equipment of the individual automatic stations that collect data in the Cordillera Blanca. SWin, SWout, LWin, and LWout are the shortwave and longwave radiation fluxes, respectively. Air temperature and relative air humidity sensors at the AWS were replaced in July 2004 (second line).The accuracy is given according to manufacturers.

Station	Variable	Sensor manufacturer/model	Sensor height	Sampling interval	Storage interval	Accuracy
AWS	Air temperature aspirated (°C)	Vaisala/50 Y HMP45C	2 m	180 s	1 h	+/− 0.2 °C
	Relative humidity aspirated (%)	Vaisala/50 Y HMP45C	2 m	180 s	1 h	+/− 2 %
	SWin (W m^{-2})	Schenk/star pyranometer 8101	2 m	180 s	1 h	+/− 3 %
	Wind speed (m s^{-1})	R.M. Young/05103	2 m	180 s	1 h	+/− 2 %
	Wind direction (°)	R.M. Young/05103	2 m	180 s	1 h	+/− 0.3 m/s
EBS	Air temperature aspirated (°C)	Vaisala HMP45C	1 m	10 s	30 min	+/− 0.2 °C
	Relative humidity aspirated (%)	Vaisala HMP45C	1 m	10 s	30 min	+/− 2 %
	Wind speed (m s^{-1})	R.M. Young/05103	2.2 m	10 s	30 min	+/− 0.3 m/s
	Wind direction (°)	R.M. Young/05103	2.2 m	1800 s	30 min	+/− 3 °
	SWin (W m^{-2})	Kipp and Zonen/ Pyranometer CM3	1 m	10 s	30 min	+/− 3 %
	SWout (W m^{-2})	Kipp and Zonen/ Pyranometer CM3	1 m	10 s	30 min	+/− 3 %
	LWin (W m^{-2})	Kipp and Zonen/ Pyrgeometer CG3	1 m	10 s	30 min	+/− 3 %
	LWout (W m^{-2})	Kipp and Zonen/ Pyrgeometer CG3	1 m	10 s	30 min	+/− 3 %
RBS	SWin (W m^{-2})	Kipp and Zonen/ Pyranometer CM3	1.5 m	60 s	30 min	+/− 3 %
	SWout (W m^{-2})	Kipp and Zonen/ Pyranometer CM3	1.5 m	60 s	30 min	+/− 3 %
	LWin (W m^{-2})	Kipp and Zonen/ Pyrgeometer CG3	1.5 m	60 s	30 min	+/− 3 %
	LWout (W m^{-2})	Kipp and Zonen/ Pyrgeometer CG3	1.5 m	60 s	30 min	+/− 3 %
	Inclination (°)	Sommer/Inclinometer	1.5 m	60 s	30 min	+/− 0.1°
	Instrument height (cm)	Judd Com./Ultrasonic depth sensor	*	60 s	30 min	+/− 1 cm
	Air temperature (°C)	Judd Com./Ultrasonic depth sensor	*	60 s	30 min	+/− 1 C

* instrument is drilled into the ice and changes in height due to surface change.

3. Climate and glaciers in the Cordillera Blanca

3.1 Long term climate conditions

To review the long term climate conditions from 1949 to 2004 in the Cordillera Blanca monthly precipitation records from the station Parón at 4200 m a.s.l. are evaluated. No air temperature measurements over the respective time period are available from station data (see also chapter 2.2.2). Thus, air temperature is extracted from NCEP-NCAR Reanalysis data at the 500 hPa level. Although those data should be treated with care when analysing time series (Kistler et al., 2001) they still represent the general trend in air temperature. Further, it has been shown that NCEP-NCAR free-air temperatures represent observed surface air temperatures well, especially on mountain tops (Pepin and Seidel, 2005). Maximum monthly precipitation sum over the whole time period is 275 mm measured in February 1955. 188 months (28.1 %) out of the 56 years of data (672 month) are characterised by very humid conditions (P>100 mm), 156 months (23.2 %) were very dry (<10 mm) and during 70 months (10.4 %) no precipitation occurred (Table 3.1). Maximum and minimum air temperature over the whole time period are −3.3 (April 1998) and −6.7 °C (July 1975), respectively. Air temperature is between −4 to −6 °C during 87 % of all months, only in 2.2 % of the months air temperature is above −4 °C (Table 3.1). Long term mean air temperature and annual precipitation sum 1949 – 2004 is −5.2 °C and 819 mm, respectively (Table 3.2).

The mean seasonal cycle in precipitation shows the typical unimodal pattern of an outer tropical site. The humid season is from October to April (Kaser et al., 1990; Kaser et al., 2003) when 70 – 90 % of annual precipitation amounts fall. According to Georges (2005) the core humid season in the Cordillera Blanca (1958 – 1997) captures the months January, February and March (JFM, P>100 mm). Transitional months (10 < P ≤ 100 mm) from humid to dry conditions are April and March (AM), and from dry to humid conditions September, October, November and December (SOND). The core dry season (P ≤ 10 mm) occurs in the months June, July and August (JJA). During the core humid season more than 50 % of annual precipitation falls, whereas the core dry season only counts for less than 2 % (Georges, 2005). Maximum precipitation is found in March (134.4 mm), minimum precipitation in July (2.1 mm). The long term mean seasonal cycle (1949 – 2004) in precipitation measured at station Parón (4200 m a.s.l.)

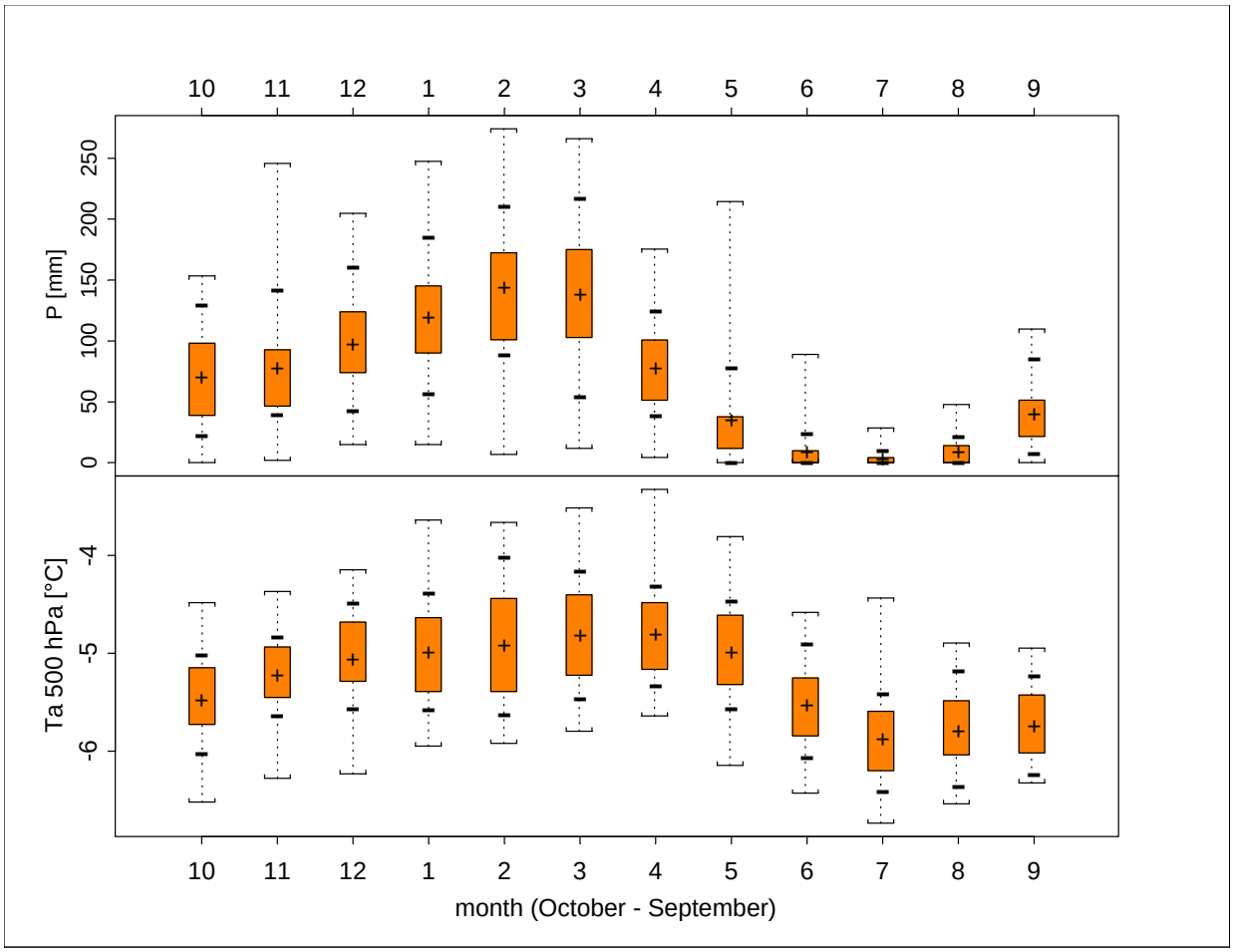

Maximum
90 % quantile
Upper quartile (75 %)
Mean
Lower quartile (25 %)
90 % quantile
Minimum

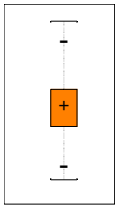

Figure 3.1: Mean seasonal cycle in precipitation and air temperature from 1949 – 2004. Precipitation is measured at station Parón (4200 m a.s.l.); air temperature is from NCEP-NCAR Reanalysis (500 hPa level). The graph shows the arithmetic mean (cross), limits of the lower and upper quartile (orange box, 25 and 75 %), 90 % quantile (vertical bar), and maximum and minimum values.

Air temperature shows the same pattern in seasonality as precipitation with low values during the dry and higher values in the humid season (Figure 3.1). Still, the amplitude in mean seasonal variability is only 1.2 °C. Mean air temperature in JFM and JJA is −4.9 and −5.7 °C, respectively. All month show a high range in possible air temperatures, only in September it is remarkable lower. This might somehow be explained by the more stable precipitation amounts in September than in all other intermediate and humid months. Still, this does not explain why the variability in daily mean air temperature is much higher in July although this is the month with the most constant precipitation amounts.

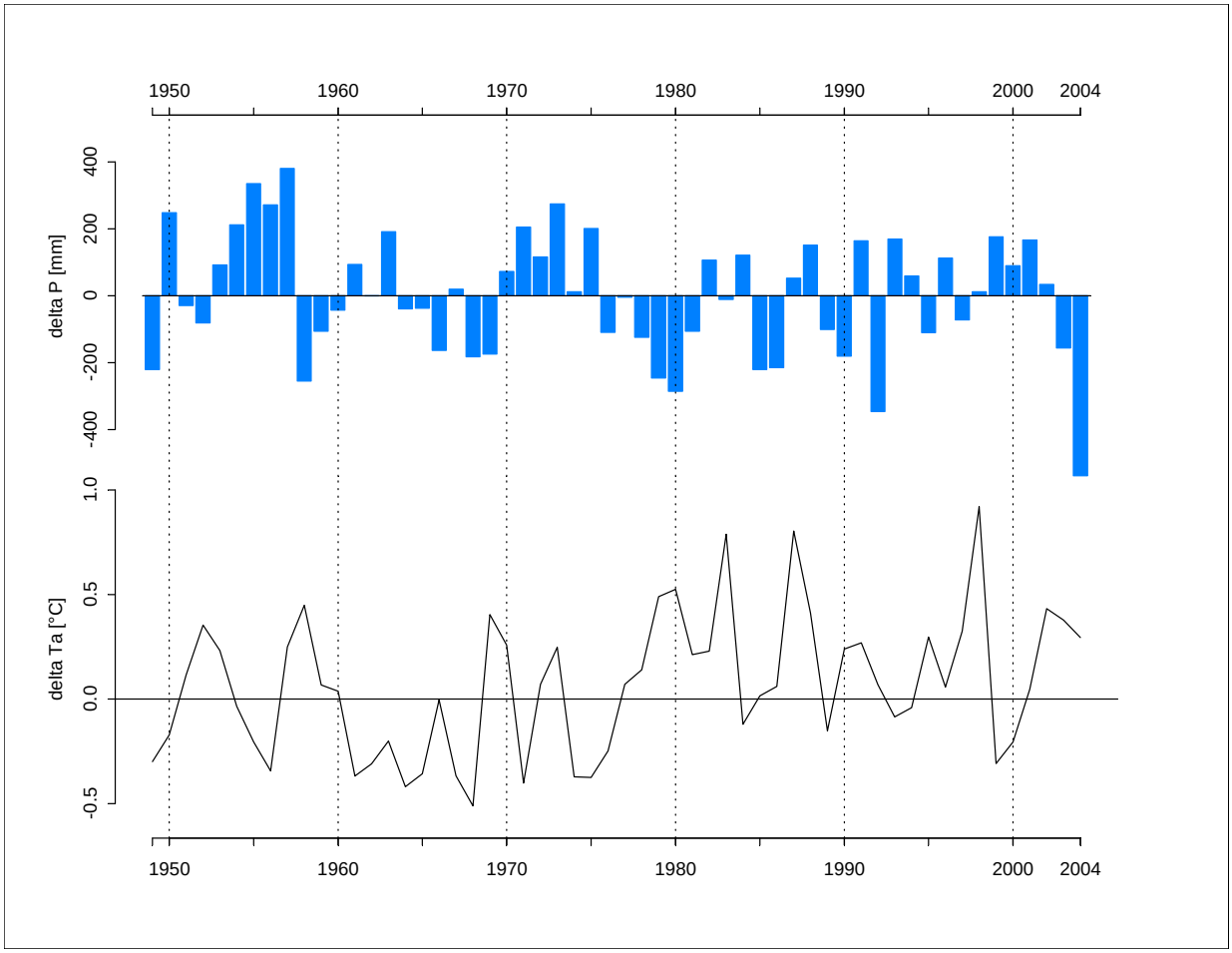

Figure 3.2: Deviation of annual precipitation sums (delta P) and mean air temperature (delta Ta) from the long term mean climate conditions 1949 – 2004. Precipitation is measured at station Parón (4200 m a.s.l.), air temperature is the NCEP-NCAR Reanalysis data set from the 500 hPa level.

Over the whole period air temperature shows an increasing and precipitation a decreasing trend (Figure 3.2). For both records a shift in the climate conditions in the mid 1970s is significant. Air temperature is characterised by mainly below average values until 1977 and mainly above average temperature afterwards (Table 3.2). Mean

air temperature for the two periods is −5.4 and – 5.1 °C, respectively. The coldest decade was from 1960 – 1969 with −5.5 °C and the warmest decade was from 1980 – 1989 with −5.0 °C. The shift in air temperature corresponds well with the general shift of ENSO mode (Trenberth and Hoar, 1995) and was also found in time series from Western North America (Hodge et al., 1998; Alley at al., 2003).

Table 3.1: Frequency of months with different precipitation amounts and air temperature means at the 500 hPa level 1949 – 2004 and for the periods before and after 1977.

Period	Frequency [%]; deviation from long term frequency			
	P 0 mm	P 0.1−10 mm	P 10.1 – 100 mm	P >100 mm
1949 – 2004	10.4	36.7	24.8	28.1
1949 – 1976	8.3; −2.1	36.9; +0.2	24.7; −0.1	30.1; +2
1977 – 2004	12.6; +2.2	36.5; −0.2	24.9; +0.1	26; −2.1
Period	Frequency [%]; deviation from long term frequency			
	T_a < −6.1 °C	T_a −6 to −4.9 °C	T_a −5 to −3.9 °C	T_a > −4 °C
1949 – 2004	10.5	55.7	31.6	2.2
1949 – 1976	13.8; +3.3	65.2; +9.5	20.4; −11.2	0.6; −1.6
1977 – 2004	7.1; −3.4	45.8; −9.9	43.2; +11.6	3.9; +1.7

Contrary to air temperature, annual precipitation sums show the inverse pattern with frequent above average precipitation until the mid 70s and a more pronounced negative deviation from the long term mean for the second half of the period (Figure 3.2 and Table 3.2). The decade with highest precipitation was from 1950 – 1959, lowest precipitation occurred from 1980 – 1989 and after 2000. The more frequent below average annual precipitation sums after 1975 can not be confirmed from the change in specific humidity from NCEP-NCAR Reanalysis data which show a more ore less permanent increase over the investigation period (Georges, 2005).

Beside the considerable decrease in annual precipitation amounts and increase in air temperature (−93 mm and +0.3 °C, respectively) after 1977 (Table 3.2) it is interesting regarding the change in frequency of different precipitation amounts and air temperature. The change in precipitation is mainly caused by a shift in the frequency of extreme months (Table 3.1). During the second, dryer period months with $P = 0$ (+4.3 %) are more, and very humid months are less frequent (−4.1 %), whereas the

amount of months with intermediate precipitation remains almost constant. Contrary, the change in air temperature is mainly caused by a shift to higher intermediate air temperatures and only primarily by more frequent extreme temperatures above −4 °C (Table 3.1). This means that the 0 °C level rises above 5050 m a.s.l. much more frequently in the second, warmer period. As discussed in chapter 2.1 this affects major parts of the glacier area and has thus a strong negative effect on the glacier mass balance. Additionally, the change in precipitation is very unfavourable in turns of glacier mass balance. Very dry months usually have a positive effect on the glacier mass balance as ablation is reduced due to increased sublimation (Kaser et al., 2004; Wagnon et al., 1999a). Analyses of the change in specific humidity from NCEP-NCAR Reanalysis data indicate an increase that took mainly place during the core dry months (Georges, 2005). Thus, the positive effect of months without precipitation is strongly reduced as with an increase in humidity the potential for sublimation decreases and more energy will be consumed by the eight times more effective process of melting. The decrease in months with very high precipitation clearly also has a negative effect on the mass balance of the glacier. The enormous amount of ablation during humid months cannot be compensated without high accumulation amounts anymore.

Table 3.2: Long term (1949 – 2004) mean annual precipitation sums (P) and air temperature (T_a) and their deviation for the period before and after 1977 and for each decade separately. Precipitation is measured at station Parón (4200 m a.s.l.), air temperature is the NCEP-NCAR Reanalysis data set from the 500 hPa level.

Period	Mean T_a (°C); deviation from long term mean T_a	Mean P (mm); deviation from long term mean P
1949 – 2004	−5.2	819
1949 – 1976	−5.4; −0.2	865; +46
1977 – 2004	−5.1; +0.1	772; −47
1950 – 1959	−5.2; +/−0	926; +107
1960 – 1969	−5.5, −0.3	785; −34
1970 – 1979	−5.3; −0.1	859; +40
1980 – 1989	−5.0; +0.2	768; −50
1990 – 1999	−5.1; +0.1	817; −2
2000 – 2004	−5.1; +0.1	738; −81

3.2 Glacier fluctuations

Table 3.3 gives an estimate of the glacier extents for the years 1920, 1935, 1970, 1990, 1997 and 2002 as obtained from Georges (2004; 2005). As discussed in chapter 2.1 the 1990 glacier extent is the most precise evaluation and taken as reference glacier extent (100%). For the 1997 glacier extent the value obtained from the inventory (value in brackets) has been reduced considering an overestimation of 5 %. For the 2002 glacier extent it is assumed that the obtained value for the three evaluated mountain groups is representative for the whole mountain range and the total glacier area is calculated with the same rate of retreat.

Table 3.3: Glacier extents in the Cordillera Blanca during the 20th century (glacier area from Georges (2004, 2005)). The reduction in glacier area (ΔA_G) is calculated with respect to the 1990 glacier extent (100 %).

Year	Glacier area[km²]	Period	ΔA_G [%]	Retreat rate [km² a^{-1}]	Retreat rate [% a^{-1}]
1920(1860)	850−900				
1935	800−850	1920−1935	0−16	0−6.7	0−0.7
1970	660−680	1935−1970	23−27	3.4−5.4	0.4−1.5
1990	620	1970−1990	6−10	2−3	0.3−0.5
1997	580 (610)	1990−1997	7	5.7	1
2002	550−570	1997−2002	1−4	2−6	0.2−0.8
		1920−2002	33−39	3.4−4.3	0.4−0.5

From the reduction in glacier area we can summarise the following characteristic of glacier retreat during the 20th century in the Cordillera Blanca:

- After the maximum ice extent in 1920 glacier retreat was strong until app. 1970;
- from 1970 – 1990 the glacier recession was considerably reduced;
- until 1997 the glaciers again lost huge amounts of mass;
- lower retreat rates are again observed at the end of the century.

Total glacier area in the Cordillera Blanca is reduced by about 1/3 of its 1920 glacier extent within 82 years. If this rate of retreat would continue, the glaciers in the Cordillera Blanca will vanish within the next 160 years. Volume changes of the small glacier Yanamarey that range from 4600 – 5100 m a.s.l. indicate a mean mass loss of 500 mm we a^{-1} from 1948 – 1988 (Hastenrath and Ames, 1995b). From 1977 – 1988 net mass loss at glacier Yanamarey increases to 1500 mm we a^{-1} (Hastenrath and Ames, 1995a). Glacier Uruashraju that range from 4500 – 5650 m a.s.l. lost 1000 mm we a^{-1} from 1977 – 1986 (Ames and Hastenrath, 1996). Ice velocity measurements on both glaciers indicate a maximum ice flow velocity of 17.5 m a^{-1} at glacier Yanamarey and 48 m a^{-1} at 4980 m a.s.l. at glacier Uruashraju. The high flow velocity of glacier Uruashraju leads to a much higher residence time of only 15 years compared to 42 years for glacier Yanamarey (Ames and Hastenrath, 1996; Hastenrath and Ames, 1995a).

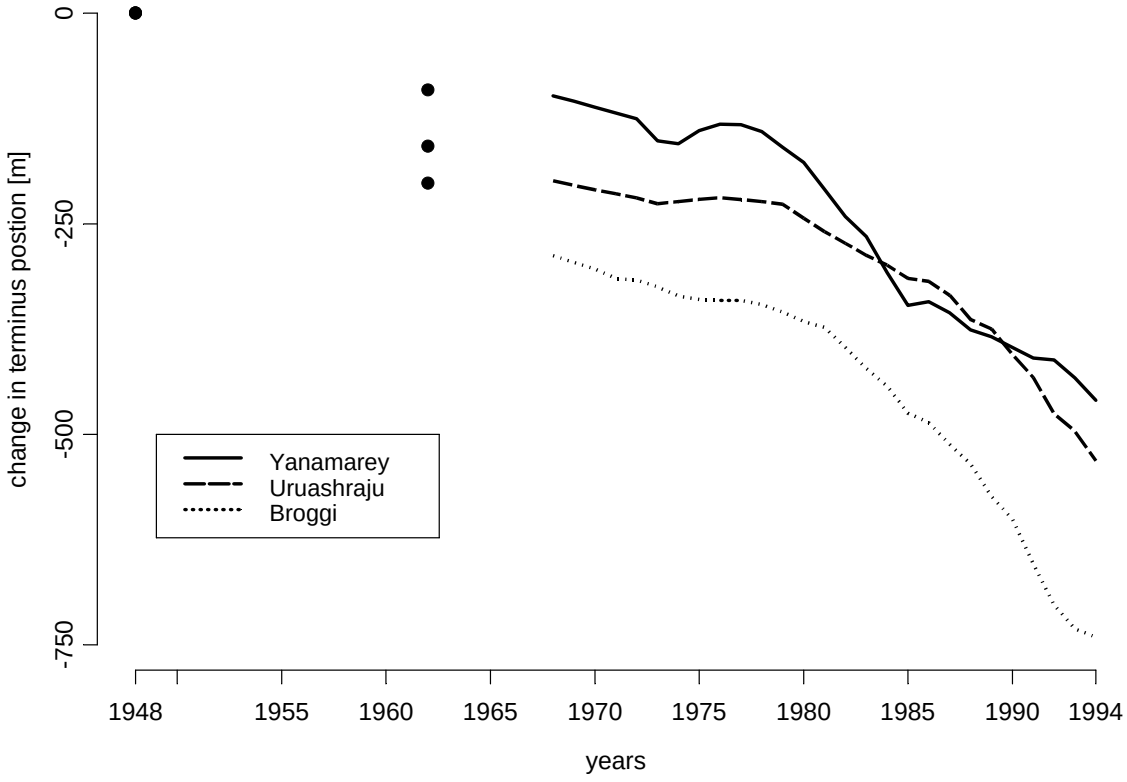

Figure 3.3: Change in the glacier terminus positions of three glaciers in the Cordillera Blanca from 1948 – 1994.

Glacier terminus changes are measured at the glaciers Yanamarey, Uruashraju and Broggi (Figure 2.1) from 1968 – 1994. A single value derived from the first air photographs in 1948 was taken as a starting point and 1962 positions are taken from

further air photographs. Total retreat of the glacier terminus position from 1948 – 1994 is 450, 500 and 750 m for the three measured glaciers (Figure 3.3). The yearly measurement of the glacier terminus position allows separating periods with stable or even advancing conditions. Glacier Yanamarey clearly advanced from 1974 – 1977, a slight advance also occurred from 1985 – 1986. The positive signal can also be seen at both other glaciers, but is less pronounced. The two periods in the mid 1970s and 1980s with at least stable glacier positions also confirm the reported low retreat rates from glacier extent mapping from 1970 – 1990 (Table 3.3). Field investigations also indicate stable glacier conditions after the 1997/98 El Niño (Kaser et al., 2003; Georges, 2005). Measurements of the glacier terminus position of Glacier Vallunaraju in May 2000 and 2001 showed a partly advance of the terminus of almost 100 m (Appendix C, Figure C.2). All other periods after 1920 were characterised by more or less pronounced glacier recession.

4. Applied methods

4.1 Mass balance reconstructions from hydrological balance (MBH)

4.1.1 Determination of runoff characteristics

To determine the runoff characteristics the variations in the water balance components was studied. The given time resolution of available data, i.e. monthly means and sums, allows to determine seasonal, annual, and inter-annual variation. The variation of runoff with time, *dQ/dt*, is due to the variations of precipitation, *dP/dt*, evaporation *dE/dt* and the reservoir volume, *dR/dt* in the respective catchment areas:

$$\frac{dQ}{dt} = \frac{dP}{dt} - \frac{dE}{dt} - \frac{dR}{dt} \qquad (4.1)$$

Owing to the fact that precipitation data at very few selected points give only limited information it is not possible to combine them directly with runoff data. In such cases usually the coefficient of variation is calculated for both precipitation and runoff. Their monthly differences then indicate the seasonal storage variation of the respective catchment basin. The coefficients are calculated as

$$C_{F,i} = \frac{F_i}{\overline{F}} \qquad (4.2)$$

with F representing any of the variables in the water balance and i being the number of individual values. If then C_q is the coefficient for runoff and C_p that for precipitation they are calculated from mean monthly values over the available time period. The analyses here were made for the hydrological year from October to September. Precipitation is calculated as a mean of the six stations Parón, Llanganuco, Chancos, Quillcay, Pachacoto and Querococha (Figure 2.1). In doing so,

the effects of possible errors in the single precipitation time series can be minimised. C_q is individually calculated for all six selected catchment areas.

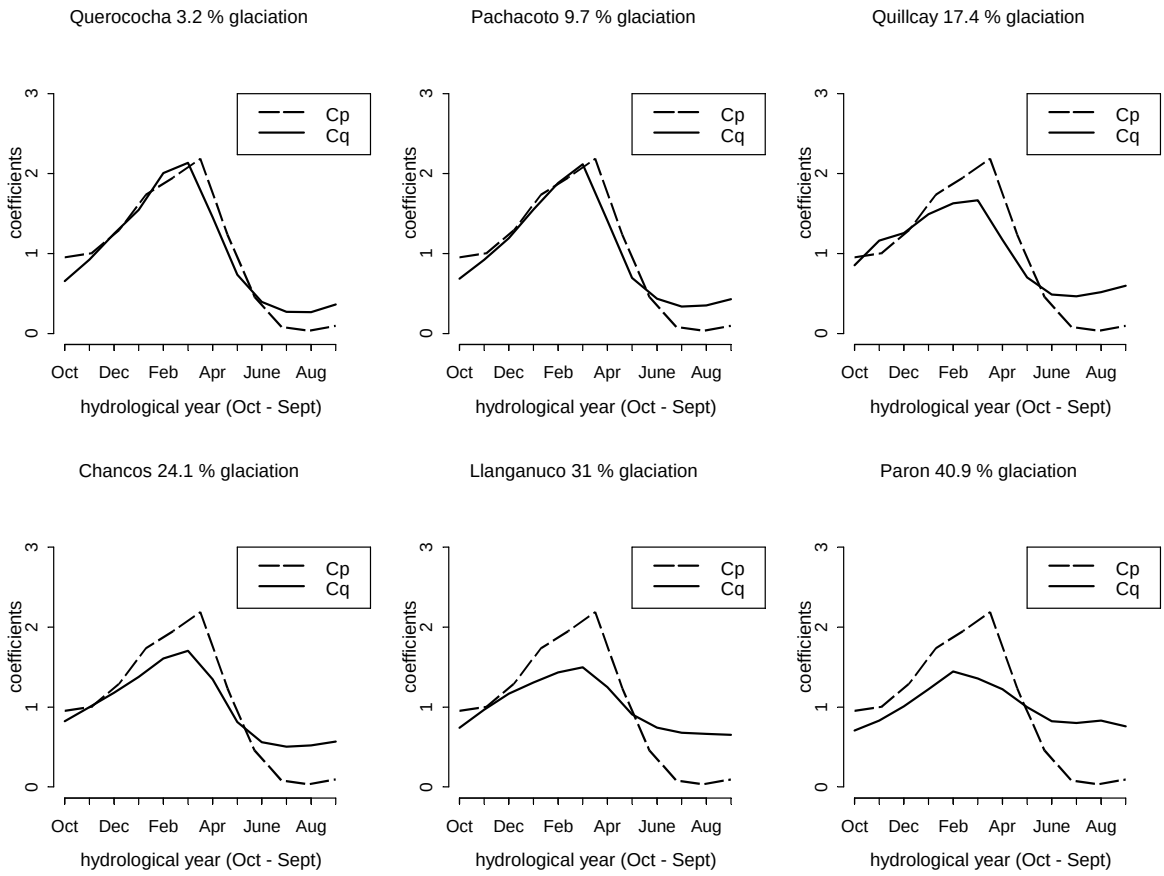

Figure 4.1: Mean monthly variation of runoff and precipitation coefficients from 1953 – 1994 (hydrological year from October to September) for six differently glacierised catchments.

The resulting mean annual variation of these coefficients for the six selected catchments with different portions of glacier area is shown in Figure 4.1. In the catchment of Querococha and Pachacoto where the portion of glacier area is minor, the annual cycle in runoff is highly related to that in precipitation and shows a high variability. With increasing percentage of glacier area in the catchments, the annual cycle in runoff is clearly reduced (Figure 4.1). This clearly shows the different impact of glaciers in the tropics compared to mid latitudes. In the latter climate, the seasonality is characterised by pronounced annual temperature variability which reduces runoff in the winter and amplifies it in spring and summer. As precipitation is higher during summer time too, runoff from glaciers amplifies the seasonal variability in runoff in the mid latitudes (Kaser et al., 2003). Contrarily, in the tropics glacier melt smoothes the runoff variability. Runoff from the glaciers compensates

for the lack in precipitation during the dry season and during the humid season precipitation is restrained. Still, one common effect on the influence of glaciers to the runoff can be found for both regions: the change in the seasonal cycle in runoff from glacier melt has a favourable effect on agricultural activities.

The extent of the impact of glaciers on the runoff seasonality can be expressed by the seasonal storage variation, *S*. This can be calculated numerically from the coefficients $C_{p,m}$ and $C_{q,m}$ which are based on the long term mean monthly precipitation and runoff:

$$S = \sum_{m=1-12} \left| C_{p,m} - C_{q,m} \right| \qquad (4.3)$$

S, obviously, summarises impacts from all possible reservoirs of the respective catchment area on time scales greater than months. Yet, for non artificially influenced catchment areas the following considerations allow further simplification:

- Interception does not last for more than some hours.
- Lakes of the sise met in the Cordillera Blanca cause a delay of runoff information only of the order of 10^{-1} to 10^{0} hours.
- No major base flow variations can be expected from most of the Cordillera Blanca valleys since they mainly have steep flanks.
- The tropical thermal conditions prevent from any major accumulations of snow cover outside the glaciers which lasts more than a few days as a maximum. Usually, snow outside the glaciers melts within hours of the same day the snow falls or the day after.
- Whereas during the humid season the evaporation from non-glaciated surfaces in the Callejon de Huaylas is reduced due to high atmospheric water vapour pressure, the limited availability of water is the limiting factor under dry weather conditions. Thus, no major seasonal variations in evaporation can be expected.
- Extended swamps generally contribute to the seasonal storage variation. If they make up only a minor portion of the catchment area their effect on *S* can be neglected.

Under the given prerequisites, *dE/dt* can be neglected and the seasonal storage variations in the Cordillera Blanca catchment areas, *dR/dt,* are reduced to the change in mass of the glaciers, *dB/dt*. The seasonal storage variability *S* consequently becomes a measure for the impact of glaciers on the runoff. In Figure 4.2 the values of *S* for each catchment area are shown as a function of the ratio of glaciation. The values for the six stations fit well the respective regression line (r^2 = 0.96). After safety constructions at the outlet of Lake Parón in the late 1970s runoff has been regulated. The extent of the regulation is, however, small compared to the seasonal

storage variation of the extensively glaciated (40.9 %) catchment area. The clear increase of *S* with glaciation of the six catchment areas indicates the strong impact of glaciers on the runoff from the Cordillera Blanca valleys. Note that the calculated storage variation is, as a matter of fact, dependent on the mean glacier extent over the period in question whereas the values of relative glaciation are given for the situation toward the end of the period (SPOT data from 1990) because of the lack of better information as discussed in chapter 2.1.

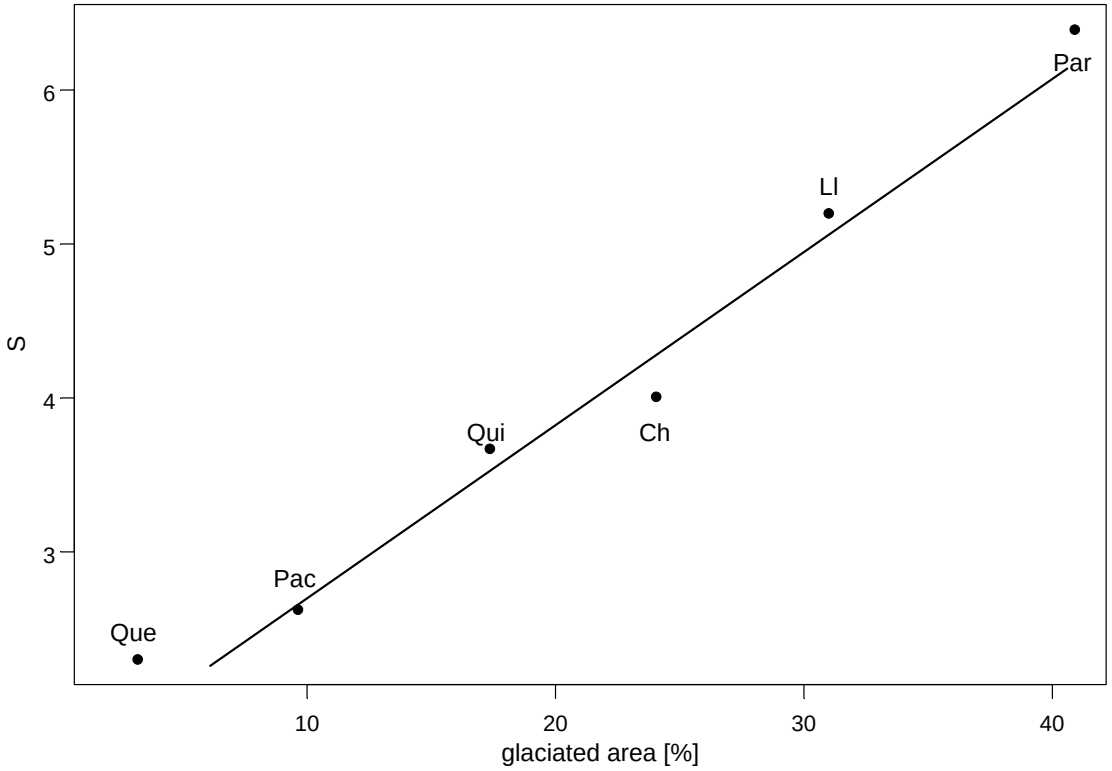

Figure 4.2: Seasonal storage coefficient S of six differently glacierised catchments against the percentage of glaciation. Que: Querococha, Pac: Pachacoto, Ch: Chancos, Qui: Quillcay, Ll: Llanganuco, Par: Parón.

The presented analyses are based on long term mean seasonal variations of precipitation and runoff. This is because an eventual inter-annual analysis of *S* does not show the storage potential of the respective catchment area but indicate primarily the change of the glacier mass turnover from year to year. Thus, the results cannot tell any variations in *S* within the analysed time range and any predictions on changes of *S* can only be made qualitatively. However, the effect of the glaciers on the dry season runoff increases with the mass loss of the glaciers. Yet, if the substantial mass loss as observed during the last century will continue, glaciers will strongly shrink or

even vanish from minor glaciated catchment areas. Consequently, the favourable impact to the runoff variation will decrease and the annual runoff variation will be dominated increasingly and quite immediately by precipitation. If, in turn, glaciers will increase their mass in the future as a result of reduced ablation, the effect on runoff during the dry season would also be reduced. Only if an advance of glaciers would be caused by a major increase of precipitation one could expect a still reasonable contribution from glaciers to runoff. In any case, it is very obvious that a high contribution of glaciers to the dry seasons runoff, such as during the last decades, cannot be expected. Therefore water resources management cannot rely on this situation on a long term.

4.1.2 The calculation of mass balance

Studies on the runoff characteristics in the Cordillera Blanca (chapter 4.1.1) indicate that, if neither human influences nor major swampy areas affect the runoff regime of the catchment area, the deviation of runoff from the precipitation cycle is exclusively due to glacier melt. Based on this, it is attempted to reconstruct the glacier mass balance variations from the available hydrological data (chapter 2.2.1). The resulting series of mass balances are referred as MBH. Normalised coefficients for precipitation and runoff as derived from equation 4.2 are the basis for the calculation again. Still, since absolute and not normalised values of the mass balance variation are approached both coefficients must be reduced to a common denominator. Here, this must be the runoff, *Q*, being the only known variable which represents the entire catchment area. Thus, and under the assumption that the variation of precipitation with time is uniform over the entire investigation area, the monthly coefficient for precipitation, $C_{p,n}$ becomes

$$C_{p,n} = \frac{p_n}{\overline{p}} = \frac{P_n}{\overline{Q}}\left(1 + \frac{\overline{E} + \overline{B}}{\overline{Q}}\right)^{-1} = \frac{P_n}{\overline{Q}}(1+k)^{-1} \qquad (4.4)$$

p_n is the precipitation per square unit calculated as an average over the six stations Querococha, Pachacoto, Quillcay, Chancos, Llanganuco and Parón for each individual month of the available time series. P_n is the monthly precipitation volume on each catchment area to be calculated as

$$P_n = \frac{p_n}{\overline{p}}\overline{Q}(1+k) \qquad (4.5)$$

$\overline{E}$, $\overline{B}$, and $\overline{Q}$ are the evaporation, the glacier mass balance, and the runoff in units of volume per time for each catchment area averaged over the entire period. The seasonal storage variation is assumed to be only from glacier mass changes which is quite reasonable as discussed in chapter 4.1.1. Consequently, $\overline{E}$ is a constant value. It is taken as 30 mm per month, multiplied by the individual surface area of the respective basin which is about 1 mm evaporation per day averaged over all altitude range and all surface types. The rather low value is taken as a best guess and is justified by high air humidity during the humid season and the lack of available water during most of the dry season. Note at this point that an eventual doubling of $\overline{E}$ would only slightly increase the amplitude of the finally approached mass balance variations. $\overline{B}$ is derived from the volume change of Yanamarey glacier (see also chapter 2.3) between 1948 and 1988 reconstructed by Hastenrath and Ames (1995b) which is equivalent to a mean specific mass balance of − 0.5 m water equivalent per year (m we a^{-1}). Being the only available estimate which is at least partly supported by measurements this value is taken for all catchment areas in question. $\overline{Q}$ is taken from measurements in each individual catchment.

In a next step a monthly mass balance coefficient $C'_{B,n}$ can be calculated as

$$C'_{B,n} = C_{p,n}(1+k) - C_{q,n} = \frac{P_n}{\overline{Q}} - \frac{Q_n}{\overline{Q}} = \frac{B_n + E_n}{\overline{Q}} \qquad (4.6)$$

Finally, monthly values for the glacier mass balance of each catchment area, B_n, can be calculated and step by step summarised to annual values B_a. At this point the catchment Querococha is not taken into account anymore since the results for this very little glacierised catchment (3.2 %) have to be expected in the same order of magnitude as the uncertainties of the applied method.

4.2 Mass balance reconstruction from a vertical mass balance profile model (ITGG-2.0)

The model presented here is developed by the Innsbruck Tropical Glaciology Group (ITGG) and referred as ITGG model, version 2.0. It is based on a vertical balance profile (*VBP*) model presented earlier (Kaser, 2001) which in turn is designed on the principles of a model published by Kuhn (1981, 1989). The *VBP* model of Kaser (2001) calculates the change in specific net mass balance with altitude. It has already been shown that modelled *VBP*s agree well with mean seasonal *VBP*s measured over several years on a glacier in the Perúvian Cordillera Blanca (Kaser, 2001). In contrast to the *VBP* model the ITGG–2.0 model is now extended to calculate the absolute mass balance of a glacier. The *VBP* is calculated according to Kaser (2001) where it is discussed in detail as a function of the following variables:

$$VBP(\partial c/\partial z, \tau, SW_{in}, \partial\alpha/\partial z, \partial T_a/\partial z, \varepsilon_a, F(f)) \qquad [\text{mm we m}^{-1}] \qquad (4.7);$$

$\partial c/\partial z$, $\partial\alpha/\partial z$, and $\partial T_a/\partial z$ are the vertical gradients of accumulation, albedo, and air temperature, respectively. τ is the duration of the ablation period. SW_{in}, ε_a are the incoming shortwave radiation and the atmospheric emissivity factor which both, differently to Kaser (2001), are no longer kept constant in time but vary with changing atmospheric moisture content (see next section). The term *F(f)* describes the contribution of melting and sublimation to ablation under the given availability of respective energy and also varies with a change in air humidity. It is

$$F = \frac{1-f}{L_M} + \frac{f}{L_S} \qquad (4.8)$$

with

$$f = \frac{L_S S}{L_M M + L_S S} \qquad (4.9)$$

with values of $0 \leq f \leq 1$ which is the ratio of energy that is consumed for sublimation to the total amount of energy. L_M and L_S are the heat constants for melting (*M*) and sublimation (*S*), respectively.

If the *VBP* is extended from the specific net mass balance at one reference level z_r, $b|_{zr}$, the mass balance at each altitude step above and below z_r and, thus, an absolute vertical balance profile VBP_a can be calculated as

$$VBP_a = b|_{zr} + VBP \tag{4.10}$$

Analogous to the *VBP* in Kaser (2001) specific net mass balance at the reference level is calculated

$$b|_{zr} = c|_{zr} - \tau F(f)\left[SW_{in}(1-\alpha)|_{zr} + \varepsilon_a \sigma T_a^4|_{zr} - \sigma T_s^4|_{zr} + C_s\left(T_a|_{zr} - T_s|_{zr}\right)\right] \tag{4.11}$$

$c|_{zr}$ is the accumulation at the reference level, σ the Stefan−Boltzmann constant, T_s the glacier surface temperature, and C_s a heat transfer coefficient. Below the 0°C−level z_0 a constantly melting ice surface is assumed. Thus, LW_{out} is a constant black body emission from the glacier surface and the variation of the sensible heat flux is determined solely by the variation of T_a. Albedo is assumed to be constant above the equilibrium line altitude *ELA*. For model application z_r should be defined below z_0 and *ELA*.

In the model, the variation of energy with altitude is solely dependent on the gradient of albedo and air temperature. When moving from z_r to higher elevations, $SW_{in}\,\partial\alpha/\partial z$ becomes zero above the *ELA* assuming α to be constant there. The temperature related terms, i.e. longwave net radiation ($\varepsilon_a \sigma T_a^4 - \sigma T_s^4$) and sensible heat flux ($C_s(T_a - T_s)$) are neglected above z_0, where the difference between air and surface temperature becomes constant (Kaser, 2001). Above the two thresholds solely the variation of accumulation with altitude counts for the *VBP*. Figure 4.3A shows the model steps along the vertical profile for dry conditions when the *ELA* is above z_0, Figure 4.3B the procedure for wet conditions with the *ELA* being below z_0 (Kuhn, 1980).

In this version of the model, the impact of air temperature on the state of precipitation is not accounted for. This limitation can be accepted for monthly time steps. As we have already seen from long term climate examination (chapter 3.1) the monthly mean 0°C level hardly ever exceeds 5200 m a.s.l. (3% of all months) and snow usually appears up to T_a = 2 – 4°C. Additionally, low latitude glacier tongues are generally short because of the all year round ablation (Kaser and Osmaston, 2002) and mostly end at 4600 – 4800 m a.s.l.. If applying shorter time steps than months, possible rainfall on the glacier tongues probably has to be accounted for.

As a final step the VBP_a has to be multiplied with the vertical distribution of the glacier surface area to obtain absolute values of the glacier mass balance.

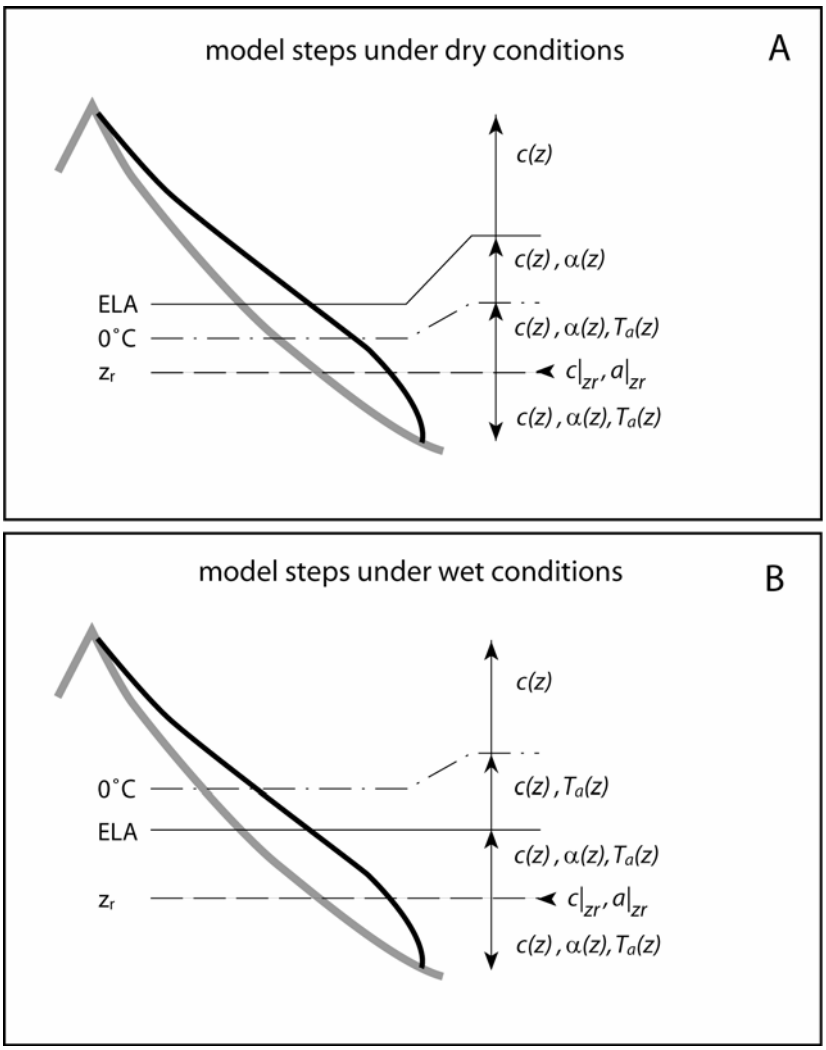

Figure 4.3: The modelling of the mass balance variation with altitude under A) dry and B) wet conditions. Calculations start with the determination of accumulation c and ablation a at z_r. From there, the mass balance varies with altitude depending on the vertical variation of accumulation c(z), albedo α(z), and air Temperature T_a(z). Above the ELA and the 0°C level the contribution of α(z) and of T_a(z) cease respectively. More details are given in the text (figure by Georg Kaser).

Determination of the value ranges for input variables

To apply the ITGG-2.0 mass balance model it is necessary to know the change of f, SW_{in}, α, ε_a, c, and T_a in time. Ideally, each input variable would be supplied from respective data sets. Yet, very few are usually measured over a longer time period. Thus, the concept of the model is that it can also be run with air temperature and one moisture related variable as input data only. From this moisture related variable (e.g. precipitation) all the other variables have to be derived e.g. by statistical parameterisation from a limited calibration period during which all variables of concern are measured. For the low latitude glaciers, not even this is possible for the time being and data sets from different sites and from different periods had to be utilised. Still, assuming that maximum as well as minimum values of moisture related parameters coincide in time, a very dry and a very wet scenario can be designed. It can be assumed that in months with high precipitation amounts accumulation, albedo and atmospheric emissivity will reach their highest values on average. Sublimation and solar radiation will be lowest. The opposite can be assumed for months without precipitation. Obviously, this assumption may be of less validity when looking at much smaller time steps such as days or hours when e.g. a strong shower in the evening cannot characterise the entire day. Even on a monthly basis, one may fail with this approach when simulating particular months within time series such as those described by Francou et al. (2003) when the wet season started with all its attributes except precipitation.

For the time being, all moisture related variables have to be derived from precipitation P which is measured at different site in the Cordillera Blanca 1953 – 1994 (Kaser et al., 2003, chapter 2.2.1). This data set also determines the time intervals, namely months, for which sums or mean values have to be calculated for each variable of concern. $P\big|_{zr}$ is calculated from the records at different sites and by applying the gradient of $\partial P/\partial z$ = 0.035 [mm m^{-1} month^{-1}] according to Fliri (1968) and Niedertscheider (1990). Considering the low wind speeds to be expected at the gauging sites and the missing of low temperatures precipitation is set equal to accumulation c (P=c) as a best guess. The data that are used to obtain possible value ranges of all moisture related variables are taken from the Perúvian Cordillera Blanca (Georges and Kaser, 2002; Kaser et al., 2003) and from Zongo Glacier in the Bolivian Cordillera Real (Wagnon et al., 1999b).

Table 4.1: Value ranges as measured for different variables and model input for monthly application as rounded from the measured ranges.

Variables	measurements		references	model input	
	from	to		dry	humid
$P\|_{zr}$ [mm month^{-1}]	0	338	(1)	0	300
f	1	0.03	(2)	1	0.05
$SW\|_{zr}$ [MJ m^{-2} d^{-1}]	23.2	11.8	(3)	23	12
$\alpha\|_{ELA}$	0.21	0.86	(2)	0.4	0.86
ε_a	0.66	0.86	(2)	0.66	0.86
$\partial P/\partial z = \partial c/\partial z$ [mm m^{-1} month^{-1}]	0.03 − 0.04		(4)	0.035	
$\partial\alpha/\partial z$ [m^{-1}]			(5)	0.00066	
$\partial T_a/\partial z$ [K m^{-1}]			(5)	−0.0065	
C_S [MJ m^{-2} d^{-1} K^{-1}]			(5)	1.7	
s			(6)	1.25	

Data sources:

(1) 6 precipitation gauges in the Rio Santa catchment basin, Cordillera Blanca, Perú; 2,840−4,185 m a.s.l; 1953 – 1993 (ElektroPerú S.A.)
(2) Zongo Glacier, Cordillera Real, Bolivia; 5150 m; 1996−1998 – (Wagnon et al., 1999b)
(3) Automatic Weather Stations, Rurichinchey, Cordillera Blanca, Perú; 4600; 1999−2001; 5000 m; 2000−2003 – (Georges and Kaser, 2002; unpublished data see also Appendix C.)
(4) Rio Santa catchment basin, Cordilera Blanca, Perú; 1953 − 1986 − (Fliri, 1968; Niedertscheider, 1990)
(5) (Kaser, 2001)
(6) the value is derived from model calculations and measured data taken from several sources mentioned in the text.

The value range for mean monthly global radiation (SW_{in}) is obtained from two automatic weather stations operated in the Cordillera Blanca at 4.600 and 5.000 m, respectively, since 1999. The ranges of f, α, and ε_a are derived from energy balance measurements carried out in the ablation zone of Zongo Glacier in the Cordillera Real, Bolivia, between 1996−1998 (Wagnon et al., 1999b). The assumption that

extreme wet or dry conditions assemble moisture related parameters in the same way both in the Cordillera Blanca and the Cordillera Real does not require the same hygric seasonality and can, thus, easily be made. Intermediate values of each parameter are calculated from precipitation amounts with a linear interpolation between the two extreme scenarios (Table 4.1). The gradients $\partial\alpha/\partial z$ and $\partial T_a/\partial z$ as well as C_s are adopted from Kaser (2001), where they are extensively discussed. The obtained values are compiled in Table 4.1 and used to construct the extreme dry and wet scenario.

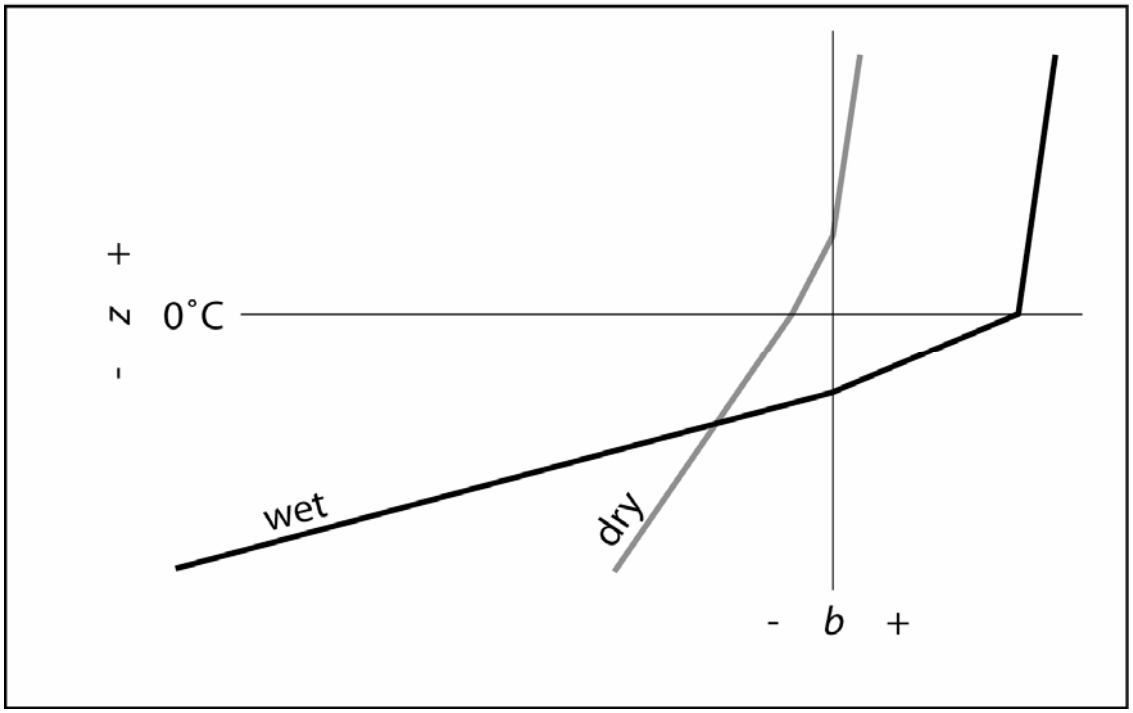

Figure 4.4: Vertical mass balance profiles calculated wit the ITGG-2.0 model with input variables from Table 4.1 for very dry and very wet conditions.

The value range of α given in Table 4.1 is from data measured close to the mean equilibrium line at Zongo Glacier (Wagnon et al., 1999b) and should therefore be inserted at *ELA*. Still, the *ELA* is not known at this point and α is necessary to calculate it. Thus, by starting with a provisional *ELA*, a best approximation of α at *ELA* can be reached after running a number of iterations. So far, the model does not meet the fact that under dry and well ventilated conditions sublimation occurs also from subfreezing glacier surfaces causing reasonable amounts of ablation (Ginot et al., 2001; Stichler et al., 2001; Schotterer et al., 2003). In order to compensate for this, the calculated sublimation amount is multiplied with a constant ratio *s*, which is calculated as $s = S_m/S_c$. S_m is a sublimation amount accumulated from 2 mm d^{-1}, a maximum daily value repeatedly measured at different sites (e.g. Kaser, 1982; Wagnon et al., 1999b; Schotterer et al., 2003). S_c is the sublimation modelled for T_a =

273.15 K and driest conditions. The amount of $S_c\big|_{zr}$ is then multiplied with *s* in order to determine b_{zr}. For the conversion of energy fluxes into mass fluxes, the duration of the ablation is needed and assumed to be τ = 365 days per year in the low latitudes according to the missing seasonal temperature variation.

By taking all moisture related model input parameters from each side of the dry − wet range (Table 4.1) and keeping the thermal conditions constant, a very dry and wet VBP_a is generated in Figure 4.4. Note that the dry VBP_a considers a minimum precipitation value of P = 0.01 mm month^{-1} to obtain an altitude of *ELA*. P = 0 mm month^{-1} would rise the *ELA* at infinitum as no accumulation could not lead to an equilibrium. This is possible for a limited time period but would not allow a glacier to exist on the long term. In the model, *ELA* for P = 0 mm month^{-1} is defined to be at the highest point of the glacier. The *VBP*s in a very dry and very wet tropical climate respectively have been discussed in detail earlier (Kaser and Georges, 1999; Kaser, 2001; Kaser and Osmaston, 2002). The information from the two VBP_as, is in any case of profound importance for understanding glaciers under seasonally varying hygric conditions (e.g. Trenberth and Otto-Bliesner, 2003). Dry conditions are related to an *ELA* clearly above z_0 and small mass turn-over. Under wet conditions *ELA* is far below z_0 and the mass turn-over is considerable.

4.3 Runoff modelling (ITGG-2.0-R)

The extended mass balance model ITGG-2.0 for runoff reconstructions is referred to as the ITGG-2.0-R model. For application of the ITGG-2.0-R (monthly time steps) the following assumptions are made:

- Snow cover outside the glacier usually melts within hours or days and, thus, will not cause any delay in runoff on a seasonal scale.

- Precipitation is assumed to fall as snow over the entire glacier. This is highly probable as indicated by only three months out of 528 in which the glacier terminus is below the monthly mean +2 °C level.

- No albedo feedback is provided. Snow cover usually lasts only a few days on the glacier tongues.

- The influence of different aspects of the glacier surface is neglected.

In addition, the ITGG-2.0-R model is designed and calibrated for all year round melting conditions at all elevations (Kaser, 2001; chapter 4.2). The basic structure of the model is shown in Figure 4.5. To run the model the following input data are needed: the area altitude distribution of the catchment and the glacier area, air temperature and at least one moisture related variables i.e. monthly precipitation sums.

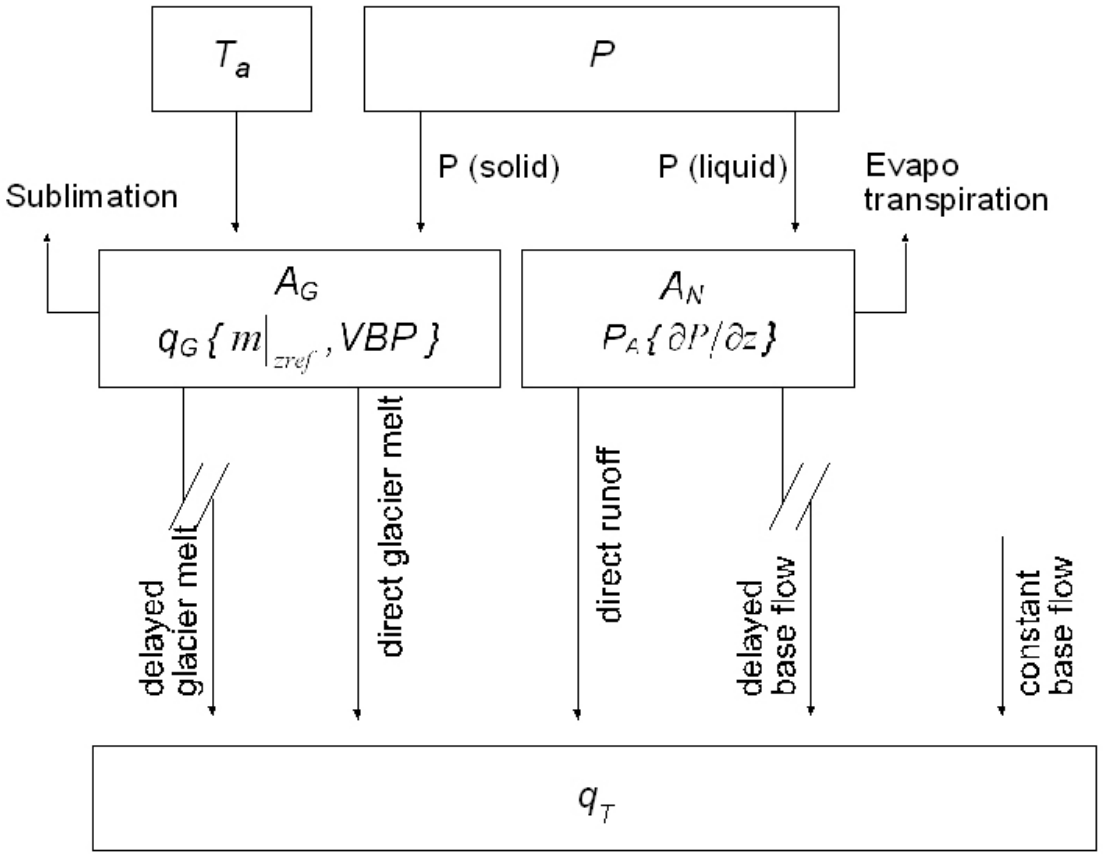

Figure 4.5: Schematic structure of the ITGG-2.0-R model. T_a is air temperature, P precipitation, A_G glacier area, A_N glacier-free area, q_G glacier melt, $m|_{zref}$ melt at reference level, VBP vertical balance profile, P_A precipitation volume, $\partial P/\partial z$ vertical gradient of P, and q_T total runoff depth.

The ITGG-2.0-R model calculates the runoff depth in mm for each month $_n$ from i) the glacier q_G, and ii) the glacier-free area q_N (Figure 4.5). The runoff depth for the total catchment area for each month q_{Tn} is obtained as

$$q_{Tn} = q_{Gn} + q_{Nn} \qquad (4.12)$$

i) The calculation of glacier melt is based on the ITGG-2.0 glacier mass balance model, deriving an absolute VBP_a with equations 4.10 and 4.11 (chapter 4.2). The ITGG-2.0-R extracts glacier melt at each altitude step along the VBP_a with vertical gradients of air temperature $\partial T_a/\partial z$, accumulation $\partial c/\partial z$, and albedo $\partial \alpha/\partial z$. The contribution of glacier melt q_G to the runoff depth of the entire catchment A_T is

$$q_G = \sum (q_{Gi} * A_{Gi}) / A_T \qquad (4.13)$$

with A_G being the glacier area.

Because of a considerable delay in the firn body of the glacier, 30 % of total melt water is considered to contribute to the runoff of the next month. The determination of the delay is discussed in chapter 4.3.1. Following this, total runoff depth derived from glacier melt for each month is

$$q_{Gn} = q_{Gn} * 0.7 + q_{Gn-1} * 0.3 \quad (4.14)$$

ii) The runoff from the non-glacierised area is calculated from precipitation P and its vertical gradient $\partial P/\partial z$. The precipitation P_i for each altitude step Δz is

$$P_i = P + \partial P / \partial z * \Delta z \quad (4.15)$$

and total spatial mean P_A for the non-glacierised area A_N is then

$$P_A = \sum (P_i * A_{Ni}) / A_T \quad (4.16)$$

A portion of $(1-k)$ of P_A goes into evaporation, transpiration, and base flow. Due to the lack of further information, a variable base flow is assumed to be 20 % of this portion and to contribute to the next month's runoff. The value of k varies from 0.5 to 0.6 with the amount of precipitation, to be discussed in the following section (chapter 4.3.1). The variable part of base flow determined this way is set on top of a constant base flow q_0. The total runoff depth for each month from the non-glacierised area is then calculated as:

$$q_{Nn} = P_{An} * k_n + P_{An-1} * (1-k_{n-1}) * 0.2 + q_0 \quad (4.17)$$

Determination of runoff specific input variables

For the determination of melt water from the firn area contributing to runoff of the subsequent month a simple linear reservoir equation is applied. Based on the discharge routing model of Baker et al (1982) discharge (Q) is calculated as

$$Q(t_2) = Q(t_1)e^{-\frac{1}{ks}} + R(t_2) - R(t_2)e^{-\frac{1}{ks}} \quad (4.18)$$

With $R(t)$ is the inflow of water to the reservoir, and ks is the storage parameter in the units of the respective time step. In the mid- and high-latitudes melt water from the firn area reaches the terminus within 10 to 20 days (Schneider, 1997). Because of the very short glacier tongues in the Cordillera Blanca (Kaser and Osmaston, 2002), and

the persistent water saturation of a tropical firn body, a *ks* of 10 days is applied. With this and assuming the amount of glacier melt is the same for each day within a given month, 60 % of the entire glacier's melt water production in the firn area will contribute to the runoff of the next month. In order to obtain the amount of melt water produced in the firn area, its extent has to be defined. Despite further information, the glacier's portion above the long-term mean 0 °C-level (5000 m a.s.l., 1965−1994) is taken as firn area. Although this is 84 % of the entire glacier area, it makes up only 50 % of q_G. Consequently, 30 % of q_G are delayed into the following month.

The runoff coefficient *k* is defined as the ratio between direct runoff and precipitation, differing with climate (Ponce and Shetty, 1995) and surface cover (Gottschalk and Weingartner, 1998) within the range 0 – 1. According to Ponce and Shetty (1995) *k* is typically less than 0.2 for arid to semiarid regions and often greater than 0.5 in wet tropical regions. In order to derive a suitable value for the non-glacierised portion in the Llanganuco catchment, *k* is determined for the minimally glacierised catchment of Querococha (3.2 %). To further minimise the influence of the glacier, the calculation was only made for the wet season from October to April. The values vary between 0.5 and 0.6, with a clear increase with enhanced precipitation. Accordingly, the value of *k* changes linearly with precipitation between 60 and 150 mm per month and remains constant below and above this value range. In order to account for a feedback effect Kadioglu and Sen (2001) suggest to calculate *k* as the arithmetic mean of the preceding and current month's value.

For the constant base flow q_0, the absolute minimum of 8 mm runoff depth per month out of the 44 years record from Querococha station was again adopted to the Llanganuco catchment.

4.4 Energy balance calculation

The energy balance for a melting surface is given by (fluxes towards the surface are positive):

$$R+H+LE+Q_C+Q_P=Q_M \quad (4.19)$$

If the surface temperature is at 0°C and the sum of net radiation (R), sensible (H) and latent (LE) heat flux, the conductive heat flux from or into the subsurface ice (Q_C) and the heat supplied by precipitation (Q_P) is positive, the remaining energy (Q_M), is consumed by melting. As precipitation mostly falls as snow over the entire glacier surface, the energy supplied by precipitation is insignificant and thus neglected in this study.

Net radiation

The energy supplied by R is the sum of incoming (SW_{in}) and reflected (SW_{out}) shortwave radiation, and incoming (LW_{in}) and outgoing (LW_{out}) longwave radiation.

$$R = SW_{in}-SW_{out}+LW_{in}-LW_{out} = SW_{in}(1-\alpha)+LW_{in}-LW_{out} \quad (4.20)$$

The shortwave radiation balance is often written as $SW_{in}(1-\alpha)$ with α being the albedo of the glacier surface.

All radiation components were directly measured in the field and taken from the *EBS*. Nevertheless, some corrections had to be considered. During the early morning hours, when sun beams hit the surface with a low angle, SW_{out} was sometimes greater than SW_{in}. We applied the correction proposed by Wagnon et al. (2003) and calculated SW_{in} when the albedo was higher than 0.9: $SW_{in}=SW_{out}/0.9$. Anyhow, the influence of the correction is very small because it only concerns the early morning hours when incoming shortwave radiation is small compared to values around midday. The albedo as calculated from the shortwave radiation fluxes is sometimes

very small with values down to 0.11. However, daily photographs of the glacier sometimes showed a very dark glacier surface which confirms this low value.

Longwave radiation was corrected with the internal temperature of the CNR1 sensor according to the manufacturer. From longwave outgoing radiation the surface temperature T_s is derived with the Stefan Boltzmann equation assuming an emissivity of 1, $T_s = (LW_{out}/\sigma)^{1/4}$ with $\sigma = 5.67\ 10^{-8}$ W m^{-2} K^{-4}. Whenever T_s exceeds 273.15 K measured LW_{out} is too high for a snow or ice surface and reduced to a maximum value of 315.6 W m^{-2}.

Turbulent heat fluxes

With an eddy correlation system (Gustafsson et al., 2001) the turbulent heat fluxes can directly be measured. Still, these measurements are rare and they do not work in conditions with precipitation or rime. Therefore, the turbulent heat fluxes are derived from air temperature, air humidity and wind speed measurements in this study by applying the bulk aerodynamic approach with stability correction. This method allows the turbulent heat fluxes to be estimated from only one level of measurements (Arck and Scherer, 2002). The calculation of the turbulent heat fluxes was done using the same approach as Wagnon et al. (2003), where it is thoroughly discussed, with the following analytical expressions:

$$H = \rho \frac{c_p k^2 u (T - T_s)}{\left(\ln \frac{z}{z_{0m}}\right)\left(\ln \frac{z}{z_{0T}}\right)} \left(\Phi_m \Phi_h\right)^{-1} \tag{4.21}$$

$$LE = \rho \frac{L_s k^2 u (q - q_s)}{\left(\ln \frac{z}{z_{0m}}\right)\left(\ln \frac{z}{z_{0q}}\right)} \left(\Phi_m \Phi_v\right)^{-1} \tag{4.22}$$

where ρ =0.55 kg m^{-3} is the air density, c_P is the specific heat capacity of air at constant pressure (1010 Jkg^{-1}K^{-1}), k is the von Karman constant (0.4), u is the wind speed (m s^{-1}), L_s is the latent heat of sublimation of snow or ice (2.834 10^6 Jkg^{-1}), T and T_s, q and q_s is the air and surface temperature and the mean specific humidity of the air and the surface, respectively. z is the height of air temperature and relative humidity measurement, and Φ_m, Φ_h, Φ_v are the stability functions for momentum, heat and moisture, respectively. The roughness length for momentum (z_{0m}), for temperature (z_{0h}) and water vapour (z_{0v}) are used as calibration parameters and set

equal as suggested by Wagnon et al (1999b). The value of z_0 was optimised to obtain the best agreement between measured and calculated sublimation. Measured sublimation could be modeled with a best fit value of z_0=0.0003 m. Although the measurement period is very short, the value obtained for a best agreement with measured sublimation was assumed for the whole period.

Subsurface energy flux and EB validation

The conductive heat flux (Q_C) is calculated with a two-layer soil model after Garratt (1992) with the formula $Q_C=\mu(T_{DS}-T_S)$. There the surface temperature (T_S) is taken as the temperature of the thin upper layer, and a constant temperature for the deeper ice layer (T_{DS}) is prescribed. For the calculation of μ the soil-specific thermal diffusivity (k_s) is required. In this study k_s for ice (0.5 W m^{-1} K^{-1}) from Paterson (1994) is applied. Since the glaciers in the Perúvian Andes are known to be temperate glaciers (Wagnon et al., 2001) the temperature of the deep ice layer was taken as 0°C. This leads to an energy flux that is nil whenever the surface reaches melting conditions. Consequently, in terms of glacier melt Q_C has no relevance and is thus neglected in the discussions of variability throughout the year. Still, we included the flux to carry out the following validation of our energy balance. For that, the EB model of Mölg and Hardy (2004) is driven with input data from the *EBS* at Glacier Artesonraju. There T_S is computed through an iterative procedure to fulfill the requirement that the sum of all energy fluxes for a non melting surface must be nil. Thus, measured (LW_{out}-obtained) and computed T_S can be compared (Figure 4.6). With the measured and modelled T_S melting conditions (T_S = 0 °C) were reached for 52 % and 48 % of the time, respectively. The small difference of only 4 % and the high correlation even on an hourly time scale of r^2=0.72 prove the quality of our energy balance calculation. Figure 5.4 shows daily mean modelled surface temperature compared to the surface temperature obtained from measured LW_{out}. Daily variability is well reflected in both data sets with r^2 = 0.76, modelled T_S being slightly higher with maximum daily differences of +2.6 °C and −1.2 °C. Over the whole period modelled T_S is only 0.1 °C higher than calculated T_S from LW_{out}.

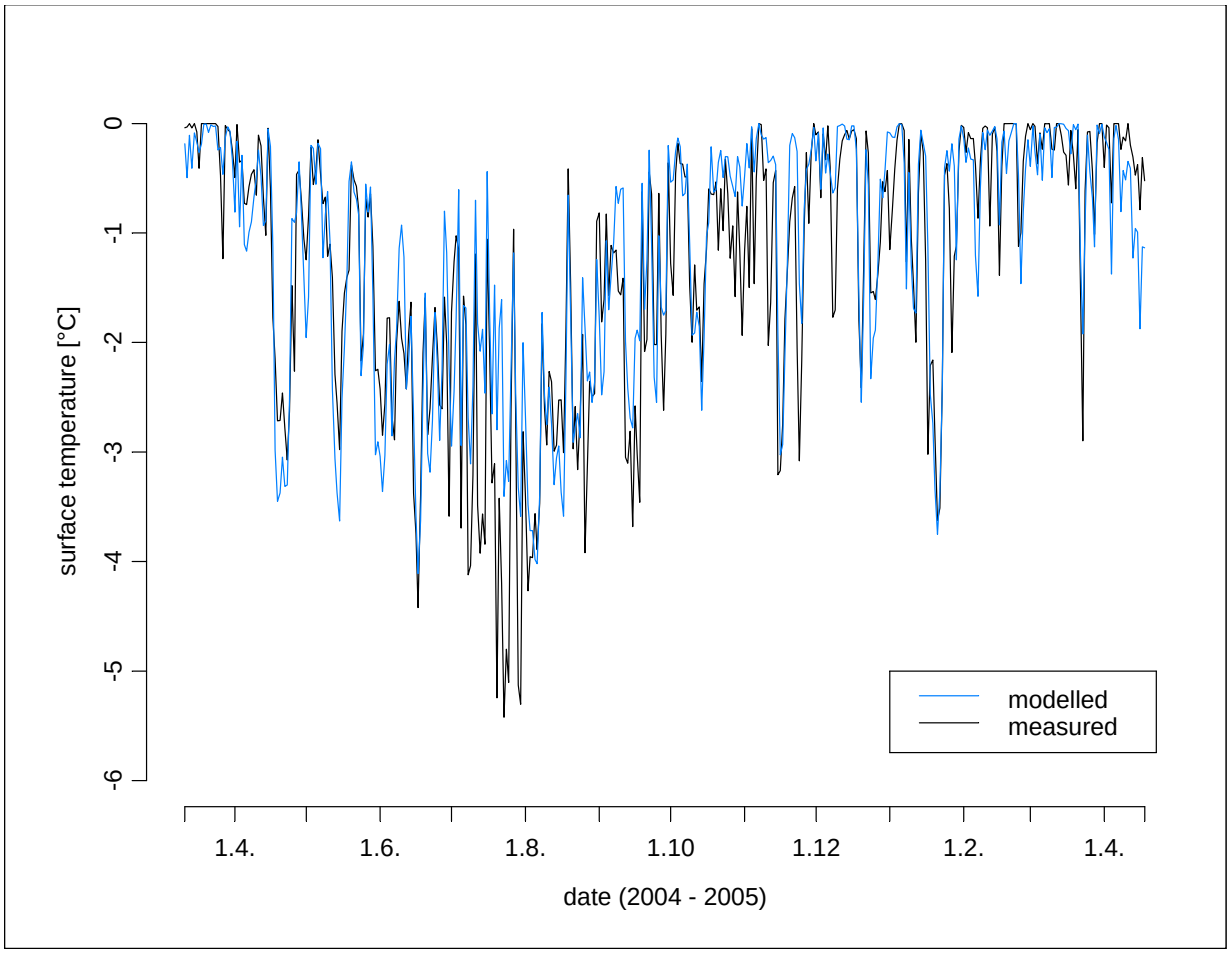

Figure 4.6: Daily mean measured and modelled surface temperature. The correlation coefficient is $r^2=0.76$, n=404.

5. Results and Discussion

5.1 Mass balance reconstructions 1953 – 1994

Monthly glacier mass balances were reconstructed from 1953 to 1994 for the glaciers in the catchments of Parón, Llanganuco, Chancos Quillcay and Pachacoto from the hydrological balance of the respective catchment area (MBH, chapter 4.1) and with a vertical mass balance profile model (ITGG-2.0, chapter 4.2). For the hydrological balance model a constant value of sublimation is assumed throughout the year. Thus, only annual sums for the hydrological years (October – September) are discussed. The ITGG model mass balance series are calculated using the calibrated values ranges as obtained for runoff modelling (chapter 5.3). The absolute value of net mass balance loss is much higher for the MBH than for the ITGG model run. This is a consequence of the higher $\overline{B}$ of −500 mm we a^{-1} taken from measurements which are adopted for the MBH reconstruction (see chapter 4.1.2). Modelled $\overline{B}$ with the ITGG-2.0 model over the entire period is only −271 mm we a^{-1} which is 54 % of $\overline{B}$ from measurements. Measured $\overline{B}$ is derived from volume changes from glacier Yanamarey from 1948 – 1988 (Hastenrath and Ames, 1995b). As this glacier only range from 4600 – 5100 m a.s.l. it is quite obvious that mean $\overline{B}$ is much lower for most of the catchments which reach much higher elevations (see chapter 2.1, Table 2.1). For the lowest catchment of Pachacoto (4700 – 5690 m a.s.l.) $\overline{B}$ is −350 mm we a^{-1}, the least negative mass balance is modelled for the glaciers in the catchment of Parón (−36 mm we a^{-1}) where the glaciers range from 4650 – 6110 m a.s.l.. Thus, for comparison all model results from MBH are scaled by 54 %.

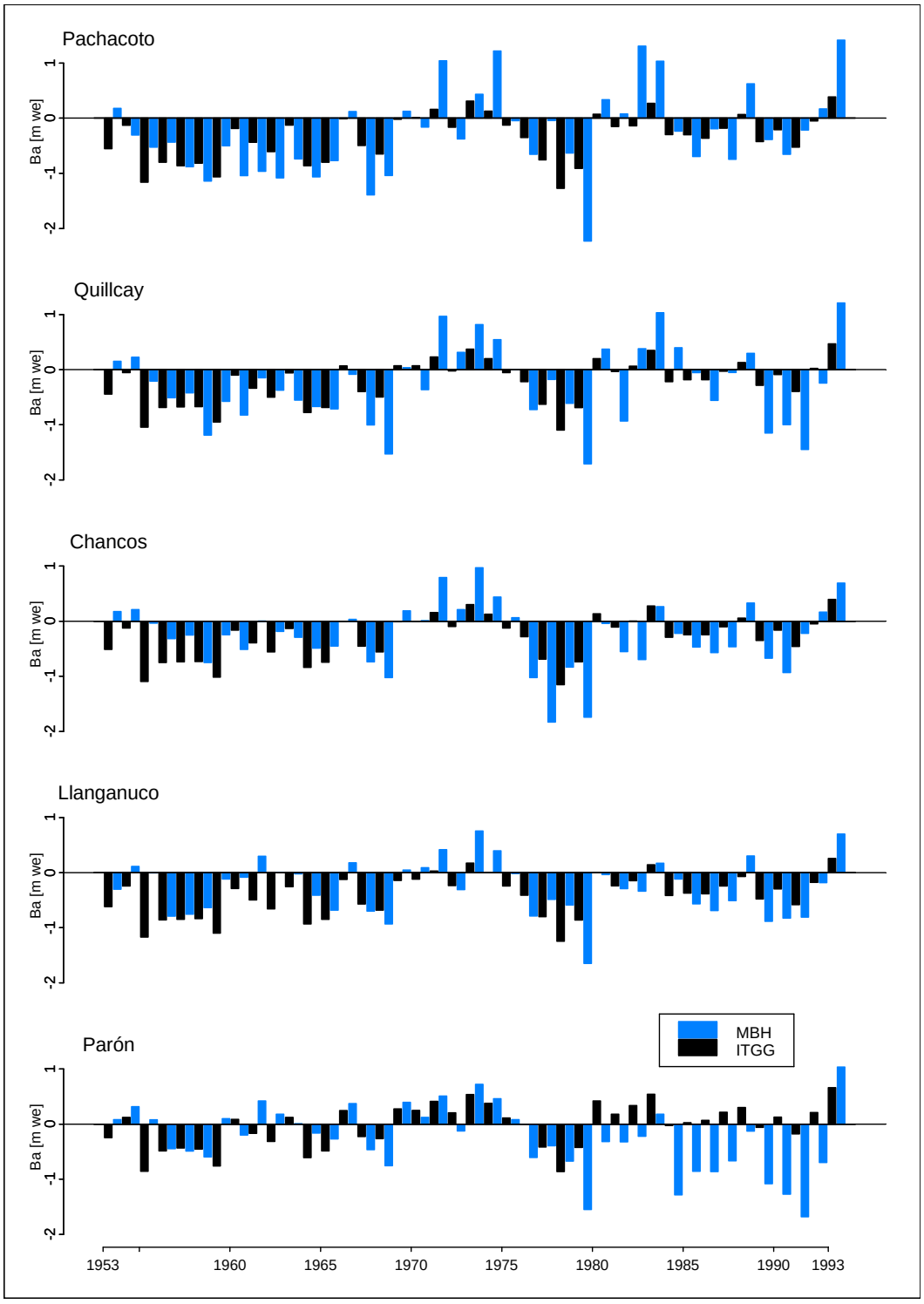

Figure 5.1: Annual specific mass balance for five catchments in the Cordillera Blanca for the hydrological years 1953/1954 – 1993/1994 modelled from the hydrological balance (MBH) and with the ITGG-2.0 mass balance model (ITGG). The MBH is scaled by 54 %. The catchments are sorted from low to high percentage of glacierisation and from North to South.

Figure 5.1 shows the specific mass balance derived from both model runs for the individual catchments. Note that the interpretation of spatial differences in the single catchments is limited as they originate only from differences in runoff and in glaciation (MBH) or from the difference in the area altitude distribution of the respective glaciers (ITGG). Note that in Figure 5.1 the graphs are not only sorted by their rate of glaciation increasing from top to bottom, but, arbitrarily, also according to their position from South to North.

First of all, a basic synchronous character can be seen in all catchments and both model runs. A slight general decrease of absolute values from Pachacoto to Parón must not be misinterpreted as a regional gradient. For the results from MBH this might be related to model uncertainties with decreasing effects from small to bigger rates of glaciation. Nevertheless, the trend can also be figured out from the ITGG model run. A possible explanation for this decrease in amplitude might be that the glaciers in the North generally range over a much higher altitude range than those in the South. As the vertical mass balance profile changes with a change in precipitation a higher portion of the glacier area is affected when they end at low altitudes. Thus, mass balance is much stronger negative or positive in the South of the Cordillera Blanca.

The series of negative mass balances in the 1950s and 1960s are more pronounced in the basins of Pachacoto and Quillcay which could origin from i) a climate gradient from North to South and/or ii) the above discussed general smaller altitude range of the glaciers in the South. The agreement of the two modelled mass balance series is lowest in the catchment of Parón. Whereas with the MBH the positive mass balances around 1980 do not appear they are very dominant in the ITGG model run. The strong negative mass balances in the 1980s in the catchment of Parón (MBH) are even slightly positive years modelled with the ITGG model. The reason for this might be the regulation of the runoff from Lake Parón which, at least partly, influences the seasonal cycle and thus the calculation of mass balance from the hydrological balance is somehow distorted.

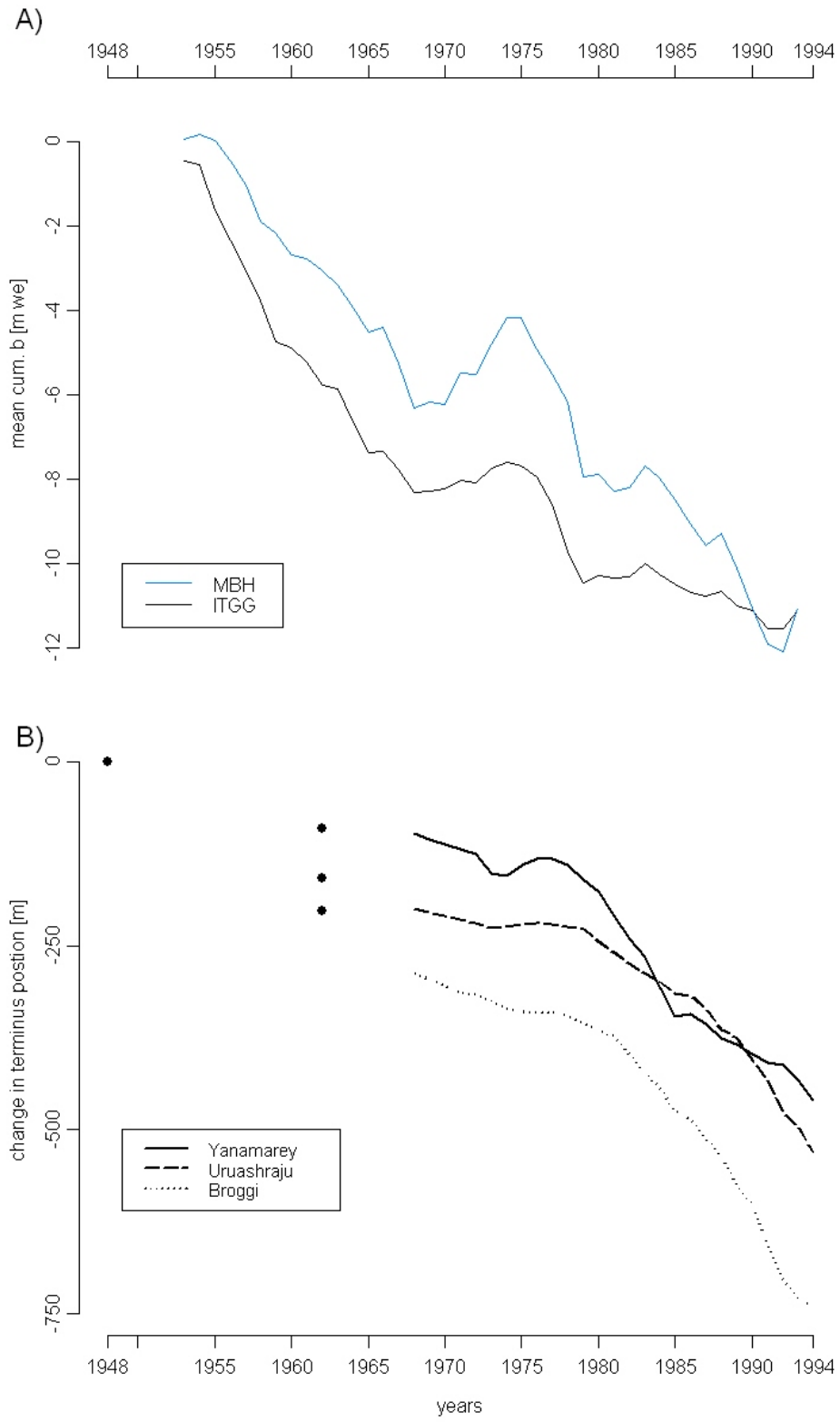

Figure 5.2: A) Mean cumulative annual specific mass balance for five catchments for the hydrological years 1953/1954 – 1993/1994 modelled from the hydrological balance (MBH) and with the ITGG-2.0 mass balance model (ITGG). The MBH is scaled by 54 %. B) Change in glacier terminus position of three glaciers in the Cordillera Blanca from 1948 – 1994.

However, the basic synchronous character of the mass balance series in the single catchments allows the interpretation of general trends of the glacier mass balance in the Cordillera Blanca between 1953 and 1994. To minimise the influence of catchment specific errors in the modelled mass balance series the cumulative mass balance for the two model runs is averaged over all catchments in Figure 5.2A. Both reconstructions show very similar trends over the whole time period. Accordingly, the 1950s and 1960s are characterised by a strong mass loss followed by a more or less marked mass gain between 1970 and 1975. Afterwards, a mass loss dominates again with the exception of two short positive periods in the 1980s.

It would be best to compare these results with measured mass balance series. Still, such data are not available for entire glaciers so far (see chapter 2.3). The mass balance data obtained on the glaciers Yanamarey and Uruashraju range only over a few years and cover only the lower portions of the respective glaciers (Kaser et al., 1990). Therefore, the only way to prove the reconstructed mass balance curves is to compare them with the terminus variations measured more or less regularly on three glaciers from 1968 to 1994 (Figure 5.2B). All three glacier tongues have responded to the 1970s mass gain with an advance of their terminus position with a time lag of only few years. Also the small mass gain in the early 1980s shows corresponding small response of the tongues. It has to be mentioned that the differences in terminus response between the three glaciers are not only due to different mass balances but also due to differences in their geometry. Still, the rapid reaction of all glaciers to mass changes can be expected on tropical glaciers where each change in the mass regime mainly affects the parts of the generally short tongues. This is obvious in the strong vertical mass balance gradients on these tongues, particularly during the humid seasons (Kaser, 2001). In the Cordillera Blanca, the steepness of the glaciers contributes additionally to short response times. The reconstructed mass balance curves are also synchronous to the global trend when glaciers all around the world advanced in the 1970s (Patzelt, 1985; Porter, 1986; Kaser, 1999).

5.2 Runoff reconstruction for a highly glacierised catchment

Runoff is simulated with the ITGG-2.0-R model (chapter 4.3) for the 31 % glacierised catchment of Llanganuco from 1953 to 1997. Model input parameters are idealised to obtain a best fit between measured and modelled runoff (Table 5.1) within the value ranges obtain from measurements (Table 4.1).

Table 5.1: Input variables and model parameters for the ITGG-2.0-R model to obtain best fit between measured and modelled runoff.

Input variables			Model parameter derived linearly from precipitation		
	dry	wet		dry	wet
P [mm month^{-1}]	0	300	f	0.85	0.15
Vertical gradients			$SW_{in}\|_{zref}$ [MJ m^{-2} d^{-1}]	23	12
$\partial P/\partial z$ [mm m^{-1} month^{-1}]	0.035		$\alpha\|_{zref}$	0.4	0.85
$\partial \alpha/\partial z$ [m^{-1}]	0.00066		ε_a	0.7	0.86
$\partial T_a/\partial z$ [K m^{-1}]	−0.0065		k	0.5	0.6

As input for air temperature the only record in the Cordillera Blanca from station Querococha at 3980 m a.s.l. (Figure 2.1) is used in a first model run. A second model run was performed by using air temperature from NCEP-NCAR Reanalysis data from the 500 hPa-level (Kistler et al., 2001). This allows extending the study from 1953 to 1997. Attempts to derive moisture-related model inputs from gridded data sets have not led to any improvement of runoff simulation so far. The application of a radiation model (Mölg et al., 2003) to improve the model input for SW_{in} did also not lead to better results in the modelled runoff (Hölzli, 2006). Thus, all moisture-related variables are solely derived from available precipitation data with a linear relation between very humid and very dry conditions (see chapter 4.2). The glacier extent is taken from the 1990 evaluation although this might not be representative over the whole period of interest (chapter 3.2). Still, if the glacier area is constantly kept 6 %

larger for the first decades, the mean difference in modelled runoff is only between +3 and −2.5% when looking at individual months.

All analyses are made for hydrological years starting with October. The calibration period was taken for the hydrological years 1965/1966 to 1974/1975 because i) this was a period of more or less constant glacier cover (Georges, 2004), and ii) air temperature records at the station Querococha start in 1965. The following ten hydrological years represent the validation period.

5.2.1 Calibration period 1965 − 74 and validation period 1975 − 84

A first model run (run1) over the calibration period was performed with measured precipitation averaged over six stations, air temperature records from Querococha station, and best fitted model parameters (Figure 5.3a). It resulted in a coefficient of determination of $r^2 = 0.82$ with the above discussed best fit model parameters as listed in Table 5.1.

For the same period, a second model run was carried out by replacing the Querococha temperature record with respective series from NCEP-NCAR Reanalysis data. The result is shown in Figure 5.3b and is almost equal to that of model run 1 with $r^2 = 0.81$.

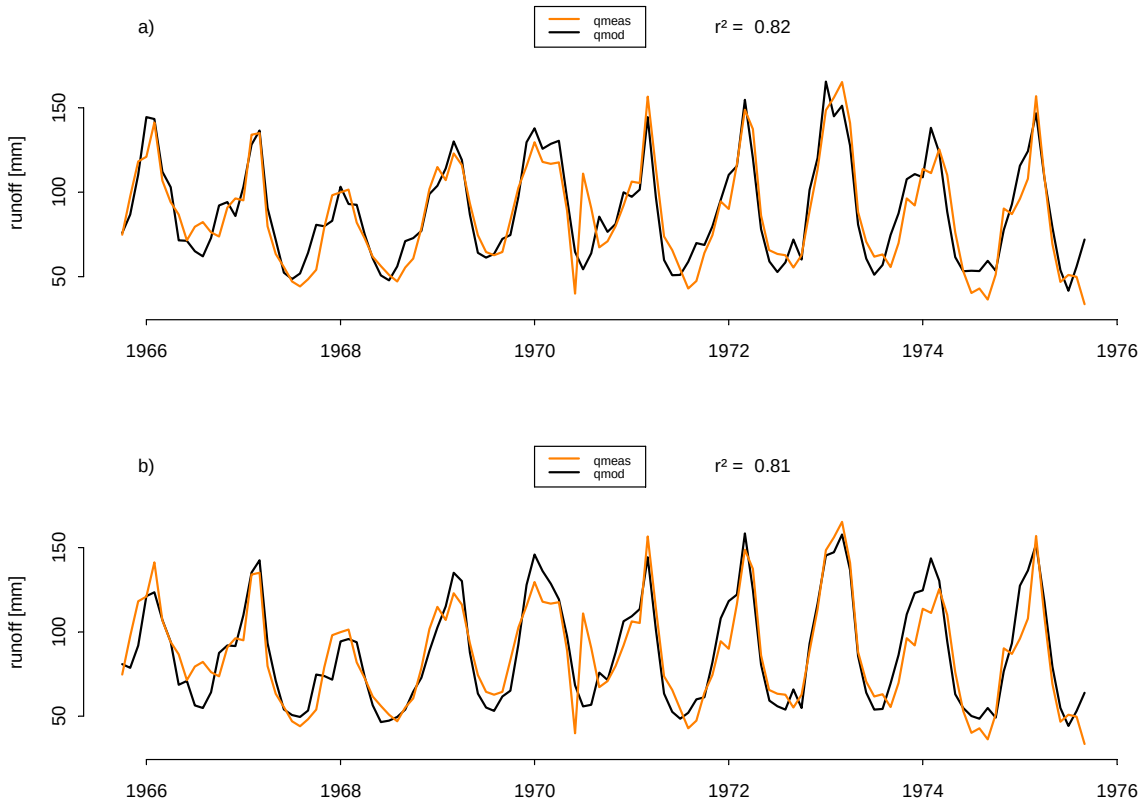

Figure 5.3: Modelled (qmod) and measured (qmeas) monthly mean runoff depths for the calibration period 1965 to 1975 with a) measured air temperature at Querococha station and b) air temperature from NCEP-NCAR Reanalysis.

In both cases the seasonal as well as the inter-annual variations are well represented by the model. When taking a closer look, some particular modelled values deviate from measured ones. The most striking one is the high runoff depth in June 1970 which is not met by the model runs. An amount of more than 110 mm is very unusual for a month in the dry season, where the long-term dry season mean is only about 60 mm month^{-1}. In all available data sets no evidence for this extraordinary high runoff was found. Precipitation in June 1970 is only 9 mm and air temperature is below the long-term mean. Runoff series available from nine other catchments in the Cordillera Blanca (Kaser et al., 2003) do not show any unusual runoff in June 1970. Hence, an underlying climatic reason is not obvious, which precludes modelling this event. One reason for the high runoff in June 1970 can be a recording error. Another explanation could relate to the catastrophic earthquake on May 31st, 1970 (Welsch and Kinzl, 1970), which might have disturbed the runoff gauge. Excluding the value, the result improves considerably with $r^2 = 0.86$ for both model runs.

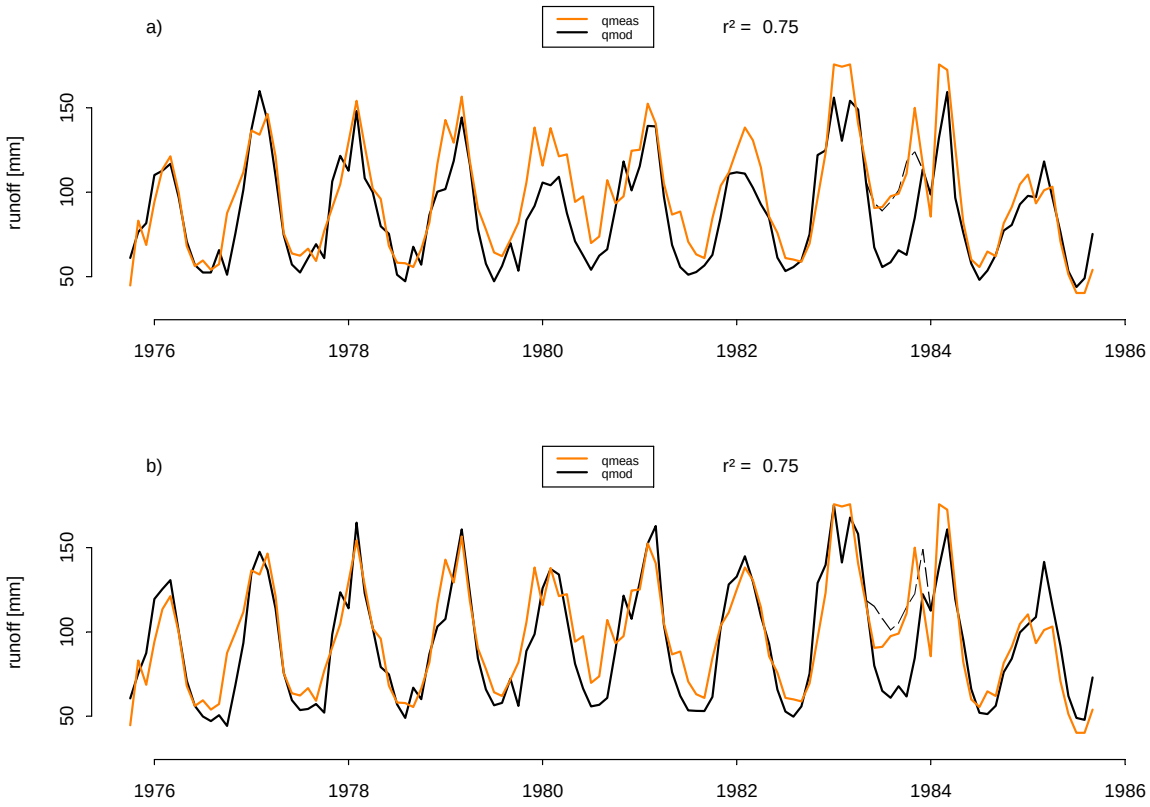

Figure 5.4: Modelled (qmod) and measured (qmeas) monthly mean runoff depths for the validation period 1975 to 1985 with a) measured air temperature at Querococha station and b) air temperature from NCEP-NCAR Reanalysis. Additionally, runoff is modelled with a reduced sublimation/melt ratio f during the dry period 1983 (dashed line, see text for further explanation).

For the validation period the coefficient of determination of modelled versus calculated runoff is $r^2 = 0.75$ for both model runs (Figure 5.4). For the dry seasons 1980 and 1982 air temperature from NCEP-NCAR Reanalysis leads to a much better result than those from Querococha station.

Particularly noticeable is the dry season 1983 when runoff is above 100 mm in each month, which is not met by neither model runs. Again, these high observed amounts cannot be explained by precipitation, since this does not deviate from the long-term mean. In addition, both air temperatures at Querococha station and from NCEP-NCAR Reanalysis data are markedly below average. Consequently, the high amount of runoff during the entire dry season of 1983 cannot be explained by the available data. A possible explanation for this high runoff is an influence of the strong 1982/1983 El Niño. Although precipitation is normal, a raise in air humidity could have caused reduced sublimation and, thus, high melting rates (Wagnon, et al.,

1999a). However, this cannot be modelled as long as all humidity-related variables are derived directly from precipitation. A reduction of the sublimation/melt ratio *f* of 0.15 as independent from precipitation can produce the unusual high runoff during the dry season of 1983 (dashed line in Fig. 5.2.2) and improves the over all coefficient of determination ($r^2 = 0.79$). In a less pronounced way, similar effects may help to explain the underestimation of runoff during several dry seasons. Thus, using an independent time series of air humidity (such as those from NCEP-NCAR Reanalysis data) is expected to improve the model results significantly. Still, the extraction of moisture-related variables from atmospheric reanalysis is not yet developed sufficiently for a glacier mass balance calculation in the tropics.

It has to be mentioned that, the pronounced seasonality of runoff given, these high values of r^2 are not surprising. Monthly analyses, however, are statistically insignificant for the limited number of years. Therefore a seasonally varying r^2 is discussed for the full time series from 1953 to 1997 in the following chapter.

5.2.2 Runoff simulation for the period 1953 − 1997

Making use of the entire length of measured precipitation and runoff as well as NCEP-NCAR Reanalysis air temperature, runoff is simulated for the 44 years period from 1953 to 1997. The result shown in Figure 5.5 reaches $r^2 = 0.76$. The coefficient of determination for each month (Table 5.2) is worst for November and January with $r^2 = 0.53$ and $r^2 = 0.42$, respectively. The highest values are reached for the months December, March and August with values above 0.85. Distinguishing between wet and dry season, the value is higher for the dry season when glacier melt dominates ($r^2 = 0.72$) than for the wet season with ($r^2 = 0.65$). This shows that the ITGG-2.0-R model simulated the glacier melt well. The monthly difference between modelled and measured runoff fluctuates between −70 and +50 mm month^{-1} (Figure 5.5). 94.3 % are within the standard deviation of +/− 32.6 mm month^{-1} of measured runoff (Juen et al., 2006), the mean positive deviation of simulations being +12 mm and the negative one –12.5 mm per month. The accumulated deviation shows a long-term trend (Figure 5.5c). Cumulative deviations increase more or less continuously until 1975 and decrease afterwards. Observed glacier area changes cannot account for it since their effect is to small and no other obvious causes for this trend can be retrieved from the available information at this point. Variations in length and intensity of seasons have to be considered the most likely reason. In particular all moisture-related variables being restrictively synchronised so far are thought to stand

for the deviations to a certain extend. Over the 528 months of simulation, overestimation and underestimation of runoff nearly balance each other.

Table 5.2: Monthly and seasonal coefficients of determination between modelled and measured runoff.

October	November	December	January	February	March	April
0.82	0.53	0.85	0.42	0.82	0.88	0.70

Wet season: $r^2 = 0.65$

	May	June	July	August	September	
	0.60	0.74	0.80	0.85	0.77	

Dry season: $r^2 = 0.72$

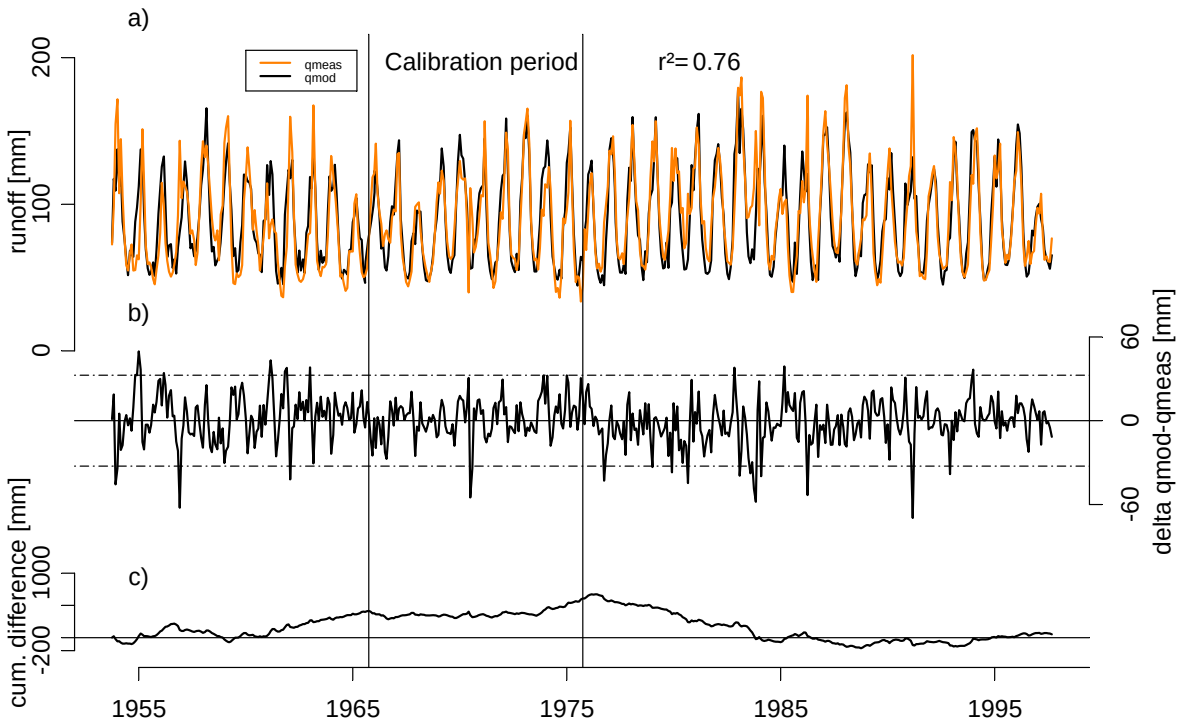

Figure 5.5: Results for the 44 years time series from 1953 to 1997 with air temperature input from NCEP-NCAR Reanalysis: a) modelled (qmod) and measured (qmeas) monthly mean runoff depth, b) difference between modelled and measured runoff with the standard deviation of measured runoff in dashed lines), and c) cumulative monthly difference.

The modelled and measured long-term mean seasonal variation of runoff is shown in Figure 5.6 ($r^2 = 0.99$). In each case the monthly standard deviation of modelled runoff is smaller than that of the measured runoff as indicated by the bars in Figure 5.6. Again the slight underestimation during the dry season as well as the slight overestimation during the period of increasing precipitation may be related to the missing dissolution of the individual moisture-related variables. Nevertheless the mean annual cycle is simulated rather well, which enables the use of the model for predicting mean seasonal runoff in different climate change scenarios.

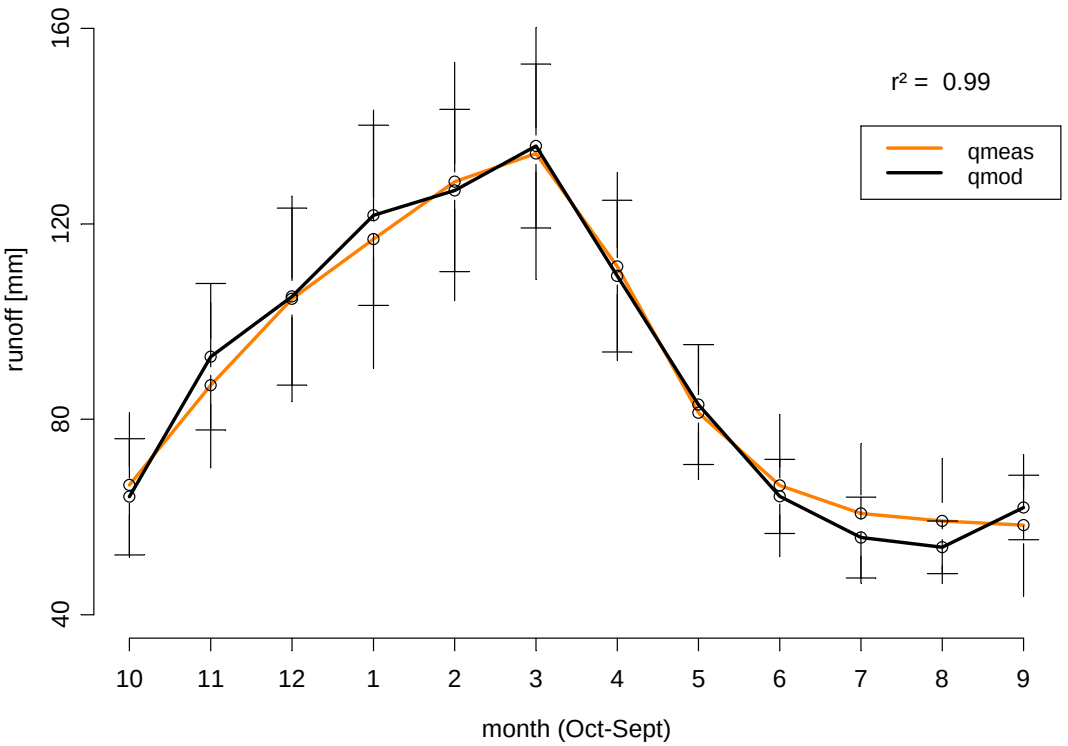

Figure 5.6: Long-term mean seasonal variation of modelled (qmod) and measured (qmeas) runoff for the hydrological year (October – September). Vertical and horizontal bars depict the standard deviation of measured and modelled runoff, respectively.

5.3 Runoff predictions under changing climate conditions

The seasonal cycle of runoff in the Cordillera Blanca is strongly influenced by the degree of glacierisation in a catchment (see chapter 4.1.1). Thus, changing climate conditions will also change this seasonality as the amount of glacier melt will change with the climate conditions and the respective change in the glacier extent. To state the sensitivity of the amount of glacier melt to a change of different climate variables a change in air temperature and precipitation is analysed separately with a step by step decrease or increase of the respective variable for all glaciers that drain into the Rio Santa (chapter 5.3.1). Runoff predictions for different climate change scenarios derived from climate models (IPCC, 2001) are made assuming that the glaciers will be in steady-state with the future climate conditions (chapter 5.3.2). Runoff is modelled with the ITGG-2.0-R model (chapter 4.3). All model runs were made with the calibrated model input variables as depicted for the simulation of runoff in the Llanganuco catchment (chapter 5.2, Table 5.1). It is also assumed that the mean annual cycle of the climate variables will not change. Steady-state glacier extents are derived by gradually reducing/increasing the glacier area until the annual specific mass balance is close to zero (+/− 50 mm we). Note that this procedure does not include any dynamic response times of the glaciers and therefore excludes prediction in time. The spatial pattern of retreat was adopted from a case study in the Santa Cruz mountain range performed by Georges (2004), where the retreat from 1930 to 1970 and 1990 was analysed in detail. The retreat in the Santa Cruz mountain group showed a typical pattern, which was adopted for this investigation. The area altitude distribution of the glacier is divided into three parts. The area in the highest third is unchanged, in the middle part the area is changed gradually by 0 to 60 %, and the area in the lowest third will change 60 to 100 % of its original area per altitude step.

5.3.1 Runoff predictions for climate change scenarios

To analyse the influence of a climate change on the amount of melt water from all glaciers in the Cordillera Blanca the climate parameter precipitation and air temperature are changed step by step from −20 to +20 % and −2 to +2 °C, respectively. It is obvious that each change in the climate conditions affects runoff from glacier melt on different timescales (Hock et al., 2005). Thus, in this evaluation the influence of a climate change on the amount of glacier melt is depicted as the immediate reaction before the glacier area changes considerably as well as the long-term effect after the glaciers have adapted to the new climate conditions (steady-state glacier extent). To outline the change in glacier area the investigation should start with a present-day steady-state condition. For the glacier area distribution (1990) of all glaciers that drain into the Rio Santa this can be approximated by taking the mean annual cycle of precipitation from the station Parón (4200 m a.s.l.) and air temperature from NCEP-NCAR Reanalysis data for the hydrological years 1999/2000 and 2000/2001 as input data. Mean annual precipitation sum over the two years is 100 mm above, mean air temperature is 0.2 °C below the long term average (see chapter 3.1). Modelled net mass balance for this period is +12 mm. Field investigations on Glacier Vallunaraju from 1999 to 2002 also point out that the glaciers were indeed close to steady-state conditions or even experienced small advances during this period (Appendix C, Figure C.2). The catchment characteristics of the Rio Santa catchment (8.4 % glacierised) are summarised in chapter 2.1.1. Runoff from glacier melt contributes to app. 20 % of total runoff, during the dry season glacier melt provides app. 40 % of the total runoff.

Figure 5.7a shows the immediate influence of a 0.2−2°C warming and cooling on the amount of glacier melt as well as for a new steady-state glacier extent with respect to the present-day situation (100 %). Figure 5.7b illustrates the same for a 2−20 % change in precipitation. Table 5.3 gives a summary of the obtained changes in runoff from glacier melt and glacier area for a change in air temperature of +/− 1 and 2 °C and a change in precipitation of +/− 10 and 20 %.

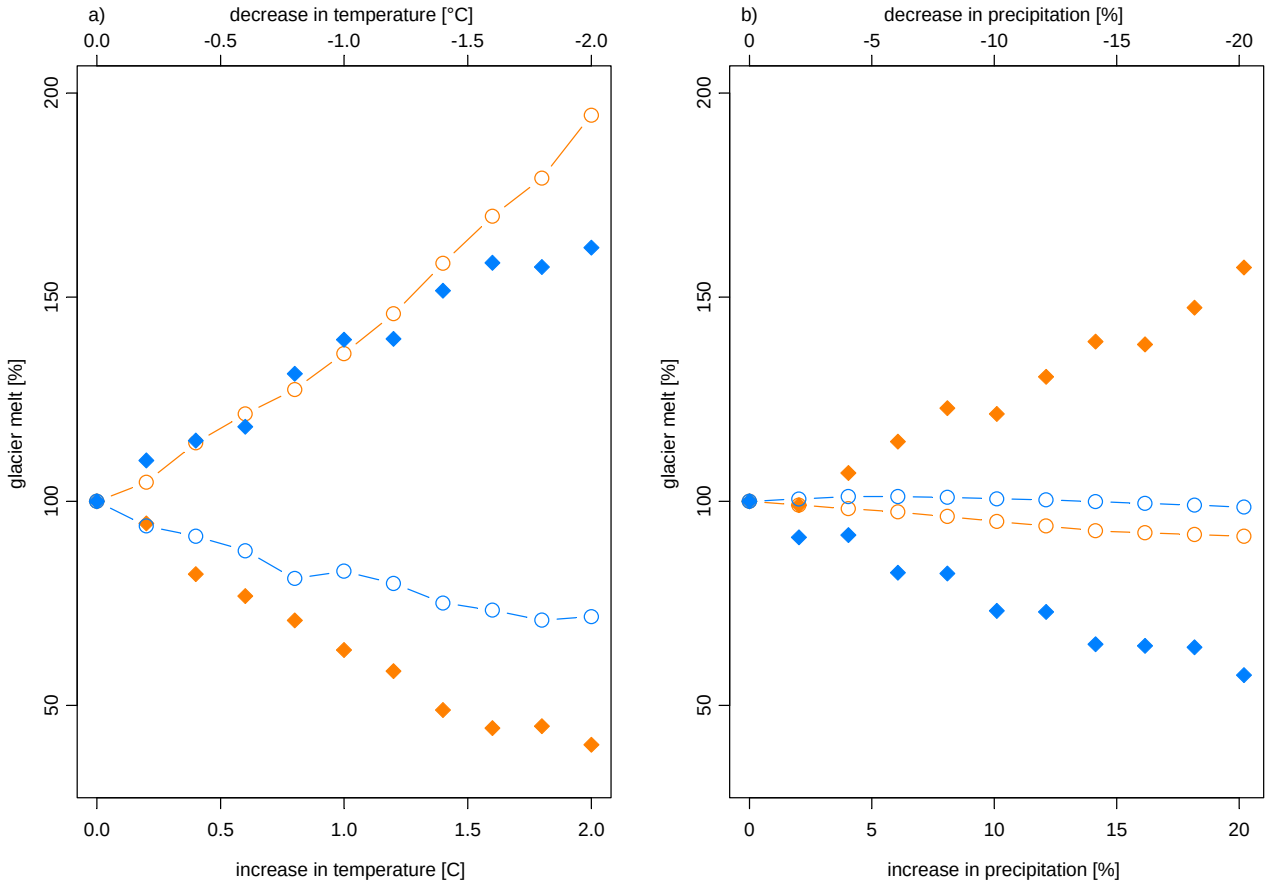

Figure 5.7: Modelled influence of a climate change on the amount of glacier melt for a) a change in air temperature of +/− 0.2−2 °C and b) a change in precipitation by +/− 2−20 %. Lines with circles indicate the immediate change in the amount of glacier melt and filled triangles the change after the glacier has reached steady-state conditions with the respective new climate. Blue represents a decrease, orange an increase of the respective climate variable.

A change in air temperature impacts the amount of energy that is available for ablation. Assuming that the sublimation/melt ratio will not change this influences mainly the amount of melt. At the beginning, the melt water production increases with a warming and decreases with a cooling. An increase in air temperature of 2 °C will almost double the amount of glacier melt during the first years (Table 5.3, Figure 5.7a). This, in turn, will lead to a reduction of the water stored in the glacier and consequently the glacier will loose volume and shrink. On a long term, the glacier will adapt to the changed climate and reach a new steady-state glacier extent. After this adoption to the climate change a 2 °C warming would result in a new steady-state glacier extent with a reduced glacier area of 62 % compared to the glacier extent in 1990. As a final result, melt water production will be reduced by 60 %. In contrast, a −2 °C cooling will decrease glacier melt only by 28 % (Table 5.3, Figure

5.7a) in the beginning. This is quite reasonable as reduced melting conserves the snow cover of the glacier surface and thus albedo is higher and the energy that is available for ablation decreases. On a long term this will lead to an advance of the glacier and increase the glacier area by 75 % and, consequently, also increase in the amount of glacier melt by 62 %.

The influence of a change in precipitation on the melt water production is minor during the first years. This is due to the compensating effects of the change in all moisture-related variables. A higher amount of precipitation will decrease incoming shortwave radiation and the sublimation/melt ratio, but increase the albedo and the emissivity of the atmosphere (cf. Table 4.1). Total energy that is available for ablation will slightly decrease. Nevertheless, the total amount of glacier melt is almost unchanged due to the higher portion of energy that will be used for melting, which is eight times less energy consuming than sublimation. As a consequence, net ablation increases. On the other hand, accumulation also increases due to higher precipitation amounts. All together, net balance will be positive and force the glacier to grow. A decrease in precipitation will produce the opposite effect. After the adoption of the glacier area to the changed climate conditions glacier melt changes considerably as the glacier volume and area has changed too. An increase in precipitation by +20 % leads to a glacier surface growth of +38 % and a rise in the amount of melt water by +57 % (Table 5.3). A precipitation decrease of −20 % will result in a reduced glacier area of −31 % and a change in the mean annual amount of melt water of −43 %.

Table 5.3: The immediate and long term change in mean annual glacier melt (q_G) for a change in air temperature (T_a) and precipitation (P). ΔA_G is the change in the glacier area for a new steady-state glacier extent.

	immediate	long-term			immediate	long-term	
climate variable	Δq_G [%]	Δq_G [%]	ΔA_G [%]	climate variable	Δq_G [%]	Δq_G [%]	ΔA_G [%]
T_a +1°C	+ 36	− 37	− 39	T_a − 1°C	− 17	+ 39	+ 44
T_a + 2°C	+ 94	− 60	− 62	T_a − 2°C	− 28	+ 62	+ 75
P + 10 %	− 6	+ 22	+ 17	P – 10 %	+ 1	− 27	− 20
P + 20 %	− 9	+ 57	+ 38	P – 20 %	− 1	− 43	− 31

Comparing the changes in the melt water production for a new steady-state glacier extent for precipitation or air temperature changes it is striking that:

i) a change in air temperature changes the amount of glacier melt almost equivalent with the change in glacier area, whereas a change in precipitation causes much higher changes in the amount of glacier melt than in the glacier area.
ii) the decrease in the melt water production of a 2 °C warming can almost be covered by 20 % wetter conditions. A decrease in air temperature of −2 °C increases the amount of melt water considerably which can only partly be compensated by a decrease in precipitation of −20 %.

Both differences can be explained by the following consideration. With a change in precipitation the gradient of the vertical mass balance profile (*VBP*) and the *ELA* will change; both effects partly compensating each other. In contrast, a change in air temperature only affects the *ELA* but does not change the shape of the *VBP*. As a consequence, the change in the net mass balance is higher for a change in air temperature and thus the change in glacier area for a new steady-state glacier extent is higher too. The small change in runoff from glacier melt for a decrease in precipitation is because this affects only the melt water production during the wet season. During the dry months the sublimation/melt ratio already is at its maximum and thus cannot rise anymore. An increase in precipitation mainly increases the melt water production during the dry season.

5.3.2 Runoff predictions for IPCC climate change scenarios

Global climate model (GCM) computed climate scenarios (Hulme and Sheard, 1999) as based on different IPCC emission scenarios (IPCC, 2001) quantify the change in mean annual air temperature and precipitation at sea level for the years 2050 and 2080. To predict the influence of the climate change on runoff the five catchments with available runoff data and different portion of glacier area, i.e. Parón, Llanganuco, Chancos, Quillcay, Pachacoto and Querococha are evaluated individually (see chapter 2.1). To derive the range of possible changes in runoff the influence of the two extreme scenarios, i.e. b1-low and a2-high (Table 5.4) are modelled for 2050 and 2080 separately. The IPCC predicted changes proceed from 1961 – 1990 mean climate conditions. Thus, the changes in glacier extend and runoff is simulated accordingly. To predict the change in runoff for a new steady-state

glacier extent it would be best to start with a steady-state glacier situation. Therefore, it is first evaluated if the glaciers in the different catchments are in balance with the climate conditions from 1961 – 1990.

Table 5.4: Predicted mean annual change in air temperature Δ Ta and precipitation Δ P (sea level) for two IPCC climate change scenarios (b1-low, a2-high) with respect to the mean conditions from 1961−1990 (IPCC, 2001; Hulme and Sheard, 1999). Values are taken as a mean from the four GCM grid points surrounding the Cordillera Blanca.

	2050		2080	
	Δ T_a [°C]	Δ P [%]	Δ T_a [°C]	Δ P [%]
b1-low	+1.1	+2.5	+1.45	+3.5
a2-high	+3.0	+8.5	+4.67	+13.0

Steady-state glacier extent for the mean climate conditions from 1961 – 1990

For all glaciers in the 6 catchments mean specific mass balance $\overline{B}$ was calculated with the ITGG-2.0 model with mean climate conditions from 1961 to 1990 and the glacier extent from 1990. Model input data were monthly mean precipitation sums (calculated as a mean over the six selected catchments for the altitude of 4000 m a.s.l., see chapter 2.2) and air temperature (NCEP-NCAR Reanalysis data, 500 hPa level). Mean annual precipitation, air temperature and *ELA* over the time period of interest is 1000 mm, −5.2 °C and 5130 m a.s.l., respectively. Steady-state glacier extent is reached when $\overline{B}$ is close to zero, here defined to be between +/− 50 mm we per year.

Out of the six selected catchments this is only the case in the region of Llanganuco and Parón, where $\overline{B}$ is −27 and −44 mm we, respectively (Table 5.5). In the catchments of Chancos, Quillcay and Pachacoto $\overline{B}$ is negative with −362, −291, and −446 mm we, respectively. Steady-state glacier extent in the individual catchments could be modelled with 0.6, 0.5 or 0.65 °C colder or 15, 10, or 17 % wetter conditions than mean climate from 1961 – 1990, respectively (Table 5.5). The glaciers in the catchment of Querococha end at 5200 m a.s.l. which is only slightly above mean *ELA* (5130 m a.s.l.). Thus, $\overline{B}$ is strongly negative with −2053 mm we. A steady-state glacier extent in this catchment could only be modelled with a decrease

in air temperature of 1.85 °C or an increase in precipitation of 70 % (Table 5.5). With the mean climate conditions from 1961 – 1990 the glaciers in this region will not survive. Thus, the catchment of Querococha is not taken into account for further studies concerning runoff predictions since a steady-state glacier extent with warmer conditions cannot be obtained.

Table 5.5: Modeled mean specific mass balance for the mean climate conditions from 1961 – 1990 ($\overline{B}$ 1961 – 1990) and the required change in air temperature (ΔT_a) or precipitation (ΔP) to reach steady-state glacier extents with the 1990 glacier area extent in the individual catchments.

	$\overline{B}$ 1961 − 1990	ΔT_a [°C]	ΔP [%]
Parón	−27	–	–
Llanganuco	−44	–	–
Chancos	−362	−0.6	+15
Quillcay	−291	−0.5	+10
Pachacoto	−446	−0.65	+17
Querococha	−2053	−1.85	+70

The mean altitude of the glaciers that have a steady-state glacier extent in the region of Parón and Llanganuco is 5475 and 5550 m a.s.l., the percentage of glacier area above *ELA* – also called the accumulation area ratio (*AAR*) – is 72 and 69 %, respectively. The glaciers in the Chancos and Quillcay catchments are close to equilibrium and will have to lose 14 and 11 % of their area to reach equilibrium conditions, respectively. Their mean altitude is 5300 and 5325 m a.s.l. (Figure 5.8A), the *AAR* is 64.5 and 63 % (Figure 5.8B), respectively. The glaciers in the catchment of Pachacoto have a mean altitude of 5200 m a.s.l. and only 51 % of the glacier area is above mean *ELA*. To reach steady-state glacier extent the glaciers have to retreat 27 % of their actual sise. The very low glaciers in the Querococha catchment with a mean altitude below 5000 and only 2 % of the area above *ELA* will almost vanish (>99% loss of area) to be in balance with the 1961−1990 climate conditions.

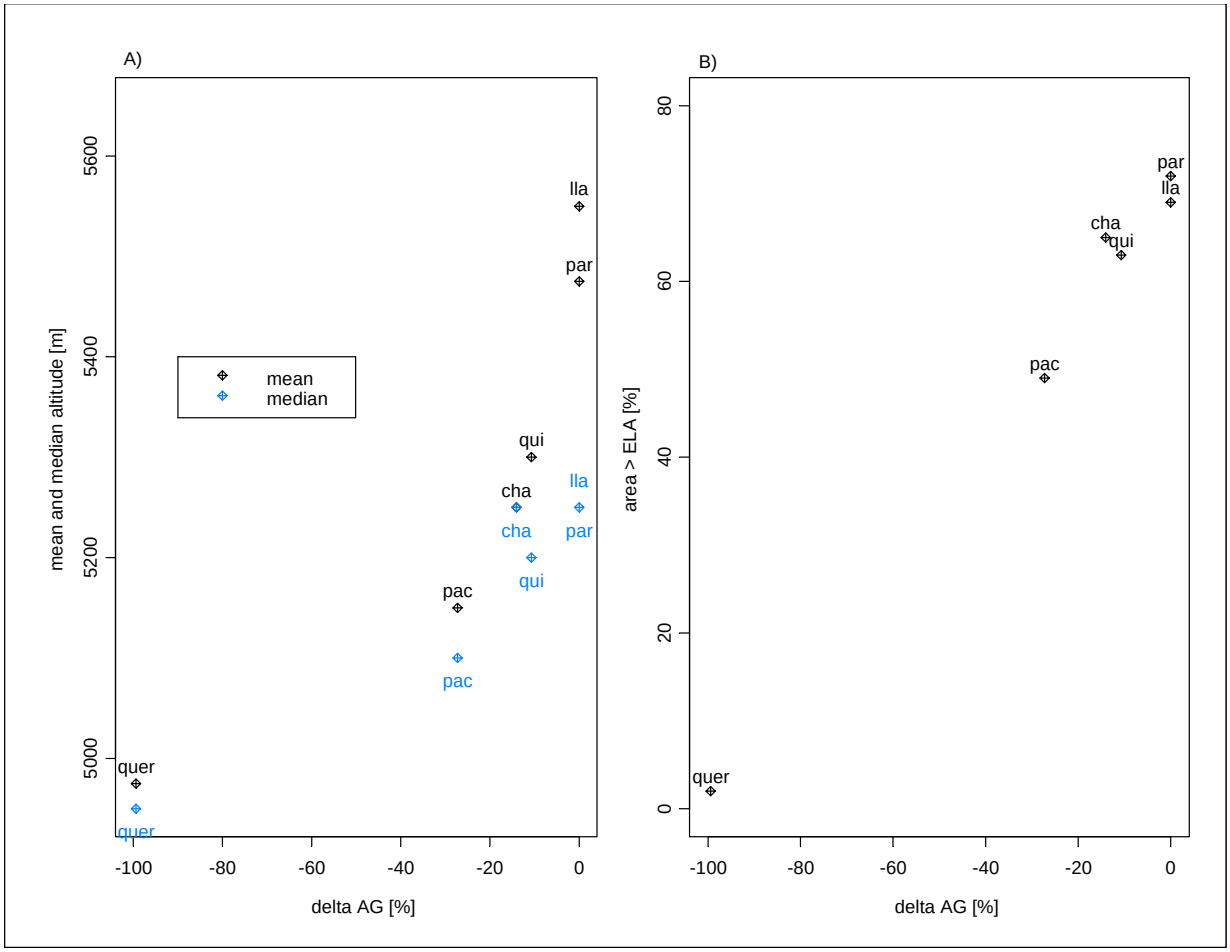

Figure 5.8: Relative change in glacier area (delta AG 1990) to reach steady-state glacier extent for mean climate conditions from 1961−1990 dependent on A) the arithmetic mean and median altitude of the glaciers in the individual catchments and B) on the percentage of glacier area above mean ELA (5100 m a.s.l.). The abbreviations for the single catchments are: par=Parón, lla=Llanganuco, cha=Chancos, qui=Quillcay, pac=Pachacoto, quer=Querococha.

A quite good relation can also be seen between the mean altitude of the glacier and the relative change in glacier area to reach steady-state glacier extent (Figure 5.8 A). The median altitude of the catchment (50% of the area below and above that altitude) seems not to be a suitable number to distinguish glaciers that are in balance or not as the median altitude of the glaciers in the region of Chancos with negative $\overline{B}$ is the same altitude as for both catchments that are in balance (Parón and Llanganuco; see Figure 5.8 A).The relative change in glacier area until the glaciers in the single catchments reach steady-state glacier extent is linear to the percentage of glacier area above *ELA* (Figure 5.8 B). This is somehow a relict of the ITGG-2.0 model that does not take into account any differences in aspect so far. The vertical mass balance profile is the same in all catchments and thus *AAR* has to be > 68 to be able to compensate glacier ablation with accumulation. As all catchments of interest are on

the western side of the mountain ridge and drain to the west the difference in aspect is not very crucial. All glaciers in the individual catchments show a very similar orientation to south, west and north. Additionally, it has to be expected that mean vertical mass balance profiles do not differ considerably on the west ridge of the Cordillera Blanca. This might be of concern when modelling glacier mass balances on the east, more humid ridge of the mountain group. For the mean climate conditions from 1961 – 1990 it can be stated that the mean area of the glacier and *AAR* have to be above 5450 m a.s.l. and 71 % to reach equilibrium conditions, respectively. The degree of imbalance in the catchments increases with the deviation from these values.

To explain why the 1990 glacier extent is not representing the steady-state extent in all catchments it is necessary to evaluate ice flow dynamics and response time of the glacier. In general, the steep slopes and short tongues of the glaciers in the Cordillera Blanca lead to a fast mass transport and thus a fast response on positive mass balances (cf. chapter 5.1). On the other hand, negative mass balance will not lead to an immediate retreat as the accumulation area still supplies the glacier tongue with ice from the former years. The flow rate of a glacier is highly dependent on ice thickness and slope of the glacier. Measurements of the ice flow dynamics have been performed for two glaciers in the Cordillera Blanca (Hastenrath and Ames, 1995; Ames and Hastenrath, 1996). The response time of the two glaciers is very different depending on the steepness of the glacier. Due to the high ice flow velocity on the steep glacier Uruashraju response time is comparable small with 15 years. Glacier Yanamarey is much smoother and thus ice velocity is lower and response time is calculated to be 40 −55 years (see also chapter 3.2). Additionally to the more favourable area altitude distribution, the glaciers in the region of Parón and Llanganuco are steeper than those in the other catchments. Their mean slope is 32 and 34 %, respectively. This means that ice flow velocity is relatively high and response time is short. In all other catchments mean slope of the glaciers is below 30 %. The combination of i) higher area altitude distribution and ii) higher ice flow velocity might explains why the glaciers in the catchments of Parón and Llanganuco already reached steady-state glacier extent in 1990 whereas the other catchments were still retreating.

Runoff predictions

Table 5.6: Change in annual total runoff q_T, glacier melt q_G, and direct runoff q_N for a new steady-state glacier extent for two IPCC climate change scenarios for the individual catchments as predicted for the years 2050 and 2080. A_G is the change in the glacier area relative to the steady-state glacier extent for mean climate conditions from 1961 – 1990. The catchments are listed from a high to low ratio of glacier area/total catchment.

	b1-low 2050 change [%]				a2-high 2050 change [%]			
	Δq_T	Δq_G	Δq_N	ΔA_G	Δq_T	Δq_G	Δq_N	ΔA_G
Parón	−1.2	−37.7	+32.1	−38.4	+1.5	−78.7	+75.5	−80.9
Llanganuco	+0.1	−37.6	+23.5	−40.8	+3.9	−61.4	+45	−67.5
Chancos	+1.5	−23.7	+11.9	−27.5	+5.5	−65.3	+34.7	−70.7
Quillcay	+0.7	−39.5	+11.7	−40.6	+5	−75.4	+27.5	−78.7
Pachacoto	+1.2	−65.6	+8.2	−65.9	+5.8	−99.5	+17.4	−99.6
	b1-low 2080 change [%]				a2-high 2080 change [%]			
	Δq_T	Δq_G	Δq_N	ΔA_G	Δq_T	Δq_G	Δq_N	ΔA_G
Parón	−1	−50.1	+43.9	−51.5	+4.4	−93.2	+94.8	−94.7
Llanganuco	+0.6	−45.3	+29.1	−49.3	+7.2	−71.4	+57.1	−78.1
Chancos	+2.2	−31.6	+16	−36.2	+8.7	−86.1	+48	−89.2
Quillcay	+1.3	−47.2	+14.7	−49	+8.4	−89.9	+36.3	−92.1
Pachacoto	+1.9	−75.6	+10.2	−76.7	+9.5	−100	+22	−100

The portion of glacier melt that contributes to total runoff is dependent on the percentage of glacier area in the individual catchments and increases with increasing percentage (see also chapter 4.1.1). As stated above the glaciers in the catchment of Querococha are close to vanish and will not be considered anymore. In the catchment of Parón (40.9 % glacierised) annual glacier melt amounts to 43.8 %, in the catchment of Pachacoto (9.6 %) it makes up only 8.5 % of total runoff. Thus, any

changes in the amount of glacier melt effects runoff in the individual catchments very differently.

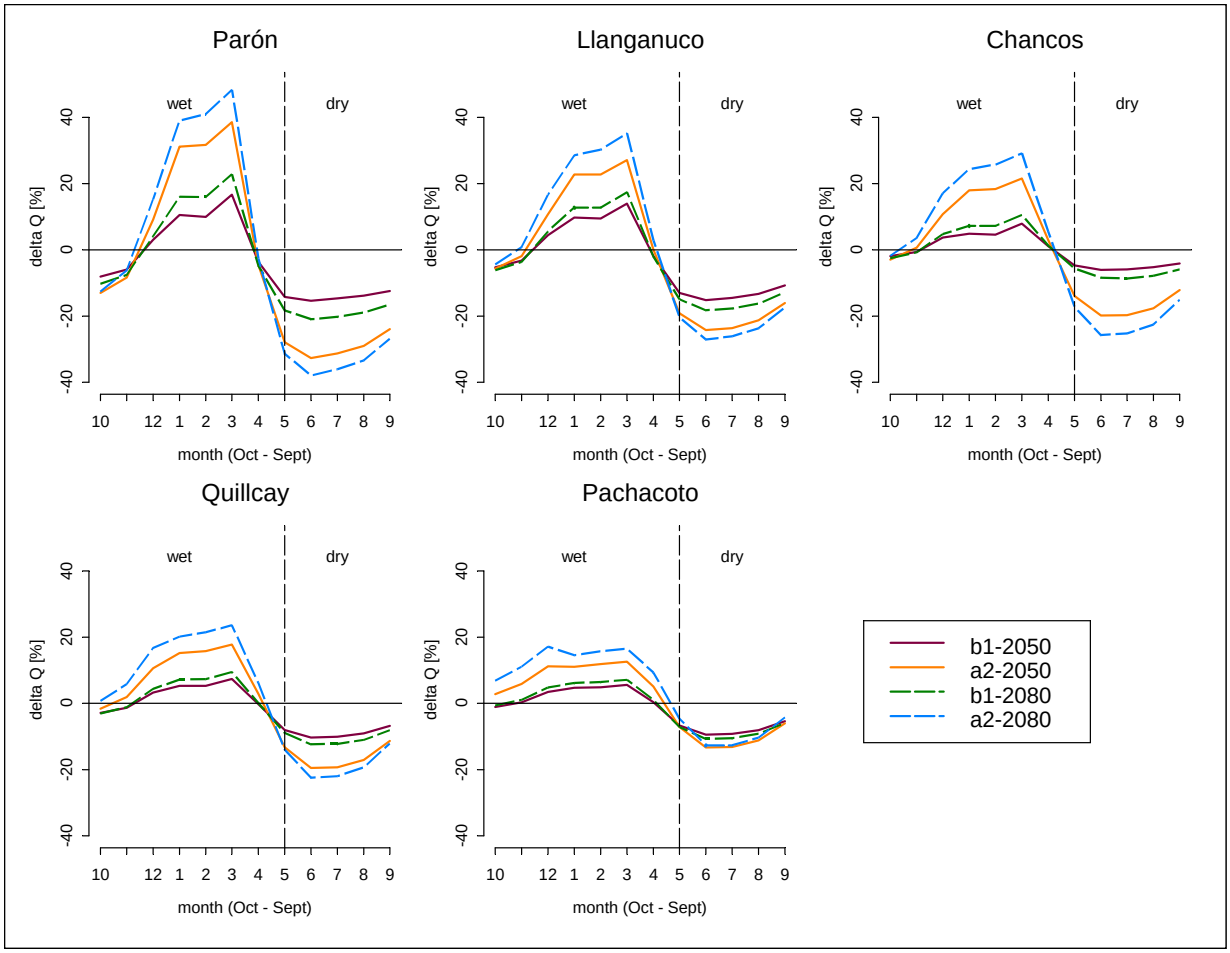

Figure 5.9: Predicted monthly relative change in total runoff (delta Q) for the two IPCC climate chance scenarios in 2050 and 2080 in the different catchments.

The mean annual change in total runoff $\Delta\ q_T$, glacier melt $\Delta\ q_G$, and direct runoff $\Delta\ q_N$ predicted for the four model runs in the five remaining catchments is summarised in Table 5.6. Additionally, the reduction in glacier area for the new steady-state glacier extent $\Delta\ A_G$ is listed with respect to the 1961 – 1990 steady-state glacier extent. Total annual runoff remains almost unchanged for the b1-low scenarios (−1.2 – 2.2 %, Table 5.6) and changes only minor with the a2-high model runs (−1 – 9.5 %). This is due to the compensating effect of increased direct runoff and reduced glacier melt that balance the amount of annual runoff. For the b1-low scenarios glacier area is reduced by 27 – 66 % and glacier melt decreases 24 – 66 % in 2050. The predicted changes until 2080 are roughly 10 % higher. q_N will increase 8 – 32 % until 2050 and 10 – 44 % until 2080. The increase in q_N is caused by a combination of higher amounts of total precipitation and the increase of the glacier

free area in the catchment (A_N). Thus, the change in q_N is also influenced by the area altitude distribution of A_N as precipitation increases with altitude. For the higher climate change scenarios a2-high the change in all runoff components is predicted to be app. double as high as for the lower scenarios (Table 5.6). The glaciers in the Pachacoto region will even vanish.

Looking at the differences between the single catchments it is noteworthy that the highest change in the percentage of q_G and, accordingly, the lowest change in q_N, both concern the runoff in Pachacoto which is the less glacierised catchment. The lowest change in q_G is not as expected in the catchment of Parón with highest percentage of glacier area but in the higher catchments of Chancos (b1-low) and Llanganuco (a2-high). Still, as the contribution of glacier melt to total runoff is much higher in catchments with high percentage of glacier area the absolute change in runoff is a multiple of that in catchments with only little glacier area which is obvious when considering the change in the seasonal cycle of total runoff.

Although mean annual total amount of runoff is almost unchanged it is, however, crucial when looking at the change in the seasonal cycle. Figure 5.9 shows the predicted change in total runoff relative to the mean 1961 – 1990 runoff for each month separately. The Figure clearly shows that runoff increases during the wet and decreases during the dry season in all catchments. The maximum change for both seasons is predicted for the catchment of Parón and decreases with decreasing percentage of glacier area (see also Appendix E, Figure E.3, Table E.1).

During the core wet season (JFM) the increase of q_N in the region of Parón is predicted to be 27 – 63 mm until 2050 and 37 – 78 mm until 2080 (see also Appendix E, Figure E.1 and Table E.1). The amount of glacier melt decreases 12 – 21 mm until 2050 and 14 – 26 mm until 2080, respectively (Appendix E, Figure E.2). In the catchment of Pachacoto the change in q_N is less than half, q_G is less than a fourth part. The highest increase in total runoff is predicted in March when precipitation is highest. This has to be expected as precipitation also increases most as a matter of course. Additionally, the glacier free area increases with the retreat of the glacier and the reduction in glacier melt is minor.

During the dry season the decrease in total runoff is highest which has a crucial impact on the availability of water in the Rio Santa valley. Again the change is most dramatic in catchments with high percentage of glacier area and decreases with the glacierised area in a catchment. The increase in q_N is minor in all catchments (see Appendix E, Figure E.1). Thus, the decrease of q_G is hardly covered and is responsible for the lack in total runoff. In the catchment of Parón q_G decrease by 13 – 28 mm until 2050 and 17 – 33 mm until 2080, respectively (see Appendix E, Figure E.2, Table E.1). In the region of Pachacoto q_G is only reduced by 4 – 7 mm.

Only in the intermediate months (April, October, November) the change in direct runoff and runoff from glacier melt is more balanced and total runoff will not change considerably.

5.4 Energy balance investigations on a tropical glacier tongue

The amount of glacier melt that will contribute to runoff is the result of the energy availability on the glacier surface. Thus, in order to better understand the processes that drive glacier melt the energy balance on the tongue of Glacier Artesonraju (4850 m a.s.l.) is studied in detail. An energy balance station (*EBS*) was installed on March, 12th 2004 in the ablation area of Glacier Artesonraju at 4850 m a.s.l. (Figure 2.1, Appendix C, Figure C.6). Here the data are analysed from first of April 2004 until end of March 2005 to characterise a full year of measurements. Some data gaps in the records of air temperature at the *EBS* were filled using the data from a nearby radiation balance station (*RBS*) and an automatic weather station (*AWS*) outside the glacier at the same altitude (see Appendix D). A statistical analysis is made for hourly values as well as for daily means to obtain the daily and seasonal variations of the measured and derived components. First, the climate conditions at the glacier surface are shown by evaluating measured wind speed, air temperature, and vapour pressure (chapter 5.4.1). Wind direction is analysed separately for each month. The full energy balance is calculated as described in chapter 4.4. and analysed in chapter 5.4.2. Finally, calculated net ablation is compared to net mass balance obtained from ablation stake measurements, and glacier melt is compared to runoff (chapter 5.4.3). For some additional, more detailed Figures see Appendix F.

5.4.1 Climate conditions at the glacier surface

A summary of the statistical values for each of the hourly measurements as well as for daily means is given in Table 5.7. Over the entire period mean air temperature is 0.6 °C, mean vapour pressure is 4.8 hPa, mean wind speed is 3.2 m s^{-1}. The frequency in wind direction is analysed on a monthly scale. Overall the wind direction is clearly indicating easterly and northeasterly currents.

In Figure 5.10 the daily cycle of measured air temperature, wind speed and calculated vapour pressure is shown over the whole investigation period from April

2004 to March 2005. Beside the arithmetic mean daily cycle (crosses in Figure 5.10) the plot shows the upper and lower quartile (orange box), the 90 % quantiles as well as the maximum and minimum values of each hour throughout the day. A first view already shows that air temperature has a clear daily cycle whereas vapour pressure and wind speed show a wide range of values at almost each time of the day.

Table 5.7: Statistical mean, median (50%), standard deviation (σ), minimum and maximum, and lower and upper quartile (25 and 75 %, respectively) of measured wind speed, air temperature, and vapour pressure at the tongue of Glacier Artesonraju (4850 m a.s.l.) from April 1st 2004 to March 31st 2005. First line: hourly measurements; second line: daily means.

	Mean	Median	σ	25 %	75%	Minimum	Maximum
wind speed [m s^{-1}]	3.17	2.72	2.18	1.33	4.74	0.00	11.05
	3.17	2.77	1.62	2.01	4.07	0.60	8.56
air temperature [°C]	0.71	0.68	2.11	−0.48	2.02	−7.70	9.71
	0.71	0.75	1.08	−0.04	1.45	−2.24	3.85
vapour pressure [hPa]	4.84	5.01	1.03	4.24	5.61	0.61	8.78
	4.84	5.05	0.85	4.24	5.50	1.85	6.59

The daily cycle in air temperature is strongly influenced by the cycle of the sun. During daytime (10 – 18 local time (l. t.)) air temperature is mainly positive (>90 %), negative air temperature is measured chiefly after midnight until sunrise. Maximum air temperature is reached just after midday at 13 – 15 l. t., the minimum occurs in the early morning hours at 5 – 7 l. t. (Figure 5.10). The range of possible air temperatures measured at the surface of Glacier Artesonraju is −7.7 – 9.7 °C, 50 % of the hourly measurements are within −0.5 – 2 °C (Table 5.7). The mean daily amplitude of air temperatures is 4.2 °C. The minimum daily amplitude in air temperature is measured in the core humid season in March (2.9 °C), but also the highest amplitude (5.6 °C, November) occurs in the humid season (see Appendix F, Figure F.2) and not as expected during the dry season. In addition to the strong cooling during the clear sky nights in the dry season the angle of the sun is also lowest. Thus the warming during the day is weaker and the amplitude in air temperature stays low.

The daily cycle in vapour pressure (*e*) is dominated by the cycle in air temperature and thus shows the same pattern. Still, the daily cycle is less pronounced as the maximum of air humidity is measured during the night and thus smoothes the influence of air temperature on the daily cycle of vapour pressure. It ranges from 0.6

– 8.8 hPa, 50 % of the time e is above 4.2 and below 5.6 hPa (Table 5.7). The mean daily amplitude of e is 1.2 hPa. The difference in the mean cycle of e throughout the year is very small and mainly caused by a shift to higher/lower values (see also Appendix F, Figure F.4). The lowest amplitude of e is measured in March (0.8 hPa), the highest in January (1.5 hPa).

Wind speed peaks just before midday (10 – 11 l. t.) and the minimum wind speeds occur in the early evening (20 – 21 l. t.). Hourly measurements of wind speed vary from 0 – 11 m s^{-1}, 50 % of the time wind speed is between 1.3 – 2.7 m s^{-1}. The mean daily amplitude in wind speed is 2.3 m s^{-1}. During dry months, this amplitude increases, whereas during the humid months wind speed is almost constant throughout the day (see also Appendix F, Figure F.1). The maximum mean daily amplitude in wind speed is measured in July (3.4 m s^{-1}), in March wind speed is more constant throughout the day with an amplitude of only 1.6 m s^{-1}.

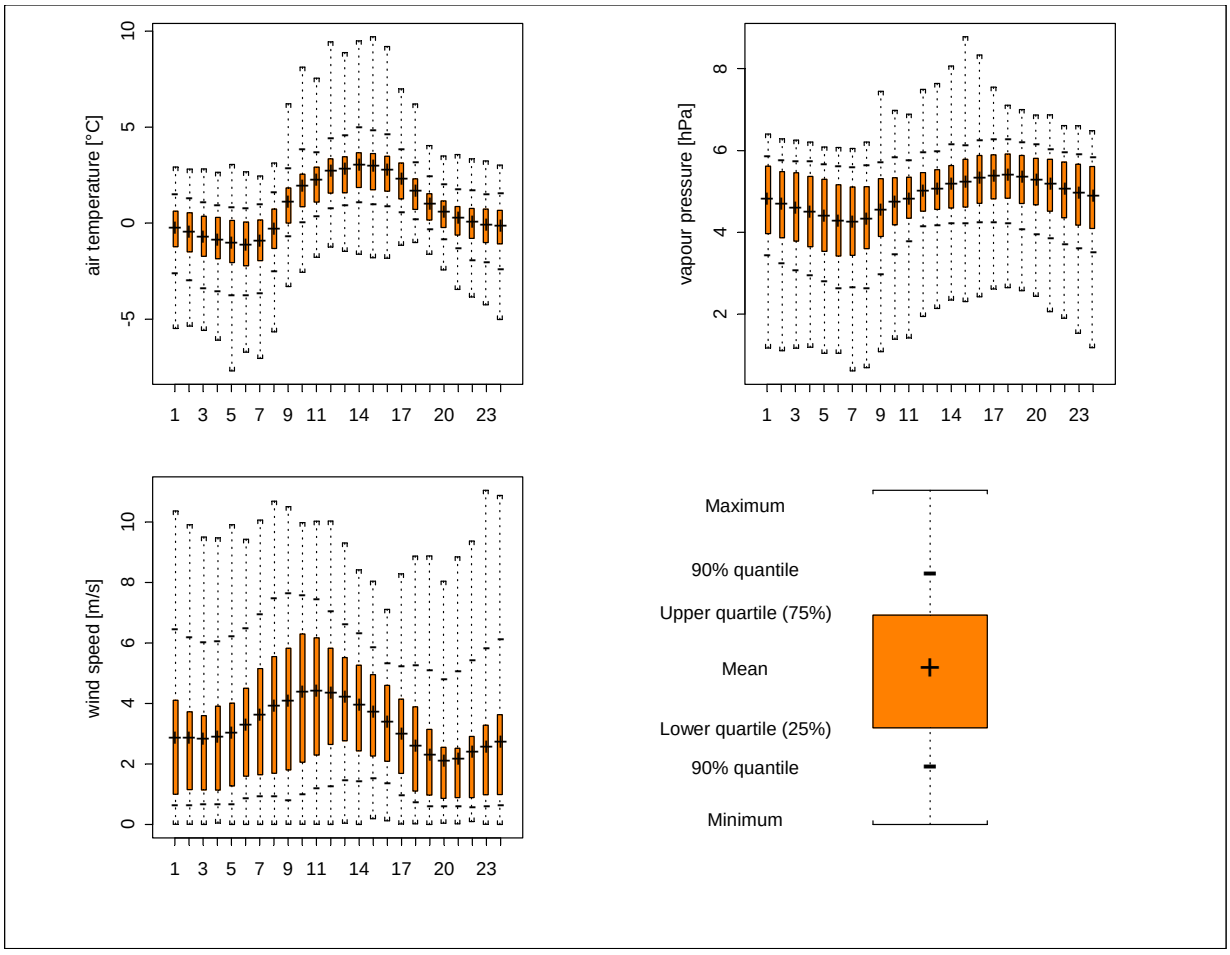

Figure 5.10: The daily cycle in measured air temperature, wind speed, and vapour pressure at the surface of Glacier Artesonraju (4850 m a.s.l.). The graph shows the arithmetic mean (cross), limits of the lower and upper quartile (orange box, 25 and 75 %), 90 % quantile (vertical bar), and maximum and minimum values.

To characterise the seasonal pattern in wind speed, air temperature, and vapour pressure daily mean values as well as daily maximum and minimum (7 day running mean) values are shown in Figure 5.11. Wind speed is highest in the dry season, whereas air temperature and vapour pressure show lower values at this time of the year.

Mean wind speed during the core dry (JJA) and core humid (DJF) season is 4.7 and 2.4 m s^{-1}, respectively (see also Appendix F, Table F.1). Daily mean wind speed varies from 0.6 – 8.6 m s^{-1} throughout the year, which is 73 % of the variability of hourly measurements. The seasonal variability is 3.4 times higher than the mean daily amplitude. In general, the months with high wind speed (JJA) also show the highest variability. Most stable wind conditions are clearly measured in November, lowest wind speed is measured in March (see also Appendix F, Figure F.14).

Daily mean negative air temperature is more or less only measured in the core dry season, the core humid season is dominated by air temperatures clearly above 0 °C. Seasonal means are −0.5 and 1.5 °C, respectively. The lower air temperature during the dry season has to be expected due to the strong cooling during the clear sky nights. Still, a considerable increase in the amplitude of daily maximum and minimum air temperature is not visible. The lower air temperature during the dry season results much more from a combination of lower air temperature during the night and, at the same time less warming during the day (see Appendix F, Figure F.2). Most variable daily mean air temperatures occurred in January, March and December, which might be caused by a frequent alternation of cloudy and clear sky days. The lowest variability in air temperature from day to day can be seen in October and November (see also Appendix F, Figure F.14).

Mean vapour pressure during the dry and humid season is 3.9 and 5.4 hPa, respectively (see also Appendix F, Figure F.14). From November to end of March maximum daily *e* is frequently above 6.1 hPa, whereas during the dry period *e* never exceeds 5.1 hPa. The lowest variability of both, air temperature and vapour pressure, is found in October, the highest variability from day to day is measured in January. (see also Appendix F, Figure F.14).

On the face of it, air temperature and vapour pressure show the same seasonality with lower values during the dry and higher values during the humid season. Still, if taking a closer look on the difference between daily amplitudes and daily mean values it is obvious that this seasonality is much higher for vapour pressure than for air temperature. Daily mean values of air temperature over the whole investigation period range from −2.2 – 3.9 °C, which is only 10 % of the variability of hourly values and 40 % of the mean daily amplitude. In contrast, mean daily vapour

pressure varies from 1.9 – 6.6 hPa, which is almost 60 % of the range of hourly values and 3.9 times higher than the mean daily amplitude of *e*. However, these differing patterns in air temperature and vapour pressure have to be expected for a tropical investigation site and confirm that the seasonality in the tropical Cordillera Blanca is mainly driven by humidity related variables.

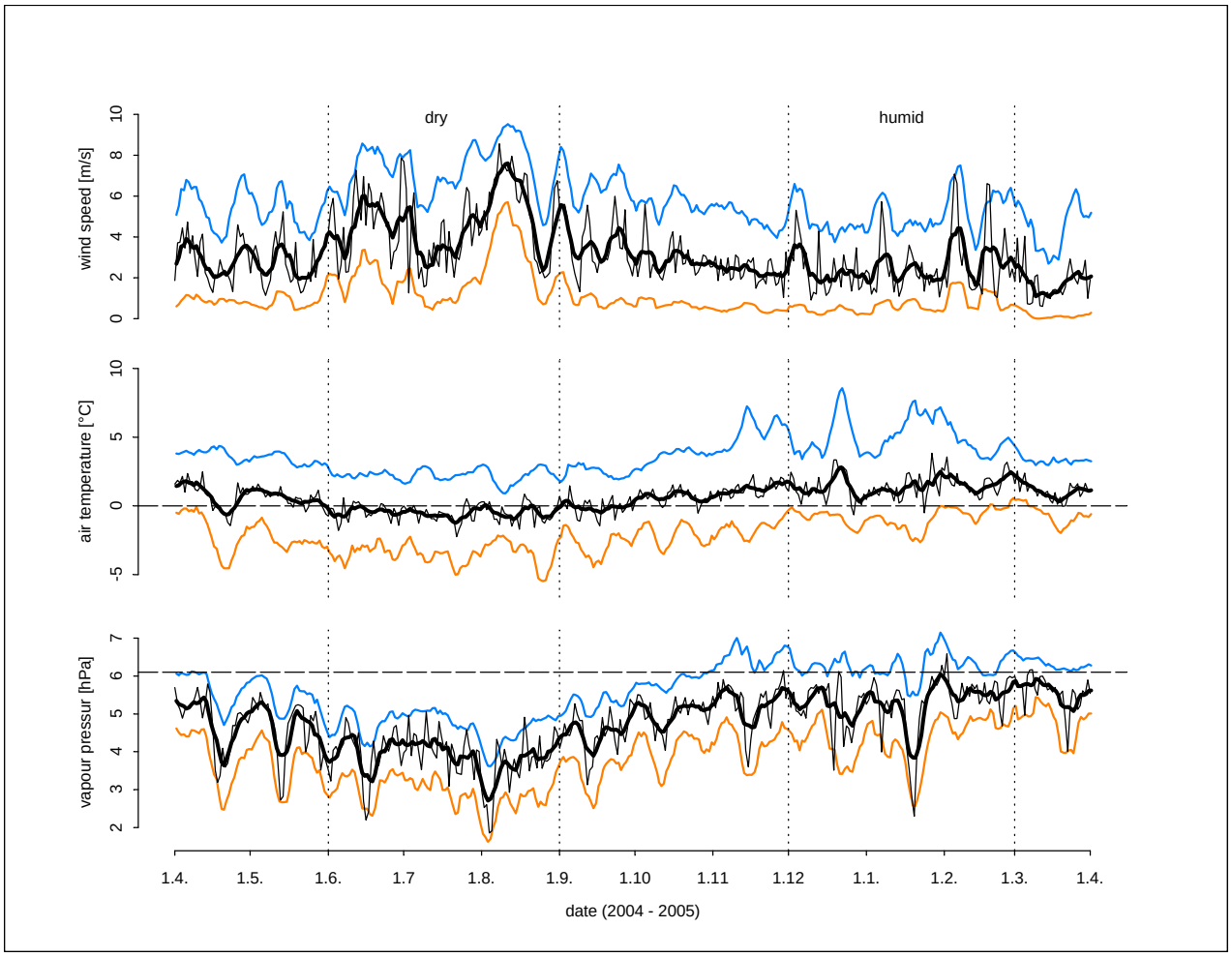

Figure 5.11: Daily mean wind speed, air temperature, and vapour pressure measured at the surface of Glacier Artesonraju (4850 m a.s.l.) from 1.4. 2004 – 31.03. 2005 (black lines). The blue, orange, and thick black lines are 7 day running means of the daily maximum, minimum, and mean values, respectively. Horizontal lines represent the 0 °C air temperature and the vapour pressure of a saturated glacier surface at melting point (6.1 hPa), respectively.

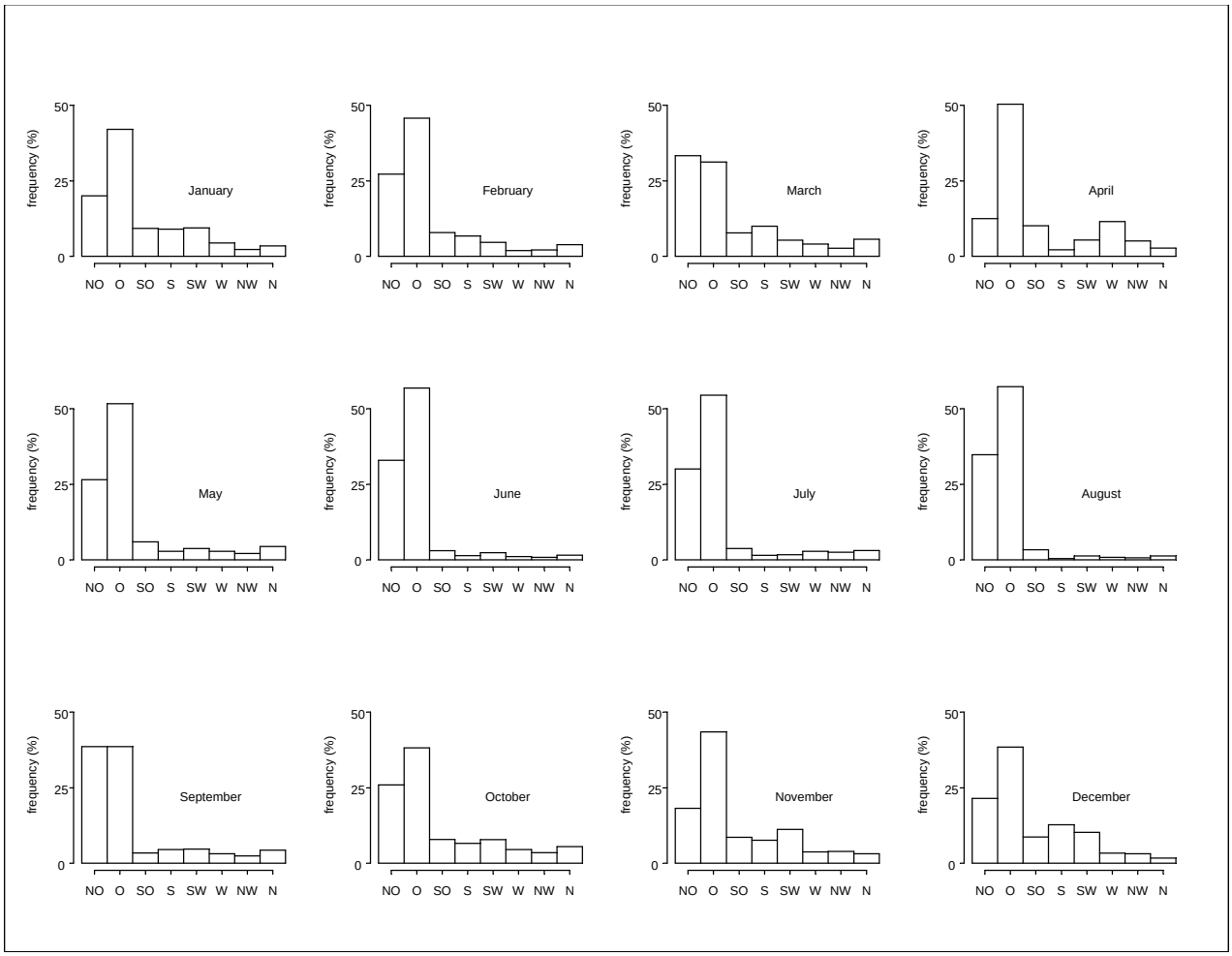

Figure 5.12: Frequency of wind directions (45 ° bins) measured at Glacier Artesonraju (4850 m a.s.l.) for each month from April 2004 – March 2005.

The frequency in wind direction for each month separately is shown in Figure 5.12. The wind direction measured at the energy balance station on Glacier Artesonraju is clearly dominated by easterly and northeasterly currents throughout the year. Still, we can detect changes in the wind direction frequencies for wet and dry month. In the dry month (May to August) more than half of the time wind comes from east, northeast directions are still very presence and occur during >25 % of all hours. The remaining wind directions are of minor importance (Figure 5.12). This confirms with analyses from Georges (2005) who found dominating east trajectories in the lower troposphere (850 hPa) in the Cordillera Blanca for dry (<10mm) and moderately dry (10−50mm) months during the dry season (JJA) and the intermediate season (AM). During the humid season (JFM) and the moderately humid intermediate season (SOND) trajectories in the lower troposphere converge over the Cordillera Blanca from north to northeast. This can only partly be confirmed by measurements in March, where northeast currents slightly dominate. A balance between northeast and east wind direction frequency was measured in September, in all other months

easterlies still dominate. Glacier Artesonraju is mainly west orientated and thus the katabatic glacier wind is expected to come from east. Consequently, the katabatic glacier wind seems to overlay the general wind direction at the glacier surface and may explain the high occurrence of easterly wind throughout the year. If high wind speeds (>5.5 m s^{-1}) are measured, 98.7 % of the wind direction is northeast or east. A high dominance of east and northeast currents (>96 %) is also true for low air temperature (<−1.4 °C) and low vapour pressure (<3.8 hPa).

5.4.2 The energy balance at the glacier surface

The energy balance (*EB*) on the surface of Glacier Artesonraju is calculated as described in chapter 4.4. All energy fluxes, i.e. SW_{in}, SW_{out} (including albedo), LW_{in}, LW_{out}, and the turbulent fluxes *H* and *LE* are discussed separately. Their mean daily cycles are shown in Figure 5.13 and 5.14, Table 5.8 gives an overview of their statistical measures.

Table 5.8: Statistical mean, median (50%), standard deviation (σ), lower and upper quartile (25 and 75 %, respectively), and minimum and maximum of the energy fluxes at the tongue of Glacier Artesonraju (4850 m a.s.l.) from April 1st 2004 to March 31st 2005. First line: hourly values; second line: daily means.

	Mean	Median	σ	25 %	75 %	Minimum	Maximum
SW_{in} [W m^{-2}]	230.67	7.67	340.73	0.00	409.09	0.00	1350.00
	230.67	225.57	64.91	178.06	276.72	110.02	406.21
SW_{out} [W m^{-2}]	109.96	5.33	169.01	0.00	184.44	0.00	948.50
	109.96	104.59	43.35	75.76	135.60	29.75	243.33
Albedo	0.54	0.54	0.22	0.34	0.73	0.11	0.90
	0.54	0.53	0.18	0.38	0.71	0.20	0.87
LW_{in} [W m^{-2}]	281.49	298.95	41.44	246.34	315.20	177.00	471.75
	281.49	293.60	34.28	255.95	309.98	199.07	341.70
LW_{out} [W m^{-2}]	309.73	315.64	9.61	306.65	315.64	260.05	315.64
	309.73	311.21	5.48	306.20	314.40	291.71	315.64
H [W m^{-2}]	9.2	5.6	10.1	1.6	14.2	−17	75.6
	9.2	7.7	6.4	4.6	12.5	−0.4	37.5
LE [W m^{-2}]	−13.4	−5.4	18.7	−1.1	−20.8	18.7	−148.6
	−13.4	−8.9	13.2	−3.9	−17.6	6.2	−76.8

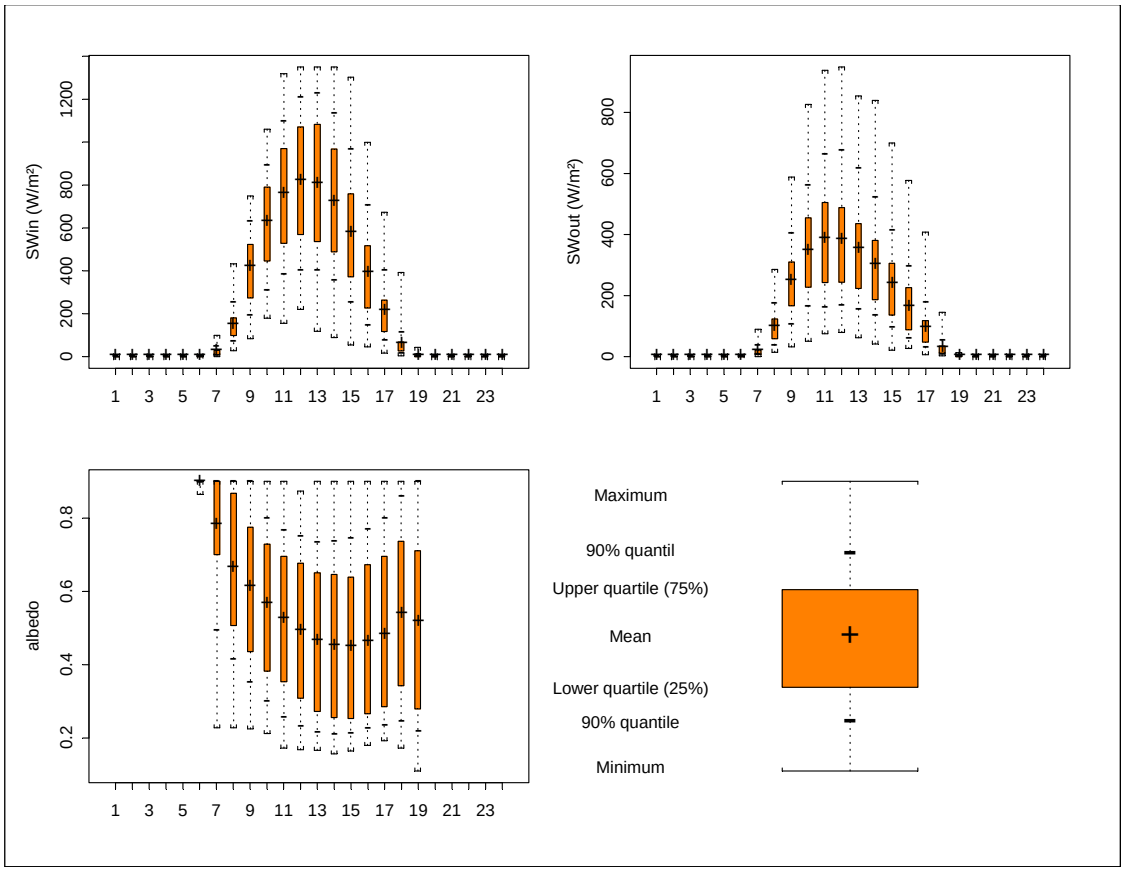

Figure 5.13: The daily cycle in measured SW_{in}, SW_{out}, and albedo at the surface of Glacier Artesonraju (4850 m a.s.l.). The graph shows the arithmetic mean (cross), limits of the lower and upper quartile (orange box, 25 and 75 %), 90 % quantile (vertical bar), and maximum and minimum values.

The shortwave radiation terms, SW_{in} and SW_{out}, show a very high hourly variability (σ = 341 and 169 W m^{-2}) as they are both zero during the night (Table 5.8, Figure 5.13). They range from 0 – 1350 and 0 – 949 W m^{-2}, mean values are 231 and 110 W m^{-2}, respectively. Daily maximum SW_{in} is measured at 12 – 13 l. t., for SW_{out} the maximum value already occurs at 11 – 12 l. t.. Throughout the year the daily cycle in SW_{in} is almost constant (see Appendix F, Figure F.6). The lowest daily maximums are measured from May to August when the sun is in zenith on the northern hemisphere, maximum amplitudes are reached from September to February. The minimum daily amplitude of SW_{out} is measured from April to June, the maximum in September (see Appendix F, Figure F.7). Mean albedo during the investigation period is 0.54, hourly values range from 0.11 – 0.9. The daily cycle of albedo shows maximum values in the morning hours, which then decrease until 14 – 15 l. t. and rise again (Figure 5.13). This decrease in albedo after sunrise might be an artefact of measurements as the instruments are mounted horizontally (Ohmura, 1981). Still, after a slope correction for albedo measurements on Glacier Zongo

(Sicart et al., 2001) the daily cycle also showed this maximum in the morning. The rise in albedo after 15 l. t. might be caused by frequent snowfall events in the late afternoon: 64 % of all precipitation events occur from 15 – 24 l. t.. This pattern of the daily cycle in albedo is very similar throughout the year and only changes in amplitude (see Appendix F, Figure F.5). Constantly high values and thus minor amplitude in the daily cycle of albedo is solely measured in July. Contrary, in March almost the full range of albedo can occur each time of the day.

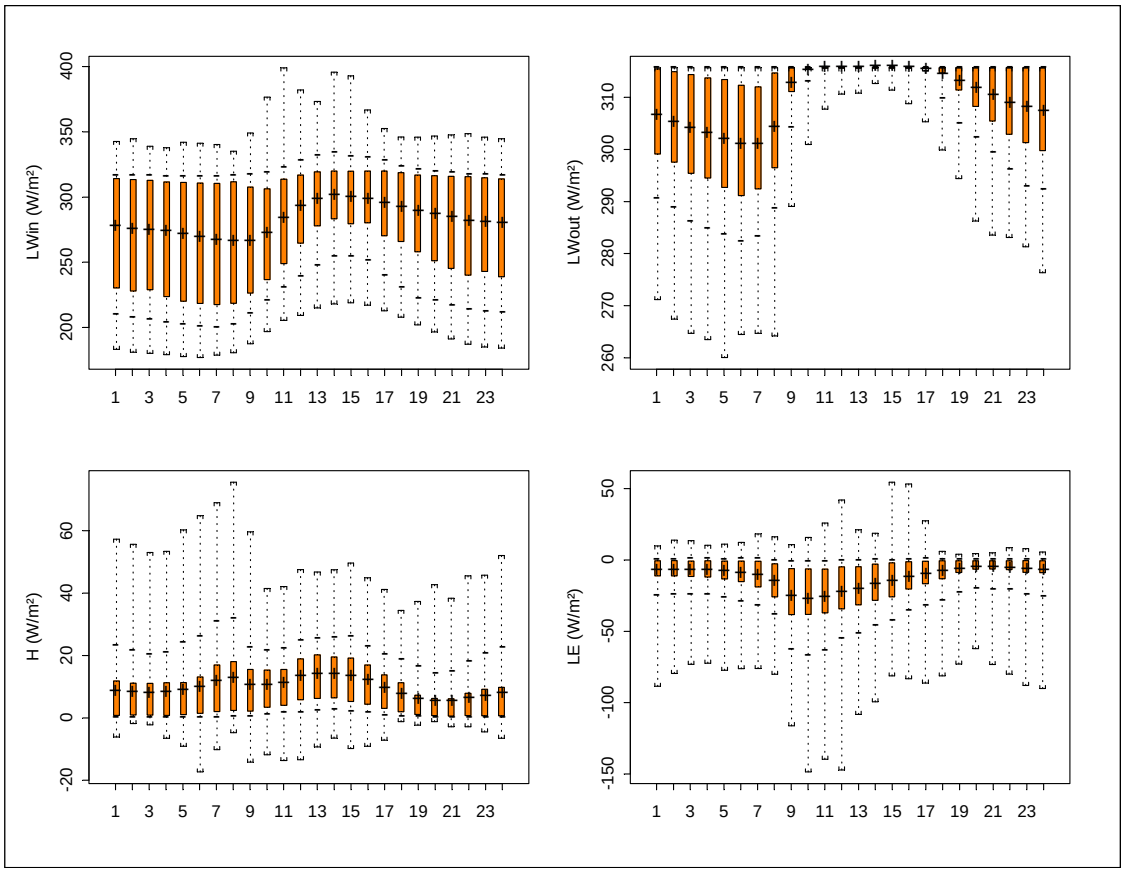

Figure 5.14: The daily cycle in measured LW_{in}, LW_{out}, and the calculated sensible (H) and latent (LE) turbulent fluxes at the surface of Glacier Artesonraju (4850 m a.s.l.). The graph shows the arithmetic mean (cross), limits of the lower and upper quartile (orange box, 25 and 75 %), 90 % quantile (vertical bar), and maximum and minimum values. For legend see Figure 5.13.

The longwave radiation terms LW_{in} and LW_{out} vary from 177 – 472 and 260 – 316 W m^{-2} (Table 5.8), respectively. The daily cycle of LW_{in} is characterised by slightly higher values around noon with low variability and lower values during night time with higher variability (Figure 5.14). This is caused by higher air temperatures and vapour pressure which both increase LW_{in} during the day. The mean daily amplitude is 35 W m^{-2} with a variability throughout the year from 25 W m^{-2} in March to 55 W m^{-2} in September (see Appendix F, Figure F.8). The mean daily cycle of LW_{out}

also shows higher values during the day and lower values during the night. The mean amplitude in the daily cycle is 15 W m^{-2} and varies from 5 W m^{-2} in March to 30 W m^{-2} in July. The same months also show the longest and shortest period when melting occurs: from 10 – 18 l. t. in March and from 12 – 15 l. t. in July (see Appendix F, Figure F.9).

Hourly values of sensible heat flux *H* vary from −17 to 75.6 W m^{-2} (Table 5.8), the mean daily amplitude is 9 W m^{-2}. Negative *H* occurs when surface temperature is higher than air temperature which is the case during 5 % of the hourly measurements. The mean daily cycle of *H* is characterised by two maxima; the first just after sunrise (9 – 11 l. t.) and the second around midday (12 – 14 l. t., Figure 5.14). The first maximum is even higher than the second in months with very low surface temperature during the night (June – September). This is due to the fast increase in air temperature after sunrise which leads to a huge gradient between the still cold surface and the air, and thus a high sensible heat flux. From February to March, when surface temperature is close to melting conditions even during the night, this maximum is not visible (see also Appendix F, Figure F.10).

Latent heat flux *LE* varies from 19 – −149 W m^{-2} (Table 5.8) which implies the occurrence of accumulation by condensation (deposition). Positive *LE* (12 % of the hours) mainly occurs from October to February when the saturation of the atmosphere is high. The mean daily maximum of *LE* always occurs before midday (9−11 l. t., Figure 5.14). At this time wind speed is already high and vapour pressure still low (see also Figure 5.10). During the night the turbulent exchange of latent heat is small due to low gradients and wind speed. The mean daily amplitude of *LE* is 23 W m^{-2} and varies from 8 W m^{-2} in March to 48 W m^{-2} in August (see Appendix F, Figure F.11).

Compared to the mid latitudes the seasonal cycle of SW_{in} is minor. Nevertheless, it is the most variable energy flux at this tropical glacier site with maximum amplitude of monthly means of 71 W m^{-2} (see also Appendix F, Table F.2). During the dry season SW_{in} in reduced, highest values are measured in November and February (Figure 5.15). This is a matter of course from the position of the sun at this time of the year. In July the sun is at its northern turning point and thus stands in a lower angle over the Cordillera Blanca whereas in December the sun is closer to its zenith. In March and September, when the sun crosses the Cordillera Blanca, precipitation is high and thus cloud cover decreases the energy supplied by solar radiation (Figure 5.15).

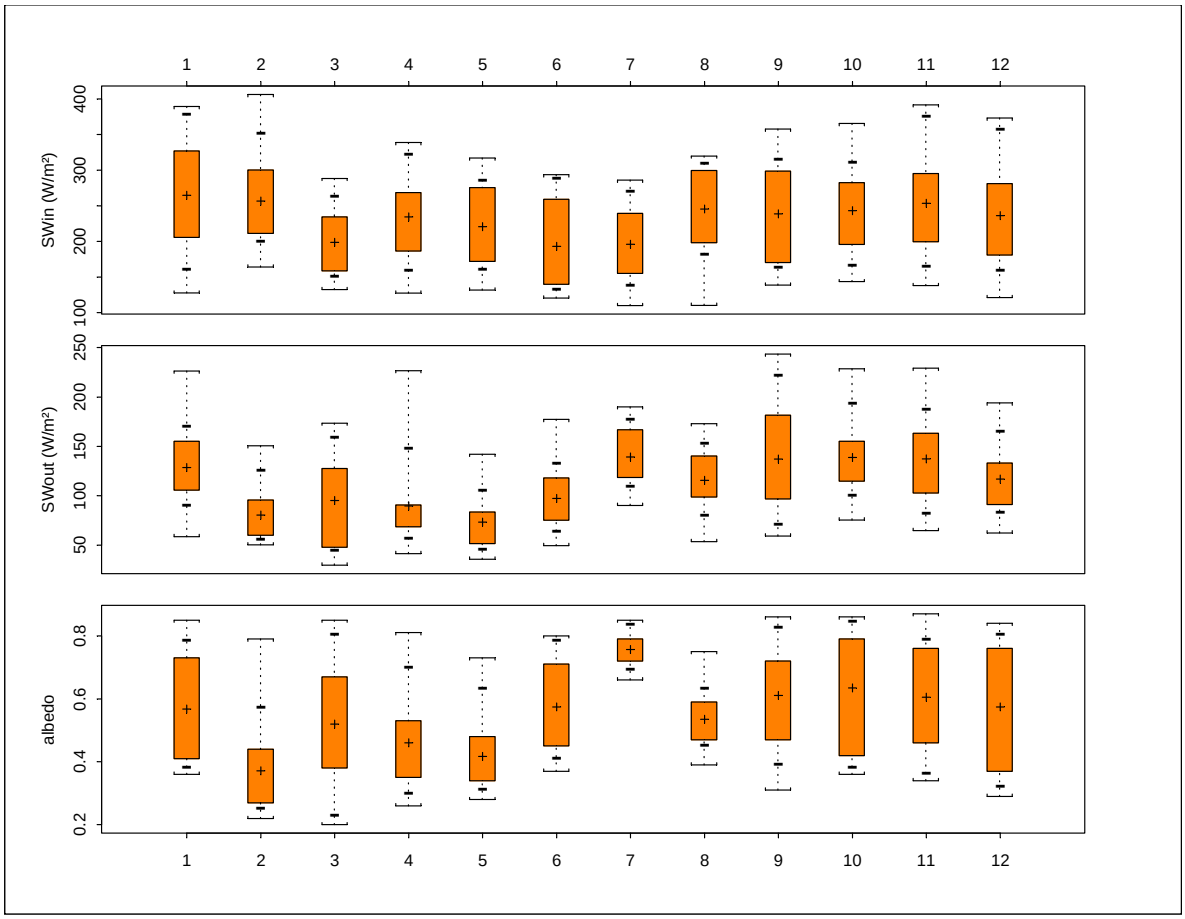

Figure 5.15: Statistics of daily means of the SW radiation terms and albedo measured at the EBS at the surface of Glacier Artesonraju (4850 m a.s.l.) for each month. The graph shows the arithmetic mean (cross), limits of the lower and upper quartile (orange box, 25 and 75 %), 90 % quantile (vertical bars), and maximum and minimum daily values. For legend see Figure 5.13.

Albedo (SW_{out}/SW_{in}), which controls SW_{out}, is constantly and remarkable high in July with daily means always above 0.6 and a mean of 0.75. In contrast, in February albedo is mainly below 0.57 with a mean of only 0.34 and huge differences from day to day. This may imply that in February most precipitation fell as rain and thus decreases albedo whereas snowfall kept albedo constantly high in July. This is only partly true as will be demonstrated with Figure 5.16. The left picture shows a typical day during the dry season, the right picture is representative for the surface conditions after a snowfall event during the wet season. It is obvious, that albedo is much higher in the first case than in the latter. This is mainly due to the increased sublimation which dries out the snow surface and thus it appears whiter. A typical situation during the wet season is that a few centimetres of wet snow fall during the night and already melt during the morning hours. This leads to a very wet, dark surface and thus low albedo. Nevertheless, this does not explain why albedo is much

higher in July than in June and August when sublimation is higher. Thus, only an intense and dry snowfall event at the end of June can explain this constantly high albedo in July. Indeed, albedo substantially rises in the night from 29.−30. June which indicates a snowfall event. The still high sublimation reduced glacier melt and thus the dry snow cover could last over a long time period. Minor snowfall events that also occurred in June and August increased albedo only over a few days. Still, albedo did not reach such low values as during the wet season.

Figure 5.16: EBS on Glacier Artesonraju (4850 m a.s.l.) at 11:30 a.m. The left photo is taken by Irmgard Juen during a dry period in August 2005. The right Photo is taken by Robert Galliere after a snowfall event during the night in March 2004.

Mean daily LW_{in} varies from 200 – 340 W m^{-2}, LW_{out} only from 290 – 315 W m^{-2}. In general, the variability from day to day is higher during the dry season when both fluxes are lower. In February and March both radiation terms are quite stable from day to day (Figure 5.17). During the core dry season energy supplied by LW_{in} is reduced due to lower atmospheric temperature and lower vapour pressure (compare chapter 5.4.1). The colder conditions (−1.9 °C, see Appendix F, Table F.1) decreases LW_{in} by 9 W m^{-2}. The decrease in atmospheric moisture content (−1.5 hPa) reduces cloudiness and thus atmospheric emissivity. It is responsible for a reduction of LW_{in} by 40 W m^{-2}. The lower surface temperature (−2.1 °C) during the core dry season reduces LW_{out} by 10 W m^{-2}.

The turbulent fluxes *H* and *LE* are considerably higher during the dry than during the wet season (Figure 5.17). This is quite obvious when considering the climate conditions (compare chapter 5.4.1). Both gradients between atmosphere and the glacier surface of temperature as well as vapour pressure are higher during the dry season. The gradient of air and surface temperature is 2.2 °C in the dry and 2 °C in the wet season. The gradient of vapour pressure is even more than doubled during the

dry season (1.1 vs. 0.5 hPa). Additionally, the higher wind speed during the dry season forces the turbulent exchange.

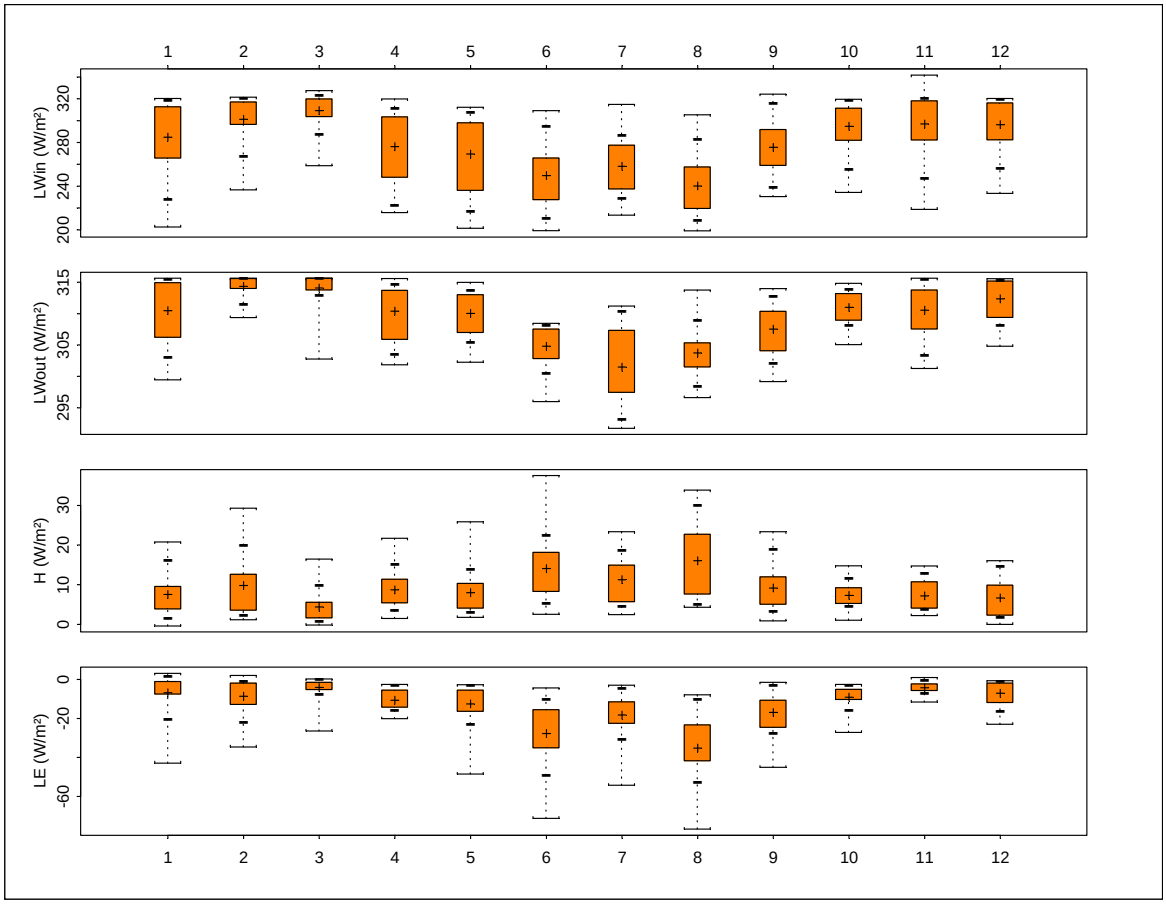

Figure 5.17: Statistics of daily means of the LW radiation terms measured at the EBS at the surface of Glacier Artesonraju (4850 m a.s.l.) and calculated turbulent fluxes (H and LE) for each month. The graph shows the arithmetic mean (cross), limits of the lower and upper quartile (orange box, 25 and 75 %), 90 % quantile (vertical bars), and maximum and minimum daily mean values. For legend see Figure 5.13.

Table 5.9: Mean monthly, seasonal and annual energy fluxes by shortwave and longwave net radiation (SW_{net}, LW_{net}) and the turbulent fluxes (H and LE). Albedo is derived from the ratio of SW_{in} and SW_{out}. The amount of melt (m) and sublimation (s) is calculated from the EB from station Artesonraju (4850 m a.s.l.) and calculated as monthly and annual sums, and seasonal mean monthly sum, respectively. The core dry and wet seasons are defined from June to August and from January to March, respectively.

Month	SW_{net} [W m^{-2}]	LW_{net} [W m^{-2}]	H [W m^{-2}]	LE [W m^{-2}]	*Albedo*	m [mm we]	s [mm we]
4	144.6	−34.3	8.7	−10.7	0.46	991.2	9.8
5	147.6	−40.7	8.0	−12.6	0.42	993.6	11.9
6	95.9	−55.1	14.1	−27.7	0.57	434.1	25.4
7	56.8	−43.4	11.3	−18.3	0.75	218.9	17.5
8	129.8	−63.6	16.1	−35.2	0.53	629.7	33.2
9	101.4	−32.1	9.2	−17.0	0.61	607.4	15.7
10	104.5	−16.3	7.3	−9.1	0.63	746.3	8.8
11	116.2	−13.6	7.2	−4.2	0.60	840.1	4.5
12	119.5	−16.1	6.7	−7.1	0.57	891.0	7.1
1	136.2	−25.6	7.5	−6.8	0.57	987.3	7.0
2	176.3	−13.2	9.8	−8.6	0.37	1249.5	7.7
3	103.5	−4.9	4.4	−4.1	0.52	829.3	4.0
dry	94.2	−54.0	13.8	−27.0	0.62	427.6	25.4
wet	133.9	−15.0	7.1	−6.7	0.51	989.3	6.4
$\Delta_{dry-wet}$	−39.7	−39.1	6.7	−20.4	0.11	−561.7	19.0
annual	119.4	−29.9	9.2	−13.4	0.55	9418,4	152,5
$\Delta_{max-min}$	119.5	58.7	11.7	31.0	0.38	1030.6	29.2

As a consequence of less energy supplied by SW_{in} and higher SW_{out} during the core dry season net shortwave radiation SW_{net} is reduced by −40 W m^{-2} compared to the core wet season (Table 5.9, see also Appendix F, Figure F.12, Table F.2). The very high albedo in July even reduces SW_{net} to only 57 W m^{-2}. Longwave net radiation LW_{net} is strongly negative during the core dry season whereas it is almost balanced in March (Table 5.9). The strong reduction of LW_{in} during the core dry season and the minor decrease in LW_{out} decreases LW_{net} by −39 W m^{-2} compared to the core wet season. Both turbulent heat fluxes are higher during the dry season (Table 5.9). Still, *LE* is more than double of *H* and the energy supplied by turbulent heat flux is lower by 14 W m^{-2} during the dry season. As a result, total energy that is available for melt is strongly reduced during the dry season compared to the wet season. Only 13.6 % of total annual glacier melt is due to melt during the core dry period. In contrast, glacier melt during the core wet season counts for almost a third (31.5 %) of total annual glacier melt.

5.4.3 Glacier mass balance, glacier melt and runoff

To evaluate the accuracy of calculated glacier melt and sublimation amounts from the *EB* it would be best to check it with measured ablation or, if accumulation is known, with net mass balance. Net mass balance can be measured with a stake drilled into the ice and a sensor that measures the distance to the glacier surface continuously, which also provides information about the amount of accumulation and thus net ablation can be subtracted. Still, the noise of the measurement makes it very difficult to filter out net ablation amounts. Ablation stakes that are measured periodically can, however, only give information about net mass balance as accumulation is also included. For the year where the *EB* on Glacier Artesonraju is analysed only ablation stake measurements carried out every month are available. In April 2005 a continuous measurement of net mass balance with an ultrasonic height sensor at the *RBS* 100 m below the site of the *EBS* (see also Appendix C, Figure C.6) is available over a period of 16 days. This period of high resolution data will now be used for a validation of calculated ablation amounts from the EB.

Net ablation at the *EBS* is calculated as the sum of glacier melt and sublimation. Accumulation is derived from precipitation measurements at the nearby *AWS* outside the glacier at the same altitude (Appendix C., Figure C.6) assuming that accumulation is equal to precipitation. In Figure 5.18 measured and calculated cumulative net mass balance are compared. Until April 9th (day 99) 2004 calculated and measured mass balances are in excellent agreement. After that, measured net mass balance is less negative than the calculated one. Over the 16 days net mass balance is calculated to be −507 mm we (melt 547, sublimation 6, precipitation 46 mm we, respectively). Measured net mass balance at the *RBS* is slightly less negative with −493 mm we although the station is 100 m lower than the *EBS*. The error is, however smaller than 3 % of the total net mass balance over the 16 days. The overestimation of calculated net mass balance could be due to i) underestimation of accumulation, and/or ii) overestimation of glacier melt. The assumption that accumulation is equal to precipitation might account for a part of the underestimation in accumulation. After day 99 precipitation is less frequent but more intense as during the first few days. This could easily cause an underestimation of measured precipitation because the error of measuring precipitation increases with the intensity of precipitation. Still, even if adding 10 % of precipitation for each of the possible error sources it can only partly explain the underestimation of net mass balance. Thus, the overestimation of calculated glacier melt can not be ruled out.

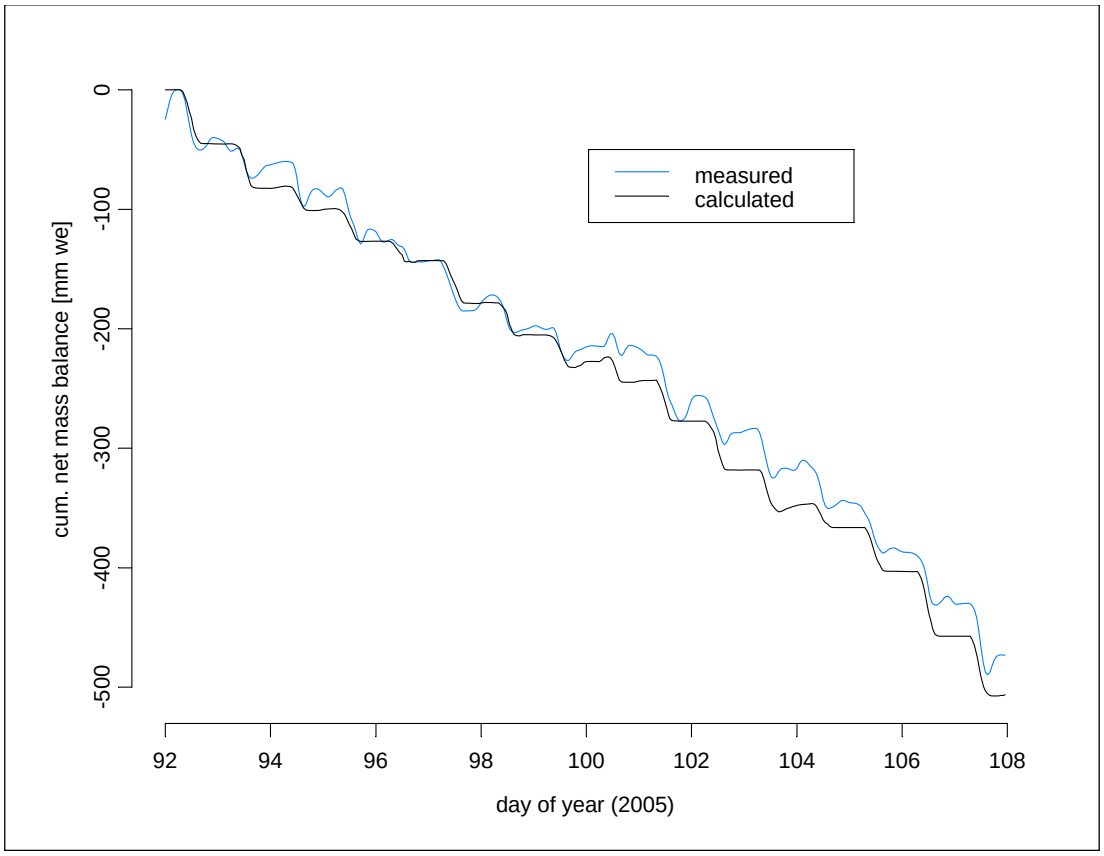

Figure 5.18: Measured (RBS, ultrasonic height sensor) and calculated cumulative net mass balance (EBS, melt + sublimation – accumulation) from 2. – 18. April 2005 at the tongue of Glacier Artesonraju (4750 and 4850 m a.s.l., respectively). Accumulation is obtained from precipitation measurements at the AWS outside the glacier (4850 m a.s.l.).

Over the whole year of investigation net mass balance can not be calculated as no information about accumulation is available. Thus, measured net mass balance can only be compared to net ablation calculated from the EB (Figure 5.19). Nevertheless, the agreement between measured net mass balance and calculated net ablation from the EB is very high with r^2=0.98. During the core dry period when melting is low net mass balance is only slightly negative (−8.6 mm we day^{-1}), during the core wet season when melting is highly effective net mass balance is strongly negative (−22 mm we day^{-1}, Figure 5.19). As a single energy balance term daily net mass balance rates correlate most with mean albedo during the same period (r^2= 0.67, n=12). The period with the strongest (least) negative mass balance (February 2005 and July 2004, respectively) clearly coincides with the lowest (highest) albedo (Figure 5.19). The same has been found at Glacier Antizana (Favier et al., 2004) and Glacier Zongo (Sicart et al., 2005). Still, the most significant change in the amount of available energy between the core dry and wet season is clearly from LW_{in} (−49 W m^{-2}, see also Appendix F., Table F.2). It is responsible for 45 % of the

difference in energy that is available for melt during the core dry season compared to the core wet season. This also agrees with findings at Glacier Zongo where Sicart et al. (2005) pointed to the importance of the variability in LW_{in} due to changes in the moisture content of the atmosphere and thus changes in the atmospheric emissivity. The increased latent heat flux (−20 W m^{-2}, Table 5.9) during the dry season accounts for 19 % of the decrease in energy for melt. Still, sublimation amounts at Glacier Artesonraju are comparable small for a tropical glacier and only half of the amount that was measured at Glacier Antizana and Glacier Zongo (Favier et al., 2004, Sicart et al., 2005). This is due to higher wind peed at Glacier Antizana (mean annual wind speed is 1.6 m s^{-1} higher than on Glacier Artesonraju, during the dry season wind speed is even 1.9 m s^{-1} higher) and a drier climate at Glacier Zongo.

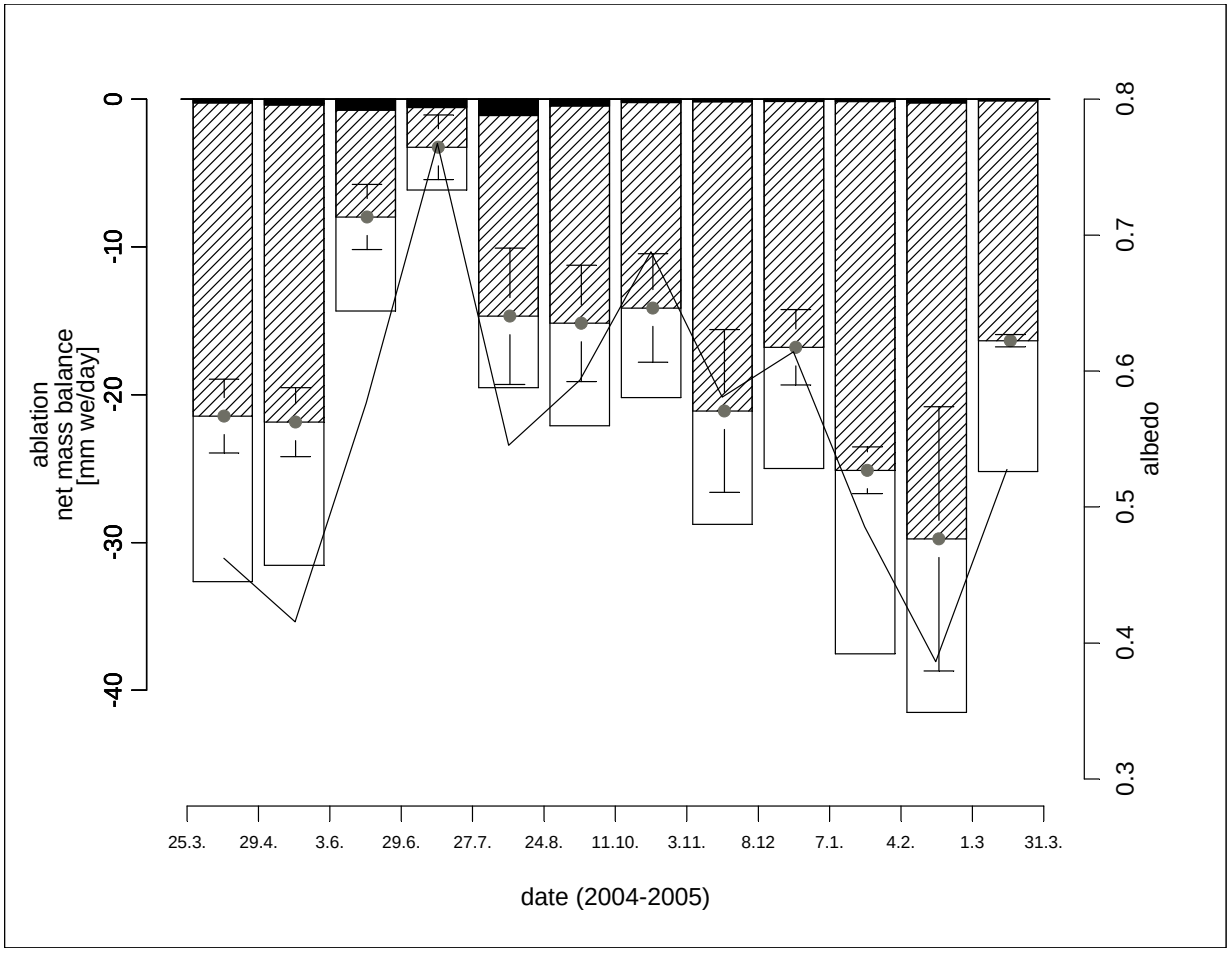

Figure 5.19: Net mass balance rates as measured at four ablation stakes close to the EBS (striped bars with error bars of the standard deviation) and net ablation rates calculated from the EB (sublimation + melt; empty bars). The black bars are net ablation rates from sublimation. Albedo is averaged over the respective time period (right hand axis).

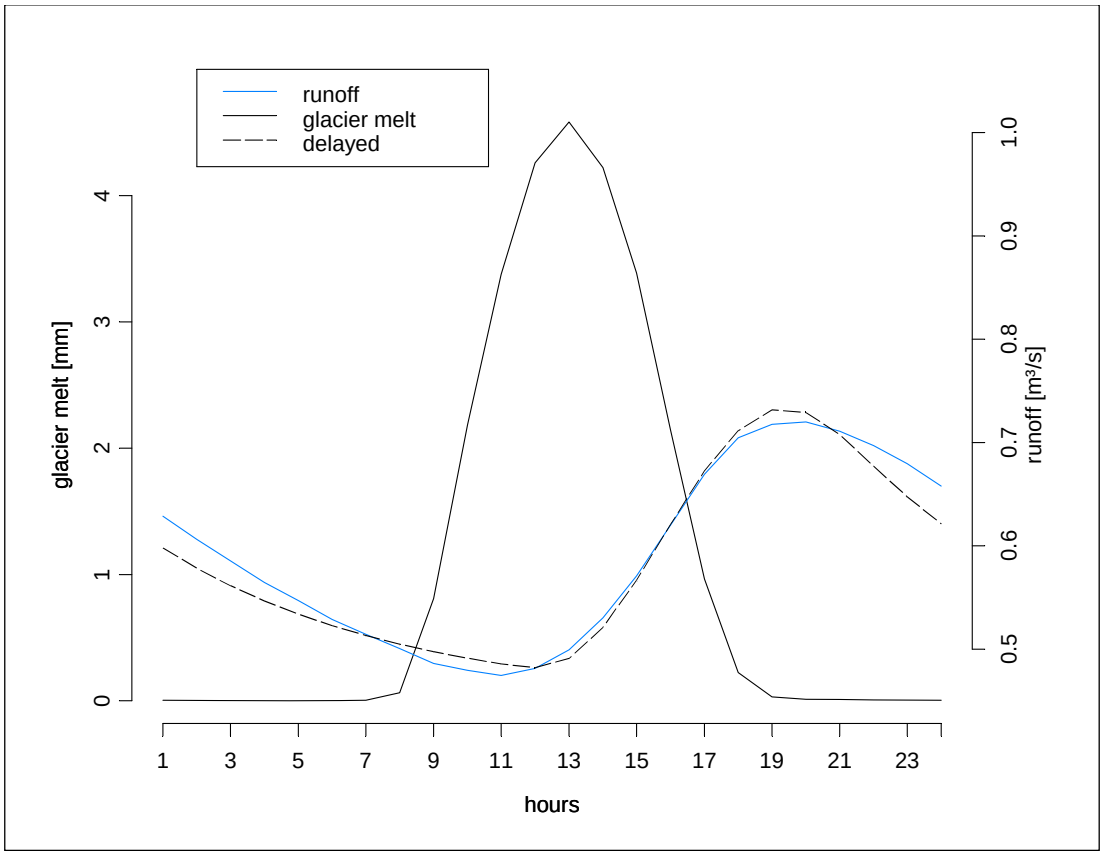

Figure 5.20: Mean daily cycle in glacier melt calculated from the EB at the tongue of Glacier Artesonraju (4850 m a.s.l.) and runoff measured at the outlet of Lake Artesoncocha (4200 m a.s.l.). The dashed line is calculated glacier melt applying a linear reservoir equation with a storage parameter ks=7.

The energy balance on a glacier surface can only give information about the energy and mass fluxes at the site of the station. Measured runoff, in contrast, includes glacier melt from the whole glacier surface. Thus, the amount of glacier melt calculated at the station site cannot be compared to measured runoff quantitatively. For this, the EB has to be extrapolated to the entire glacier surface to obtain the total amount of glacier melt. For SW_{in} this can easily be modelled by applying a simple radiation model (e.g. Mölg et al., 2004). For all other components of the EB, however, the spatial distribution is unknown which makes its extrapolation to the whole glacier surface quite problematic. Still, it can be expected that the temporal variation in total glacier melt does not differ considerably from the variation obtained from the point measurement. With this assumption, glacier melt calculated at the *EBS* can be compared qualitatively to runoff measured at the outlet of Lake Artesoncocha (75 % glacierised, compare chapter 2.2; Appendix C., Figure C.6). Glacier melt was calculated starting on day 70, 2004, runoff data are available until day 58, 2005. Due to problems with the energy supply at the runoff station no data are available in May, August, and November 2004. The four periods with available runoff data, i. e. from

day 70 – 120, 158 – 209, 245 – 311, and 346 – 58 are referred to P1, P2, P3, and P4. P1 and P4 are representative for runoff conditions during the wet, P2 and P3 during the dry and intermediate season, respectively.

Figure 5.20 shows the mean daily cycle in runoff and calculated melt water, respectively. Melting starts at eight in the morning, reaches maximum values at 13 l. t. and lasts until 18 – 19 l. t.. Runoff starts to rise only after 11 l. t. and reaches maximum amounts in the evening at 20 l. t.. This indicates that peak runoff is delayed to maximum glacier melt by 7 hours. Applying a linear reservoir equation (equation 4.19) with a storage parameter (*ks*) of 7, the mean daily cycle in glacier melt can be approximated to the shape of the runoff curve quite satisfactory (Figure 5.20, dashed line).

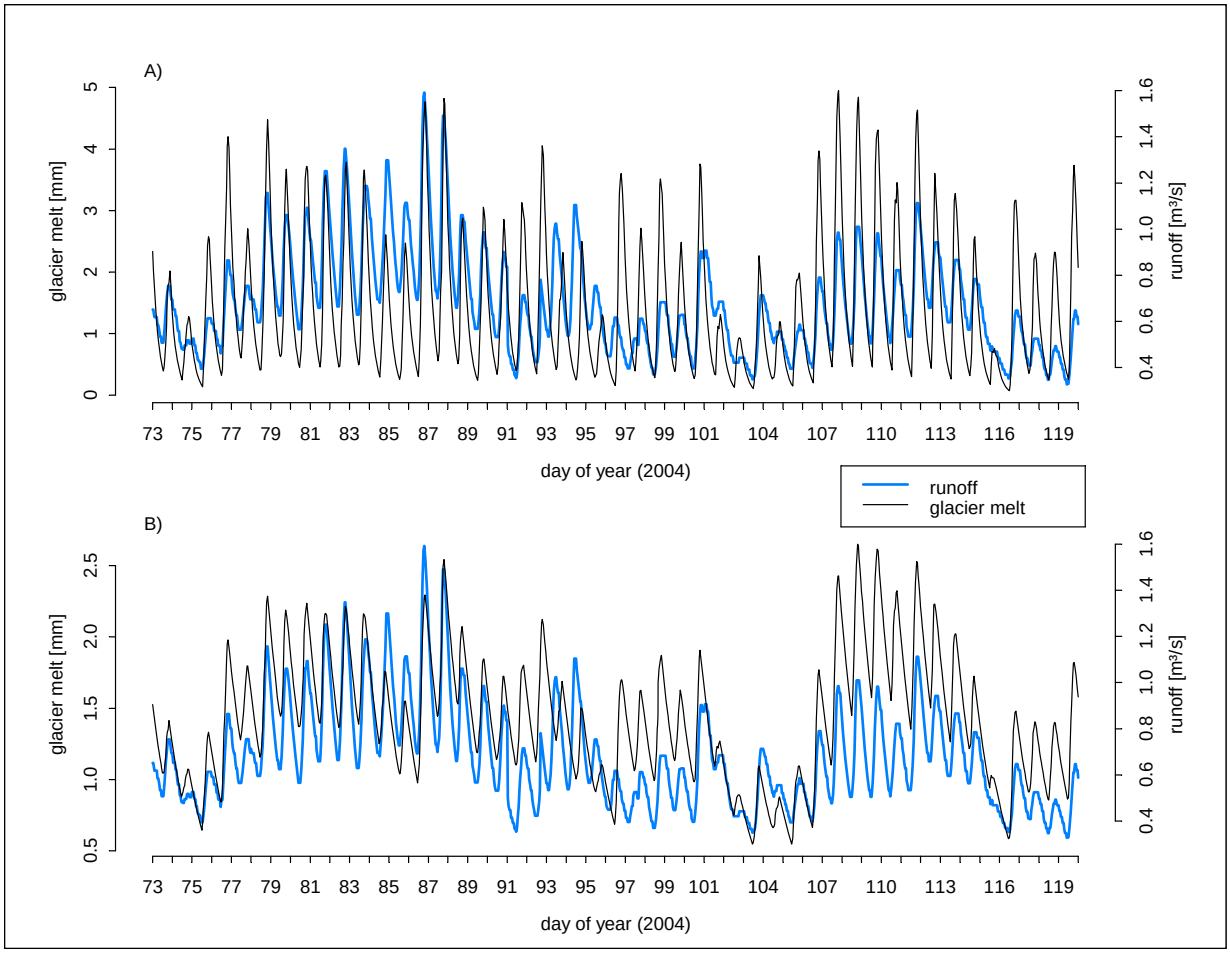

Figure 5.21: Comparison of runoff (blue) measured at the outlet of Lake Artesoncocha (4200 m a.s.l.) and calculated glacier melt (black) from Glacier Artesonraju for period P1 (Day 73 – 120, 2004). Glacier melt is calculated from the EB at 4850 m a.s.l. applying a linear reservoir equation with A) ks=7 and B) ks=55.

This does, however, not necessarily mean that runoff from glacier melt will reach the runoff station within the same day. To analyse the period P1 the first three days were excluded as no information about glacier melt from the former days is available and thus could disturb the result. A comparison of glacier melt and runoff with *ks*=7 reproduces the daily cycle but does not represent long term changes (Figure 5.21 A). With an increase of *ks* by another 48 hours, increased runoff during the night could be reconstructed much better (Figure 5.21 B). With *ks*=55 the correlation coefficient between resulting glacier melt and runoff increases from 0.44 to 0.54. For the periods P2 and P3 (dry and intermediate season, Appendix F, Figure F.16 and F.17) best agreement could be obtained by increasing *ks* by 4 days (P2: 7h r^2=0.14, 103h r^2=0.71; P3: 7h r^2=0.23, 103h r^2=0.50). For the very wet period P4 the correlation coefficient between runoff and glacier melt is highest for *ks*=55 (r^2=0.69). With the increased storage parameter also high runoff amounts during the night can be reconstructed much better (compare Appendix F, Figure F.18).

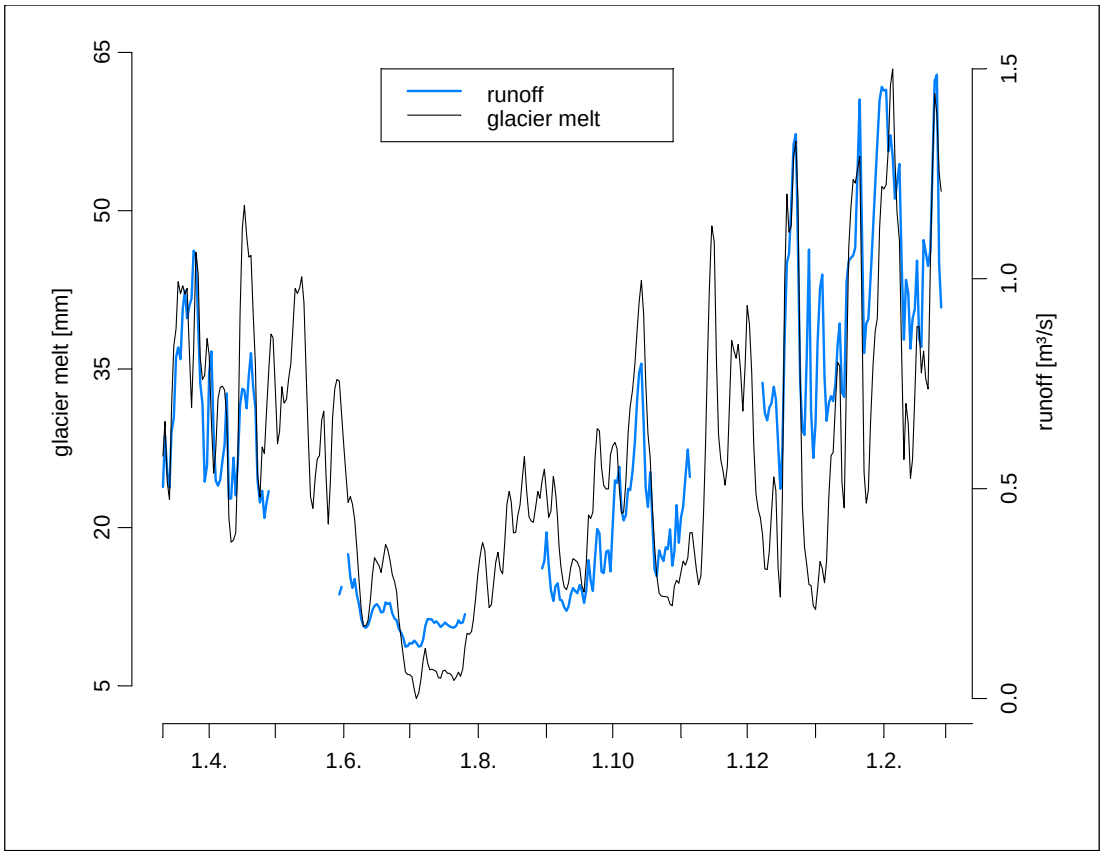

Figure 5.22: Daily mean runoff as measured at the outlet of Lake Artesoncocha (4200 m a.s.l.) and delayed glacier melt calculated from the energy balance at Glacier Artesonraju at 4850 m a.s.l. from day 73, 2004 to 58, 2005.

All together it can be stated that during the wet season glacier melt drains twice as fast as during the dry season. This is most probably caused by the different development of surface and subsurface discharge channels. During wet periods discharge channels are well developed and thus melt water can rapidly run off. In contrast, in the dry season the cold surface temperature impedes the development of discharge channels which, additionally, might refreeze every night. Following this, runoff from glacier melt is calculated with *ks*=55 for the wet periods P1 and P4, and with *ks*=103 for the drier periods P2 and P3. The distance from the *EBS* to the glacier terminus is app. 800 m. This implies that melt water drains with 14 – 15 m h^{-1} in the wet season and decreases to 7 – 8 m h^{-1} in the dry and intermediate season. Defining the firn area of the glacier above mean 0 °C level (app. 5000 m a.s.l.) a minimum delay time from the firn reservoir can be approximated. The distance from the 5000 m altitude line to the *EBS* is 1200 m along the central flow line. This implies that runoff from the firn area will reach the terminus at the earliest within 11 – 12 days in the dry and within 5 – 6 days in the wet season.

The daily sum of melt water is compared with daily runoff as measured at the outlet of Lake Artesoncocha in Figure 5.22. The agreement of daily amounts of glacier melt as calculated at the *EBS* without considering any delay is only r^2=0.52. By applying a linear reservoir model as discussed above the correlation coefficient between measured runoff and calculated delayed runoff from glacier melt is r^2=0.73 on a daily basis. Runoff as well as glacier melt show a significant annual cycle of low values during the dry period in June and July, and five times higher amounts during the wet season. To make a rough estimation of the melt water contribution to total runoff it is assumed that the amount of glacier melt calculated at the *EBS* is representative for the entire glacier area between 4825 – 4875 m a.s.l. which is 5 % of the total glacier area. Overall the contribution of runoff from glacier melt to total runoff is higher during the dry and intermediate season (P1 and P3; 21.5 % of total runoff) than during the wet periods (P1 and P4; 13.2 % of total runoff). During P1 23.6 % (8.1 – 31.5 %) of total runoff originate from this small portion of the glacier. The highest portion of runoff from glacier melt to total runoff is, as expected, found for P2 and P3 with 24.5 (9.4 – 37.7 %) and 27.1 % (8 – 44.7 %), respectively. In the wettest period P4 total runoff is highest but the contribution of runoff from glacier melt is lowest (16.3 %; 5.1 – 24.3 %) as the portion of direct runoff from precipitation is high. In this period total runoff also deviates most from the amount of glacier melt (e.g. beginning of January). Still, the general seasonal trend in runoff clearly reflects the variation in glacier melt throughout the year.

6. Summary and Conclusions

The investigation contributes to important and topical issues. The water resources management for fast developing societies in low latitude regions is an increasingly serious challenge for the near future. Especially in the tropical Cordillera Blanca glacier melt plays a significant role for the availability of fresh water. The changing climate conditions will thus considerably influence the amount of runoff. Studies on the glacier mass balance and the energy budget of the glacier surface are needed to improve the understanding of the glacier-climate interaction in the tropics – which is also considered as a vital aspect in the discussion of global climate change.

The climate in the Cordillera Blanca is characterised by one humid and one dry season which is due to the oscillation of the ITCZ. Air temperature varies little throughout the year. During the dry season, the runoff is low and almost exclusively fed from melt water. Thus, the impact of changes in the glacier extent is essential to the populated and cultivated Callejon de Huaylas. The analysis of a 41-year series of precipitation and runoff shows, in contrast to the mid latitudes, a smoothing effect of glaciers on the annual runoff variation. This effect, expressed by a seasonal storage variation, *S*, increases with the relative portion of glacierisation in the investigated catchment areas.

The thermally almost constant climate, in addition to a steep topography in the Cordillera Blanca, makes direct measurements of glacier mass balances very difficult. The particular circumstances, on the other hand, allow respective reconstructions from hydrological data which are available for several catchments from 1953 – 1994 (precipitation and runoff). Glacier mass balance was reconstructed from the hydrological balance (MBH) for five catchments that are neither influenced by extended swamps nor human irritation. With the ITGG-2.0 model, a vertical mass balance profile model that was specially adapted to model glacier mass balance under tropical climate conditions, a second series of modelled mass balance could be derived. The model is principally driven by air temperature and at least one variable that is related to atmospheric moisture content. Because of the limited availability of data records, incoming shortwave radiation, albedo, atmospheric emissivity, and a sublimation/melt ratio are empirically related to precipitation. A comparison of the reconstructed mass balance series from the five different catchments shows a strong

similarity between the model results. The comparison of the mean cumulative mass balance curves of the two different approaches averaged over the five catchment basins is in good agreement with measured glacier terminus variations of three glaciers in the Cordillera Blanca. Glacier terminus advances are measured 4 – 5 years after positive modelled mass balance. This indicates a rapid response of glaciers to mass changes which agrees with theoretical considerations for tropical conditions. Further, the derived mass balance series show a good synchronicity with a global trend in the last half of the twentieth century. In general, mass balance is negative. The negative trend is only interrupted by mass gains 1970 – 1975 and two short positive periods around 1982 and 1987.

The runoff model ITGG-2.0-R extracts glacier melt from the ITGG-2.0 mass balance model and estimates direct runoff from non glacierised areas separately. Here the model is applied to reconstruct runoff for the 31 % glacierised catchment of Llanganuco from 1953 − 1997. Different model runs show a high correlation with observed runoff ($r^2 = 0.76$). Seasonally obtained r^2 are only slightly smaller for the dry ($r^2 = 0.72$) and again decrease for the wet season ($r^2 = 0.65$) when the portion of direct runoff increases. The measured and modelled mean annual cycles of runoff have a correlation of $r^2 = 0.99$. This implies a successful validation of the ITGG-2.0-R model.

Based on the good agreement in modelled and measured mean annual cycles of runoff, runoff predictions with the ITGG-2.0-R model for different climate change scenarios are quite trustworthy. An evaluation of a change in precipitation and air temperature separately is performed predicting the change in the mean annual amount of glacier melt from all glaciers that drain into the Rio Santa valley. It is obvious that an increase in air temperature will increase the amount of glacier melt during the first years. With the shrinkage of the glacier extent afterwards, the amount of glacier melt will then decrease. On the other hand an increase in precipitation will influence the amount of glacier melt during the first years only slightly. The decrease in energy due to increased cloud cover will be compensated by less latent heat loss. Thus, the amount of energy that is available for melting will not change considerably. On a long term, when the glacier extent has adopted to the changed climate conditions, glacier melt will increase. The change in direct runoff from precipitation, glacier melt and total runoff is also calculated four different IPCC climate change scenarios for the years 2050 and 2080. For this analysis five differently glacierised catchments are investigated. All runoff scenarios are calculated assuming respective steady-state glacier extents. In each case, the reduced glacier area leads to a decreased amount of glacier melt. Over the year, mean annual total runoff remains almost unchanged because the decrease in runoff from glacier melt is compensated by the increase in direct runoff. In all catchments an increase in runoff during the wet and a decrease in the dry season can be expected. The change

in the seasonal cycle in runoff increases with the portion of glacier area in the catchment. In the highest glacierised catchment of Parón glacier melt increase up to 48 % in March and decrease up to 40 % in July. Especially the decrease of runoff during the dry season – when runoff is already low nowadays – will challenge future water management considerably.

Studies of the energy balance *EB* on the surface of Glacier Artesonraju (4850 m a.s.l.) gives detailed information about the influence of different climate conditions on the amount of glacier melt. The variability of the energy balance terms throughout the year is shown in Figure 6.1. In the core dry season (June to August) the amount of energy that is available for melt is strongly reduced compared to the amounts during the core wet season (January to March). The low amount of energy that is available for melt during the dry season is caused by a combination of reduced energy from different energy balance terms (see below). Melting rates during the core dry season are only half of those during the core wet season. Analyzing the different terms in the *EB* the reduction in melt during the dry season is due to (core dry minus core wet season):

- Reduced SW_{net} (−40 W m^{-2}). The combination of the lower angle of the sun (northern turning point) but less cloudiness is responsible for a reduction in SW_{in} of −28 W m^{-2}. Albedo is higher and enhances SW_{out} by 12 W m^{-2}. The high albedo is probably due to the increased sublimation that dries out the surface. Additionally, one single dry snowfall events has a lasting effect on the albedo due to low melting rates. In the wet season snow is mostly very wet and melts until midday, opening a wet, dark glacier ice surface.
- Enhanced energy loss from LW_{net} (−39 W m^{-2}). LW_{in} is reduced by 49 W m^{-2} due to lower atmospheric temperature (−1.9 °C) and moisture content (−1.5 hPa) which reduces cloudiness and entails a lower atmospheric emissivity. The decrease in emissivity reduces LW_{in} by 40 W m^{-2}, which is 81 % of the total difference in LW_{in}. LW_{out} is lowered by 10 Wm^{-2} due to more negative temperature of the glacier surface (−2.1 °C).
- Enhanced turbulent fluxes (ΔH=+7 W m^{-2}, ΔLE=−20 W m^{-2}). Higher gradients between the atmosphere and the surface as well as higher wind speeds (+2.3 m s^{-1}) during the dry season are responsible for increased turbulent exchange. *LE* is almost three times as high as *H* which is due to the much higher difference in the gradient of vapour pressure (−0.6 hPa) than in air temperature (−0.2 °C). Still, the amount of energy lost by sublimation is only half of the energy loss of SW_{net} or LW_{net}. Monthly mean dry season ablation due do sublimation is 25 mm we. This corresponds to 210 mm we of monthly ablation if the energy would be available for the eight times more effective melting.

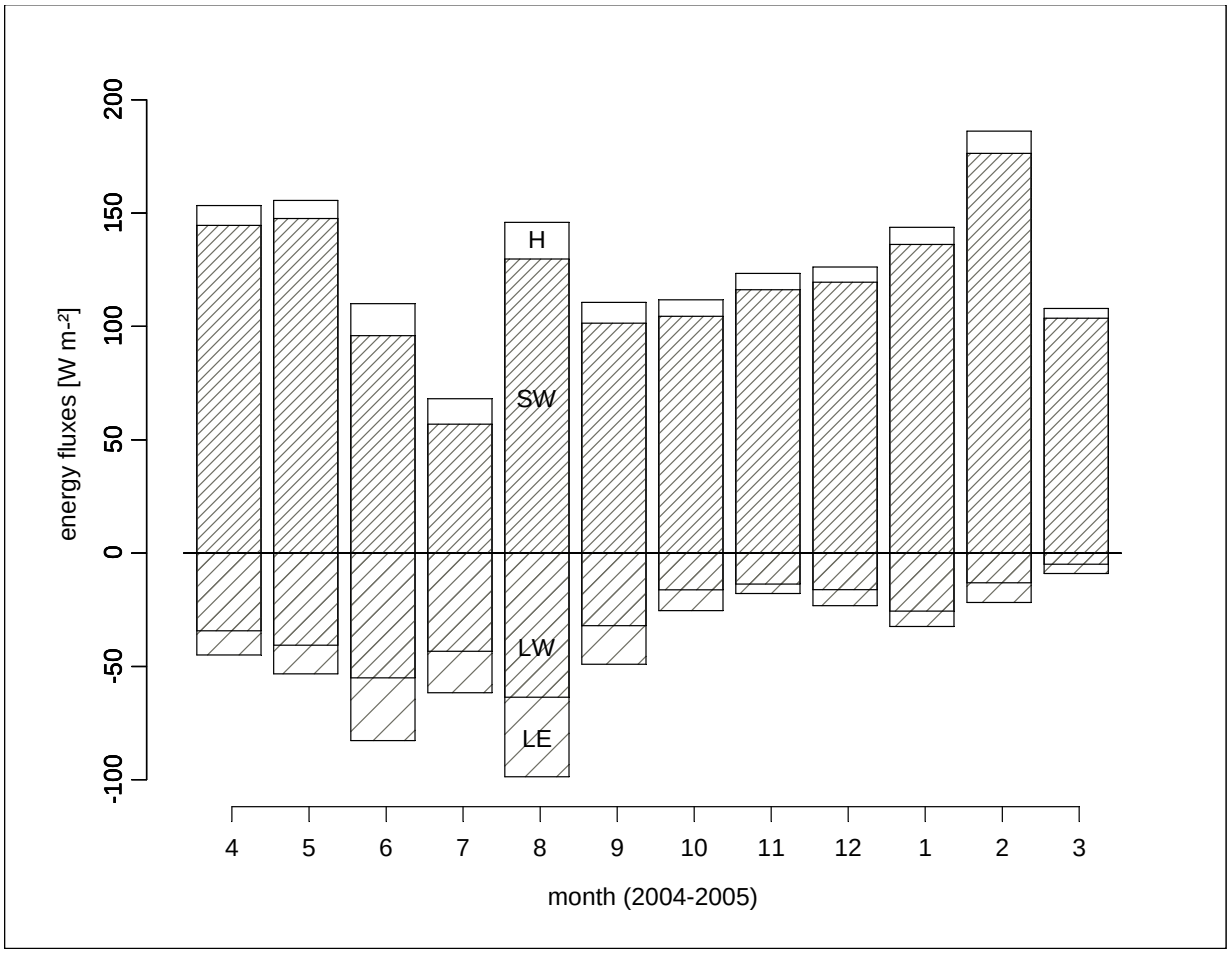

Figure 6.1: Mean monthly energy fluxes from SW_{net} (SW) and LW_{net} (LW) radiation, and the turbulent fluxes (H, LE) on the surface of Glacier Artesonraju (4850 m a.s.l.) from April 2004 to March 2005.

Finally, calculated variation in glacier melt from the EB is qualitatively compared to runoff variation at the outlet of Lake Artesoncocha (4200 m a.s.l., 75 % glacierised). Daily peak runoff is delayed to maximum amounts of glacier melt by 7 hours. Applying a linear reservoir model with a storage parameter *ks*=7 the mean daily cycle of runoff is represented well by the cycle in glacier melt. To also reconstruct changes in the amount of runoff on daily to seasonal scales, *ks* has to be increased to 55 for the two wet periods and to 103 for the dry and intermediate periods. This implicates that there is a substantial difference in the development of discharge channels during dry and wet periods. During the wet periods discharge channels are well expanded and melt water can run off very quickly. During the dry season when surface temperature is low discharge channels are probably refreezing during the night and thus melt water drains much slower. Melt water from the firn area will reach the terminus at the earliest within 5 – 6 days in the wet and within 11 – 12 days in the dry season. Thus, the mean time delay in glacier melt from the firn area of 10

days used for the ITGG-2.0-R model is not a bad value. Still, for future work it might be an improvement to also change this value with the change in humidity related variables.

On a daily basis, 73 % of the fluctuations in runoff at Lake Artesoncocha can be explained by runoff from glacier melt. Assuming the calculated amount of glacier melt at the *EBS* is representative for the whole glacier surface between 4825 – 4875 m a.s.l. a careful qualitative interpretation of daily runoff from glacier melt can be made. The 5 % of total glacier area provide 5 – 45 % of total runoff in the catchment. The highest portion of the glacier melt to total runoff can be seen in June and September (8 – 45 %), whereas in December and January runoff from glacier melt does not significantly contribute to runoff (5 – 32 %). The deviation of measured runoff and the amount of glacier melt is highest at the beginning of January 2005. This period was also a period with intense precipitation and thus runoff is highly driven by direct runoff from precipitation.

After all, the investigation contributes to a better knowledge about the contribution of glacier melt to runoff in the Cordillera Blanca. To calculate the amount of glacier melt it is very important to model the humidity related variables very precisely. To improve runoff modelling with the ITGG-2.0-R model in future, some important issues should be considered:

- From the energy balance study on Glacier Artesonraju we clearly see that albedo does not necessarily increase with increasing precipitation as it is assumed to be in the ITGG-2.0-R model. Additionally, SW_{in} does not decrease with increasing precipitation as it is assumed in the model so far. Both inverse parameterisations, however might have compensated each other so far. Still, to be physically more precise this should be changed in the next model version.
- So far the variability of LW_{net} is only driven by the variability in LW_{in} in the model as a constantly melting surface is assumed. Especially during the dry season surface temperature is frequently far below 0°C and, thus, melting is reduced. In the model the reduction in glacier melt during the dry season is much more due to the high portion of energy that will be consumed by sublimation. This could, however, not be confirmed by the EB on Glacier Artesonraju. Sublimation can only explain 19 % of the reduction in energy whereas the reduction in LW_{net} is responsible for a reduction of 36 % of the energy that is available for melt during the core dry season compared to the core wet season.
- Discharge channels are differently developed during the dry and wet season. The delay in runoff from the firn area varies from 6 – 12 days. Thus, varying the storage parameters with humidity could also improve the model.

Bibliography

- Ageta, Y. and Higuchi, K., 1984. Estimation of mass balance components of a summer−accumulation type glacier in the Nepal Himalaya. Geografiska Annaler, 66A, 249−255.
- Alley, R. B., Marotzke, J., Nordhaus, W. D., Overpeck, J. T., Peteet, D. M., Pielke, R. A., Pierrehumbert, Jr., R. T., Rhines, P. B., Stocker, T. F., Talley, L. D. and Wallace, J. M., 2003. Abrupt Climate Change. Science, 28, 2005−2010, doi: 10.1126/science.1081056.
- Ames, A., 1985. Estudio de mediciones glaciológicas efectuadas en la Cordillera Blanca por ELECTROPERÚ S.A. − Variación y balance de masas de los glaciares y su contribución en el caudal de las cuencas. Laboratoire de Glaciologie & Géophysique de l'Environnement, C.N.R.S., Grenoble, publication No. 457.
- Ames, A. and Francou, B., 1995. Cordillera Blanca glaciares en la historia. Bulletin de l'Institut Francais d'Etdudes Andines, 24, (1), 37−64.
- Ames, A. and Hastenrath, S., 1996. Mass balance and ice flow of the Uruashraju glacier, Cordillera Blanca, Peru. Zeitschrift für Gletscherkunde und Glaczialgeologie, 32, 83−89.
- Ames, A., Munoz, G., Verástegui, J., Vigil, R., Zamora, M. and Zapata, M., 1989. Glacier Inventory of Perú. Huaraz, Perú.
- Arck, M., and Scherer, D., 2002. Problems in the determination of sensible heat flux over snow. Annals of Geophysical Research, 84A, 157−169.
- Arnell, N., 1996. Global Warming, River Flows and Water Resources. Wallingford.
- Arnold, N. S., Willis, I. C., Sharp, M. J., Richards, R. K. and Lawson, W. J., 1996. A distributed surface energy-balance model for a small valley glacier. I. Develepment and testing for Haut Glacier d'Arolla, Valais, Switzerland. Journal of Glaciology, 42, (140), 77−89.

- Backer, D., Escher−Vetter, H., Moser, H., Oerter, H., and Reinwarth, O., 1982. A glacier discharge model based on results from field studies of energy balance, water storage and flow. In: Glen, J. W. (Ed.) Hydrological aspects of alpine and high-mountain areas. Proceedings of the Exeter Symposium 1982: IAHS Publication, 138, 103−112.

- Bergstrøm, E., 1955. The British Ruwenzori Expedition, 1952. Journal of Glaciology, 2, (17), 468 − 476.

- Braithwaite, R. J. and Zhang, Y., 2000. Sensitivity of mass balance of five Swiss glaciers to temperature changes assessed by tuning a degree-day model. Journal of Glaciology, 46, (152), 7−14.

- Braun, L. M., Weber, M. and Schulz, M., 2000. Consequences of climate change for runoff from Alpine regions. Annals of Glaciology, 31, 19−25.

- Borchers, P., 1935a. Cordillera Blanca. Topographical map, scale 1:100000. Published with support of the Deutschen and Österreichischen Alpenverein.

- Borchers, P., 1935b. Die weiße Kordillere. Berlin.

- Chen, J. and Ohmura, A., 1990. On the influence of alpine glaciers on runoff. In: Lang, H. and Musy, A., (Eds.), Hydrology in Mountainous Regions I Hydrological Measurements, The Water Cycle. Lausanne. IAHS Publication, 193, 117−125.

- Collins, D. N., 1987. Climatic fluctuations and runoff from glacierised Alpine basins. In: Solomon, S. I., Beran, M. and Hogg, W., (Eds.), The influence of Climate Change and Climatic Variation on the Hydrological Regime and Water Resources. Vancouver. IAHS Publications, 168, 77−89.

- Collins, D. N., 1989. Hydrometeorological conditions, mass balance and runoff from alpine glaciers. In: Oerlemans, J., (Eds), Glacier Fluctuations and Climatic Chance, 235−260.

- Deutscher Alpenverein 1945. Cordillera Blanca Südteil. Topographical map, scale 1:100000.

- Favier, V., Wagnon, P., Chazarin, J. P., Maisincho, L., and Coudrain, A., 2004. One-year measurements of surface heat budget on the ablation zone of Antizana Glacier 15, Ecuadorian Andes. Journal of Geophysical Research, 109, D18105, doi:10.1029/2003JD004359.

- Fliri, F., 1968. Beiträge zur Hydrologie und Glaziologie der Cordillera Blanca (Perú). Alpenkundliche Studien. Veröffentlichung Universität Innsbruck 1, 26−52.

- Francou, B., Ribstein, P., Saracia, R., and Tiriau, E., 1995. Monthly balance and water discharge of an inter-tropical glacier: Zongo Glacier, Cordillera Real, Bolivia, 16°S. Journal of Glaciology, 44, (137), 61−67.

- Francou, B., Vuille, M., Wagnon, P., Mendoza, J., and Sicart, J. E., 2003. Tropical climate change recorded by a glacier in the central Andes during the last decades of the 20th century: Chacaltaya, Bolivia, 16°S. Journal of Geophysical Research − Atmospheres, 108, (D5), 4154−4165.

- Garratt, J. R., 1992. The Atmospheric Boundary Layer, Cambridge University Press, New York.

- Georges, C., 2004. 20th century glacier fluctuations in the tropical Cordillera Blanca (Perú). Arctic, Antarctic, and Alpine Research, 36(1), 100−107.

- Georges, C., 2005. Recent Glacier Fluctuations in the Tropical Cordillera Blanca and Espects of the Climate Forcing. Doctor Thesis, University of Innsbruck, Department of Geographie, Austria.

- Georges, C. and Kaser, G., 2002. Ventilated and unventilated air temperature measurements for glacier-climate studies on a tropical high mountain site. Journal of Geophysical Research, 107, (D24), 4775, doi:10.1029/2002JD002503.

- Ginot, P., Schwikowski, M., Gäggeler, H. W., Schotterer, U., Kull, C. Funk, M., Rivera, A., Stampfli, F., and Stichler, W., 2002. The Patagonian Icefields, First results of a Paleoatmospheric Chemistry and Climate study of Cerro Tapado Glacier, Chile. Kluwer, New York. 157−167.

- Gleick, P. H., 1987. Global climatic changes and regional hydrology: impacts and responses. In: Solomon, S. I., Beran, M. and Hogg, W., (Eds), The Influence of Climate Change and Climatic Variation on the Hydrological Regime and Water Resources. Vancouver. IAHS Publication, 168, 389−388.

- Gottschalk, L. and Weingartner, R., 1998. Distribution of peak flow derived from a distribution of rainfall volume and runoff coefficient, and a unit hydrograph. Journal of Hydrology, 208, 148−162.

- Gustafsson, D., Stähli, M., and Jansson, P. E., 2001. The surface energy balance of a snow cover: Comparing measurements to two different model simulations. Theoretical and Applied Climatology, 70, 81−96.

- Hastenrath, S., (1984): The Glaciers of Equatorial East Africa. D. Reidel Publishing Company, Dordrecht.

- Hastenrath, S., 1991. Glaciological Studies on Mount Kenya 1971 − 83 − 91. University of Wisconsin, Madison.

- Hatenrath, S. and Ames, A., 1995a. Diagnosing the imbalance of Yanamarey Glacier in the Cordillera Blanca of Peru. Journal of Geophysical Research, 100, D3, 5105−5112.

- Hastenrath, S. and Ames, A., 1995b. Recession of Yanamarey Glacier in Cordillera Blanca, Perú, during 20th century. Journal of Glaciology, 41, (137), 191−196.

- Hastenrath, S. and Kruss, P. D., 1992. The dramatic retreat of Mount Kenya's glaciers between 1963 and 1987: greenhouse forcing. Annals of Glaciology, 16, 127−133.

- Held, I. M. and Hou, A. Y., 1980. Nonlinear axially symmetric circulations in a nearly inviscid atmosphere. Journal of Atmospheric Sciences, 37, 515−533.

- Hock, R., 1998. Modelling of glacier melt and discharge. Zürcher Geographische Schriften, 70, 1−70.

- Hock, R., 1999. A distributed temperature-index ice- and snowmelt model including potential direct solar radiation. Journal of Glaciology, 45, 149, 101−111.

- Hock, R., 2003. Temperature index melt modelling in mountain areas. Journal of Hydrology, 282, (1−4), 104−115.

- Hock, R., Jansson P. and Braun, L., 2005. Modelling the response of mountain glacier discharge to climate warming. In: Huber, U.M., Reasoner, M. A., and Bugmann, H., (Eds.), Global Change and Mountain Regions - A State of Knowledge Overview. Advances in Global Change Series, Springer, Dordrecht, 243-252.

- Hodge, S. M., Trabant, D. C., Krimmel, R. M., Heinrichs, T. A., March, R. S., and Josberger, E.G., 1998. Climate variations and changes in mass of three glaciers in western North America. Journal of Climate, 11, 9, 2161−2179.

- Hölzli, M., 2006.Weiterentwicklung des Abflussmodells ITGG2.0-R durch hochaufgelöste Strahlungsmodellierung: Anwendung in einem tropischen, vergletscherten Einzugsgebiet (Cordillera Blanca, Peru). Master thesis, University of Innsbruck, Departement of Meteorology, Austria.

- Hope, G.S., Peterson, J.A., Radok, U., and Allison, I., 1976. The Equatorial Glaciers of New Guinea. Results of the 1971 − 1973 Australian Universities Expeditions to Irian Jaya: survey, glaciology, meteorology, biology and paleoenvironments. In: Johnson, A. M., (Ed.), The Climate of Perú, Bolivia and Ecuador. World Survey of Climatology, 12, 147 − 218.

- Hulme, M. and Sheard, N., 1999: Escenarios de Cambio Climático para Países de los Andes del Norte. http://www.cru.uea.ac.uk/~mikeh/research/andes.pdf

- IPCC, 2001. Special Report on Emission Scenarios. Cambridge University Press, UK, pp570.

- Jansson, P., Hock, R., and Schneider, T., 2003. The concept of glacier storage: a review. Journal of Hydrology, 282, (1−4), 116−129.

- Juen, I., Kaser, G., and Georges, C., 2006. Modelling observed and future runoff from a glacierised tropical catchment (Cordillera Blanca, Perú). Global and Planetary Change, in press.

- Kadioglu, M. and Sen, Z., 2001. Monthly precipitation−runoff polygons and mean runoff coefficients. Hydrological Sciences, 46, (1), 3−11.

- Kaser, G., 1982. Measurements of Evaporation from Snow. Archives for Meteorology, Geophysics, and Bioclimatology, Ser. B, 30, (4), 333−340.

- Kaser, G., 1995. Some Notes on the Behaviour of Tropical Glaciers. Bulletin Institute fr. études andines, 24, (3), 671−681.

- Kaser, G., 1999. A review of the modern fluctuations of tropical glaciers. Global and Planetary Change, 22, 93−103.

- Kaser, G., 2001. Glacier−Climate Interaction at Low−Latitudes. Journal of Glaciology, 47, (157), 195 − 204.

- Kaser, G., Ames, A., and Zamora, M., 1990. Glacier fluctuations and climate in the Cordillera Blanca. Annals of Glaciology, 141, 136−140.

- Kaser, G., Georges, C., and Ames, A., 1996a. Modern glacier fluctuations in the Huascarán−Chopicalqui Massif of the Cordillera Blanca, Perú. Zeitschrift für Gletscherkunde und Glazialgeologie, 32, 91−99.

- Kaser, G. and Georges, C., 1999. On the mass balance of low latitude glaciers with particular consideration of the Perúvian Cordillera Blanca. Geografiska Annaler, 81, (A (4)), 643−651.

- Kaser, G., Georges, Ch., Juen, I., Mölg, T., Wagnon, P., and Francou, B., 2004. The behaviour of modern low−latitude glaciers. Past Global Changes News, 12, (1), 15−17.

- Kaser, G., Hastenrath, S. and Ames, A., 1996b. Mass Balance Profiles on Tropical Glaciers. Zeitschrift für Gletscherkunde und Glazialgeologie 32, 75−81.

- Kaser, G., Juen, I., Georges, C., Gomez, J., and Tamayo, W., 2003. The impact of glaciers on the runoff and the reconstruction of mass balance history from hydrological data in the tropical Cordillera Blanca, Perú. Journal of Hydrology, 282, (1−4), 130−144.

- Kaser, G. and Osmaston, H., 2002. Tropical Glaciers. International Hydrology Series, UNESCO and Cambridge University Press.

- Kinzl, H., 1942. Gletscherkundliche Begleitworte zur Karte der Cordillera Blanca (Perú). Zeitschrift für Gletscherkunde, 28 (1/2), 1−19.

- Kinzl, H., 1949. Die Vergletscherug der Südhälfte der Cordillera Blanca (Peru). Zeitschrift für Gletscherkunde und Glazialgeologie, 1, 1−28.

- Kistler, R., Kalnay, E., Collins, W., Saha, S., White, G., Woollen, J., Celliah, M., Ebisuzaki, W., Kanamitsu, M., Kousky, V., Van den Dool, H., Jenne, R., and Riorino, M., 2001. The NCEP-NCAR 50−year Reanalysis: monthly means CD−Rom and documentation. Bulletin of the American Meteorological Society, 82, (2), 247−267.

- Klok, E. L. and Oerlemans, J., 2004. Modelled climate sensitivity of the mass balance of Morteratschgletscher and its dependence on albedo parameterisation. International Journal of Climatology, 24, 231−245.

- Kuhn, M., 1981. Climate and Glaciers. Sea Level, Ice and Climatic Change Proceedings of the Canberra Symposium, 1979. IAHS Publication, 131, 3−20.

- Kuhn, M., 1989. The response of the equilibrium line altitude to climatic fluctuations: theory and observations. In: Oerlemans, J. Glacier fluctuations and climatic change. Cordrecht, Kluwer AcaDEMish Publishers, 407−417.

- Lliboutry, L., Morales, B., and Schneider, B., 1977. Glaciological Problems set by the Control of Dangerous Lakes in Cordillera Blanca, Perú. III. Study of

Moraines and Mass Balances at Safuna. Journal of Glaciology, 18, (79), 275−290.

- Mark, B. G. and Seltzer, G. O., 2003. Tropical glacier meltwater contribution to stream discharge: a case study in the Cordillera Blanca, Perú. Journal of Glaciology, 49, (165), 271−281.

- McMahon, T. A., Finlayson, B. L., Haines, A., and Srikanthan, R., 1987. Runoff variation: a global perspective. In: Solomon, S. I., Beran, M. and Hogg, W., (Eds.), The Influence of Climate Change and Climatic Variation on the Hydrolgoical Regime and Water Resources. Vancouver. IAHS Publication, 168, 3−11.

- Mölg, T., Hardy, D. R., and Kaser, G., 2003. Solar-radiation-maintained glacier recession on Kilimanjaro drawn from combined ice-radiation geometry modeling. Journal of Geophysical Research, 108, (D23), 4731, doi:101029/2003JD003546.

- Mölg, T. and Hardy, D. R., 2004. Ablation and associated energy balance of a horizontal glacier surface on Kilimanjaro. Journal of Geophysical Research, 109, D16104, doi:10.1029/2003JD004338.

- Morales Arnao, B., 2000. Los eternos nevados en el Perú están retrocediendo en forma cada vez más acelerada. In: Brack Egg, A. et al., (Eds), El Medio Ambiente en el Perú 2000. Huaraz, Perú, 17−24.

- Niedertscheider, J., 1990. Untersuchungen zur Hydrographie der Cordillera Blanca (Perú). Master thesis, University of Innsbruck, Department of Geographie, Austria.

- Oerlemans, J., 2000. Holocene glacier fluctuations: is the current rate of retreat exceptional? Annals of Glaciology, 31, 39−44.

- Oerlemans, J., 2001. Glaciers and Climate Change. A. A. Balkema Publishers.

- Oerlemans, J. and Reichert, B. K., 2000. Relating glacier mass balance to meteorological data by using a seasonal sensitivity characteristic. Journal of Glaciology, 46, (152), 1−6.

- Ohmura, A., 1981. Climate and Energy Balance on Arctic Tundra, Axel Heiberg Island, Canadian Arctic, Archipelago, Spring and Summer 1969, 1970 and 1972. Zürcher Geographische Schriften, pp. 448.

- Ohmura, A., 2001. Physical Basis for the Temperature-Based Melt-Index Method. Journal of applied Meteorology, 40, 753−762.

- Österreichischer Alpenverein, 2000. Alpenvereinskarte Cordillera Blanca Nord (Perú). 0/3a, 1:100 000, Freytag-Berndt und Artaria KG, Vienna.
- Paterson, W. S. B., 1994. The Physics of Glaciers, 3rd ed., Oxford University Press, New York.
- Patzelt, G., 1985. The Period of Glacier Advances in the Alps, 1965 to 1980. Zeitschrift für Gletscherkunde und Glazialgologie, 21, 403−407.
- Pepin, N. C. and Seidel, D. J., 2005. A global comparison of surface and free air temperatures at high elevation, Journal of Geophysical Research, 110, D03104, doi:10.1029/2004JD005047.
- Peterson, J. A. and Peterson, L. F., 1997. Ice Retreat from the Neoglacial Maxima in the Puncak Jayakesuma Area, Republic of Indonesia. Zeitschrift für Gletscherkunde und Glazialgeologie, 30, 1−9.
- Ponce, V. M. and Shetty, A. V., 1995. A conceptual model of catchment water balance. 2. Application to runoff and baseflow modeling. Journal of Hydrology, 173, 44−50.
- Porter, S. C., 1986., Pattern and Forcing of Northern Hemisphere Glacier Variations During the Last Millenium. Quaternary Research 26, (1), 27−48.
- Pouyaud, B., Francou, B. and Ribstein, P. (1995). Un réseau d'observation des glaciers dans les Andes tropicales. Bulletin de l'Institut Français d'Etudes Andines, 24, (3), 707−714.
- Raggl, M., 1996. Abschätzung von Wasserhaushaltsgrößen für das Ötztal mit Hilfe eines Geographischen Informationssystems. Master thesis, University of Innsbruck, Austria.
- Ramírez, E., Francou, B., Ribstein, P., Descloitres, M., Guérin, R., Mendoza, J., Gallaire, R., Pouyaud, B. and Jordan, E., 2001. Small glaciers disappearing in the Tropical Andes. A case study in Bolivia; the Chacaltaya Glacier (16° S). Journal of Glaciology, 47, (157), 187 − 194.
- Reynolds, J. R. and Young, F. J., 1997. Changes in areal extent, elevation and volume of Athabasca Glacier, Alberta, Canada, as estimated from a series of maps produced between 1919 and 1979. Annals of Glaciology, 24, 60−65.
- Ribstein, R., Tiriau, R., Francou, B. and Saravia, R., 1995. Tropical climate and glacier hydrology: a case study in Bolivia. Journal of Hydrology, 165, 221−234.

- Schuler, T., 1997. Hydrologie eines randtropischen Gletschers, Fallstudie Glaciar Zongo, Cordillera Real, Bolivien. Master thesis, University of Freiburg, Germany.

- Schneider, T., 1997. Water Movement and Storage in the Firn of Storglaciären, Northern Sweden. Forskningsrapport, 99.

- Schotterer, U., Grosjean, M., Stichler, W., Ginot, P., Kull, C., Bonnaveira, H., Francou, B., Gäggeler, H. W., Gallaire, R., Hoffmann, G., Pouyaud, B., Ramirez, E., Schwikowski M., and Taupin, J. D., 2003. Glaciers and climate in the Andes between the Equator and 30°S: what is recorded under extreme environmental conditions? Climatic Change, 59, 1−2, 157−175.

- Sicart, J. E., 2002. Contribution a l'Etude des flux d'Energie, du bilan de masse et du debit de fonte d'un Glacier tropical: le Zongo, Bolivie. Doctor thesis, Universite Paris VI, Department of Pierre et Marie Curie, Paris, France.

- Sicart, J. E., Wagnon, P., and Brunstein, D., 2001. Clear-sky albedo measurements on a sloping glacier surface: A case study in the Bolivian Andes. Journal of Geophysical Research, 106 (D23), 31729-31738, doi:10.1029/2000JD000153

- Sicart, J. E., Wagnon, P., and Ribstein, P., 2005. Atmospheric controls of the heat balance of Zongo glacier (16 °S, Bolivia). Journal of Geophysical Research, 110, D12106, doi:10.1029/2004JD005732.

- Stichler, W., Schotterer, U., Fröhlich, K., Ginot, P., Kull, C., Gäggeler, H., and Pouyaud, B., 2001. Influence of sublimation on stable isotope record recovered from high-altitude glaciers in the tropical Andes. Journal of Geophysical Research, 106, D19, 22613−22620.

- Tamayo, W., 1996. Influencia de los glaciares en el comportamiento hidrológico de cuencas de alta montaña, estudio de casos en Perú y Bolivia. Master thesis, University of Huaraz, Perú.

- Trenberth, K. E. and Hoar, J. T., 1995. The 1990−1995 El Nino-Southern Oscillation Event: Longest on Record. Geophysical Research Letters, 23, 57−60.

- Trenberth, K. E. and Otto-Bliesner, B. L., 2003. Toward Integrated Reconstruction of Past Climates. Science, 300, 589−591.

- Wagnon, P., Ribstein, P., Francou, B., and Pouyaud, B., 1999a. Annual cycle of energy balance of Zongo glacier, Cordillera Real, Bolivia. Journal of Geophysical Research, 104, 3907−3923.

- Wagnon, P., Ribstein, P., Francou, B., and Sicart, J. E., 2001. Anomalous heat and mass budget of Glaciar Zongo, Bolivia, during the 1997/98 El Niño year. Journal of Glaciology, 47, (156), 21−28.

- Wagnon, P., Ribstein,P., Kaser, G., and Berton, P., 1999b. Energy balance and runoff seasonality of a Bolivian glacier. Global and Planetary Change, 22, 49−58.

- Wagnon, P., Sicart, J. E., Berthier, E., and Chazarin, J. P., 2003. Wintertime high-altitude surface energy balance of a Bolivian glacier, Illimani, 6340 m above sea level. Journal of Geophysical Research, 108, (D6), doi:10.1029/2002JD002088.

- Wagnon, P., Ribstein, P., Francou, B., and Sicart, J. E., 2001. The influence of the 1997−98 El Niño−Southern Oscillation warm event on tropical glaciers. Journal of Glaciology, 47, (156), 21−28.

- Welsch, W. and Kinzl, H., 1970. Der Gletschersturz vom Huascarán (Perú) am 31. Mai 1970 − die größte Gletscherkatastrophe der Geschichte. Zeitschrift für Glescherkunde und Glaczialgeologie 6, (1−2), 181−192.

- Whittow, J. B., Shepherd, A., Goldthorpe, J. E., Temple, P. H., 1963. Observations on the glaciers of the Ruwenzori. Journal of Glaciology, 4, (35), 581−616.

.

Publications

Kaser, G., I. Juen, Ch. Georges, J. Gómez, W. Tamayo (2003): The impact of glaciers on the runoff and the reconstruction of mass balance history from hydrological data in the tropical Cordillera Blanca, Perú. *Journal of Hydrology*, 282, 130−144.

Juen, I., C. Georges, G. Kaser (2006): Modelling observed and future runoff from a glacierised tropical catchment (Cordillera Blanca, Perú). *Global and Planetary Change*, in press.

Kaser, G., Ch. Georges, I. Juen, T. Mölg, P. Wagnon, and B. Francou (2004): The behaviour of modern low-latitude glaciers. *Past Global Changes News*, 12(1), 15−17.

Kaser, G., C. Georges, I. Juen, and T. Mölg (2004): Gletscher in den Hochgebirgen der niederen Breiten. *Innsbrucker Geographische Gesellschaft, Jahresbericht 2001/2002.*

Kaser, G., C. Georges, I. Juen, and T. Mölg (2005): Low-latitude glaciers: Unique global climate indicators and essential contributors to regional fresh water supply. A conceptual approach. In: Huber, U., H. K. M. Bugmann, and M. A. Reasoner (*eds.*): *Global Change and Mountain Regions: A State of Knowledge Overview*. Kluwer: New York, vol.23, 185−196.

Conferences

AGM: Alpine Glaciological Meeting
EGU: European Geophysical Union
IAHS: International Association of Hydrological Sciences
IGS: International Glaciological Society

Lectures

AGM, Munich (Germany), February 2001:
Juen, I.: Glacier mass balance, precipitation and runoff in tropical catchment areas (Cordillera Blanca, Perú).

AGM, Zurich (Switzerland), February 2002:
Juen, I. and Kaser, G.: A rock & ice avalanche and subsequent flood in the Andes.

EGU, Nice (France), April 2002:
Juen, I., Georges, C. and Kaser, G.: Modelling Younger Dryas glacier extents in the tropical Cordillera Blanca.

Mass Balance of Andean Glaciers, Valdivia (Chile), March 2003:
Juen, I. and Kaser, G.: Modelling runoff from a glaciated tropical catchment area in Perú.

AGM, Innsbruck (Austria), February 2004:
Juen, I. and Kaser, G.: Modelling runoff from a glaciated tropical catchment area in Perú.

Conference on Mountain Hydrology, Berchtesgaden (Germany), September 2004:
Juen, I: The change of glacier runoff in the tropical Cordillera Blanca, Perú, under different climate change scenarios.

AGM, Milano (Italy), February 2005:
Juen, I.: Climate change and its impact on runoff in the Rio Santa valley, Cordillera Blanca, Perú.

IAHS VIIth Scientific Assembly, Foz do Iguaçu (Brazil), April 2005:
Juen, I., Wagnon, P., Kaser, G. and Pouyaud, B.: Modelled and measured ablation and runoff from a glacier in the tropical Cordillera Blanca, Perú.

IGS, Lanzhou (China) 2005:
Juen, I.: One year of energy balance on Glacier Artesonraju in the tropical Cordillera Blanca, Perú. Measured and modelled ablation and runoff.

Posters

Mass Balance of Andean Glaciers, Valdivia (Chile), March 2003:
Juen, I., Pouyaud, B. and Kaser, G.: Analysis of glacier runoff and climate data in the tropical Cordillera Blanca, Perú.

EGU, Nice (France), April 2004:
Juen, I. and Kaser, G.: The variability of seasonal melt water production on a glacier in the tropical Cordillera Blanca, Perú.

Mass Balance of Andean Glaciers, Huaraz (Perú), July 2004:
Juen, I.: Runoff scenarios from Cordillera Blanca glaciers under different changing climate conditions.

EGU, Vienna (Austria), April 2005:
Juen, I., Wagnon, P., Kaser, G. and Pouyaud, B.: Modelled and measured ablation and runoff from a glacier in the tropical Cordillera Blanca, Perú.

Curriculum vitae Irmgard Juen

Born on September 18th 1972 in Innsbruck

1976 – 1987	Elementary school in Fließ
1987 – 1988	Household school in Pfaffenhofen
1988 – 1992	Academy of fashion and clothing in Innsbruck (A-level June 1992)
1992 – 1993	Tailor in Wattens
09/1993 – 01/2000	Study of Geography (diploma) in Innsbruck. Master thesis: "Blockgletscheruntersuchungen im hintersten Ultental".
01/2000 – 09/2001	Co-worker at several projects at the Department of Geography in Innsbruck
Since 10/2001	Research scientist within the Innsbruck Tropical Glaciology Group.
Research fields	Glaciology and Hydrology in the Tropics
Main tasks	Data processing and analyses
	Field work and organisation
	Programming and maintenance of automatic stations
	Project organisation
Languages	German English Spanish (conversational)

Appendixes

A. Generating a digital elevation model (DEM)

A digital elevation model for the whole Cordillera Blanca was generated using the software ArcInfo 7.1 and Surfer 6. A report about generating the *DEM* with ArcInfo is performed by Georges (2005).

Export des GeländEModells cbtin in ein Ascii-File

Arc: ungeneratetin cbtin tinasc

Dabei werden nur die Stützpunkte des Tins verwendet, die bereits auf den Höhenlinien vorhanden waren. Dadurch wird das neue GeländEModell nicht durch interpolierte Stützpunkte des Tin-GeländEModells manipuliert.
Das Ascii-File enthält vier Spalten mit den Informationen:

Id	X-Koordinaten	Y-Koordinaten	Z-Koordinaten
1	24574000000000000D+06	900202000000000000D+07	3705000E+04
2	24588000000000000D+06	.....	.....
3	.....	.....	.....

Ascii – File zerlegen

Die Berechnung des SurfergeländEModells ist nur in kleinen Teilstücken möglich, da sonst die Berechnungszeit exponentiell ansteigt. Dazu wurde das Programm GAWK (Linux-Unix-Tool) verwendet. Die Zerteilung wurde mit einer Doppelbedingung durchgeführt (wenn x kleiner als 207870 und x größer als 169870 und y kleiner als9044670 and y größer als 8999570 = cbdgm11.dat.....). Dadurch entstanden 12 Teilstücke mit je 1000 m Überlappung in folgenDEM Schema:

11	12	13
21	22	23
…	…	…

Eckkorrdinaten des cblat		xmin	xmax	ymin	ymax
		169870	180750	886790	9044670
Teile:		dx	dy	xueberlapp	yueberlapp
		38000	45000	1000	1000
teily	teilx	xmin	xmax	ymin	ymax
1	1	169870	207870	8999570	9044670
1	2	206870	244870	8999570	9044670
1	3	243870	281870	8999570	9044670
2	1	169870	207870	8955570	9000570
2	2	206870	244870	8955570	9000570
2	3	243870	281870	8955570	9000570
3	1	169870	207870	8911570	8956570
3	2	206870	244870	8911570	8956570
3	3	243870	281870	8911570	8956570
4	1	169870	207870	8867570	8912570
4	2	206870	244870	8867570	8912570
4	3	243870	281870	8867570	8912570

Erstellung des GeländEModells im Surfer

Grid-Data:

Input: cbdgm11.dat
Data: x = Spalte B
Y = Spalte C
Z = Spalte D
General: Spacing: 20
Min und Max jeweils – 10 m da der Surfer vom Eckpunkt unten links aus misst und Arc/Info vom Mittelpunkt aus.
Methode: Kriging
Output: cbdgm11.grd

Umwandlung der GeländEModelle im Surfer:

Grid – Transform – MirrowY

Spiegelung des Grids

Input: cbdgm11.grd

Output: cbdgm11s.grd

Grid – Convert – GS ASCII (*.grd)

Input: cbdgm11s.grd

Output: cbdgm11se.grd

Header im Word verändern:

Die ersten fünf Zeilen müssen geändert werden, damit es ArcInfo lesen kann.

Ursprung	Neuer Header
DSAA 1901 2251 169870 207870 8955570 9000570 2165.4619140625 6301.8623046875	Ncols 1901 Nrows 2251 Xllcorner 169870 Yllcorner 8999570 Cellsise 20 Nodata_value -9999

Importieren und zusammenfügen der Einzelteile in Arc/Info

Arc: asciigrid cbdgm11se.grd cbdgm11 float

=> Importieren des Asciigrids.

Grid: gridclip cbdgm11 dgm11 169870 9000070 207370 9044670

=> Da die Überlappung 1000 m beträgt, werden die Grids an den Schnittstellen jeweils 500 m kleiner gemacht (-500 bzw. +500 bei den Koordinatenpunkten).

Grid: dgmsurfer = merge (dgm11, dgm12, dgm13, ...dgm43)

=> Zusammenfügen der einzelnen Grids zu einem großen Grid.

Grid: if

:: (cblat eq –9999) cbsurfer = -9999

:: else cbsurfer = dgmsurfer

:: end

=> Ausschneiden des Grids auf die genaue Größe des Grids cblat.

Grid: cbsurfin = int (cbsurfer + 0,5)

=> Umwandlung des GeländEModells in ein integer Grid, da sonst die Füllung der
Sinks nicht funktioniert

B. Watershed deviation from DEM

1. Berechnung der hydrologischen Einzugsgebiete vom GeländEDEModell cblat (Lattice)

Import des DGM

Arc: import grid cblat.e00 cblat

Pourpoints setzen

Zur Watershed-Berechnung in Arc/Info müssen die Endpunkte der Einzugsgebiete händisch gesetzt werden. Dazu wurde bei jeDEM Einfluß in den Hauptfluß ein Punkt gesetzt und mit der Gletscherinventarnummer versehen. Mehrere Zuflüsse in einem Einzugsgebiet wurden mit einer zusätzlichen Nummer am Ende versehen z. B. 1P005CL1, 1P005CL2 ...
Die Zuflüsse des Rio Santa von Westen sind durchgehend von Norden nach Süden mit W1 bis W63 durchnummeriert. Einzugsgebiete im Osten, die keine Gletscherinventarnummer haben sind mit E1 bis E6, Einzusgebiete des Rio Santa von Osten, die zwischen den Begrenzungen der Gletscherinventare liegen mit 1P1, 1P2, 2P1 usw. nummeriert.
Die so gesetzten Punkte sind in den Kopien aus *DEM* Glacier Inventory of Peru eingezeichnet. Die Coverage heißt pourpoint und beinhaltet 201 Punkte.

Aml zur Berechnung der Einzugsgebiete – einzug.aml

cbdir = flowdirection (cblat)
cbacc = flowaccumulation (cbdir)
cbpour = snappour (pourpoint, cbacc, 500)

snappour ist eine Funktion die notwendig ist um die eingezeichneten Punkte auf den wirklichen Zufluß zu snappen, der durch die Funktion flowaccumulation für das DGM berechnet wird.

Cbwater = watershed (cbdir, cbpour)

Probleme des Ergebnisses

- Durch die Funktion snappour werden die Punkte genau auf den Fluß Rio Santa gesnappt, wodurch die Einzugsgebiete natürlich auf die West- und auf die Ostseite reichen.
- Das GeländEDEModell hat an Stellen, wo die Höhenlinien nicht nahe genug beieinander liegen Löcher interpoliert, wodurch die hydrologischen Einzugsgebiete hier enden und nicht bis zur Wasserscheide reichen.

Problemlösung

- Das DGM wird beim Fluß Rio Santa durchgetrennt und für beide Teile eine separate Berechnung durchgeführt.
- Die Löcher müssen ermittelt und aufgefüllt werden. Dazu dient die Funktion sinks und fill

Aml einzug2.aml

fill cblat cbfill sink 40 cbdirfill
gridclip cbfill cbost cover clipost
gridclip cbfill cbwest cover clipwest
gridclip pourpoint pointost cover clipost
gridclip pourpoint pointwest cover clipwest
ostdir = flowdirection (cbost)
westdir = flowdirection (cbwest)
ostacc = flowaccumulation (ostdir)

westacc = flowaccumulation (westdir)
ostsnap = snappour (pointost, ostacc, 500)
westsnap = snappour (pointwest, westacc, 500)
waterost = watershed (ostdir, ostsnap)
waterwest = watershed (westdir, westsnap)

Zusammenfügen der beiden Grids und Umwandlung in eine Coverage

Grid: waterall = merge (waterost, waterwest)
Grid: einzug = gridpoly (waterall)

Attributierung der Einzugsgebiete

Durch die Umwandlung des Grids in eine Coverage ist die Attributierung verloren gegangen. Diese kann mit linken wieder gewonnen werden

Ae: sel einzug.pat
Ae: relate add
Relation name: link
Table identifier: waterall.vat
Database Name: info
Info item: Grid-code
Relate column: value
Relate type: linear
Relate Access: rw

Ae: Additem s_value 10 10 c
Ae: Calculate s_value = link//s_value

2. Berechnung der hydrologischen Einzugsgebiete vom GeländEModell cbsurfer

Aml einzug3.aml starten im Grid

```
Grid: &r einzug3.aml

surferdir = flowdirection (cbsurfer)
surfersink = sink (surferdir)
fill cbsurfin surferfill sink 40 surferdirf
gridclip surferfill surferost cover clipost
gridclip surferfill surferwest cover clipwest
/*gridclip pourpoint pointost cover clipost
/*gridclip pourpoint pointwest cover clipwest
surfostdir = flowdirection (surferost)
surfwestdir = flowdirection (surferwest)
surfostacc = flowaccumulation (surfostdir)
surfwestacc = flowaccumulation (surfwestdir)
surfostsnap = snappour (pointost, surfostacc, 500)
surfwestsnap = snappour (pointwest, surfwestacc, 500)
surfwaterost = watershed (surfostdir, surfostsnap)
surfwaterwest = watershed (surfwestdir, surfwestsnap)
```

Die weiteren Arbeitsschritte wurden genau wie beim GeländEModell cblat durchgeführt

3. Expostions- und Neigungsanalysen der beiden DEM

```
Grid: surferexpo = aspect (cbsurfer)
Grid: cbexpo = aspect (cblat)

Grid: surferneig = slope (cbsurfer)
Grid: cbneig = slope (cblat)
```

Reklassifikation der Expositionsgrids

Flach	-1	1
Nord	0-22,5; 337,5-360	2
Nordost	22,5-67,5	3
Ost	67,5-112,5	4
Südost	112,5-157,5	5
Süd	157,5-202,5	6
Südwest	202,5-247,5	7
West	247,5-292,5	8
Nordwest	292,5-337,5	9

Vergleich der reklassifizierten Expositionsgrids expoai und surfexpore:

	Expoai	Surferexpore
Exposition	Count	Count
Flach	2089951	0
N	2770092	3074027
NE	3174111	3359338
E	2971319	3307611
SE	2878829	3061424
S	2619265	2946198
SW	3173712	3356086
W	3120787	3488014
NW	2976033	3181401

Hierbei fällt auf, daß beim GeländEModell expoai sehr viele Ebenen sind, was auf die Art der Berechnung zurückzuführen ist. Gering geneigte Flächen erscheinen

vollkommen eben, was die Unzulänglichkeiten der Einzugsgebiete im Bereich des Flußbettes erklärt. Im Gegensatz dazu hat das GeländEModell keine ebenen Flächen, was den Gegebenheiten in der Natur eher entsprechen dürfte.

Reklassifikation der Neigungsgrids

0	0
0,1-10	1
10,1-20	2
20,1-30	3
30,1-40	4
40,1-50	5
50,1-60	6
60,1-70	7
70,1-80	8
80,1-85,422	9

Vergleich der reklassifizierten Neigungsgrids cblatneigre und surfneigre:

	Cblatneigre	surfneigre
Neigung	Count	Count
Flach = 0	2227791	0
0,1-10	3078791	5052842
10,1-20	6502985	7173717
20,1-30	6910596	6928582
30,1-40	4621859	4513037
40,1-50	1851127	1621516
50,1-60	478010	6,397672
60,1-70	89496	77788
70,1-80	13356	8857
80,1-85,442	86	88

C. Field work report

At the beginning of the project one glacier for the west (Rajupaquinan) and one glacier for the east (Chinchey) site of the mountain was chosen to investigate the influence of the more humid (east) and the drier (west) situation of the Cordillera Blanca mountain ridge on the glacier mass balance. During the first field trip in October 1999 an automatic weather stations (*AWS*) was installed at both glaciers (Table C.1 and C.2). The selected glacier on the west site, the Rajupaquinan, had to be given up because of the inacceptance of the local people. Therefore a third *AWS* was installed at Glacier Vallunaraju in May 2000. After the take town of the *AWS* at Rajupaquinan in October 2000 the station was rebuild as a second, higher station at Chinchey. To obtain information about the ice flow velocities a digital camera was installed at the higher *AWS* in May 2001 to take one picture each day. The lower station at Chinchey was taken town in November 2001 because the glacier snout advanced and the station was in danger to be destroyed by the ice. For hydrological studies a runoff gauge (R) was installed below the Glacier Chinchey during the same field trip. The *AWS* at Vallunaraju was stolen in March 2002 but could be got back in May 2002. Nevertheless the field works on Glacier Vallunaraju were given up totally and thus the lower *AWS* from Chinchey was reinstalled at Glacier Shallap as a new glacier for the west side. The situation at Glacier Shallap would have been perfect for runoff measurements. Because of lake safety works during the following year this could not be realised. In March 2004 the runoff station at Chinchey was stolen too and the intention to install a precipitation balance also failed as a matter of course because of the missing logger. As the glacier is very difficult to reach, very crevassed and dangerous, and the ablation area could never been reached we decided to give it up and took the higher *AWS* town in April 2004. With joined efforts with the France group of IRD (Institut de recherche pour le Développement) we concentrate all our field work on Glacier Artesonraju from now on. At the outlet of Lake Artesoncocha the IRD group already runs a runoff gauge since 2000. End of April 2004 we installed a radiation balance station (*RBS*) on the glacier only some days after the installation of an energy balance station (*EBS*) from the IRD. The very bad weather conditions prevented the installation of the two *AWS* which were then installed in July 2004. The *AWS* at Artesonraju-south was extended by a precipitation balance and the northern station by a pressure sensor. One additional precipitation balance was installed at the lake Llanganuco, where the French also run a runoff gauge since 2000.

Table C.1: Field visits in the Cordillera Blanca during the two FWF projects P13567-GEO and P13116-N06

When	Where	Who	What
03.Sep – 10.Oct 1999	Rajupaquinan, Chinchey	Georg Kaser, Bernd Öggl, Michael Butscheck, P Jörg, Klaus Kleebinder, Mathias Knaus, Wolfgang Thomaseth	*AWS* installation, Pluviometer installation, drilling of ablation stakes, Radar and GPS-measurements
17.Apr – 22.May 2000	Vallunaraju, Chinchey	Georg Kaser, Bernd Öggl, Mathias Knaus, Klaus Kleebinder, Wolfgang Thomaseth, Daniela Gerstgrasser	*AWS* installation and data transfer, Pluviometer installation and reading, reading of ablation stakes, snow pits, GPS-measurements
27.Sep – 20.Oct 2000	Vallunaraju, Chinchey, Rajupaquinan	Georg Kaser, Regina Sterr, Norbert Span	*AWS* installation, dismantling and data transfer, Pluviometer reading, reading and drilling of ablation stakes, snow pits, Radar and GPS-measurements
6.May – 25.May 2001	Vallunaraju, Chinchey	Georg Kaser, Regina Sterr, Adam Montein, Daniela Brugger	*AWS* data transfer, digital camera installation, Pluviometer reading, reading and drilling of ablation stakes, snow pits, GPS-measurements
16.Oct – 25.Nov 2001	Chinchey, Shallap, Vallunaraju	Georg Kaser, Irmgard Juen	*AWS* data transfer, Pluviometer reading, GPS-measurements, Runoff gauge installation, runoff calibration measurements, inspection of new glacier
03.Jun – 30.Jun 2002	Chinchey, Shallap, Vallunaraju	Georg Kaser, Irmgard Juen	*AWS* installation and data transfer, runoff calibration measurements, GPS-measurements
16.Mar – 31.Mar 2003	Chinchey, Shallap	Irmgard Juen	*AWS* data transfer
02.Mar – 23.Mar 2004	Shallap, Artesonraju	Georg Kaser, Irmgard Juen, Martin Hölzli	*EBS* installation, *AWS* data transfer
27.Jun – 25.Jul 2004	Shallap, Artesonraju	Georg Kaser, Irmgard Juen	*AWS* installation, extension, and data transfer, sublimation measurements, *EBS* extension
30.Oct – 20.Nov 2004	Shallap, Artesonraju	Irmgard Juen, Lisette Klok	*AWS* and *EBS* data transfer, sublimation measurements
11.Dec – 18.Dec 2004	Artesonraju	Irmgard Juen	Change of energy supply regulators
17.Jun – 28. Aug 2005	Artesonraju, Shallap	Irmgard Juen, Michael Winkler	*AWS* data transfer, change of Ta/Rh sensor *AWS* Shallap, sublimation measurements (Winkler)

Table C.2: Automatic stations in the Cordillera Blanca during the two FWF projects P13567-GEO and P13116-N06

Site	1999 S/O	1999 N/D	2000 J/F	2000 M/A	2000 M/J	2000 J/A	2000 S/O	2000 N/D	2001 J/F	2001 M/A	2001 M/J	2001 J/A	2001 S/O	2001 N/D	2002 J/F	2002 M/A	2002 M/J	2002 J/A	2002 S/O	2002 N/D	2003 J/F	2003 M/A	2003 M/J	2003 J/A	2003 S/O	2003 N/D	2004 J/F	2004 M/A	2004 M/J	2004 J/A	2004 S/O	2004 N/D	2005 J/F	2005 M/A	2005 M/J	2005 J/A	Station [m]
Rajupaquinan	/x°	x°	x°	x°	x°	x°	x°/																														*AWS* 4750
Chinchey	x	x	x	x	x	x	x	x	x	x	x	x	x	x/																							*AWS* 4600
Chinchey							/x	x	x	x	x#	x#	x#	x#	x	x	x	x	x	x	x	x	x	x	x	x	x	x									*AWS* 4950
Chinchey														x			/x	x	x	x	x	x	x/															R 4200
Vallunaraju					x	x	x	x	x	x	x	x	x	x	x	x/																						*AWS* 4800
Shallap																	/x	x	x	x	x	x	x	x	x	x	x	x	x	x°*	x°*	x*	x*	x*	x*	x*	*AWS* 5000
Artesonraju																													x	x	x	x	x	x	x	x	*RBS* 4750
Artesonraju																														x°*	x°*	x°*	x°*	x°*	x°*	x°*	*AWS* 4850
Artesonraju																														x#	x#	x#	x#	x#	x#	x#	*AWS* 5100
Llanganuco																														x	x	x	x	x	x	x	P 3850

° missing and/or unconvincing data >50%
AWS extended by a digital camera
* *AWS* extended by a precipitation balance

The time series of data that are available from the different sites are listed in Table C.2. Although not a single *AWS* could be left at the same site during the five years we can obtain a continuous time series of data from 2000 to 2005 when we combine the data different stations (Table C.2).

Beside the installation of automatic stations field measurements were carried out during the field trips at the different sites. Glacier Rajupaquinan on the west side had to be given up immediately after the installation field trip in November 1999. Thus no field data could be collected. Glacier Chinchey, Vallunaraju and Shallap could be measured at least one year. From April 2004 on field work is concentrated at Glacier Artesonraju with joined efforts with the French group of IRD.
To obtain glacier thickness and surface velocity GPR and GPS measurements were carried out during the field trips. For GPR-measurements (Ground Penetrating Radar) a transmitter from Narod Inc. with 15 m half length antennas has been used. The operating frequency was about 6.5 MHz and the signal was displayed on a digital 100 MHz Scopemeter. Measurements and interpretation of the signal have been performed by Norbert Range and Michael Butscheck. High precision Trimble GPS (Global Positioning System) with a base station and a rover was used for stake measurements. The derived accuracy is below +/- 0.5 m and +/- 1 m horizontally and vertically, respectively. Glacier mass balance information is restricted to very few point measurements and could not be extended to full mass balance calculations. Sublimation measurements during several field trips were carried out on Glacier Artesonraju.

Glacier Chinchey

Glacier Chinchey is situated on the east, more humid side of the Cordillera Blanca at 9°23’ South and 77°18’ West in the valley Rurichinchey. The highest point of the glacier is Nevado Chinchey with 6222 m a.s.l. and the tongue reaches down to app. 4.600 m a.s.l. (Fig. C.1). In 1990 the glacier area was 6.2 km². 90 % of the glacier is east orientated, some minor upper parts are north and south orientated, respectively. The installation field trip was in November 1999 with a seasonal return until November 2001. Because of the heavy crevasses and the dangerous approach of the glacier the mass balance measurements were then given up.

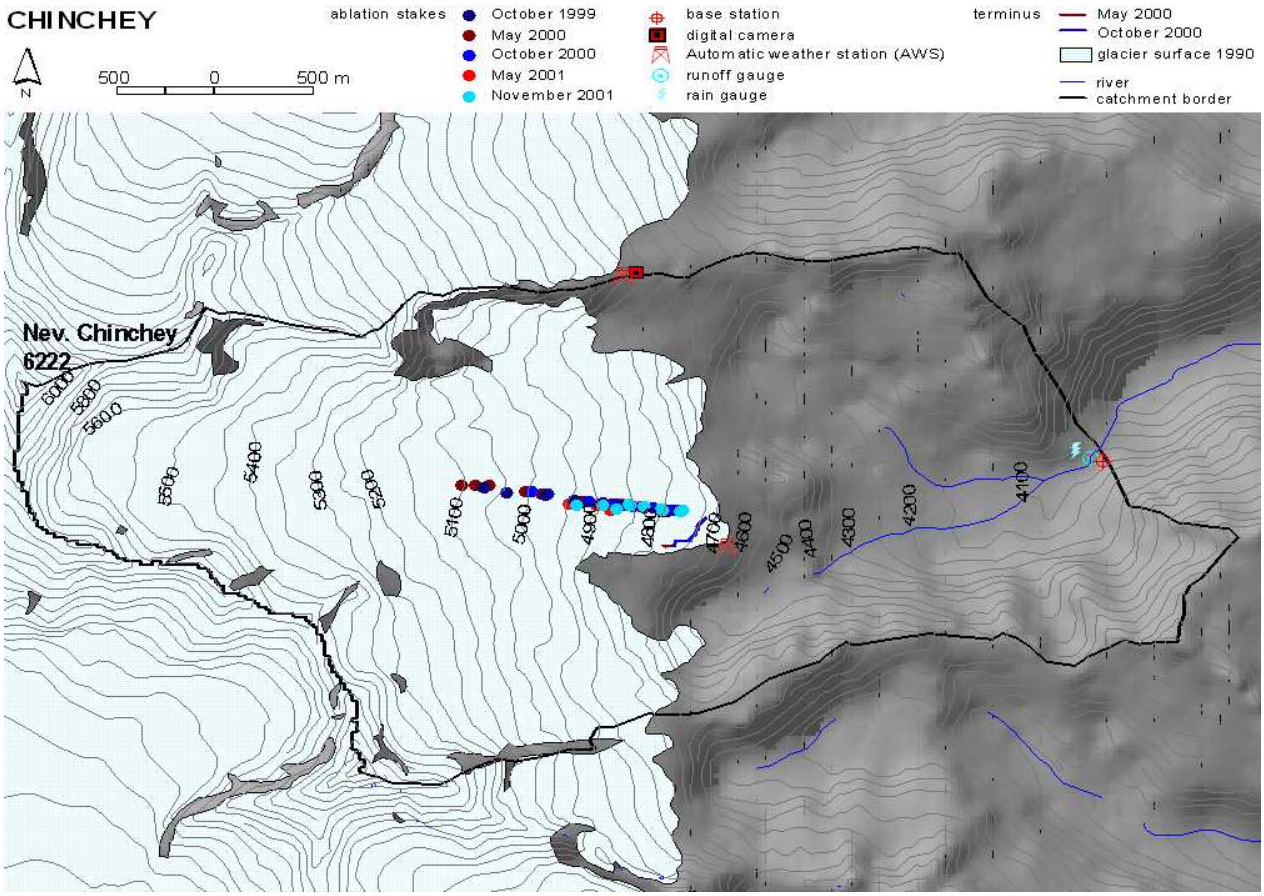

Figure C.1: Map of Glacier Chinchey its station equipment, stake and terminus position (measured with DGPS).

Ground penetrating (GPR) measurements were made along one profile (ablation stakes in Figure C.1) in November 1999 between 4760 and 5060 m a.s.l. and showed a mean ice depths of 47 m and a mean slope of 17 ° (Range et al., 2002). Glacier thickness as well as the slope of the glacier is very uniform along the profile. In October 1999 eight stakes were drilled into the ice and in May 2000 the network was extended by two higher stakes. During each field visit until November 2001 the position of the ablation stakes was measured with a differential global positioning system (DGPS) to obtain seasonal glacier surface movements (Table C.3). Only two stakes could be found at each time. All the other stakes were buried by snow, fell into crevasses or could not be reached because of bad weather conditions and/or high amounts of snow. The calculated velocity for the two year time period of the stakes shows a clear trend of increasing velocity with altitude indicating that measurements did not reach the accumulation area. In the first year velocity is much higher during the wet than during the dry season whereas during the second year the difference in velocity is minor. The mean ice velocity during this two year period is 60 m per year with slightly slower movement during the second year. Additionally to the calculated velocity from DGPS-measurements a digital camera was installed at *AWS* Chinchey-high to take a picture each day. The distance to the glacier is 1300 m; the field of vision of the camera is 55 °. Feature tracking from May to November 2001 with the use of crevasses gave a very high velocity in this part of the glacier of 62 m which is almost double of the measured velocity at the ablation stakes.

Table C.3: Seasonal and annual stake movements obtained from DGPS measurements on Glacier Chinchey from October 1999 to November 2001.

		Stake movement [m]			
Stake	***Altitude [m]***	***Wet season 1999/2000***	***Dry season 2000***	***Wet season 2000/2001***	***Dry season 2001***
y7	*5040*		*31*		*37*
y6	*4970*		*30*		*36*
y5	*4940*	*49*	*26*		*34*
y4	*4880*	*40*	*23*	*33*	*30*
y3	*4850*	*40*	*19*	*31*	*24*
y2	*4800*				*21*
y1	*4780*	*24*	*13*		*18*
		Annual 1999/2000		***Annual 2000/2001***	
y5	*4940*	*75*			
y4	*4880*	*64*		*63*	
y3	*4850*	*59*		*55*	
Y1	*4780*	*37*			

Stake measurements for glacier mass balance calculations were carried out during the same time period than the GPS measurements. Although field work was done very carefully the measurements of the second year are unconvincing and thus not shown. The stakes y6 and y2 could not be found in May 2000. Therefore only annual ablation could be calculated (Table C.4). Ablation is very high at the tongue and decreases quasi linear with altitude. Only stake y2 does not fit perfect into the shape of the mass balance gradient. Mean equilibrium line altitude (ELA) was above 5070 m a.s.l. for the wet and the dry season. Daily melting and refreezing prevents any layering and thus makes snow pit interpretation very difficult. As high altitudes (above 5100 m a.s.l.) could never been reached no full mass balance calculation was possible.

Table C.4: Seasonal net mass balance on Glacier Chinchey from October 1999 to November 2000.

		Stake ablation [mm we]	
Stake	***Altitude [m]***	***Wet season 1999/2000***	***Dry season 2000***
y8	*5070*	*-920*	
y7	*5040*	*-150*	*-95*
y6	*4970*	*-470*	
y5	*4940*	*-35*	*-720*
y4	*4880*	*-90*	
y3	*4850*	*-650*	*-850*
y2	*4800*	*-1160*	
y1	*4780*	*-1440*	*-1580*

DGPS glacier tongue measurements resulted in a mean glacier tongue retread of 70 m from the 1990 glacier extent to 2000 and with almost no change between October 2000 and October 2001.

Data from two automatic weather stations (*AWS*, Figure C.1), one at 4650 m a.s.l. (Chinchey-low) and one at 4950 m a.s.l. (Chinchey-high) are available from November 1999 to November 2001 and from October 2000 to May 2004, respectively. The runoff gauge constructed in November 2001 was stolen after the field visit in May 2003 and only partly covers one dry and one wet season.

Glacier Vallunaraju

Glacier Vallunaraju is situated on the west and drier side of the Cordillera Blanca app. 10 km north of Huaraz at 9°25’ South and 77°28’ West. The top of Nevado Vallunaraju is 5686 m a.s.l., the glacier tongue at app. 4700 m a.s.l (Figure C.2). The glacier area is 5.2 km² and mainly west orientated. In October 2000 investigations on Glacier Vallunaraju were initialised. After the huge avalanche that eroded the glacier unto the rocks just beside the ablation stakes in November 2001 measurements were given up.

DGPR-measurements were made along one profile (ablation stakes in Figure C.2) in October 2000 between 4720 and 5080 m a.s.l. and showed a mean ice depths of 41 m and a mean slope of 19 ° (Range et al., 2002). In Mai 2000 ten ablation stakes were drilled into the ice. During each field visit until Mai 2001 the position of the ablation

stakes was measured with GPS to obtain seasonal glacier surface movements (Table C.5). Four stakes could be found at each time. The calculated velocity for the dry season shows similar to the results at Glacier Chinchey a trend of increasing velocity with altitude. Also similar is the much higher velocity during the wet than during the dry season but with an inversed trend of decreasing velocity with altitude. Mean annual stake movement is 60 m at Glacier Vallunaraju. At the two lower stakes ice velocity at the steeper Glacier Vallunaraju is above 75 m per year which is much higher then at Glacier Chinchey where only 50 m during the same time period were obtained.

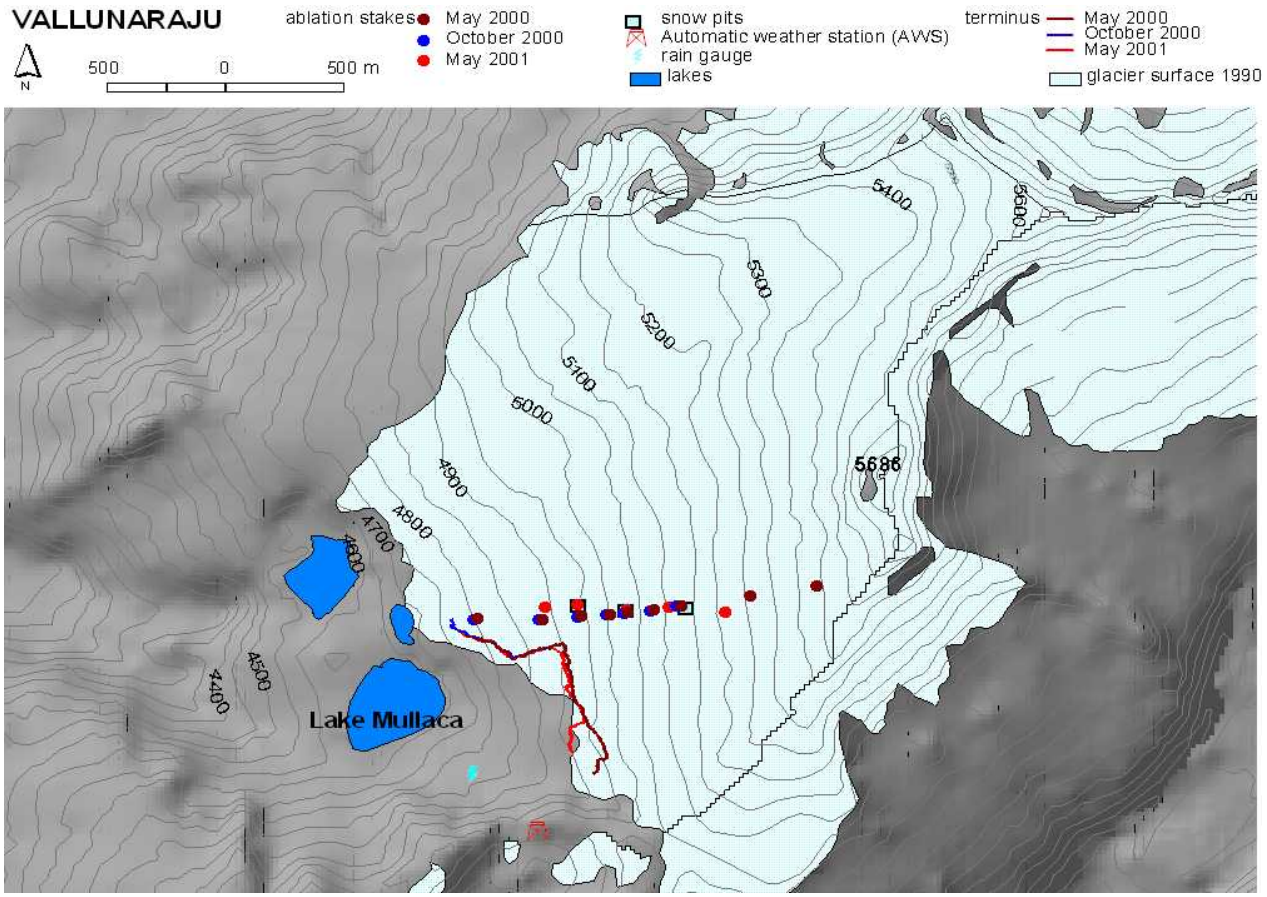

Figure C.2: Map of Glacier Vallunaraju its station equipment, stake and terminus position (measured with DGPS).

Stake measurements for glacier mass balance calculations were carried out during the same time period than the GPS measurements (Table C.5). During the dry season 2000 mean equilibrium line altitude (ELA) was around 5000 m a.s.l. where stakes above and below experienced a mass gain and loss, respectively. The wet season 2000/2001 was a positive period with mass gain at all altitudes. The mass balance year 2000/2001 was positive with a mass loss only at vr4 and probably below. Mean *ELA* from May 2000 to May 2001 was at 4950 m a.s.l.

Glacier tongue measurements with GPS show a mean retreat of the glacier tongue of 50 m from 1990 to 2000. From May 2000 to May 2001 the glacier tongue was stable

or even advanced up to 150 m in the southern part of the glacier (Figure C.2) which is in good agreement with the mass gain we observed at the ablation stakes.

Table C.5: Seasonal and annual stake movements obtained from GPS measurements and stake ablation on Glacier Vallunaraju from May 2000 to May 2001.

		Stake movement [m]		***Stake ablation [mm we]***	
Stake	***Altitude [m]***	***Dry season 2000***	***Wet season 2000/2001***	***Dry season 2000***	***Wet season 2000/2001***
vr8	*5110*	*23*	*31*	*+32*	*+750*
vr7	*5050*	*21*		*+92*	
vr6	*5000*	*16*	*18*	*+193*	*+390*
vr5	*4970*	*16*	*54*	*-900*	*+250*
vr4	*4920*	*17*	*68*	*-660*	*+545*
vr3	*4850*	*16*		*-1999*	
		Annual 2000/2001		***Annual 2000/2001***	
vr8	*5110*	*54*		*+782*	
vr6	*5000*	*34*		*+197*	
vr5	*4970*	*70*		*+650*	
vr4	*4920*	*85*		*-115*	

The *AWS* at Vallunaraju (Figure C.2) was installed in May 2000 and taken down by thieves in March 2002.

Glacier Shallap

Glacier Shallap is situated on the west side of the Cordillera Blanca app. 80 km east of Huaraz at 9°25’ South and 77°20’ West in the valley of Shallap. Glacier Shallap is one of the hugest glaciers in the Cordillera Blanca with 8.4 km². The glacier tongue is separated into a northern and a southern part by a middle moraine. Measurements were concentrated on the southern part with the accumulation area reaching up to 6000 m a.s.l. The upper part is mainly north orientated whereas the glacier tongue is more west to southwest orientated. In 1990 the glacier reached down to 4400 m a.s.l. but has strongly retreated since then to app. 4600 m a.s.l. in 2001 (personal guess). A network of ablation stakes between 4785 and 4940 m a.s.l. was initialised in July 2001. From March 2002 to March 2004 the glacier was visited by the glaciologists of INRENA every month to measure the stake network.

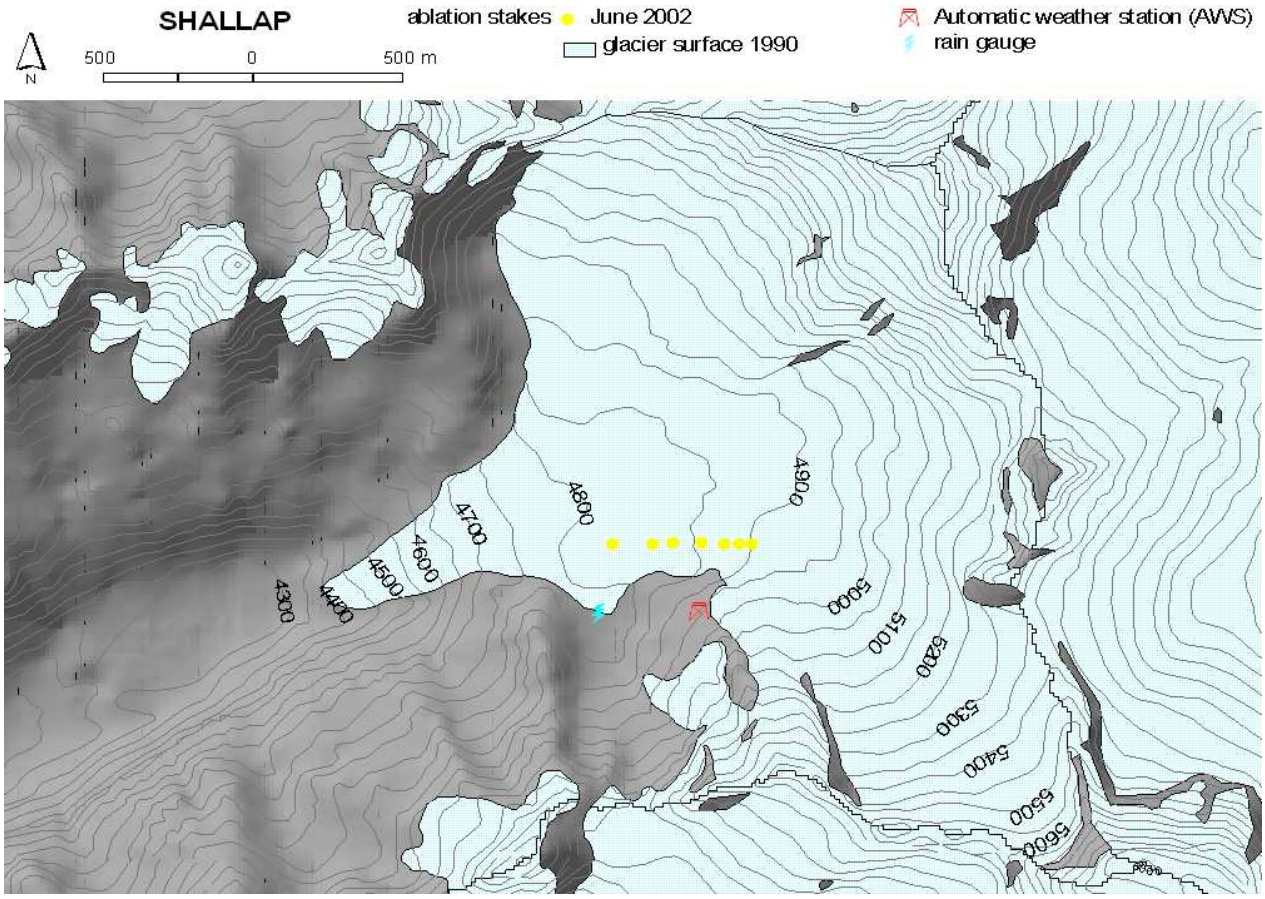

Figure C.3: Map of Glacier Shallap its station equipment and stake position.

Seasonal stake ablation for the two year time period is shown in Figure C.4. A trend towards steeper mass balance gradients during the dry seasons can clearly be seen (regression lines in Figure C.4). Below 4800 m a.s.l. ablation is very high with values up to almost 5 m we per season, at 4900 m a.s.l. ablation varies between 1 – 3 m we per season. Annual net balance is strongly negative for both years at all measured altitudes varying between 2 – 5.7 m we in the first and 4 – 7 m we in the second year (Table C.6). A calculation of total mass balance from stake ablation is not possible because the stakes only give information about a very small part of the ablation area. In the accumulation area no measurements exist. Mean net balance derived from the ablation stakes for three months is shown in Figure C.5 for the lowest and highest stake and as a mean between 4800 – 4850 and 4850 – 4900 m a.s.l.. Only from October – December 2002 slightly positive mass balance was measured above 4850 whereas all other periods are characterised by more or less strong mass losses.

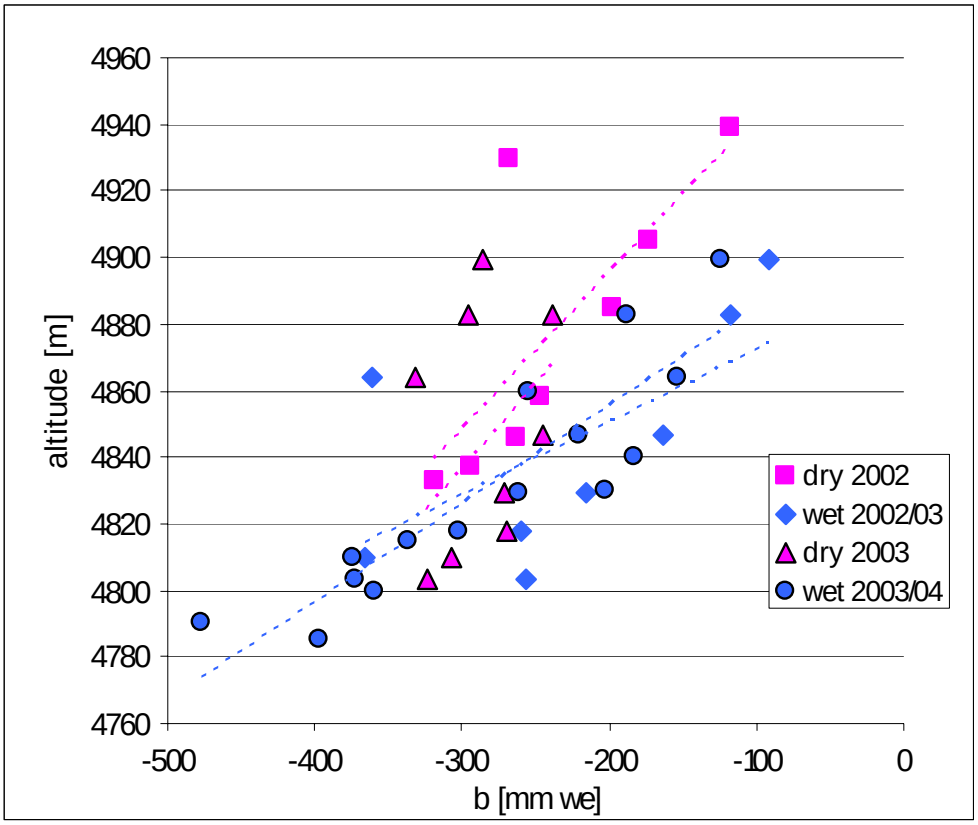

Figure C.4: Seasonal stake ablation at Glacier Shallap between 4785 to 4940 m a.s.l. from April 2002 to March 2004. The dry season is defined from April to September, the wet season from October to March. The lines indicate the regression between the stakes (dashed line is 2003/2004).

Table C.6: Seasonal stake ablation measured at Glacier Shallap at 4800, 4850 and 4900 m a.s.l.

		Stake ablation [mm we]			
Stake	***Altitude [m]***	***Dry season 2002***	***Wet season 2002/2003***	***Dry season 2003***	***Wet season 2003/2004***
a3	*4803*	*-3194*	*-2566*	*-3230*	*-3732*
a7	*4847*	*-1984*	*-1641*	*-2453*	*-2209*
a10	*4899*	*-1170*	*-917*	*-2857*	*-1240*
		Annual 2002/2003		***Annual 2003/2004***	
a3	*4803*	*-5760*		*-6962*	
a7	*4847*	*-3625*		*-4662*	
a10	*4899*	*-2087*		*-4097*	

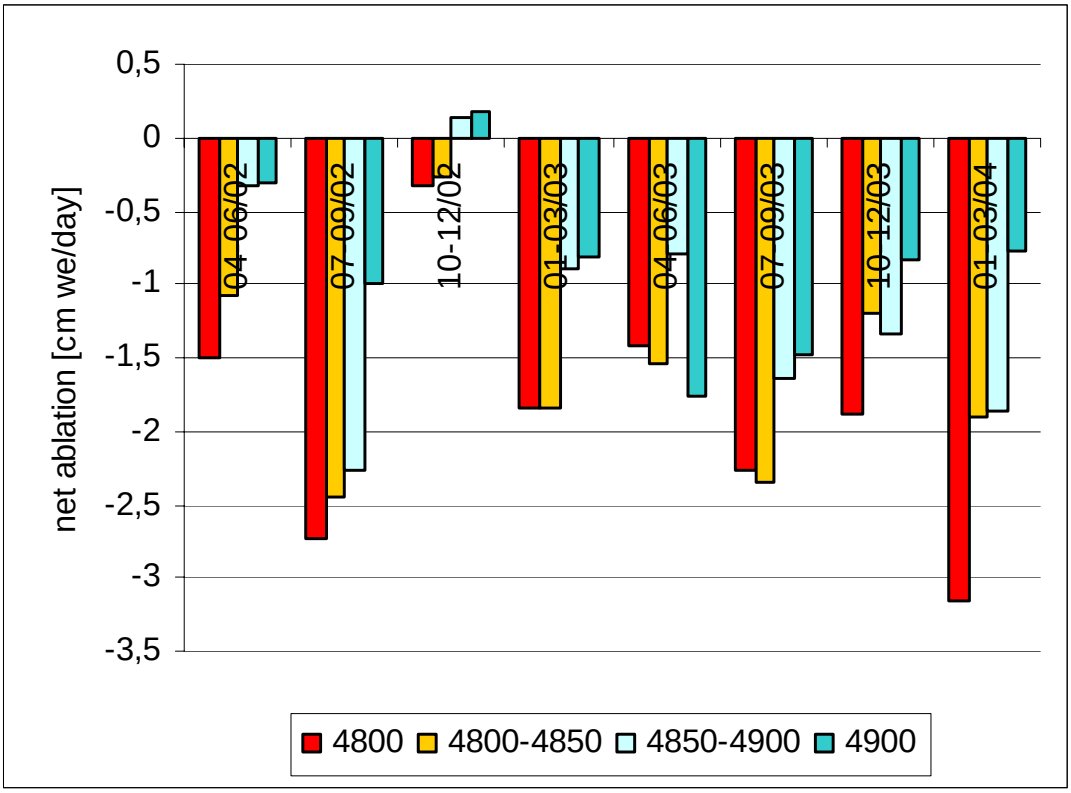

Figure C.5: Mean net mass balance derived from ablation stake measurements at Glacier Shallap averaged over three months.

The *AWS* Shallap (Figure C.3) was installed in June 2002 at 5000 m a.s.l. and extended by a precipitation gauge in July 2004. Due to bad energy regulators data are incomplete after June 2003.

Glacier Artesonraju

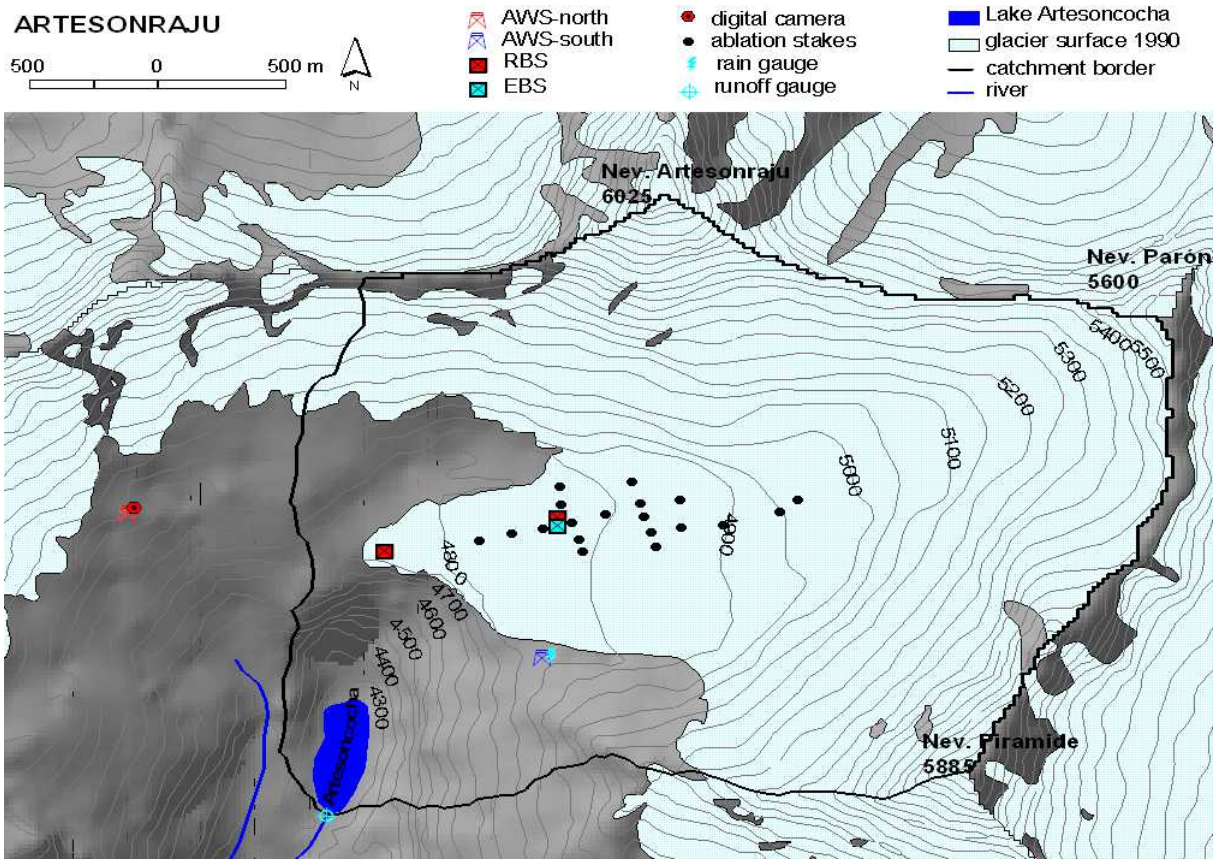

Figure C.6: Map of Glacier Artesonraju its station equipment and stake position. AWS = automatic weather station; RBS = radiation balance station (moved to lower side on 17th of November 2004); EBS = energy balance station.

Glacier Artesonraju is situated in the northern part of the Cordillera Blanca at 8°58' S and 77°38' W in the valley of Paron (Figure C.6). The glacier covers an area of 5.7 km² from the highest top Nevado Artesonraju with 6025 m a.s.l. down to the tongue at app. 4750 m a.s.l. The runoff gauge at the outlet of Lake Artesoncocha was built in 1999 by the French group of IRD. The catchment covers an area of 7.7 km² with a glacierised area of 74 %. The stake network was initialised in 2000 and extended in July 2004. Sublimation measurements were carried out through several field trips when the weather conditions allowed it (Table C.7).

Table C.7: Daily sublimation as measured during field trips in July and November 2004 and in August 2005. Measurements were made at 10 a.m. each day.

Date	***Daily sublimation [mm we]***	
	4850 m a.s.l.	***5010 m a.s.l.***
21.-22.7.2004	*0.07*	*0.06*
22.-23.7.2004	*0.42*	*0.45*
23.-24.7.2004	*0.64*	*0.79*
24.-25.7.2004	*0.85*	-
25.-26.7.2004	-	*0.35*
27.-28.7.2004	*0.84*	-
14.-15.11.2004	*1.72*	*1.44*
15.-16.11.2004	*1.84*	*1.55*
2.-3.8.2005	*2.47*	-
3.-4.8.2005	*2.08*	*1.76*
4.-5.8.2005	*0.62*	-
5.-6.8.2005	*0.80*	*0.58*
6.-7.8.2005	*1.17*	*1.06*
7.-8.8.2005	*1.16*	*0.95*
10.-11.8.2005	*2.49*	*1.36*
11.-12.8.2005	*3.63*	*4.09*
17.-18.8.2005	*3.19*	-
18.-19.8.2005	*2.04*	-
19.-20.8.2005	*0.93*	-
20.-21.8.2005	*4.91*	-

Daily sublimation amounts vary between 0.07 to 0.85 mm we and 0.06 to 0.79 mm we during a seven day measuring period in July 2004 and between 1.72 to 1.82 mm we and 1.44 to 1.55 mm we during a two day period in November 2004 at 4800 and 5010 m a.s.l., respectively (Tab. C.7). At two days out of five where measurements at both altitudes were successful sublimation is higher at the higher site. This may be caused by higher wind speeds and thus enhanced sublimation. During the field work in 2005 sublimation amounts are generally higher and even reach 4.9 mm we per day. Surprisingly, during this period of measurements sublimation amounts at the higher site are generally lower than at the *EBS*.

Data from automatic stations

Mean daily data from the *AWS* Chinchey-low and -high, Vallunaraju, Shallap, Artesonraju-north and –south as well as from the *EBS* at Artesonraju are shown as a 9-day running mean in Figure C.7. Unconvincing data as relative and consequently specific humidity for several stations, and wind direction of station Shallap are not shown.

Annual variability of mean daily incoming solar radiation is low for all stations and varies mainly between 100 to 300 W/m². The most standing out periods are from November 4th to 15th and from December 12th to 16th, 2000 where radiation is constantly above 350 W/m² at all three stations that cover this period. These days of very clear sky are also recorded in an extraordinary high air temperature and low relative and specific humidity at all three stations. During the dry season incoming solar radiation is tendentious slightly higher than during wet season. The overlapping time period of *AWS* Chinchey-high and Shallap show good agreement in their fluctuations. Although both stations are almost at the same altitude and latitude (4950 and 5000 m a.s.l.; 9°29’ and 9°24’ respectively) mean daily values are 50 W/m² higher at *AWS* Shallap. The reason for the reduced incoming shortwave radiation at *AWS* Chinchey-high might be caused by the higher cloud cover at the more humid eastern side of the Cordillera Blanca. The higher values at *AWS* Shallap seduces to interpret the misleading optical impression that solar radiation increases during the last two years which is not the case when you take the difference in cloudiness into account. At the *EBS* SWin is slightly higher which might be due to increased diffuse radiation from the surrounding snow and ice surface.

Air temperature is calculated for 5000 m a.s.l. with a gradient of -0.0065 °C m^{-1} for all stations and varies between -2 to 4 °C. A tendency towards slightly higher temperature during the wet period because of less cooling during the night is proved from all time series. Daily variability is very similar at all stations. Mean daily air temperature at *AWS* Chinchey-low and Vallunaraju is 1.2 °C and 1.7 °C lower than at Chinchey-high. Temperature at Chinchey-high is very similar to the temperature recorded at *AWS* Shallap. Thus these two time series can be taken for a long-term trend analyses. Over the entire five years mean air temperature shows a slight increasing trend. Daily mean values at the *EBS* are lower than outside the glacier due to the cooling effect of the ice or snow surface.

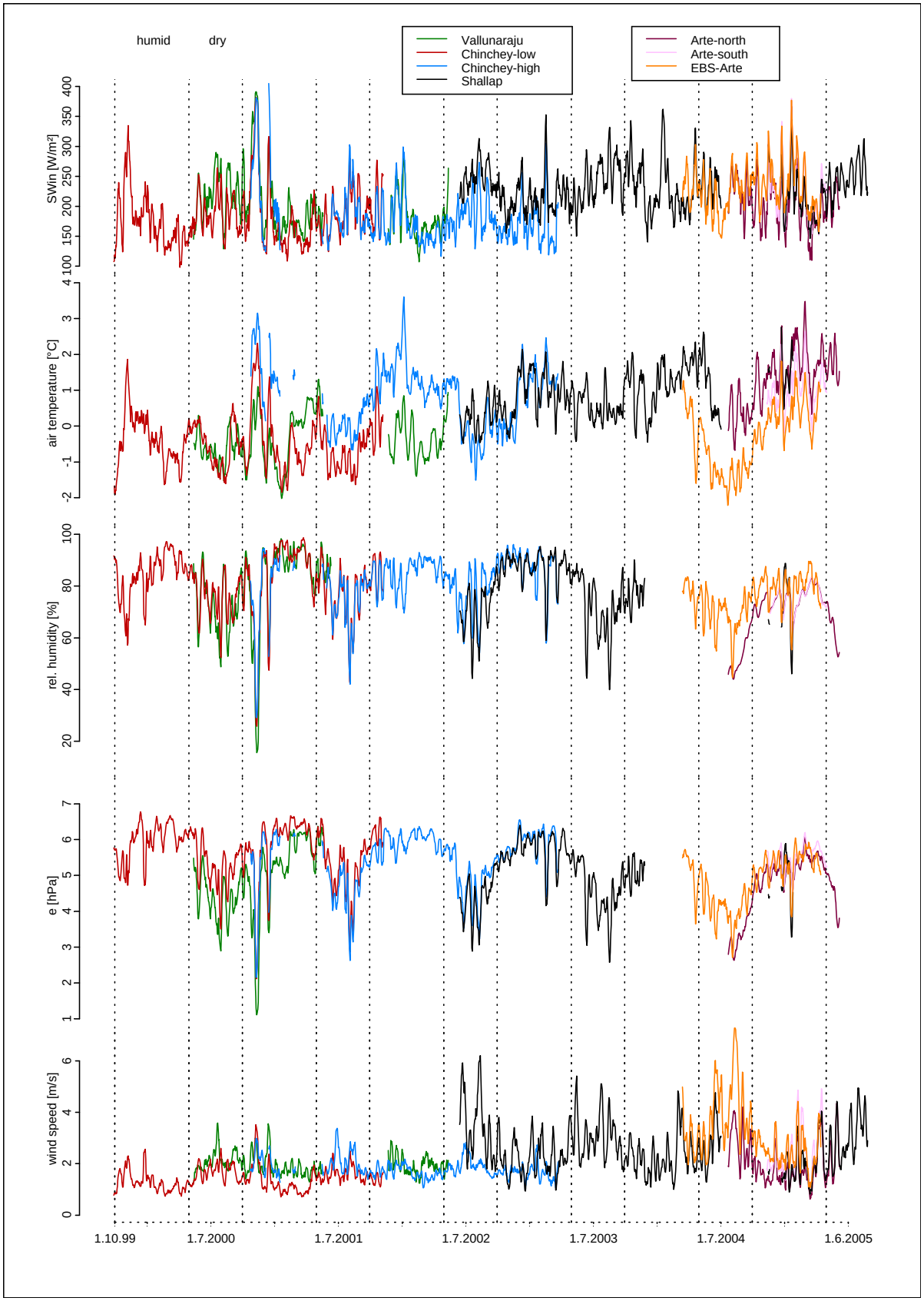

Figure C.7: Daily means (9-day running mean) of solar incoming radiation (SWin), ventilated air temperature (calculated for 5000 m a.s.l.), relative humidity and vapour pressure (e) humidity, and wind speed as measured at the AWS at Chinchey-low and –high, Vallunaraju, Shallap, Artesonraju-north and -south, and EBS Artesonraju.

Relative humidity does not drop below 45 %, vapour pressure not below 3 hPa. Only during the period of extraordinary high solar radiation in November 2000 values trop to 18 % and to 1 hPa, respectively. During the wet season humidity usually varies between 80 to 100 % (5 to 7 hPa) and between 40 to 80 % (3 to 5 hPa) during dry season. Day to day variability is much higher during the dry season then during the wet season. On a long term a slight decrease for both seasons is recorded.

Wind speed varies between 1 to 3 m/s for both Chinchey *AWS* and at *AWS* Vallunaraju. Much higher wind speeds with much higher daily variability are recorded at *AWS* Shallap and all stations in the region of Glacier Artesonraju with up to 6-7 m/s. For all stations wind speed and daily variability is higher during the dry season.

Daily cycle of the different climate variables of all stations is shown in figure C.8 as an annual mean and for the wet and dry season respectively.

Daily sunrise is at 6:00 at *AWS* Chinchey-high and at all other stations at 7:00, sunset at 20:00. Maximum solar radiation is at 12:00 at *AWS* Vallunaraju and at all other stations at 13:00. Values are much lower for both Chinchey stations due to the higher cloud cover in the more humid eastern side of the Cordillera Blanca than for all the others which may be due to the higher cloud cover at the more humid east side of the Cordillera Blanca. During dry season daily amplitude is a little bit higher than for the wet season.

Annual mean daily variability of air temperature is 4 to 5 °C for all stations. Minimum temperature occurs in the early morning hours between 6 – 7 l. t.. Daily maximum follows the cycle of solar incoming radiation with a time delay of one to two hours. Daily variability of air temperature is higher during the dry season due to the cooling in clear sky nights and the higher warming during the day when solar incoming radiation is less reduced by clouds.

The cycle of specific humidity follows more or less the cycle of air temperature with its minimum in the early morning hours and its maximum around midday. At the more humid Chinchey stations the minimum is less developed than at the others. Maximum specific humidity is reached at around 10:00 and remains high during the whole day. At station Shallap the maximum occurs in the late afternoon. At *AWS* Vallunaraju and Artesonraju-north the maximum value is reached at 13:00 with a rapid drop to very low values at the later station. Daily amplitude is more than double at *AWS* Artesonraju-north than at both Chinchey stations which is mainly caused by the much more pronounced daily variability during the wet season at *AWS* Artesonraju-north.

Wind speed reaches its maximum at around midday at *AWS* Shallap, Artesonraju-north, and Chinchey-high, whereas at Chinchey-low maximum is delayed by two hours and Vallunaraju has its minimum around midday and reaches its maximum

wind speed in the late afternoon at 17:00. Seasonal daily cycle is similar with higher wind speeds during the dry season.

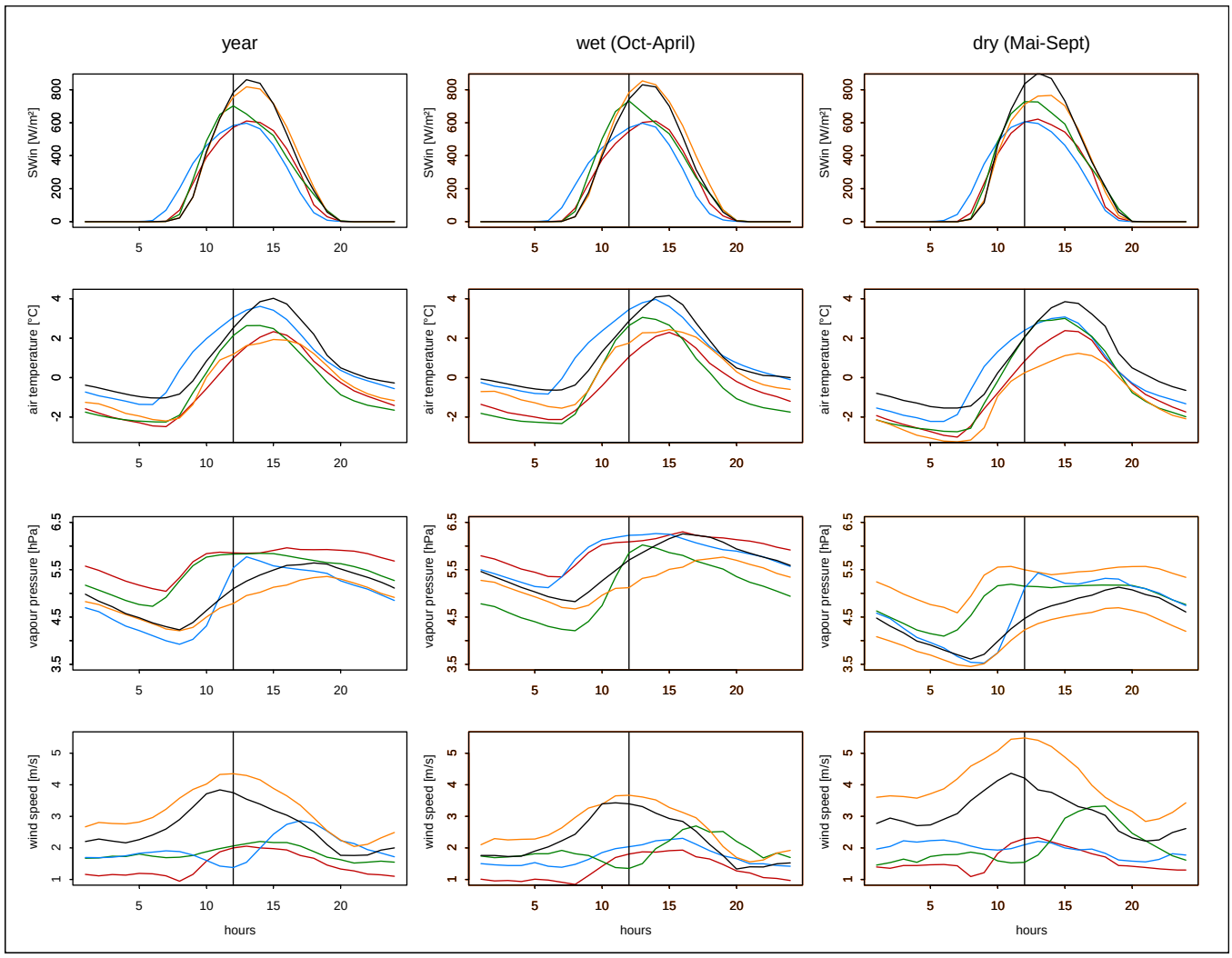

Figure C.8: Mean annual and seasonal daily cycle of solar incoming radiation (Swin), air temperature, specific humidity, and wind speed as recorded at AWS Chinchey-low (red) and –high (blue), Vallunaraju (green), Shallap (black) and the EBS Artesonraju (orange).

Figure C.9: AWS-south at Glacier Artesonraju (4850 m a.s.l.) with a precipitation gauge. Photo taken by Irmgard Juen in July 2004.

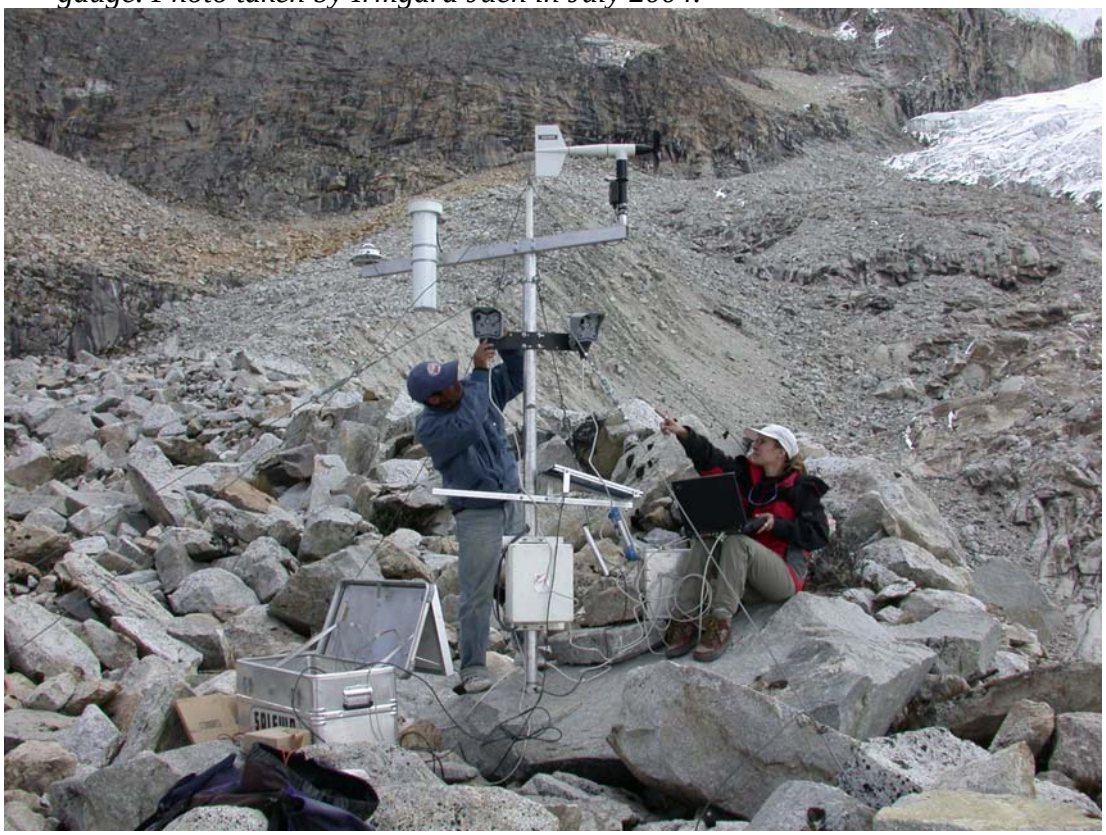

Figure C.10: AWS-north (Artesonraju) at 5100 m a.s.l. with two digital cameras. Photo taken by Georg Kaser in July 2004. The cameras take a picture of Glacier Artesonraju and Chacraraju at 10 and 15 l. t. each day.

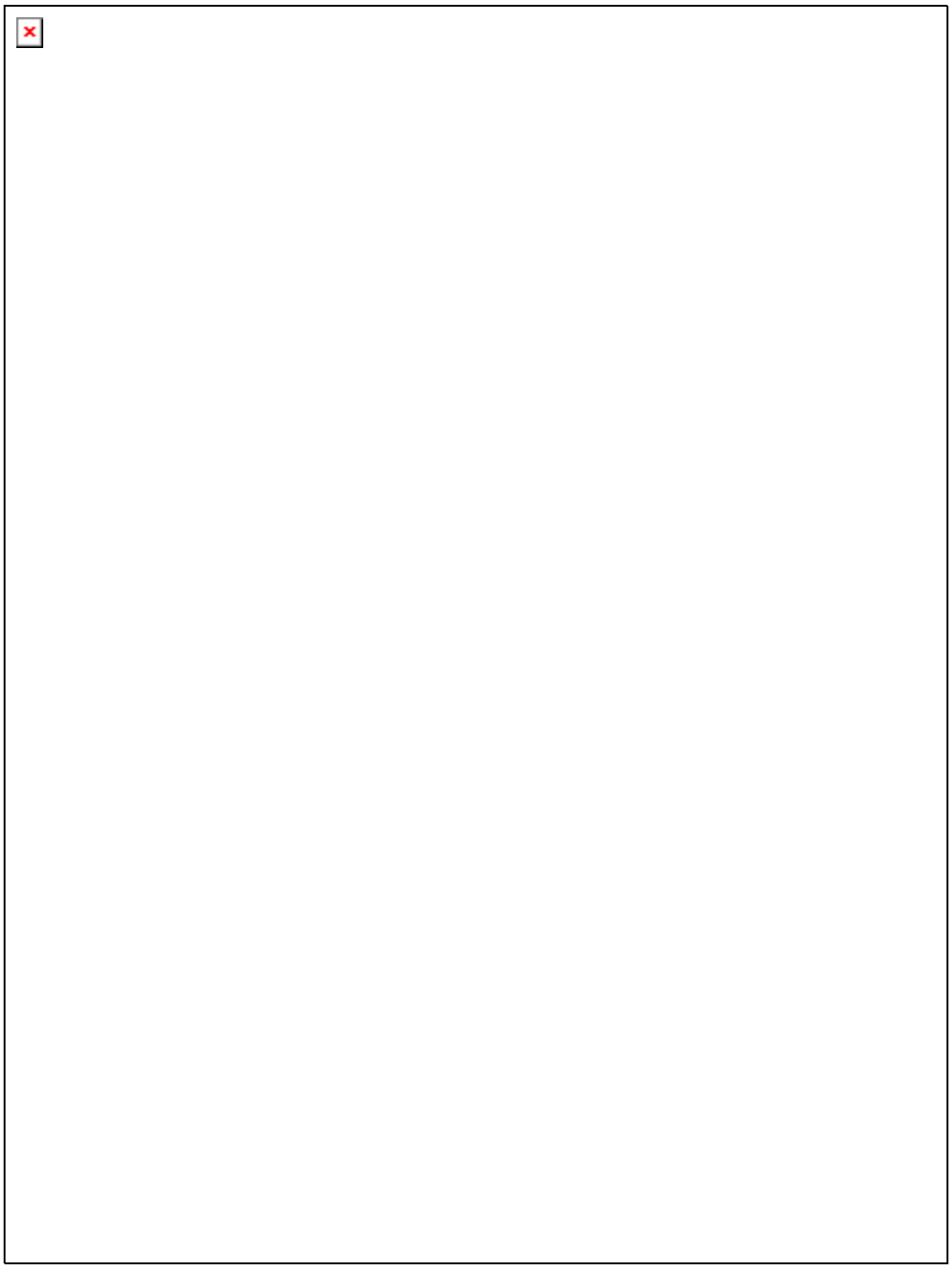

Figure C.11: Connection of the instruments to a Campbell Datalogger CR10X at station AWS-north including pressure sensor (Setra) and storage module. Photo taken by Irmgard Juen in November 2005.

Figure C.12: Photo of Glacier Artesonraju from the digital camera 1 at AWS-north.

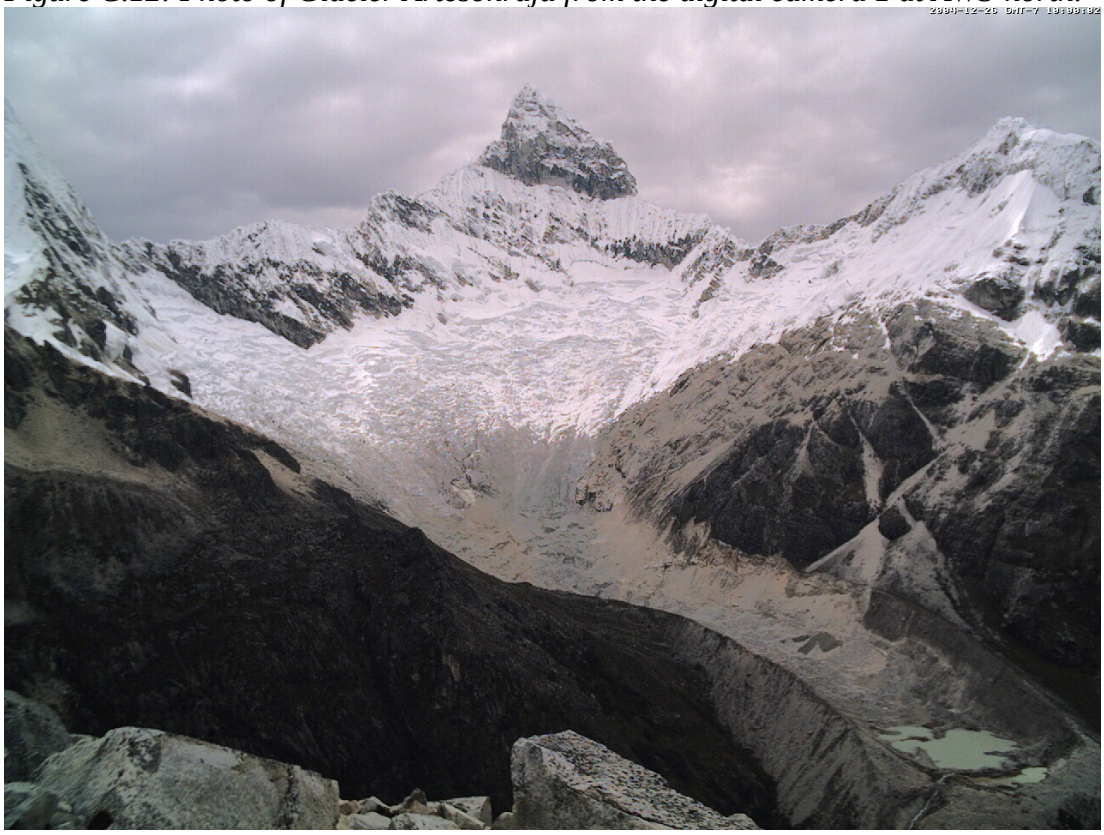

Figure C.13: Photo of Glacier Chacraraju from the digital camera 2 at AWS-north.

Figure C.14: RBS at Glacier Artesonraju (4850 m a.s.l.). Photo taken by Irmgard Juen in July 2004.

Figure C.15: Campbell Datalogger CR23X installed at the RBS on Glacier Artesonraju. Photo taken by Irmgard Juen in March 2004.

Hydrological data

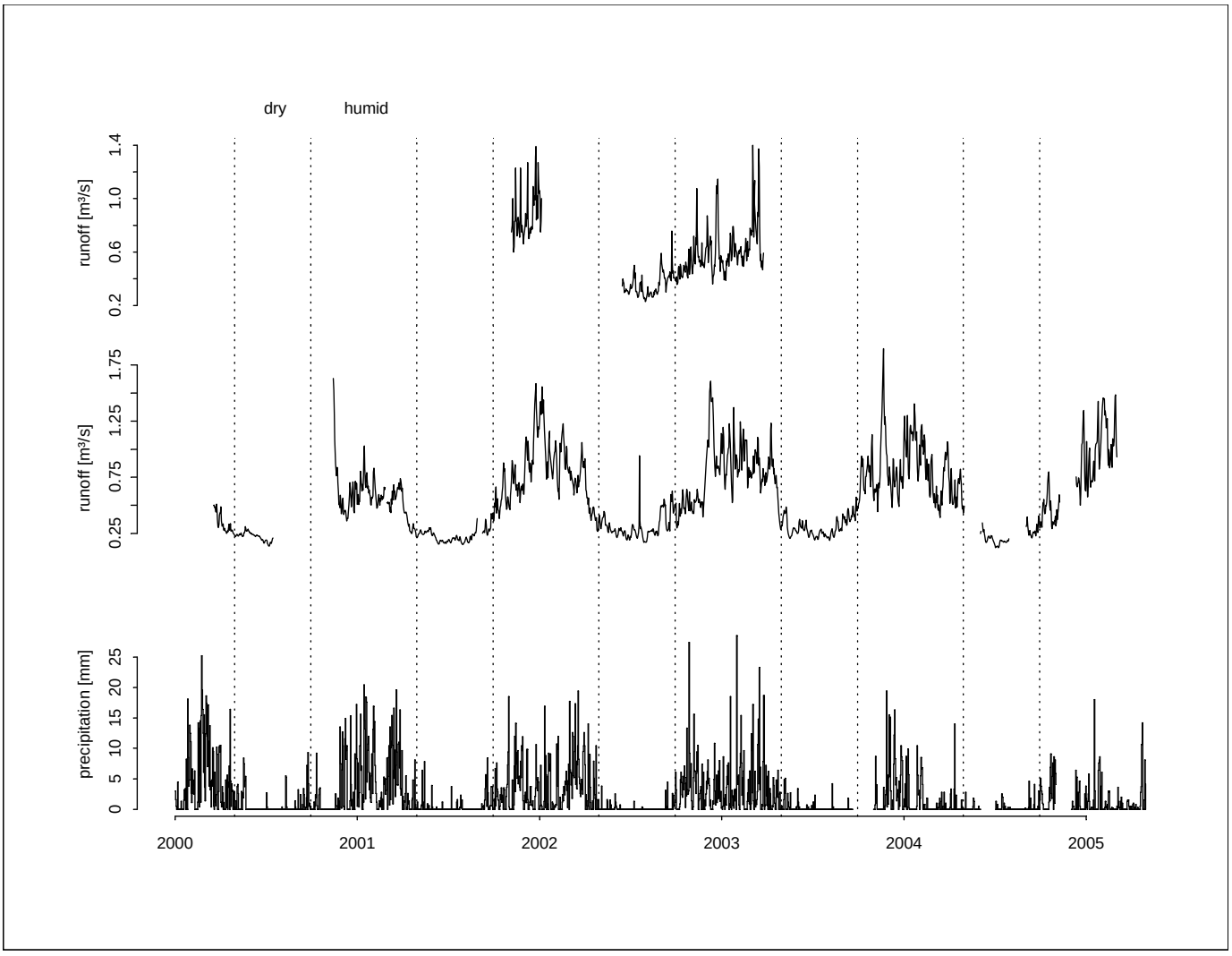

Figure C.16: Daily mean runoff recorded at station Chinchey (first graph) and Artesoncocha (38 % and 75 % glacierised, respectively) and daily sums of precipitation measured at lake Parón (4200 m a.s.l.). The dry season is defined from May to September, the humid season from October to April.

A distinct annual cycle in runoff as well as in precipitation can clearly be seen in all measured data sets (Figure C.16). Although the catchment of Chinchey is much less glacierised than the catchment Artesoncocha runoff during the dry period is almost the same. During the wet season runoff is considerably higher in the Artesoncocha catchment. This might be caused by enhanced glacier melt during the wet season when sublimation is minor and mass exchange on the glacier is high. High amounts of precipitation do not necessarily cause high runoff, whereas extraordinary high temperature like in November 200 and December 2001 raise runoff to high amounts.

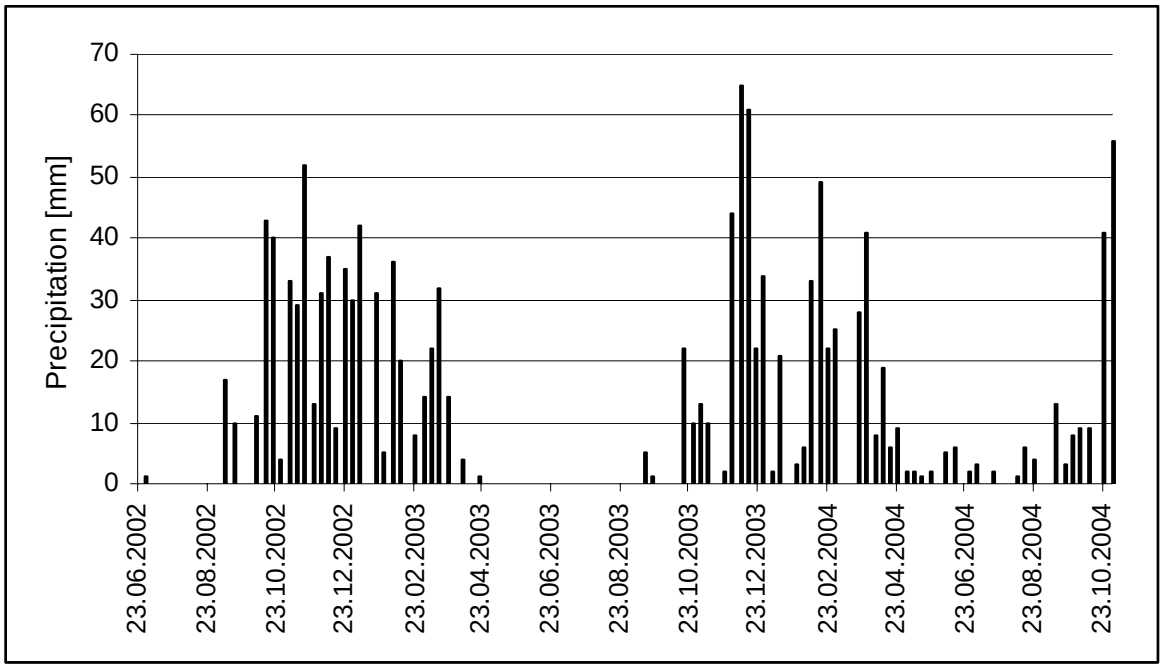

Figure C.17: Weekly precipitation sums at Llupa, 3600 m a.s.l.

Seasonal precipitation amounts were measured at each field visit at several precipitation gauges at different and altitudes. As many stations have never been controlled between the field visits the results are very poor. Although a layer of oil should prevent sublimation mass loss was up to 900 mm during one dry period. Additionally some of the precipitation gauges were destroyed and/or manipulated by local people or animals. Thus the data are not convincing and not used. Efforts to involve local people for a weekly reading mainly failed with exception of the precipitation gauge near Huaraz in Llupa at app. 3600 m a.s.l. measured by Hector Oropeza from June to 2002 to July 2005. The difference in the amount of precipitation during the first and the second year is noticeable (Figure C.17). Whereas the wet season 2002/2003 is characterised by a more or less continuous precipitation from September 2002 to end of March 2003 and during the dry season 2003 no precipitation occurs over 4 months the following year shows much more variability. Even in the wet season weeks without any precipitation are not rare but during the dry season 2004 there was not a single month without precipitation. The same can be seen in the daily amounts of precipitation at station Parón which vary much more in the wet season 2003/2004 than during the previous wet season 2002/2003.

Figure C.18: EPROM Datalogger installed at Lake Artesoncocha (4200 m a.s.l.) where runoff is recorded. Photo taken by Bernard Pouyaud.

Figure C.19: Calibration measurement at the runoff station at Glacier Chinchey (4200 m a.s.l.). Photo taken by Georg Kaser in November 2001.

D. Data gaps at the energy balance station

The energy balance station (*EBS*) has been installed in the ablation area of Glacier Artesonraju at 4850 m a.s.l. in March 2004. Due to a failure in the instrument temperature measurements failed during two periods from March 2004 to April 2005:
1st period: 13.3. 14:30 to 26.3. 15:30
2nd period: 7.11. 13:00 to 11.2. 12:00

Data from the radiation balance station (*RBS*, Figure C.6) station at the same altitude are available from 15.3. until 15.11. 2004. After that period the station has been moved to the tongue to an altitude of app. 4750 m a.s.l.. An automatic weather station (*AWS*, Figure C.6) has been installed outside the glacier at the same altitude as the *EBS* in November 2004. During the 1st period of data gaps air temperature at the *EBS* was reconstructed using the data from the *RBS*, for the 2nd period data from the *AWS* are used. To correct the data from the different stations a mean deviation from air temperature measured at the *EBS* and at the *RBS* and *AWS*, respectively has to be found. For both corrections, the mean daily cycle of the following ten days after the end of the data gap were used. Figure D.1 shows the mean daily cycle in air temperature from 27.3. – 5.4. 2004 measured at the *EBS* and at the *RBS*, and from 12.2. – 21.2. measured at the *EBS* and at the *AWS*. During the first period, the difference in air temperature is very small although air temperature is not ventilated at the *RBS*. This is, however quite reasonable as a natural ventilation from the glacier wind has to be expected. The difference between air temperature measured outside the glacier and on the glacier surface is quite large especially during the day. Thus, the correction is up to 2 °C during the day. This is due to the influence of the cold glacier surface that prevents high air temperature. During the night air temperature is still lower on the glacier surface but with minor difference. The data gaps are then filled by the data from the *RBS* and *AWS* using the mean difference of this ten day period (Figure D.1)

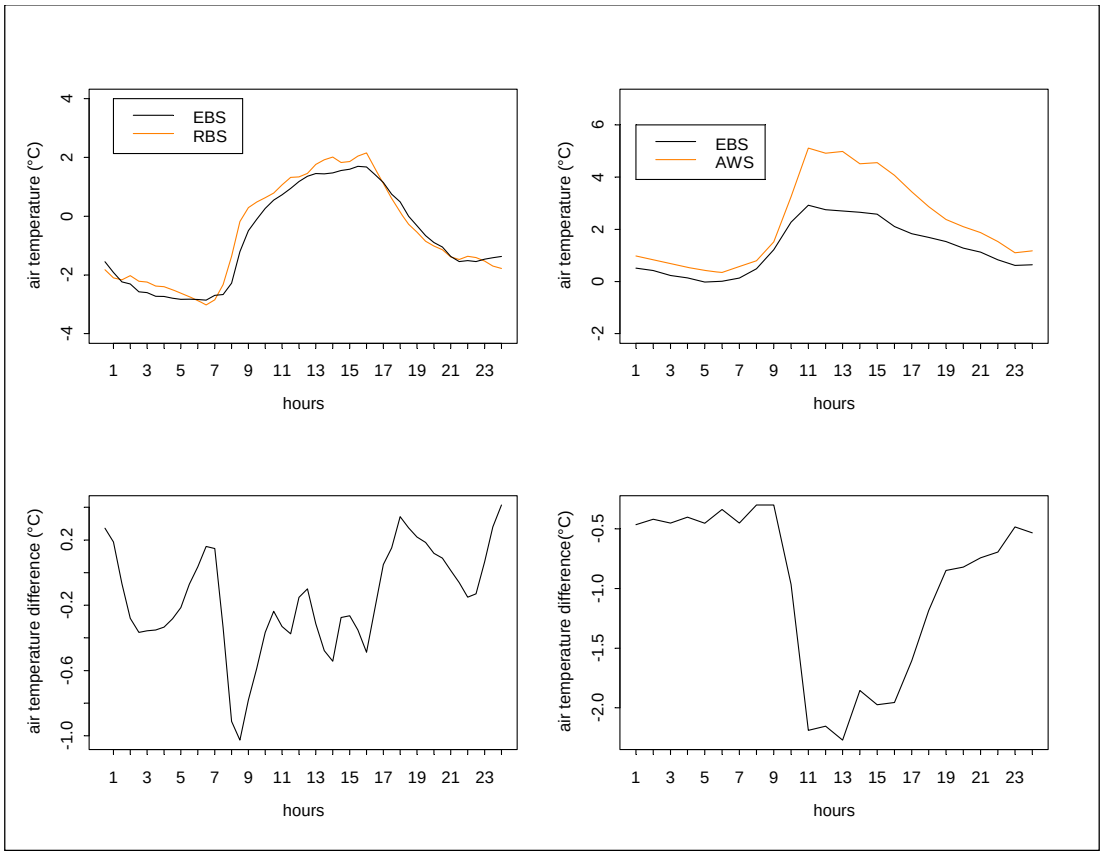

Figure D.1: Mean daily cycle in air temperature from 27.3. – 5.4. 2004 measured at the EBS and at the RBS, and from 12.2. – 21.2. measured at the EBS and AWS. The lower graphs show the mean difference in the daily cycle between EBS and RBS and EBS and AWS, respectively.

E. Additional Figures to chapter 5.3

The Figures show the change in season cycle of direct runoff (Qn), runoff from glacier melt (Qg) and total runoff (Qt) to their mean cycles from 1961 – 1990.

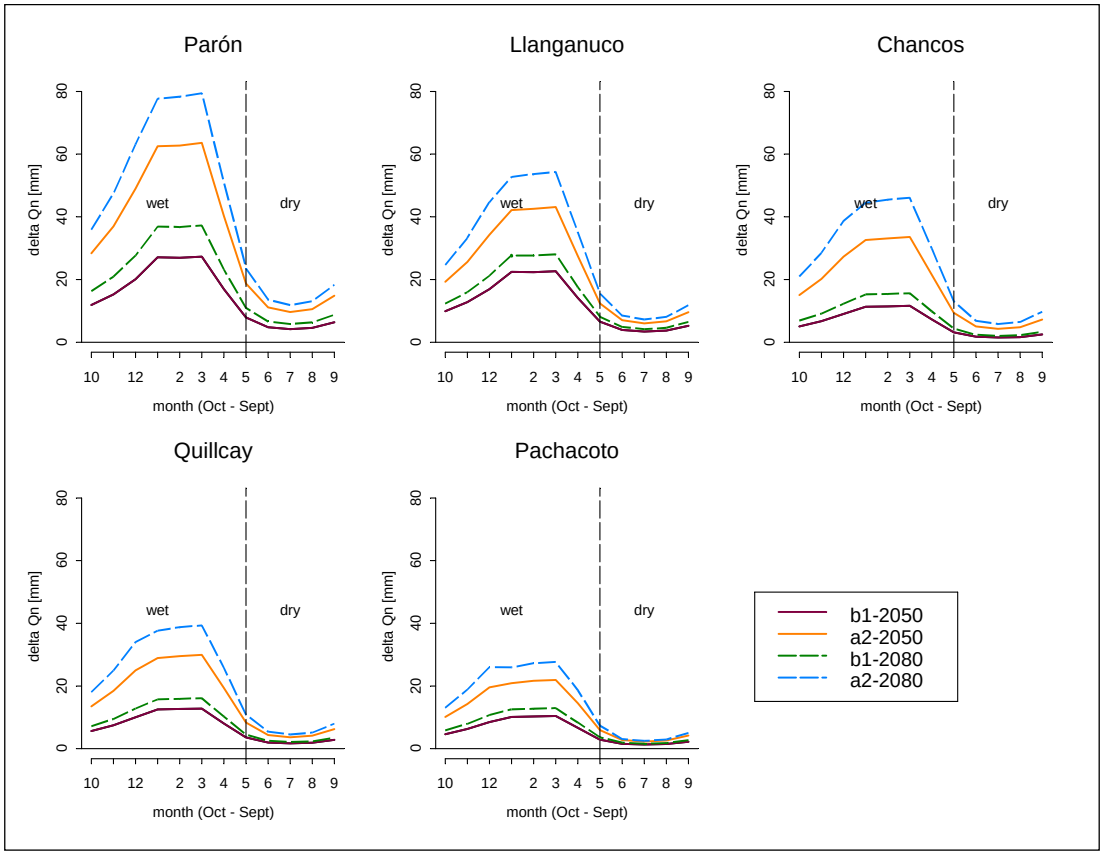

Figure E.1: Predicted change in direct runoff from precipitation (delta Qn) for five differently glacierised catchments in the Cordillera Blanca in 2050 and 2080. For detailed information see chapter 5.3.

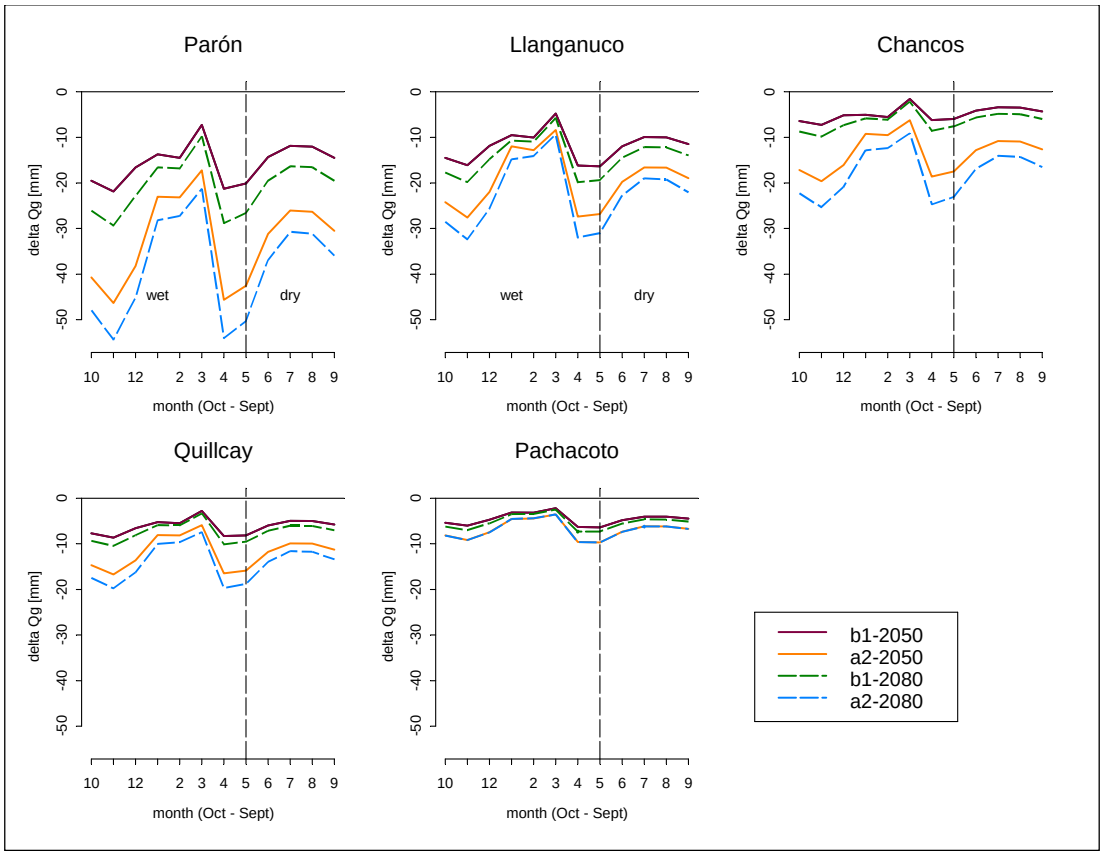

Figure E.2: predicted change in the amount of glacier melt (delta Qg) for five differently glacierised catchments in the Cordillera Blanca in 2050 and 2080. For detailed information see chapter 5.3.

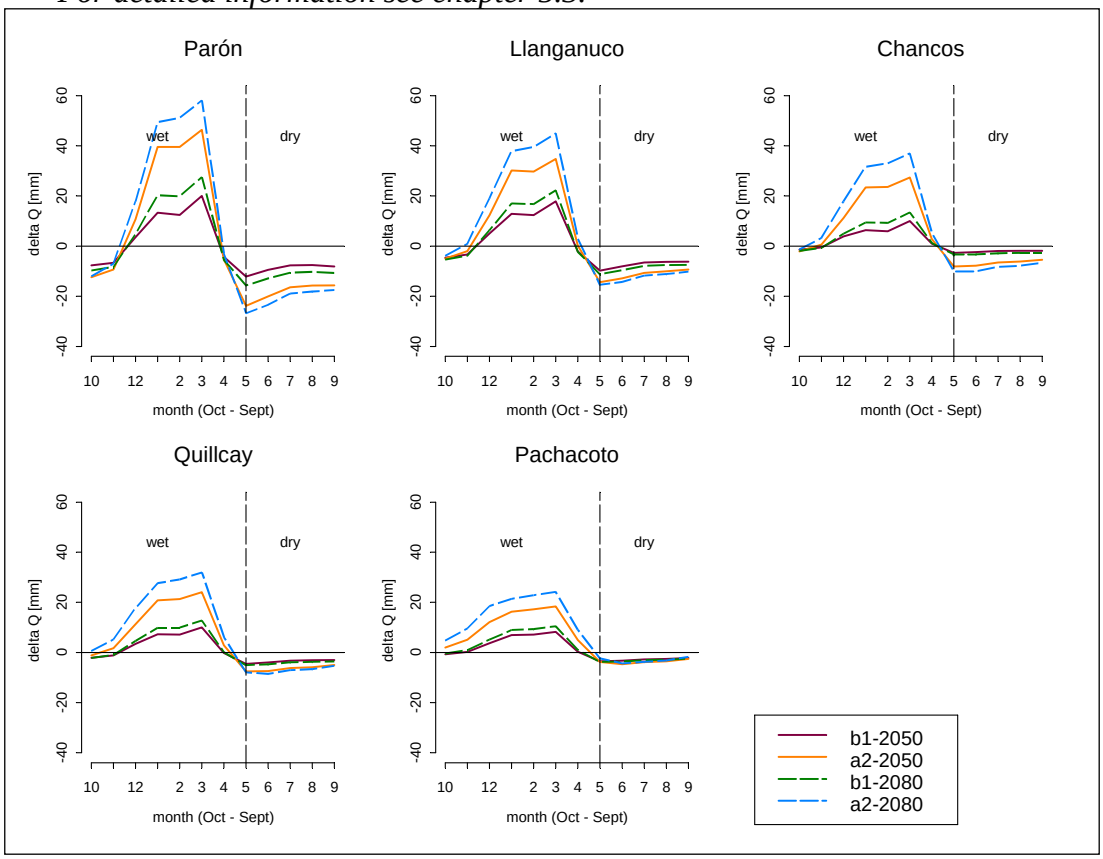

Figure E.3: Predicted change in total runoff (delta QT) for five differently glacierised catchments in the Cordillera Blanca in 2050 and 2080. For detailed information see chapter 5.3.

Table E.1: Predicted seasonal change in total runoff (q_T), direct runoff (q_N), and runoff from glacier melt (q_G) for the core wet and the core dry season in 2050 and 2080. The catchments are listed with decreasing percentage of glacier area from top to bottom. For more detail see chapter 5.3. The core wet season is from January to March, the dry season from June to August.

	Δ q_T 2050 [mm]				Δ q_T 2080 [mm]			
	wet season		dry season		wet season		dry season	
	b1	a2	b1	a2	b1	a2	b1	a2
Parón	15	42	-8	-18	23	52	-11	-20
Llanganuco	14	31	-7	-10	19	41	-8	-12
Chancos	7	25	-2	-7	10	34	-3	-9
Quillcay	8	22	-3	-7	11	30	-4	-7
Pachacoto	7	17	-3	-4	10	23	-3	-4
	Δ q_N 2050 [mm]				Δ q_N 2080 [mm]			
	wet season		dry season		wet season		dry season	
	b1	a2	b1	a2	b1	a2	b1	a2
Parón	27	63	5	10	37	78	6	13
Llanganuco	22	42	4	7	28	54	5	8
Chancos	11	33	2	5	15	45	2	6
Quillcay	13	29	2	4	16	39	2	5
Pachacoto	10	21	1	3	13	27	2	3
	Δ q_G 2050 [mm]				Δ q_G 2080 [mm]			
	wet season		dry season		wet season		dry season	
	b1	a2	b1	a2	b1	a2	b1	a2
Parón	-12	-21	-13	-28	-14	-26	-17	-33
Llanganuco	-8	-11	-11	-17	-9	-13	-13	-20
Chancos	-4	-8	-4	-12	-5	-11	-5	-15
Quillcay	-5	-7	-5	-11	-5	-9	-6	-12
Pachacoto	-3	-4	-4	-7	-3	-4	-5	-7

F. Additional Figures to chapter 5.4

The following Figures F.1 – F.13 show the mean daily cycle of all measured parameters as well as for calculated vapour pressure and turbulent fluxes at the *EBS* on the tongue of Glacier Artesonraju (4850 m a.s.l.) for each month separately. Figure F.14 – F.15 are plots for daily mean values each month. The graphs shows the arithmetic mean (cross), limits of the lower and upper quartile (orange box, 25 and 75 %), 90 % quantile (vertical bar), and maximum and minimum values.

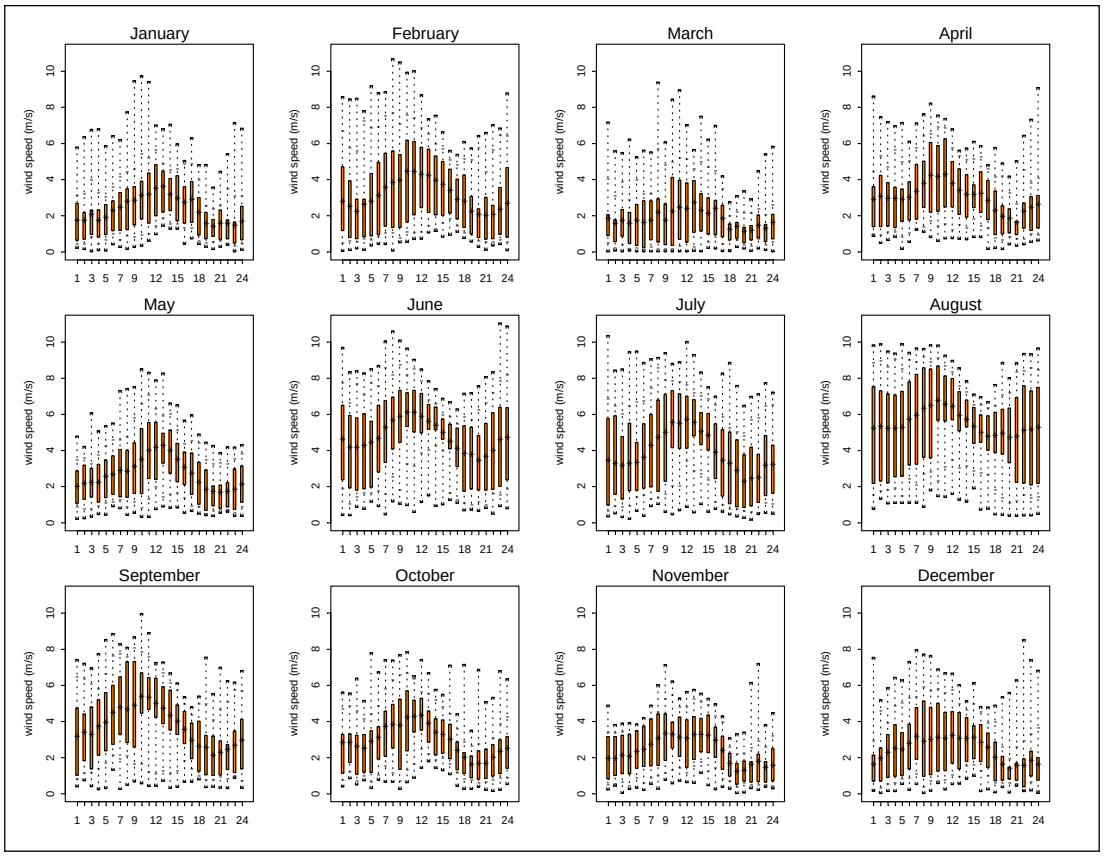

Figure F.1: Monthly daily cycle of wind speed.

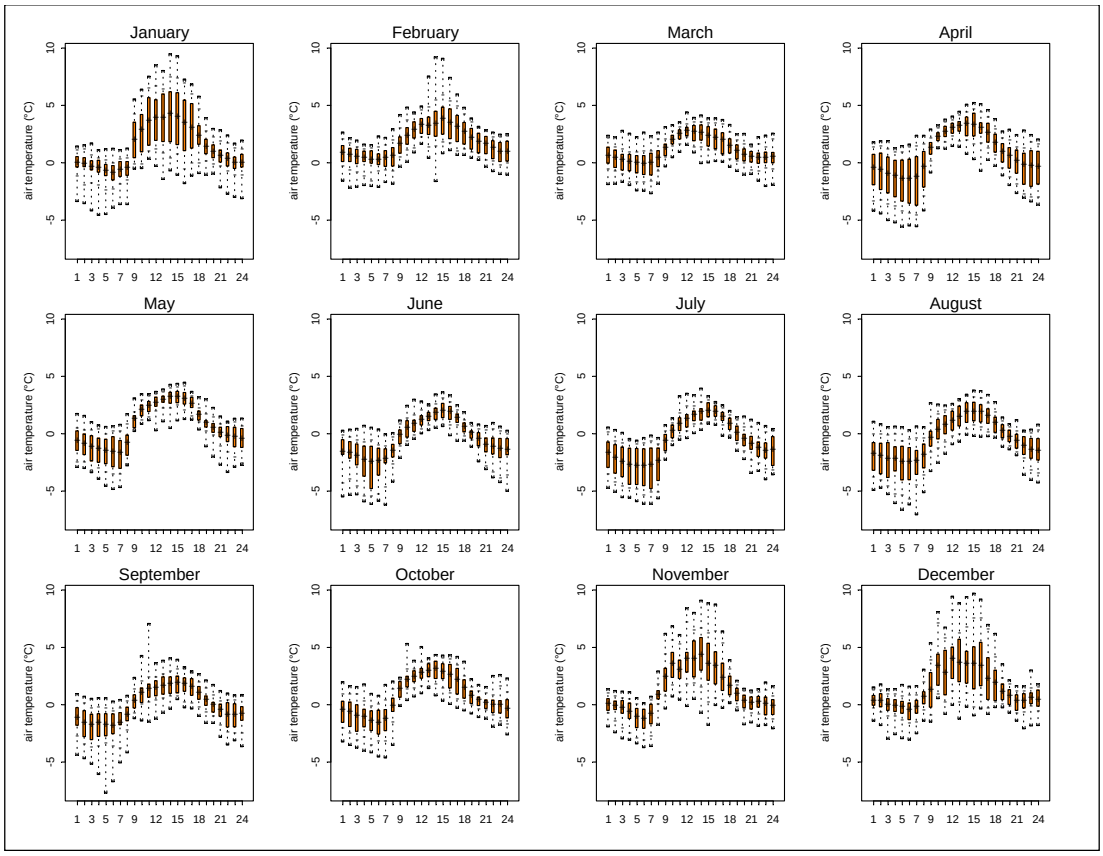

Figure F.2: Monthly daily cycle of air temperature.

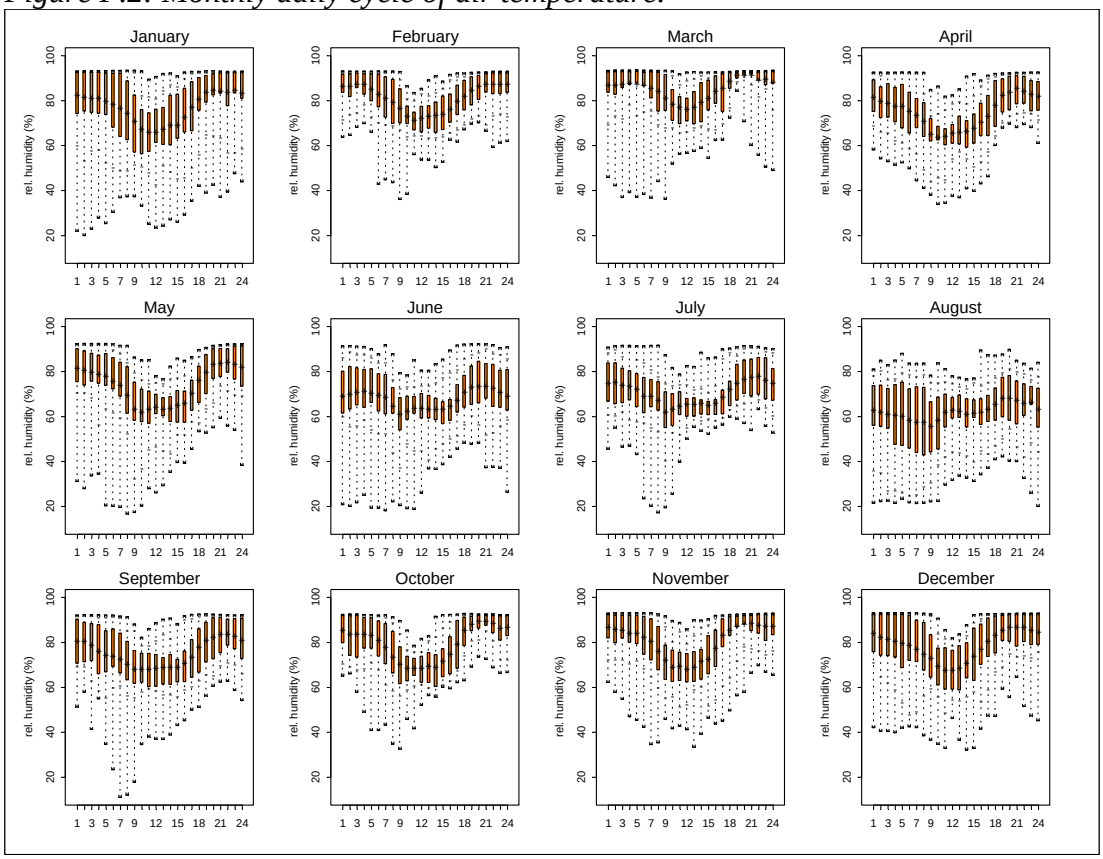

Figure F.3: Monthly daily cycle of air humidity.

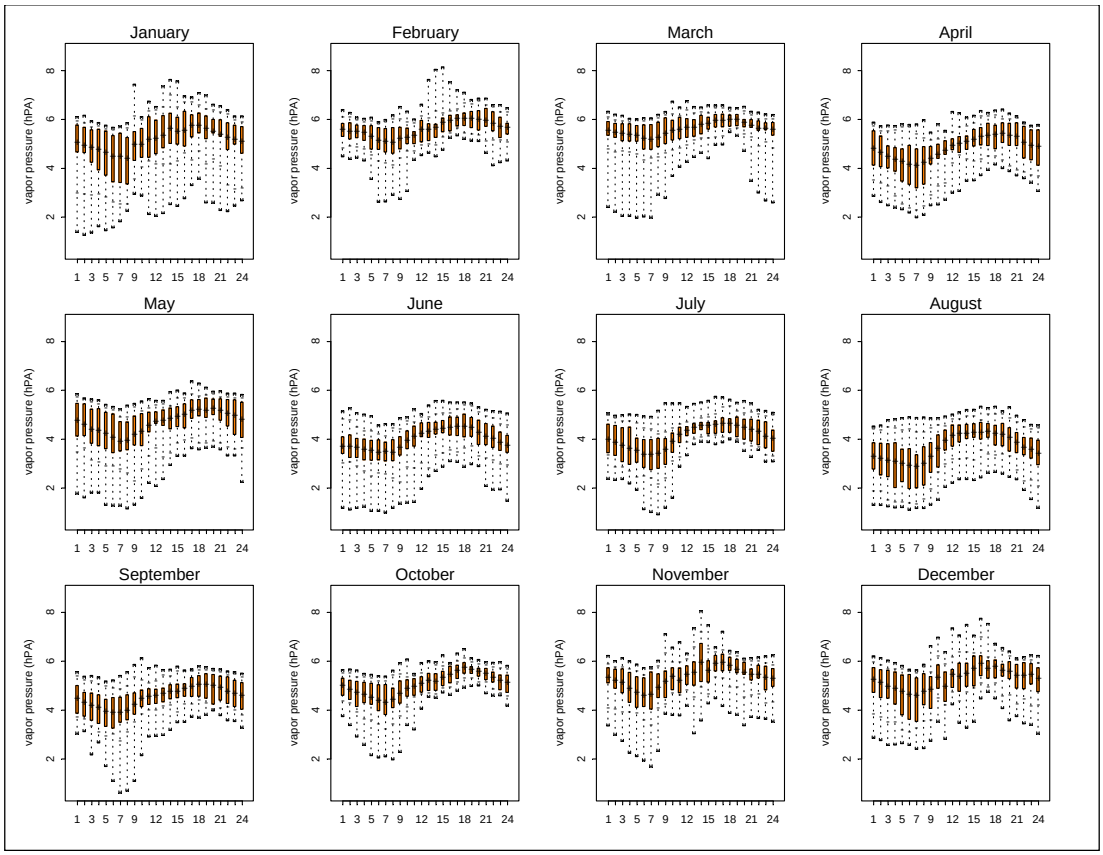

Figure F.4: Monthly daily cycle of vapour pressure (e).

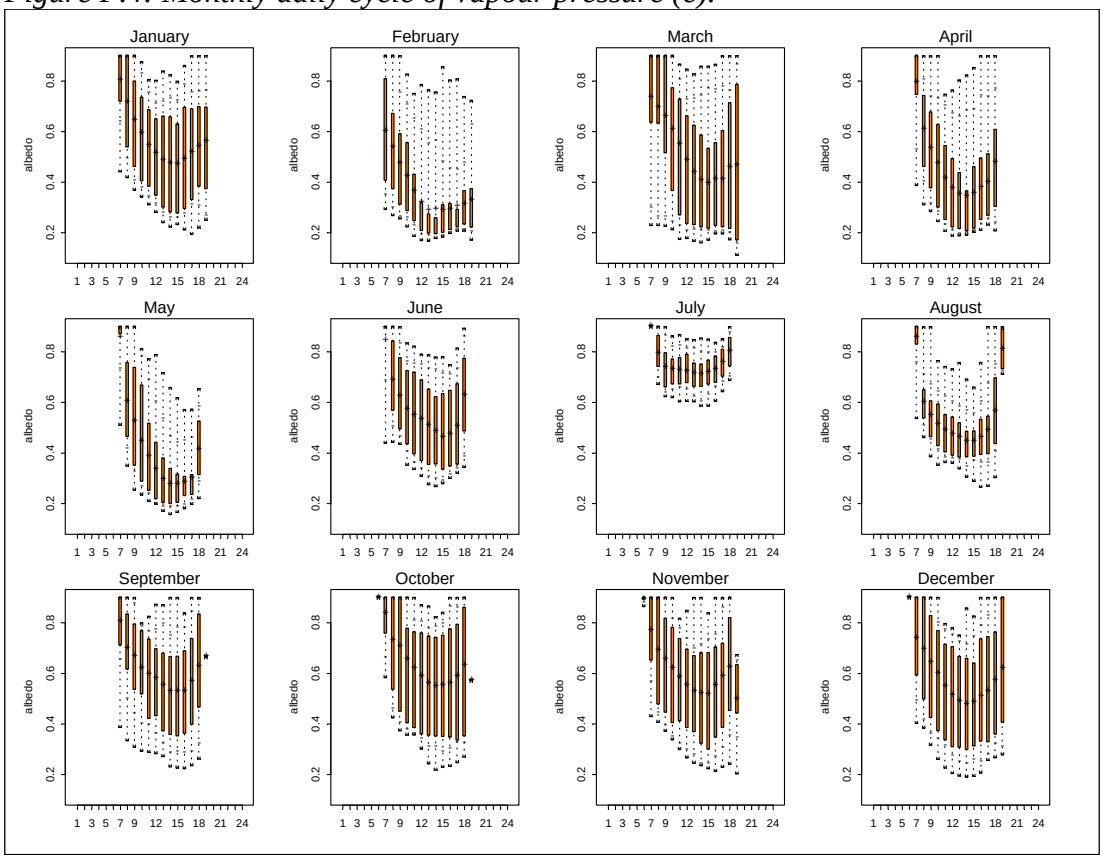

Figure F.5: Monthly daily cycle of albedo.

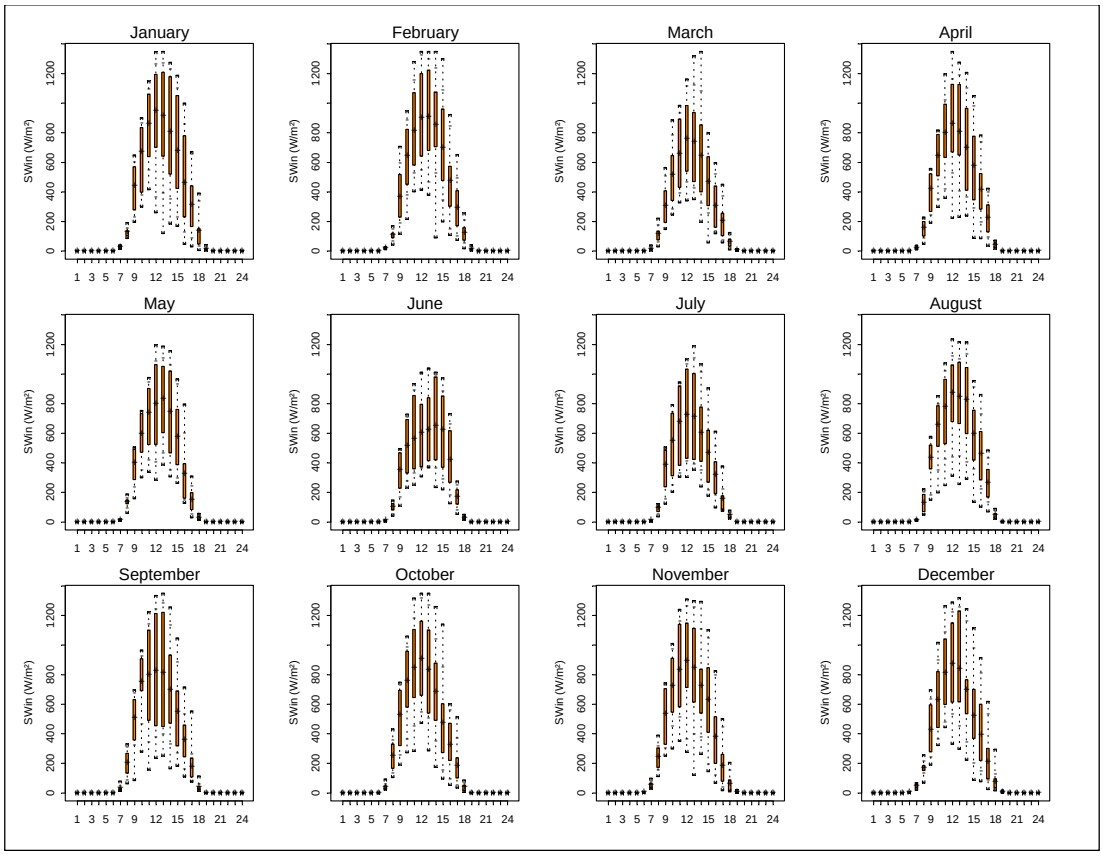

Figure F.6: Monthly daily cycle of SW_{in}.

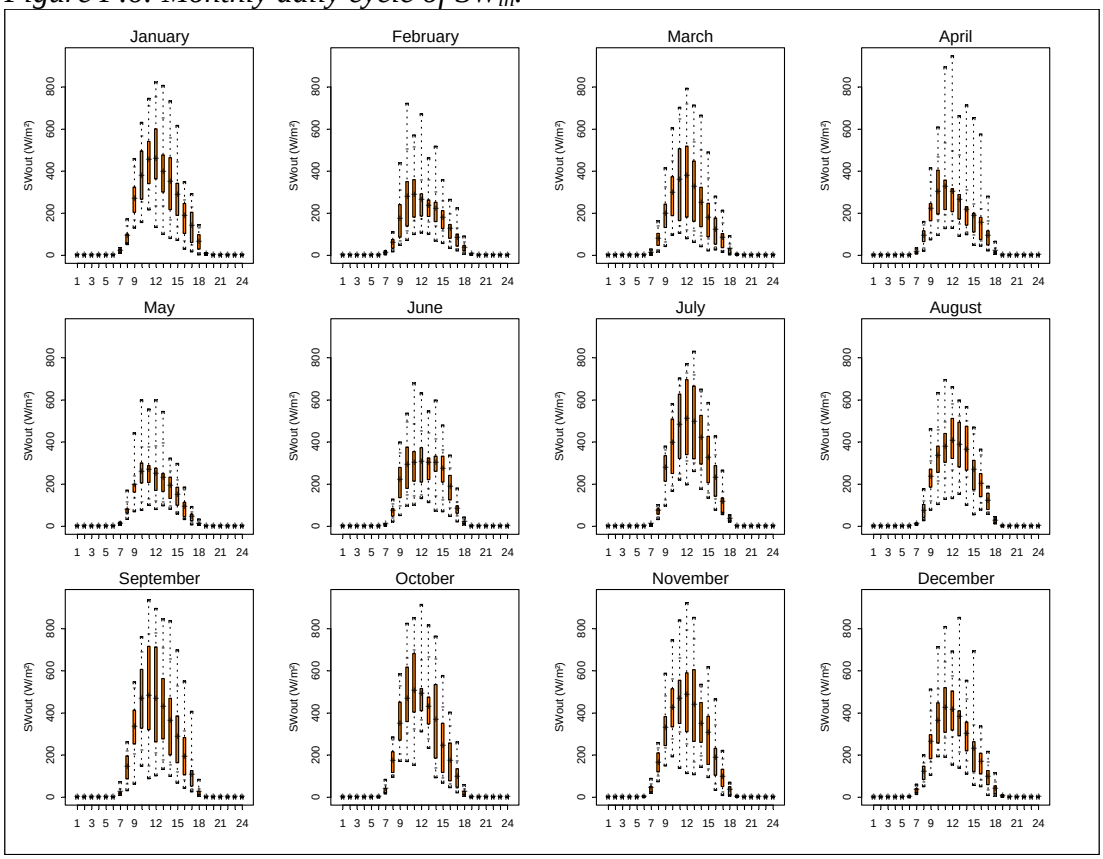

Figure F.7: Monthly daily cycle of SW_{out}.

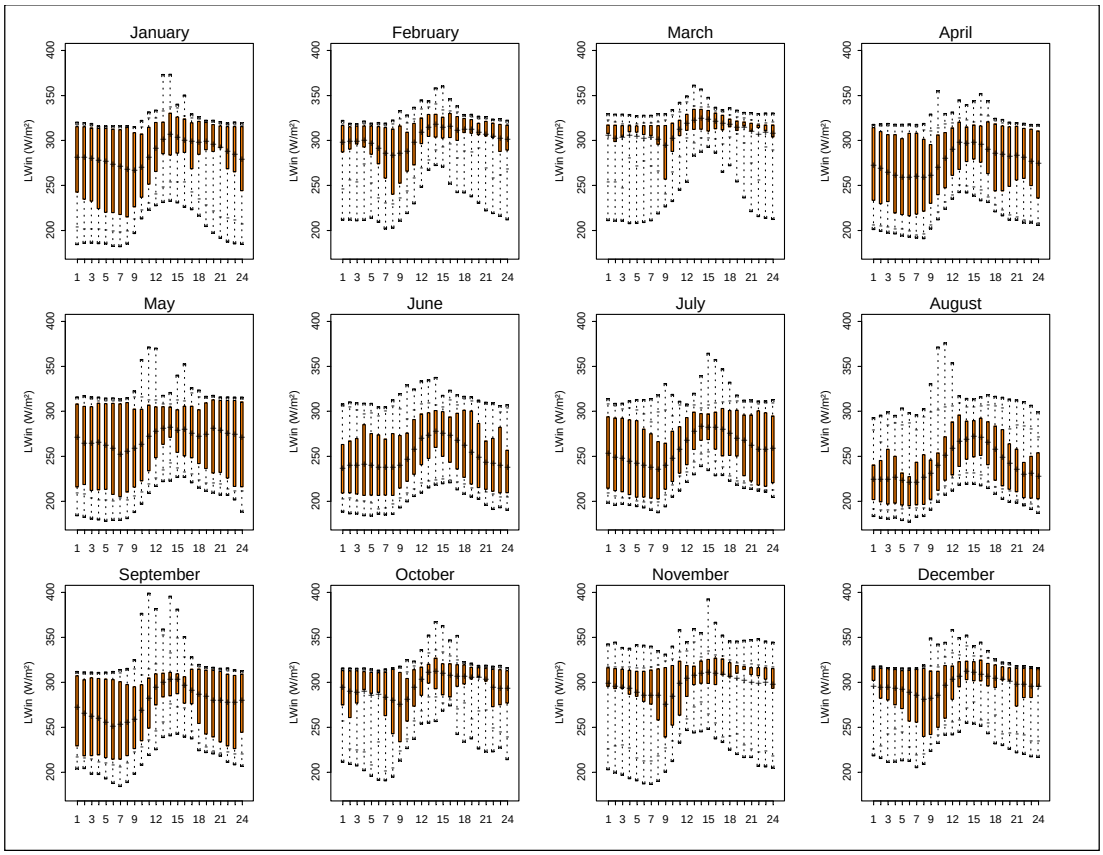

Figure F.8: Monthly daily cycle of LW_{in}.

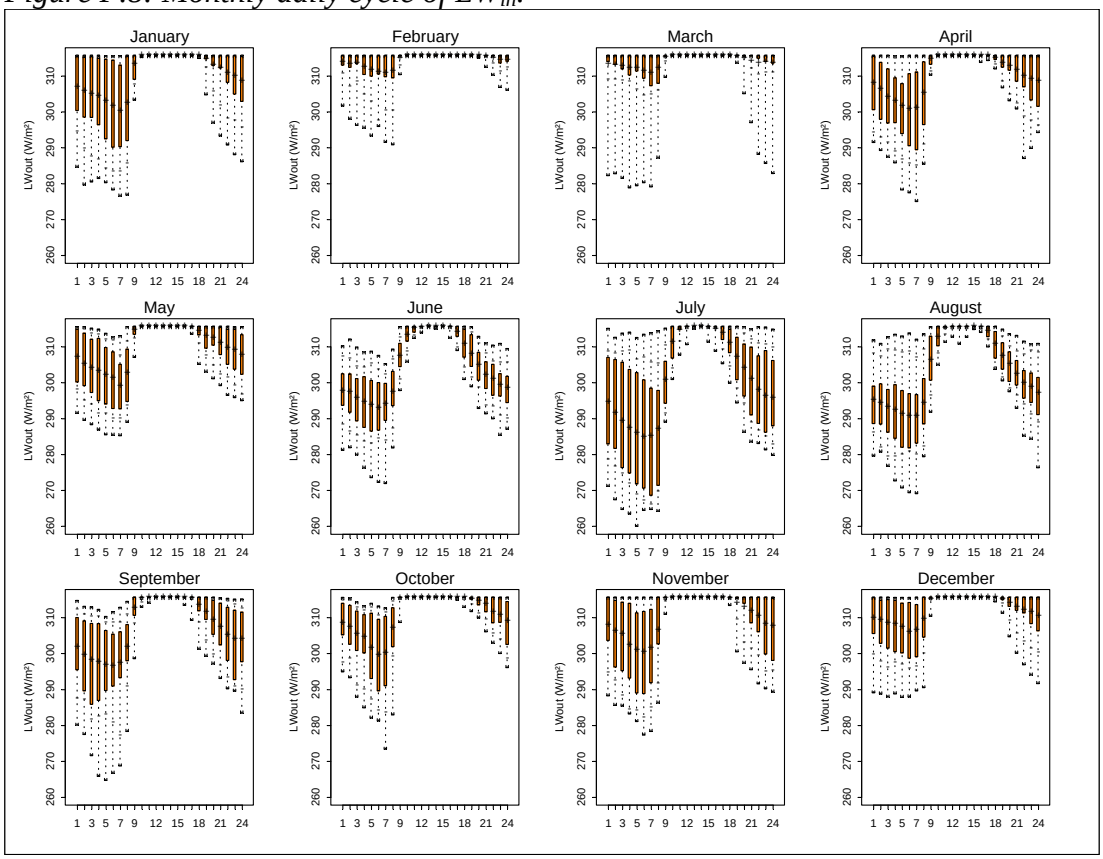

Figure F.9: Monthly daily cycle of LW_{out}.

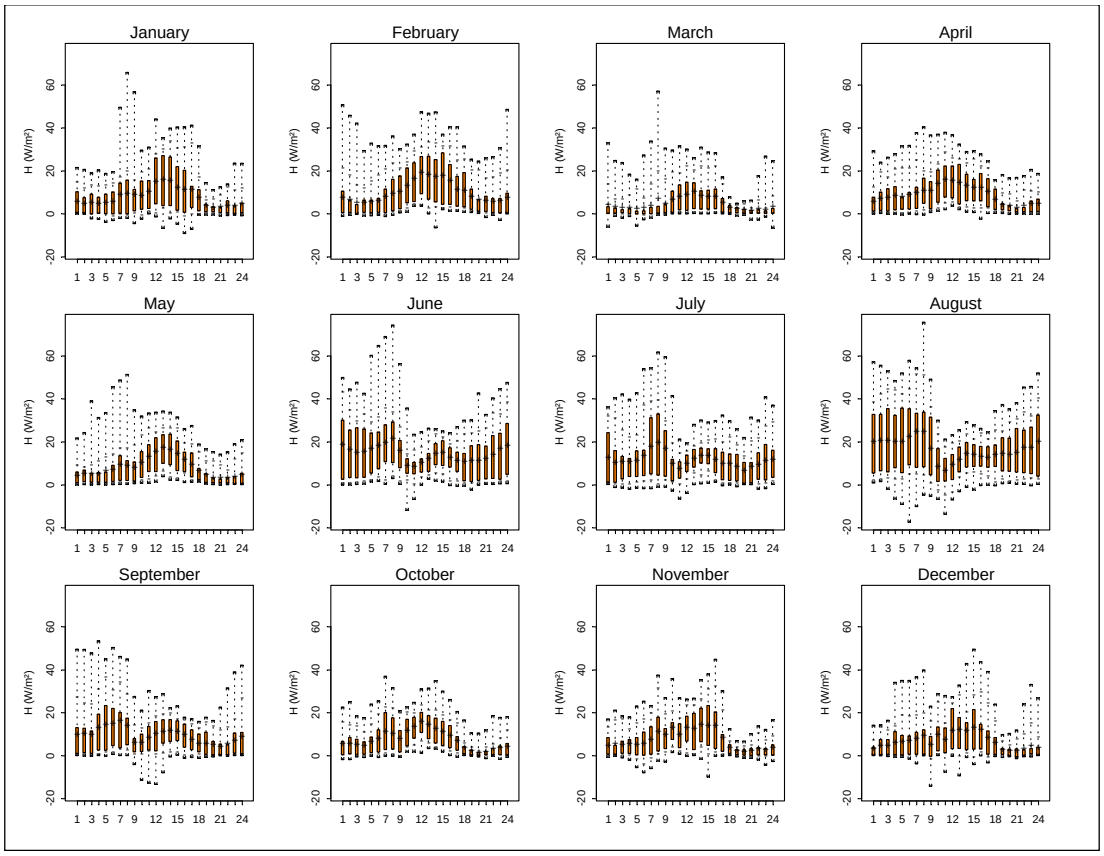

Figure F.10: Monthly daily cycle of sensible heat flux (H).

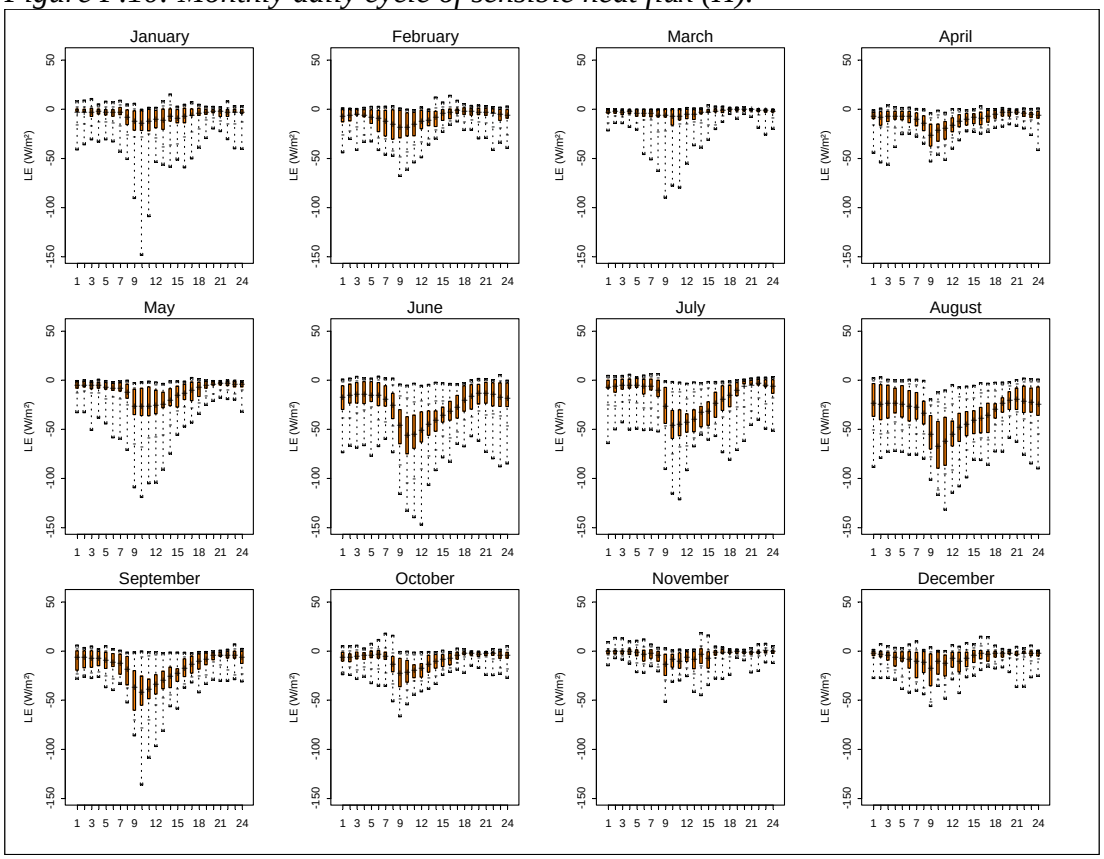

Figure F.11: Monthly daily cycle of latent heat flux (LE).

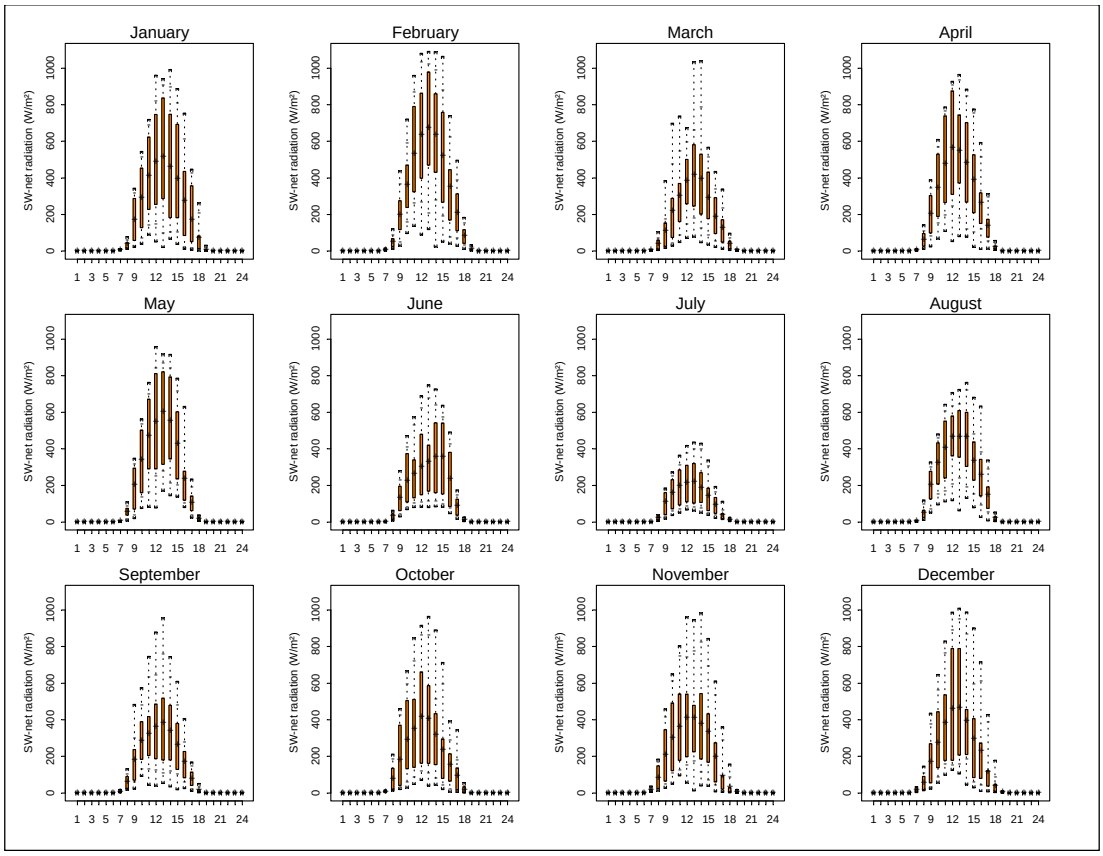

Figure F.12: Monthly daily cycle of SW_{net}.

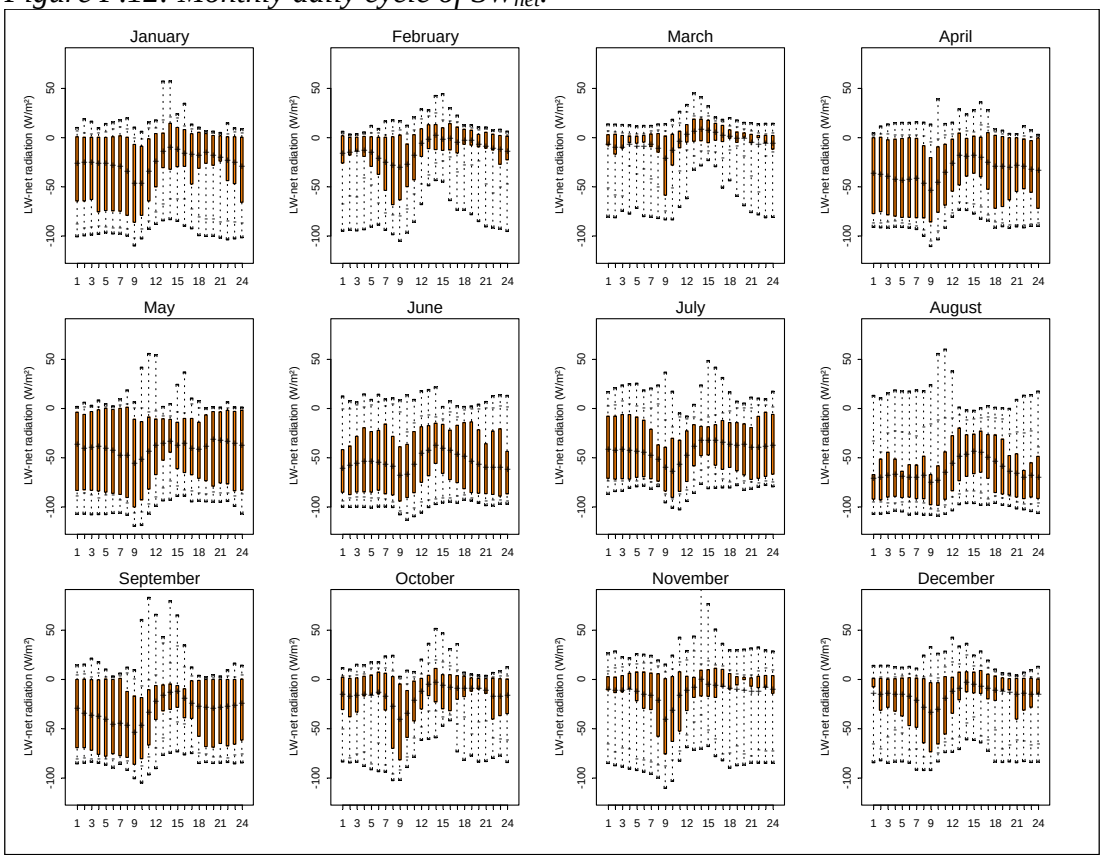

Figure F.13: Monthly daily cycle of LW_{net}.

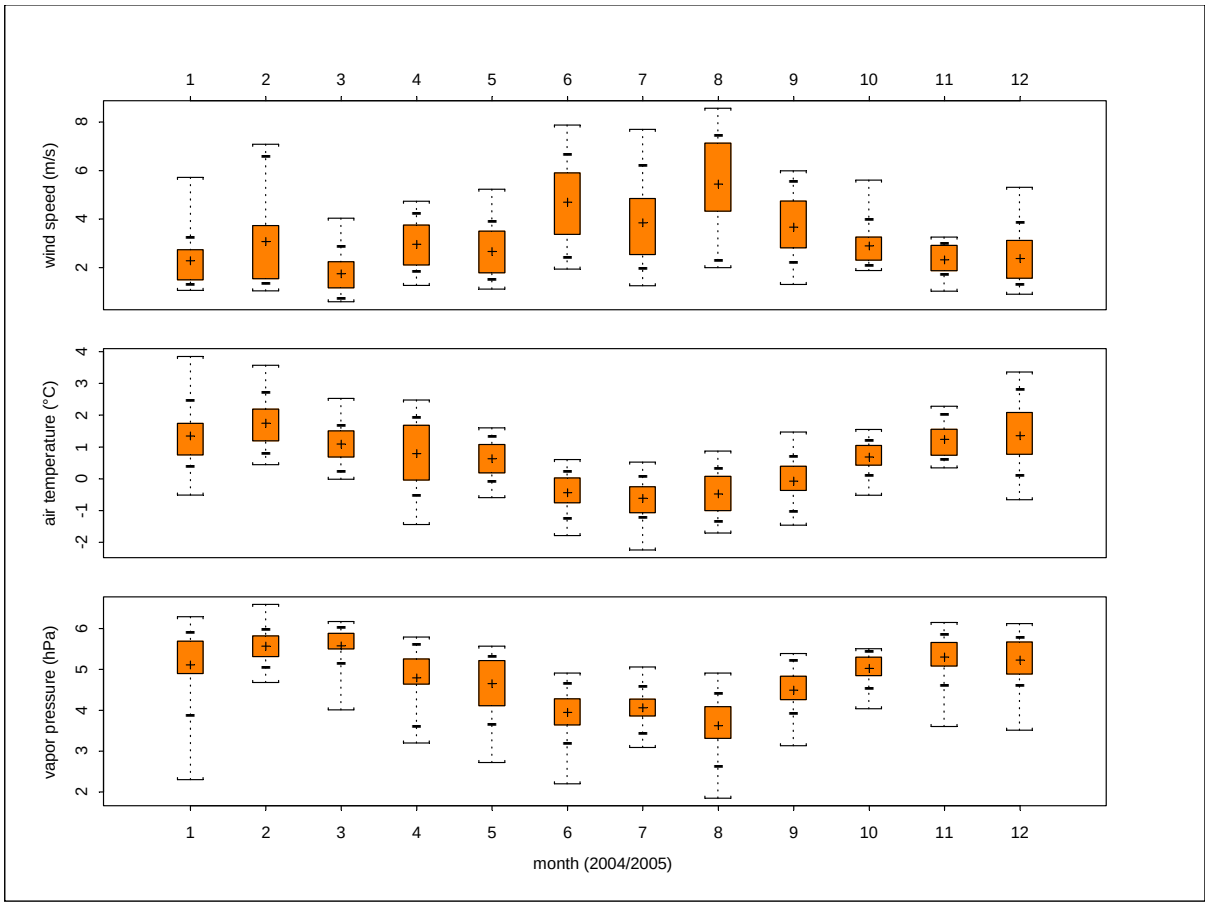

Figure F.14: Daily mean values of wind speed, air temperature and vapour pressure each month.

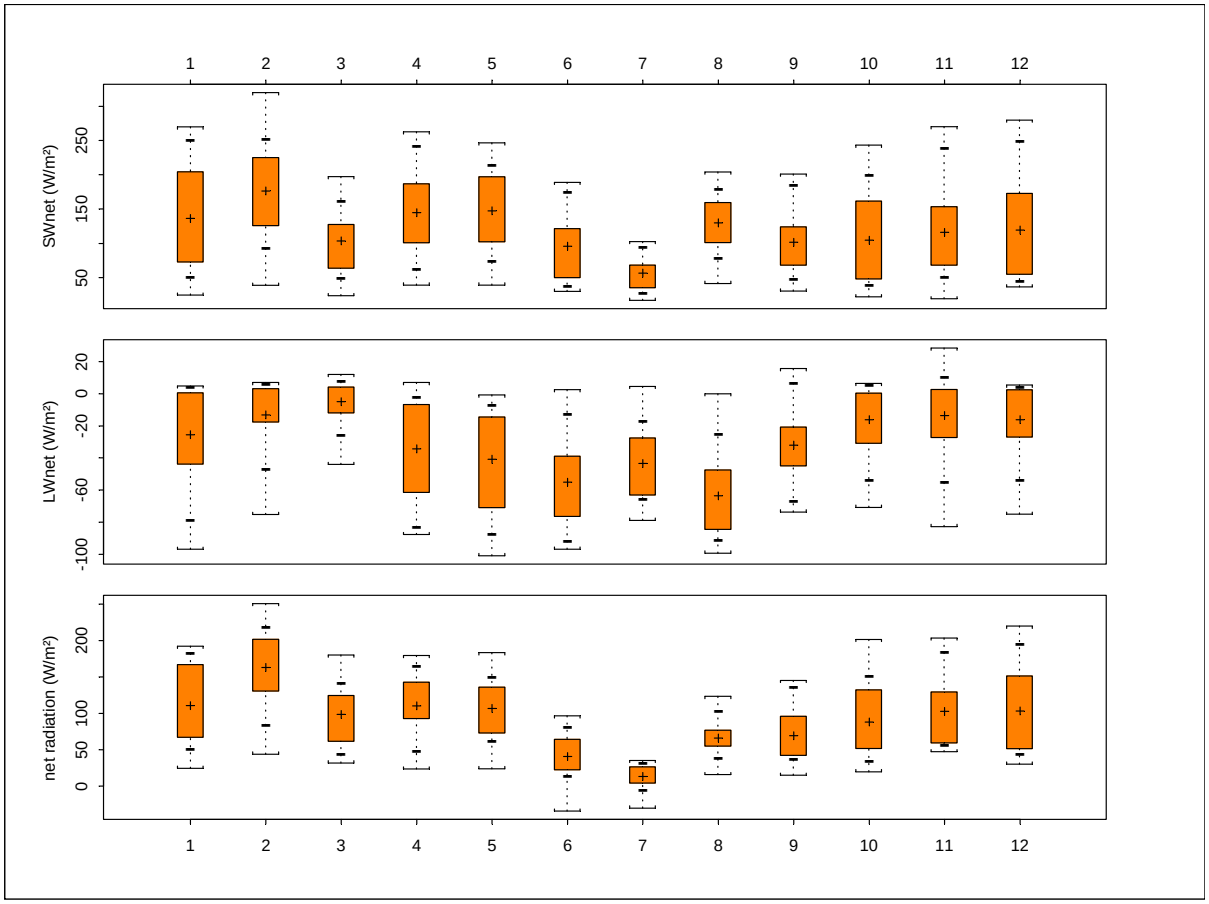

Figure F.15: Daily mean values of SW_{net}, LW_{net} and total net radiation each month.

Table F.1: Mean monthly (April 2004 to March 2005) and seasonal climate variables measured at the EBS on Glacier Artesonraju (4850 m a.s.l.). The dry season is defined from June to August, the wet season from January to March.

Month	u (m s^{-1})	R_H (%)	e (hPa)	T_a (°C)
4	3.0	74.3	4.8	0.8
5	2.7	73.3	4.6	0.6
6	4.7	67.4	4.0	-0.4
7	3.9	70.0	4.1	-0.6
8	5.4	61.7	3.6	-0.5
9	3.7	74.6	4.5	-0.1
10	2.9	78.9	5.0	0.7
11	2.3	79.9	5.3	1.2
12	2.4	78.1	5.2	1.4
1	2.3	76.4	5.1	1.3
2	3.1	80.7	5.6	1.7
3	1.8	84.6	5.6	1.1
dry	4.7	66.3	3.9	-0.5
wet	2.4	79.9	5.4	1.4
$\Delta_{dry\text{-}wet}$	2.3	-13.6	-1.5	-1.9
annual	3.2	75.0	4.8	0.6
$\Delta_{max\text{-}min}$	3.7	22.9	2.0	2.4

Table F.2: Mean monthly (April 2004 to March 2005) and seasonal radiation fluxes measured at the EBS on Glacier Artesonraju (4850 m a.s.l.). Resulting energy available for melt Q_M is derived from the energy balance calculation (see chapter 4.4). The dry season is defined from June to August, the wet season from January to March.

Month	SW_{in} (W m^{-2})	SW_{out} (W m^{-2})	LW_{in} (W m^{-2})	LW_{out} (W m^{-2})	Q_M (W m^{-2})
4	234.4	89.8	276.1	310.4	127.7
5	220.9	73.3	269.3	310.0	123.9
6	193.2	97.3	249.7	304.8	55.9
7	196.1	139.3	258.1	301.5	27.3
8	245.5	115.7	240.1	303.7	78.5
9	238.6	137.1	275.5	307.5	78.3
10	243.2	138.7	294.7	311.0	93.1
11	253.5	137.3	296.9	310.5	108.3
12	236.5	116.9	296.2	312.3	111.3
1	264.7	128.5	284.9	310.5	123.1
2	256.8	80.5	301.2	314.3	172.5
3	198.6	95.1	309.2	314.1	103.4
dry	211.6	117.4	249.3	303.3	53.9
wet	239.1	105.3	297.9	312.8	127.6
$\Delta_{dry\text{-}wet}$	-27.5	12.2	-48.5	-9.5	-73.7
annual	231.8	112.5	279.3	309.2	100.3
$\Delta_{max\text{-}min}$	71.4	66.0	69.1	12.8	145.2

In the following Figures F.16 – F.18 hourly glacier melt calculated at the *EBS* on Glacier Artesonraju (4850 m a.s.l.) and runoff measured at the outlet of Lake Artesoncocha (4200 m a.s.l.) are compared for the three periods P2, P3, and P4. The first graph shows glacier melt calculated with a storage parameter *ks* of 7 (hours). In the second graph, glacier melt is calculated with *ks*=55 (P2 and P3, Figure F.16 and F.17) and *ks*=103 (P4, Figure F.18).

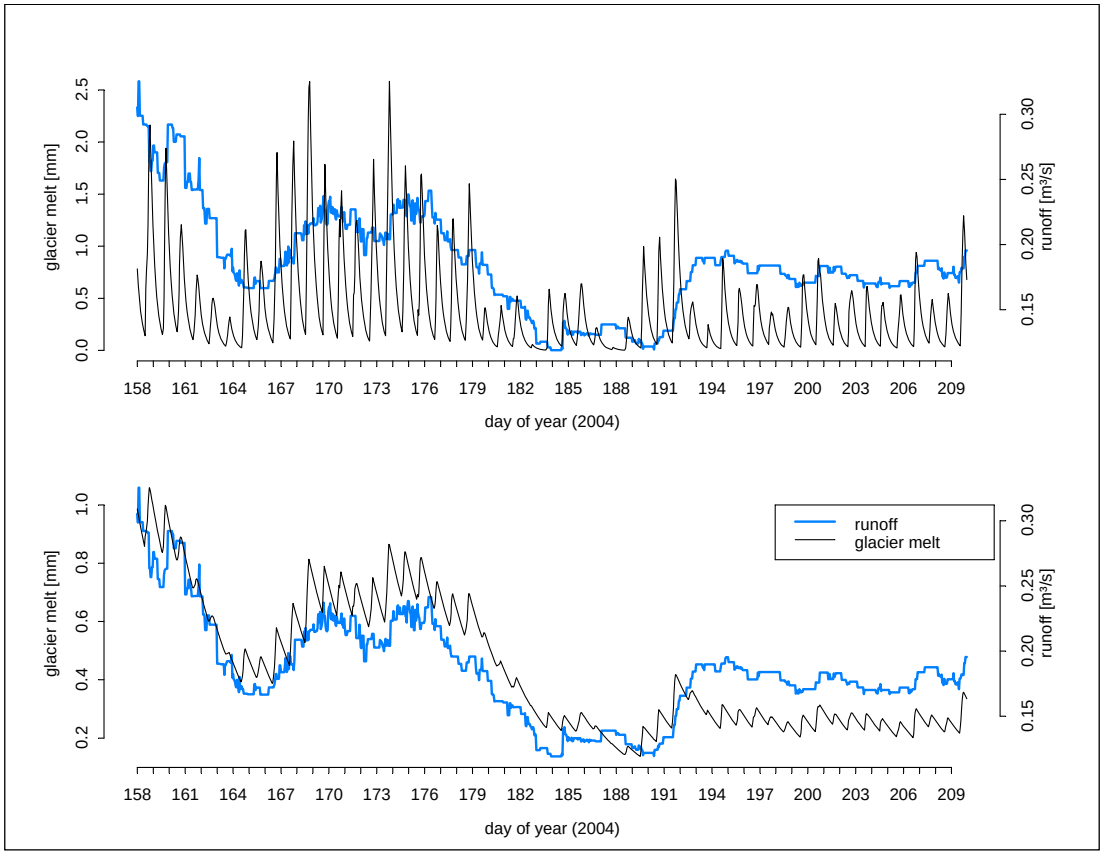

Figure F.16: Runoff and delayed glacier melt with ks=7 and ks=55 (P2: day 158 – 209).

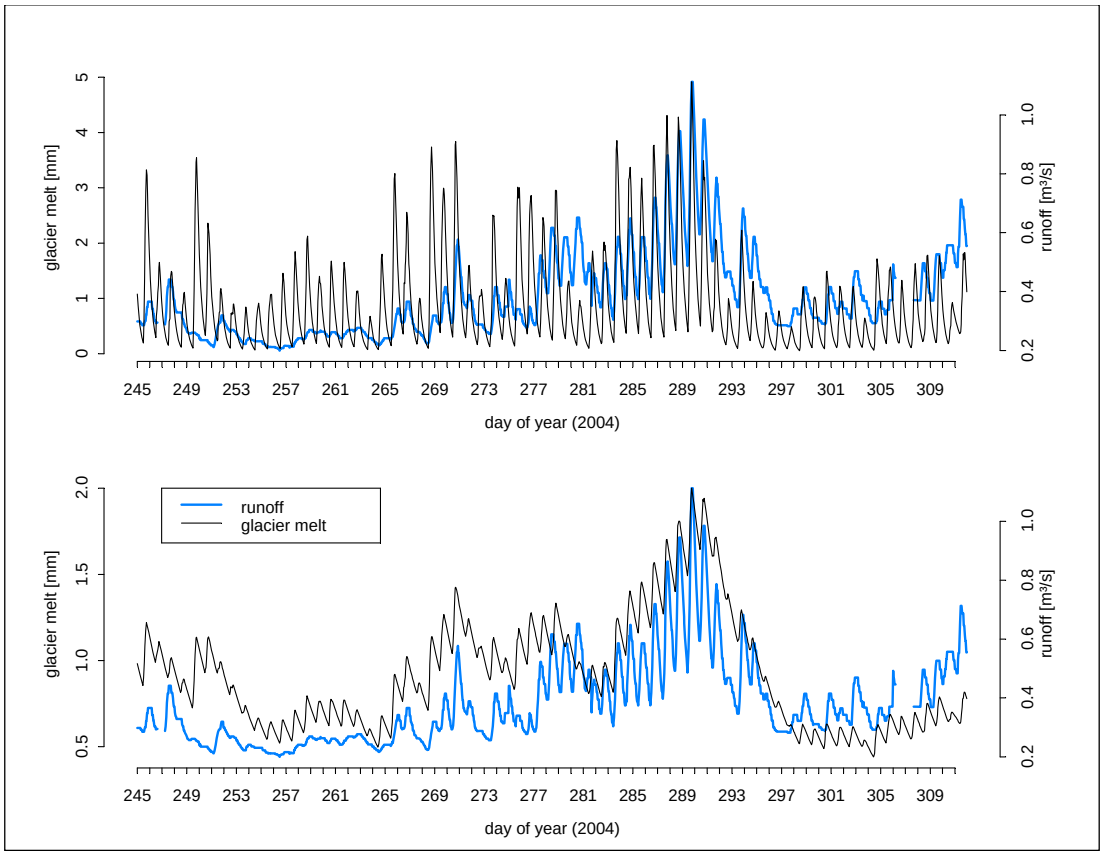

Figure F.17: Runoff and delayed glacier melt with ks=7 and ks=55 (P3: day 245 – 311).

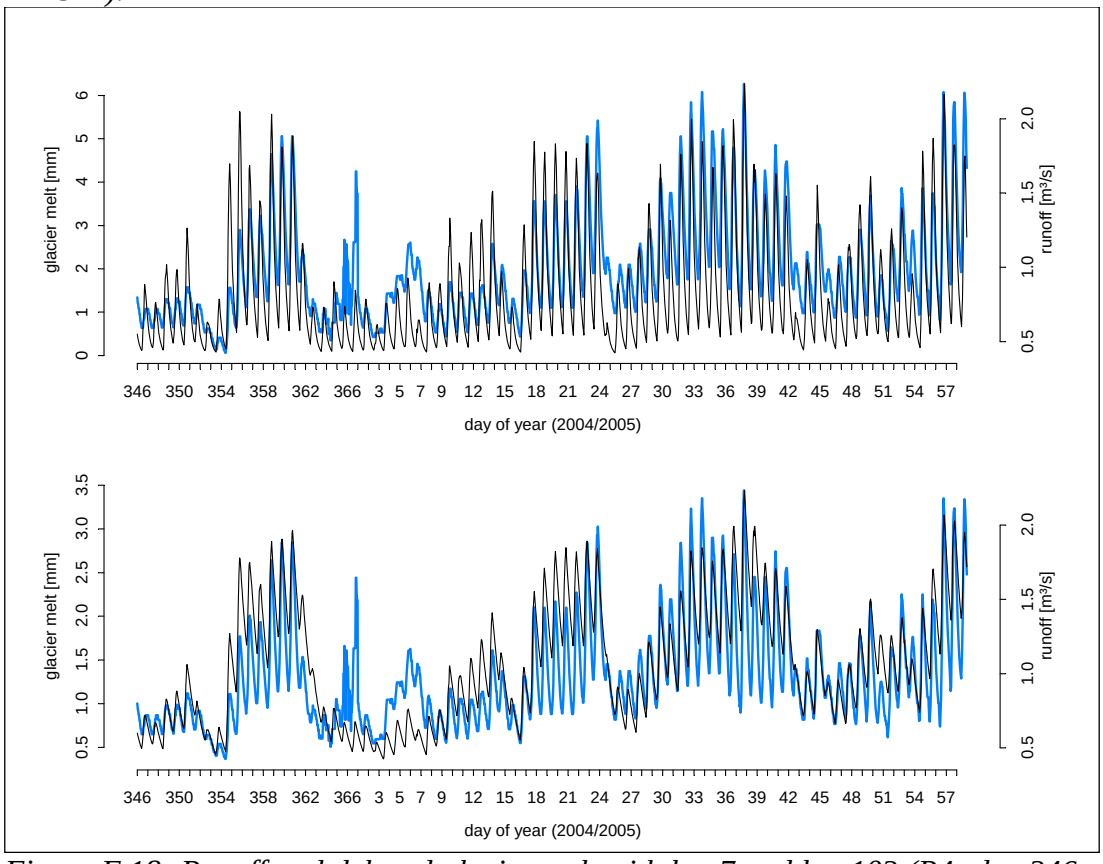

Figure F.18: Runoff and delayed glacier melt with ks=7 and ks=103 (P4: day 346 – 58).